ASTROCYTE – NEURON SIGNALLING BY SYNAPTIC STIMULATION IN THE VENTROBASAL THALAMUS

TIINA MARIA PIRTTIMÄKI

Doctor of Philosophy

ASTON UNIVERSITY

February 2009

Aston University

Thesis summary

ASTROCYTE – NEURON SIGNALLING BY SYNAPTIC STIMULATION IN THE VENTROBASAL THALAMUS

Pirttimäki TM
Doctor of Philosophy
Year of submission 2009

In the Ventrobasal (VB) thalamus, astrocytes are known to elicit NMDA-receptor mediated slow inward currents (SICs) spontaneously in neurons. These SICs can also be evoked by activation of astrocytic mGluRs, acting via intracellular Ca^{2+} elevations and presumed vesicular glutamate release. Fluorescence imaging of astrocytes and patch clamp recordings from thalamocortical (TC) neurons in the VB of 6-23 day old Wistar rats were performed. TC neurons exhibit spontaneous SICs at low frequencies (~0.0015Hz) that were inhibited by NMDA-receptor antagonists D-AP5 (50μM), and were insensitive to TTX (1μM) suggesting a non-neuronal origin. The effect of corticothalamic (CT) and sensory (Sen) afferent stimulation on astrocytic signalling was assessed by varying stimulus parameters. Moderate synaptic stimulation elicited astrocytic Ca^{2+} increases, but did not affect the incidence of spontaneous SICs. Prolonged synaptic stimulation induced a 265% increase in SIC frequency. This increase lasted over one hour after the cessation of synaptic stimulation, so revealing a Long Term Enhancement (LTE) of astrocyte-neuron signalling. LTE induction required group I mGluR activation, as it was inhibited by the group I antagonists MTEP (50μM) and CPCCOEt (200μM), and mimicked by prolonged exposure to the mGluR agonist DHPG (100μM). LTE SICs targeted NMDA-receptors located at extrasynaptic sites since a NR2B subunit specific antagonist Ifenprodil (10μM) reduced SIC amplitude significantly but had no effect on neuronal synaptic currents. LTE showed a developmental profile: from weeks 1-3, the SIC frequency was increased by an average 50%, 240% and 750% respectively. Prolonged exposure to glutamate (200μM) increased spontaneous SIC frequency by 1800%. This "chemical" form of LTE was prevented by the broad-spectrum excitatory amino acid transporter (EAAT) inhibitor TBOA (300μM) suggesting that glutamate uptake was a critical factor. Pre-incubating in D-Aspartic acid (200μM), which is a substrate for EAATs and NMDA-receptor agonist mimicked the "chemical" LTE. Repeating the moderate synaptic stimulation experiments on pre-incubated slices confirmed the ineffectiveness of acute synaptic stimulation at increasing SIC frequency. My results therefore show complex glutamatergic signalling interactions between astrocytes and neurons. Furthermore, two previously unrecognised mechanisms of enhancing SIC frequency are described. The synaptically induced LTE represents a form of non-synaptic plasticity and a glial "memory" of previous synaptic activity whilst enhancement after prolonged glutamate exposure may represent a pathological glial signalling mechanism.

Key words: astrocytes, glutamate, plasticity, rat, SIC, thalamus

Acknowledgements

I wish to thank all of those to whom this piece of work owes its completion, especially those in the Physiology and Pharmacology research group of Aston University who have given advice, support and inspiration. In particular I would like to thank Dr. Rhein Parri for his guidance and supervision.

I also want to thank all my friends here in the UK and those in Finland and other countries. Thanks for listening, supporting and bringing some fun to life throughout these hectic years managing my PhD.

A special thanks belongs to John who deserves a medal for all the help and support and for the numerous cups of tea and coffee during the ups and downs of the writing-up of my thesis.

Finally, million thanks to my mum and dad, my sister, my grandparents and other family members for all their support, help and encouragement before and during my PhD. A special thanks to my beloved Oona, just thinking of her happy tail wagging had such a huge destressing therapeutic effect.

Table of Contents

Table of Contents

LIST OF ILLUSTRATIONS

Abbreviations

AA	amino acid
ACh	acetylcholine
aCSF	artificial cerebrospinal fluid
AMPA	α-amino-3-hydroxy-5-methyl-4-isoxazolepropionic acid
CNS	central nervous system
CT	corticothalamic
D-Asp	D-Aspartate
ΔF	(delta) fluorescence change
EAAT	excitatory amino acid transporter
EPSC	excitatory post-synaptic current
Gln	glutamine
Glu	glutamate
IEI	inter-event interval
iGluR	ionotropic glutamate receptor
IPSC	inhibitory post-synaptic current
IP3	inositol triphosphate
KA	kainate (Kainic acid)
LTD	long term depression
LTE	long term enhancement
LTP	long term potentiation
LTS	long term stimulation
mGluR	metabotropic glutamate receptor
NA	noradrenaline
NMDAR	N-methyl-D-aspartate receptor
PN	post-natal
PSC	post-synaptic current
PNS	peripheral nervous system
PSQ	post-synaptic charge
Sen	sensory (afferents)
SIC	slow inward current
TC	thalamocortical
VB	Ventrobasal thalamus
$[Ca^{2+}]_i$	intracellular calcium concentration

Chapter 1

Introduction

1.1 Brief history of neuron-astrocyte-neuron communication

Glial[1] cells within the brain tissue were first described in the early 19th century by Ramón y Cajal, Rudolf Virchow, Camillo Golgi and others, and by the end of the century Carl-Ludwig Schleich proposed the idea of glia-neuron interactions [Verkhratsky & Toescu, 2006; Garcia-Marin *et al.*, 2007; Fig. 1.1].

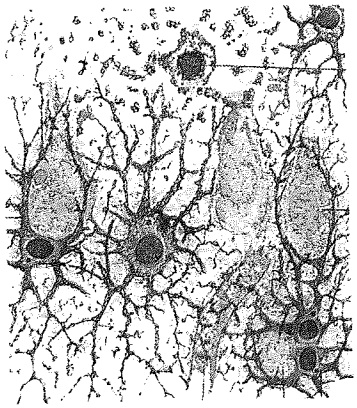

Figure 1.1: Glia in the 19th century. Cajal's drawing of neuroglia (darker highly processed cells) in the hippocampus of the human brain. The drawing shows astrocytic processes contacting blood vessel and pyramidal cells. (Figure is from Garcia-Marin *et al.*, 2007).

Nonetheless, the idea of glia-neuron interactions never achieved acceptance amongst scientists and therefore glial cells within the central and peripheral nervous system (CNS and PNS respectively) have been traditionally considered as passive elements giving mechanical, nutritional and trophic support for the neurons [Nedergaard *et al.*, 2003; Fellin & Carmignoto, 2004; Volterra & Meldolesi, 2005; Verkhratsky & Toescu, 2006].

Almost a century later, pioneering work by Cornell-Bell and his colleagues [Cornell-Bell *et al.*, 1990] showed that glutamate induced astrocytic calcium signalling, raising the question of whether glia could actually participate in nervous system signalling. Not long after, studies on cultured astrocytes established that glial cells exhibit a form of excitability based on intracellular Ca^{2+} ($[Ca^{2+}]_i$) variances leading to glutamate release and activation of neuronal glutamate receptors [Kim *et al.*, 1994; Nedergaard, 1994; Parpura *et al.*, 1994; Hassinger *et al.*, 1995]. A study by Porter and McCarthy [1996] gave the supporting evidence that astrocytes respond to glutamate released from synaptic terminals in acutely prepared brain slices (*in vitro*) whereas work by Pasti *et al.* [1997] showed that astrocytes *in vitro* do signal to neurons via glutamate release. The synaptic influence of glial cells became evident from

[1] Word glia is derived from Greek word gliok which means glue or slime

studies where glial calcium elevations induced glutamate release that was correlated with alterations in synaptic function of adjacent neurons [Araque *et al.*, 1998a-b; Kang *et al.*, 1998]; such that glial cells are now considered as active participants in the nervous system and the term "*tripartite synapse*", introduced by Araque *et al.* [1999], is now used to describe the synapses where synaptically associated astrocytes are functioning as integral modulatory elements.

The observations of signalling between neurons and glia have now been extended in many brain areas involving various neurotransmitters and cell types. Thus far the studies have covered the retina [Newman & Zahs, 1997; Newman, 2004; 2005], visual cortex [Carmignoto *et al.*, 1998], ventrobasal thalamus [Parri *et al.*, 2001], hippocampus [Angulo *et al.*, 2004; Fellin *et al.*, 2004; 2006; Perea and Araque, 2007], nucleus accumbens [D'Ascenzo *et al.*, 2007], olfactory bulb [Kozlov *et al.*, 2006] cerebellar cortex [Brockhaus & Deitmer, 2002; Bellamy & Oqden, 2006] and dorsal root ganglion [Auld & Robitaille, 2003], suggesting this is a common feature of glial cells in the nervous system. Further evidence of the glial calcium signalling was demonstrated in the intact (*in vivo*) cortical and corticothalamic systems illustrating that these are not just phenomena caused by tissue preparation [Hirase *et al.*, 2004; Wang *et al.*, 2006].

In contrast to the above, Beierlein & Regher [2006], Fiacco *et al.* [2007], Petravicz *et al.* [2008] and Shigetomi *et al.* [2008] reported evidence against the fact that astrocytic Ca^{2+} elevations readily act as an integral modulator at the synapse therefore questioning the developing consensus that astrocytic Ca^{2+} elevations and glutamate release directly affects neuronal synaptic activity *in vitro*.

It was first shown in the ventrobasal thalamus (VB) that astrocytes can display spontaneous calcium oscillations *in vitro* [Parri *et al.*, 2001], which consequently lead to neuronal excitatory *N*-methyl-D-aspartate (NMDA) -receptor mediated currents in thalamic neurons. In this thesis I extend the study of these thalamic currents to investigate how signalling between astrocytes and neurons in the VB is affected by synaptic glutamate released from thalamic afferents. This might reveal the conditions in which astrocytes cause neuronal excitation under different thalamic afferent input and would also be of great importance in illuminating communication in the tripartite synapse.

1.2 Glial cells in the CNS

The human brain is estimated to contain about 100 billion neurons and about 10 times more glial cells. Of all glial subtypes in the CNS, astrocytes appear to be the most abundant. In the rat visual cortex astroglia, oligodendroglia, and microglia are present in a ratio of 6:3:1 respectively [Gabbott & Steward, 1987]. The volume and ratio of astrocytes over neurons increases brain complexity: in a rodent cortex the ratio is 1 astrocyte per 3 neurons, but in the human cortex there are 1.4 astrocytes for each neuron, suggesting an important role in brain function [Nedergaard *et al.*, 2003; Oberheim *et al.*, 2006].

In the CNS, oligodendrocytes, ependymocytes and microglia are known to have specific functions in myelination, lining of the CNS cavities and production of cerebrospinal fluid as well as host defence, respectively. In contrast, the role of astrocytes has been less clear. Commonly accepted roles for astrocytes now include: metabolic and structural support, control of synaptic formation and function, regulation of ion concentration in the extracellular space, regulation of brain vascular tone as well as neurogenesis and repair in response to CNS injuries [Perea & Araque, 2002; Nedergaard *et al.*, 2003; Volterra & Meldolesi, 2005].

1.2.1 Astrocytes and associations with other CNS cells

1.2.1.1 Astrocytes lack ability to fire action potentials

Traditionally, astrocytes are thought to differ from neurons in that they lack a sufficient amount of sodium channels to conduct electrical activity and generate action potentials [Sontheimer, 1992]. Orkand and others showed in the 1960's that glial cells exhibit a large, almost linear K^+ conductance that makes the resting membrane potential highly negative (close to -90mV) [Orkand *et al.*, 1966; Sontheimer, 1992]. It has been shown that astrocytes express many of the same voltage-activated channels as neurons, but their functional importance is not as clear [Sontheimer, 1992]. It is noteworthy that the expression of voltage- and ligand-activated channels can be influenced by cell culture preparation methods [Miller *et al.*, 1993; Duffy & McVicar, 1994; Carmignoto *et al.*, 1998].

1.2.1.2 Astrocytic populations

Astrocytes are divided into two main classes by their anatomy and distribution: *protoplasmic astrocytes*, the major glial type in the gray matter, have fewer glial filaments and extremely dense ramification of fine shorter processes [Miller & Raff, 1984; Shepherd, 1994; Vesce *et al.*, 2001]. *Fibrous astrocytes* contain many glial filaments and are mainly found in white matter [Miller & Raff, 1984; Shepherd, 1994]. Fibrous astrocytes often have polarised shapes with one process (vascular endfeet) wrapped around blood capillaries [Magistretti & Pellerin; 1999; Zonta *et al.*, 2003]. Astrocytes can also be classified as Type 1 ($GFAP^+/A2B5^-$)[2] and Type 2 ($GFAP^+/A2B5^+$) according to their antigen binding properties [Raff *et al.*, 1983]. Astrocytes are considered to have various sub-populations based on diverse microdomain function and membrane current profiles [Steinhauser *et al.*, 1992; Grosche *et al.*, 1999; Zhou & Kimelberg, 2000, 2001; Perea & Araque, 2002; Nedergaard, 2003; Bushong *et al.*, 2002; 2004] although some may question whether the heterogeneity is a reflection of the plasticity of one astrocyte type under the influence of environmental factors rather than of the existence of distinct permanent subtypes [Walz, 2000].

1.2.1.3 Astrocytic organisation in the CNS

In the CNS astrocytes appear to be organised so that their cell bodies and larger processes are not in contact with each other [Nedergaard *et al.*, 2003]. A limited degree of overlap occurs between the smaller processes of neighbouring astrocytes and extensive overlapping is seen between the processes of distinct glial cell types such as oligodendrocytes and astrocytes [Bushong *et al.*, 2002]. Gap junctions[3] contribute greatly to the extent of astrocytic networks [Lee *et al.*, 1994]. They are mainly composed of connexin 43 and 30, abundantly distributed within astrocytic network connecting processes of the same cell as well as different cells at the narrow interfaces [Giaume & McCarthy, 1996; Giaume & Venance, 1998; Wolff *et al.*, 1998; Nedergaard *et al.*, 2003; Blomstrand *et al.*, 2004; Orthmann-Murphy *et al.*, 2008]. In the barrel field of the somatosensory cortex, the preferential orientation of coupling inside the barrels results from subpopulations of astrocytes that have different coupling properties

---

[2] Glial fibrillary acidic protein (GFAP) is a specific form of cytoskeletal intermediate filament expressed in astrocytes. A2B5 refers to positive or negative monoclonal antibody binding property

[3] Gap junctions are formed by a family of structurally related membrane proteins called connexons named after their molecular weight. They allow direct electrical and chemical communication between cells

[Houades *et al.*, 2008]: The communication between astrocytes was restricted inside a single barrel, whereas the astrocytes between barrels were either weakly or not coupled. The extent of gap-junctional coupling can also be modified, for example, with peptides such as endothelins as well as neurontransmitters, cytosolic Ca^{2+} and related molecules such as IP_3 [Giaume & Venance, 1998; Rouach *et al.*, 2000; Blomstrand *et al.*, 2004]. Gap-junctions that generally allow direct electrical and chemical communication between neurons are important, for example, in regulating extracellular K^+ concentrations, distribution of neurotransmitters as well as spreading of Ca^{2+} signalling within the astrocytic network [Giaume & Venance, 1998; Hansson *et al.*, 2000; Schools *et al.*, 2006].

1.2.1.4 Astrocytic coverage of synapses

Glial cells are thought to be a physiological barrier between the synaptic cleft and extrasynaptic space, limiting the degree of intersynaptic crosstalk caused by neurotransmitter spillout [Kullman and Asztely, 1998; Piet *et al.*, 2004]. The extent of glial ensheathment of the synapses is, however, extremely heterogenous and shows plasticity [Spacek, 1985; Theodosis & Poulain, 1992; Hatton, 1997; Castro-Alamancos, 2004]. Such plasticity is evident in the hypothalamus where glial processes are withdrawn from the synapses during lactation [Theodosis & Poulain, 1992; Hatton, 1997]. In hippocampal and cerebral synapses, the association between glia and neuronal membranes on the post-synaptic side has been shown to far exceed that on the pre-synaptic side suggesting functional specialisation [Lehre & Rusakov, 2002; Huang & Bergles, 2004]. In the visual and cerebellar cortices, dendritic spines of Purkinje cells are completely covered by the glial sheath, whereas dendritic spines of pyramidal cells are only partially covered, leaving spine stalks and synaptic clefts frequently without any glial isolation [Spacek, 1985]. In the VB, sensory afferents form synapses termed as "glomeruli" that are completely covered by glial processes, whereas cortical afferents form smaller synaptic boutons with less intimate contact with astrocytes [Matthews *et al.*, 1977; Castro-Alamancos, 2004]. Figure 1.2 illustrates astrocytic coverage of barrel cortex synapse.

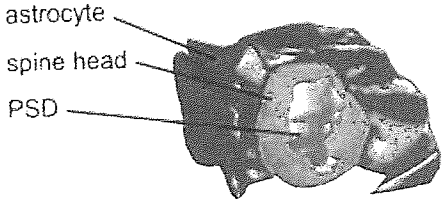

Figure 1.2: Astrocytic coverage of synaptic bouton-spine interface. This figure illustrates 3D construction of spine head, post synaptic density (PSD) and associated astrocyte with axonal bouton removed from a barrel cortex synapse. (Figure from Genoud *et al.*, 2006)

1.2.2 Astrocytes and synaptic transmission in the rodent CNS

In addition to more familiar roles of astrocytes such as maintenance of homeostasis at the synapse upon neuronal firing, several physiological signalling pathways involving glial cells have been established. The ***neuron-glia-microglia pathway*** involves release of adenosine tri-phosphate (ATP), cytokines and prostaglandins and can influence the profile of secreted microglial substances [Fellin & Carmignoto, 2004]. By releasing substances such as atrial natriuretic peptide, prostaglandins and nitric oxide, astrocytes belonging to the ***neuron - astrocyte - blood vessel pathway*** can regulate cerebral blood flow [Fellin & Carmignoto, 2004]. The recently discovered ***neuron-astrocyte-neuron/astrocyte*** pathway involving release of neuroactive substances will be disussed more in detail below.

1.2.2.1 Astrocytic maintenance of homeostasis during synaptic transmission

Clearance of excess K^+ and glutamate during neuronal activity is fundamental for preventing interference with neuronal signalling, tonic receptor activation and excitotoxicity [Huang *et al.*, 2004; Yi & Hazell, 2006]. Several mechanisms, such as spatial buffering, Na^+/K^+ pump, KCl co-transport and uptake via inwardly rectifying K^+ channels have been proposed to be involved in potassium clearance [Gardner-Medwin *et al.*, 1981; Walz & Hertz, 1983; Grafe & Ballanyi, 1987; Ballanyi *et al.*, 1987; Newman, 1993; Philippe *et al.*, 1996; Meeks & Mennerick, 2007]. Excess neurotransmitter is cleared via transporter uptake. GLAST (EAAT1) and GLT-1 (EAAT2) are glutamate transporters found on the glial membrane in rodents [Rothstein *et al.*, 1994; Lehre *et al.*, 1995; Bergles & Jahr, 1997; Anderson & Swanson, 2000; Hazell *et al.*, 2001]. Both of these transporters also have affinity for aspartate [Bergles & Jahr, 1997; Anderson & Swanson, 2000; Diamond & Jahr, 2000; Diamond, 2005; D'Aniello, 2006]. Glial cells also have transporters for GABA (GAT-1 and GAT-2/3) and glycine (GlyT1b) [Kinney & Spain, 2002; Marcaggi & Attwell, 2004]. Transporter uptake is driven by coupling with the transmembrane Na^+, H^+ and voltage gradients [Anderson & Swanson, 2000; Marcaggi & Attwell, 2004]. Glutamate can be cleared from the extrasynaptic space within 1ms [Clements *et al.*, 1992; Diamond, 2005]. However, the time course of clearance appears slower in young animals and may be diminished at room temperature [Bergles & Jahr 1997; Diamond & Jahr, 2000; Diamond, 2005].

Most of the glutamate taken up by astrocytes is recycled back to neurons via the glutamate-glutamine cycle. The classical pathway involves conversion of glutamate into glutamine by glutamine synthetase that is localised in astrocytes [Martinez-Hernandez *et al.*, 1977; Marcaggi & Attwell, 2004]. Glutamine is then exported to neurons by transporters (SNAT1-3 and 5) and converted back to glutamate by neuron specific glutaminase [Marcaggi & Attwell, 2004].

1.2.2.2 Astrocytes exhibit excitability in the form of $[Ca^{2+}]_i$ variations

Numerous studies have now revealed that astrocytes exhibit neurotransmitter/neurohormone receptors *in vitro* such as NMDA-receptors, metabotropic glutamate-receptors (mGluRs), alpha-amino-3-hydroxy-5-methyl-4-isoxazolepropionic acid receptors (AMPA-R) and kainate-receptors (KA-R) for glutamate; γ-aminobutyric acid-receptors (GABA-R) for GABA; iono- and metabotropic purinergic-receptors (P2X/P2Y-R) for ATP; CB1-R for endocannabinoids as well receptors for nitric oxide (NO), noradernaline (NA) and acetylcholine (ACh) [Porter & McCarthy, 1997; Shelton & McCarthy, 1999; Hansson & Rönnbäck, 2003; Fellin & Carmignoto, 2004; Volterra & Meldolesi, 2005; Verkhratsky & Kirchhoff, 2007; Navarrete & Araque, 2008].

During neuronal activity, astrocytes not only buffer excess K^+ ions and glutamate from the synaptic cleft, they also *respond* to the released neurotransmitters acting on G-protein-coupled receptors (GPC-Rs)[4] by elevating their $[Ca^{2+}]_i$ levels [Cornell-Bell *et al.*, 1990; Parpura *et al.*, 1994; Porter & McCarthy, 1996; Bernstein *et al.*, 1998; Araque *et al.*, 2002; Fellin & Carmignoto, 2004; Lin & Bergles, 2004; Schipke & Kettenman, 2004; Lee *et al.*, 2007; Navarrete & Araque, 2008]. In response to glutamate, there are at least two different pathways mediating the $[Ca^{2+}]_i$ elevations [Cornell-Bell *et al.*, 1990; Kim *et al.*, 1994; Shelton & McCarthy, 1999]. In the first pathway, glutamate can partially bind to GPC group I metabotropic glutamate receptor (mGluRI) of the synaptic astrocyte [Biber *et al.*, 1999]. This causes a rise in intracellular levels of phospholipase C (PLC) and hence, the second messenger inositol-1,4,5-triphosphate (IP_3) production [Biber *et al.*, 1999; Hermans & Challiss, 2001]. When IP_3 is released to the intracellular space, it binds to the IP_3 receptor on the endoplasmic reticulum (ER) releasing Ca^{2+} from the internal stores leading to cytosolic

[4] GPC-receptors belong to a large family of transmembrane receptors that bind molecules outside the cell and activate signal transductions pathways inside the cell

[Ca^{2+}] elevations [Kim *et al.*, 1994; Biber *et al.*, 1999; Parri & Crunelli, 2003; Petravicz *et al.*, 2008]. The second pathway involves glutamate binding at ionotropic glutamate receptor leading to Ca^{2+} influx and potential opening of voltage-operated calcium channels (VOCCs) engaging additional influx of Ca^{2+} [Cornell-Bell *et al.*, 1990; Kim *et al.*, 1994; Shelton & McCarthy, 1999].

Different forms of calcium signals that constitute to local, short or long range signalling have been identified. Ca^{2+} signals can manifest as global or spatially restricted calcium elevations within a single cell [Cornell-Bell *et al.*, 1990; Kim *et al.*, 1994; Nett *et al.*, 2002; Parri *et al.*, 2001; Parri & Crunelli, 2003]. These elevations can be individual spikes, oscillations or sustained elevations [Kim *et al.*, 1994; Nett *et al.*, 2002; Parri *et al.*, 2001]. Ca^{2+} signals can also vary in response to different stimulations. Cultured astrocytes, for example, have been shown to respond in graded fashion to increasing glutamate concentrations [Kim *et al.*, 1994]. In hippocampus *in vitro*, increasing afferent stimulation intensity, frequency and duration has been shown to increase the frequency and magnitude of astrocytic Ca^{2+} oscillations [Porter & McCarthy, 1996; Pasti *et al.*, 1997; Araque *et al.*, 2002; Perea & Araque, 2005].

Propagating Ca^{2+} transients originating from a single cell can sequentially engage neighbouring cells and generate intercellular Ca^{2+} waves [Cornell-Bell *et al.*, 1990; Kim *et al.*, 1994; Parri *et al.*, 2001]. Intercellular Ca^{2+} wave propagation was thought to occur via gap-junctions [Nedergaard, 1994; Giaume & Venance, 1998; Nedergaard *et al.*, 2003], but now it is commonly accepted that ATP acts as a major extracellular messenger in this mechanism [Guthrie *et al.*, 1999; Cotrina & Nedergaard, 2000]. In cell cultures, propagation depends on Ca^{2+}-dependent autocatalysis: at intermediate $[Ca^{2+}]_i$ levels, Ca^{2+} can stimulate its own release as co-agonist for IP_3-receptors, whereas high $[Ca^{2+}]_i$ levels can produce negative feedback [Bezprozvanny *et al.*, 1991; Kim *et al.*, 1994].

1.2.2.3 Astrocytes exhibit spontaneous $[Ca^{2+}]_i$ variations

Astrocytes have intrinsic properties that allow them to modulate their $[Ca^{2+}]_i$ levels independently of neuronal activity [Nett *et al.*, 2002; Parri & Crunelli, 2003]. In the hippocampus and thalamus, the mechanism seems to involve IP_3 receptor activation by Ca^{2+} independently of neurotransmitter release and GPC-receptor activation [Nett *et al.*, 2002; Parri & Crunelli, 2003]. These signals also manifest as spikes or oscillations within a single

cell or propagate as intercellular calcium waves [Nett *et al.*, 2002; Parri & Crunelli, 2003]. In addition, spontaneous astrocytic $[Ca^{2+}]_i$ signalling has also been shown to occur *in vivo* in the cortex [Hirase *et al.*, 2004]. Spontaneous neuronal activity is important for the developing brain [Katz & Shatz, 1996]. As spontaneous astrocytic Ca^{2+} waves occur in many brain regions during maturation [Aguado *et al.*, 2002], this form of signalling may also be critical for the development of precise connectivity and could be inducing specific gene activation as suggested by Rose & Konnerth [2001] and Parri & Crunelli [2002].

1.2.2.4 Astrocytes release various gliotransmitters

In addition to glutamate, astrocytes can release other gliotransmitters and substances such as GABA, aspartate, taurine, D-serine, ATP, adenosine, growth factors, steroids, eicosanoids and neuropeptides [Kimelberg *et al.*, 1990; Hansson & Rönnbäck, 2003; Fellin & Carmignoto, 2004; Perea & Araque, 2004; Volterra & Meldolesi, 2005; Kozlov *et al.*, 2006]. Release of neurotransmitters from astrocytes can occur in response to stimuli or spontaneously and is collectively termed as gliotransmission [Pasti *et al.*, 1997; Parpura & Haydon, 2000; Parri *et al.*, 2001; Nett *et al.*, 2002; Angulo *et al.*, 2004; Fellin *et al.*, 2004; Perea & Araque, 2005].

The release mechanism of astrocytic glutamate remains uncertain, however, evidence for several mechanisms has been provided. These include calcium dependent vesicular release, swelling induced anion channels, connexin hemichannels, P2X receptors, reverse operation of glutamate transporters and diffusion across the membrane [Kimelberg *et al.*, 1990; Rutledge & Kimelberg, 1996; Rutledge *et al.*, 1998; Araque *et al.*, 2000; Darby *et al.*, 2003; Duan *et al.*, 2003; Ye *et al.*, 2003; Fellin & Carmignoto, 2004; Fellin *et al.*, 2006; Takano *et al.*, 2005]. Experiments in cell cultures have demonstrated that physiological astrocytic calcium levels are sufficient to stimulate glutamate release [Parpura & Haydon, 2000]. Astrocytes express many proteins required for vesicular formation and indeed, the most commonly accepted release mechanism involves Ca^{2+}- and SNARE-dependent[5] exocytotic vesicular release [Araque *et al.*, 2000; Mazzani *et al.*, 2001; Bezzi *et al.*, 2004; Montana *et al.*, 2004; Shiga *et al.*, 2006; Xu *et al.*, 2007]. The other mechanisms, especially swelling and volume regulated release, are primarily implicated in pathological conditions such as ischemia and

[5] Soluble N-ethylmaleimide-sensitive factor (NSF) attachment receptor protein mediating fusion of cellular vesicles with membranes. The fusion of vesicles and release of neurotransmitters into extracellular space is called exocytosis.

may participate in tonic rather than transient release of glutamate [Kimelberg *et al.*, 1990; Feustel *et al.*, 2004; Fellin *et al.*, 2006].

1.2.2.5 Astrocytic modulation of synaptic activity

Gliotransmission can affect neuronal receptors presynaptically, postsynaptically or extrasynaptically at the same synapse as well as heterosynaptically at longer distance as illustrated in figure 1.3 [Haydon & Carmignoto, 2006]. Depending on the site of action and the released substance, gliotransmission can either depress or facilitate synaptic transmission or lead to additional extrasynaptic depolarising currents known as slow inward currents (SICs) [Haydon & Carmignoto, 2006].

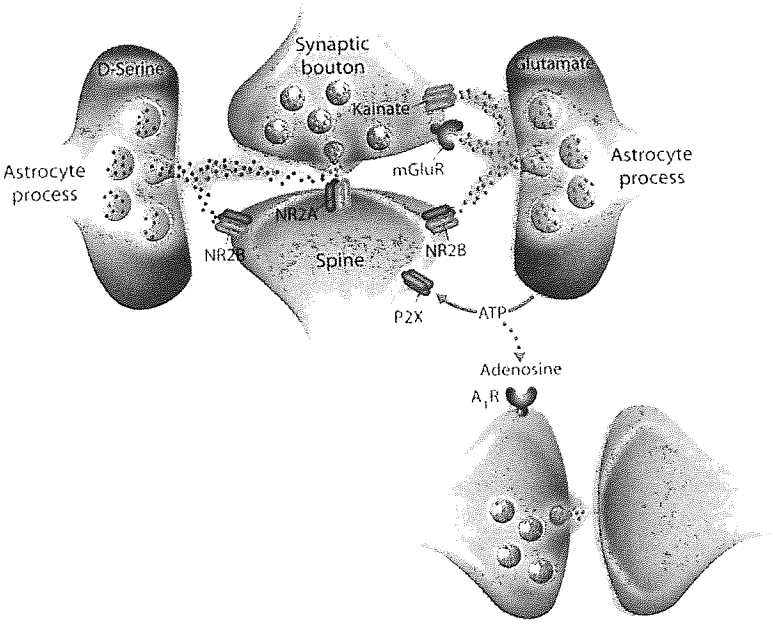

Figure 1.3: Astrocytic modulation of synaptic transmission. Astrocytes release gliotransmitters such as glutamate (red dots), D-serine (green dots) and ATP (blue arrow). These can have various effects depending on the target receptors and locations. (Figure is from Haydon & Carmignoto, 2006).

Depression. Astrocyte mediated depression of synaptic transmission is due to the activation of neuronal pre-synaptic group II/III mGluRs [Araque *et al.*, 1998, 1999; Liu *et al.*, 2004]. Activation of these receptors is known to suppress the vesicular release of neurotransmitters therefore affecting the amplitude of evoked excitatory post-synaptic currents (EPSCs) and inhibitory post-synaptic currents (IPSCs) or frequency of miniature PSCs [Gereau *et al.*, 1995; Araque *et al.*, 1998, 1999; Liu *et al.*, 2004].

Facilitation. Glutamate released from astrocytes can also bind to neuronal pre/post synaptic NMDA/non-NMDA receptors and consequently potentiate neuronal inhibitory and/or excitatory currents [Araque *et al.*, 1998; Kang *et al.*, 1998; Fiacco & McCarthy, 2004; Liu *et al.*, 2004; Lee *et al.*, 2007; Jourdain *et al.*, 2007].

Plasticity. Astrocytes also contribute to neuronal plasticity and long term potentiation (LTP) either by releasing gliotransmitters or by physically controlling neurotransmitter availability at synapses [Yang *et al.*, 2003; Panatier *et al.*, 2006; Perea & Araque, 2007]. Perea and Araque [2007] demonstrated that astrocytic Ca^{2+} and SNARE-protein dependent glutamate release acting on presynaptic group I mGluRs potentiated transmitter release leading to short-term plasticity. When this coincided with postsynaptic depolarisation, the transient potentiation became permanent therefore extending the classical rule of Hebbian LTP[6]. Astrocytes can also contribute to heterosynaptic plasticity. For example, Ca^{2+} dependent glially-released ATP is enzymatically degraded to adenosine which acts on pre-synaptic A_1 receptors at synapses distant from the original release site, and so is an important mediator of heterosynaptic depression [Pascual *et al.*, 2005; Serrano *et al.*, 2006].

Slow Inward Currents. SICs were first described on cultured cells where electrical or mechanical stimulation of astrocytes caused $[Ca^{2+}]_i$ increases that were correlated with slow inward currents in associated neurons [Araque *et al.*, 1998]. Since then SICs have been studied *in vitro* in the VB thalamus, hippocampus, cortex, nucleus accumbens, cerebellum and olfactory bulb including both glutamatergic and GABAergic neurons [Parri *et al.*, 2001; Fellin *et al.*, 2004; Angulo *et al.*, 2004; Perea & Araque, 2005; Beierlein & Regehr, 2006; Fellin *et al.*, 2006; Kozlov *et al.*, 2006; D'Ascenzo *et al.*, 2007; Ding *et al.*, 2007; Navarrete & Araque, 2008; Shigetomi *et al.*, 2008]. What is common to all these SICs *in vitro* is that they are much larger than synaptic currents as demonstrated in figure 1.4. They are insensitive to TTX and AMPA/KA-receptor antagonists but are inhibited by NMDA-receptor antagonists [Parri *et al.*, 2001; Fellin *et al.*, 2004; Angulo *et al.*, 2004; Perea & Araque, 2005; Fellin *et al.*, 2006; Kozlov *et al.*, 2006; D'Ascenzo *et al.*, 2007; Ding *et al.*, 2007; Navarrete & Araque, 2008; Shigetomi *et al.*, 2008]. Insensitivity to synaptic transmission inhibitors established that these slow currents were non-neuronal in origin [Araque *et al.*, 1998; Angulo *et al.*, 2004; Fellin *et al.*, 2004]. In the field in general, currents with amplitudes greater than 20pA and rise times

[6] Hebbian rule of LTP describes the pairing pre- and post synaptic activity leading to persistent increase in synaptic strength

longer than 10ms in the presence of TTX are accepted as SIC [Araque *et al.*, 1998; Angulo *et al.*, 2004; Fellin *et al.*, 2004].

Astrocyte mediated SICs have been shown to preferentially target extrasynaptic NMDA-receptors containing NR2B sub-unit [Cull-Candy *et al.*, 2001; Fellin *et al.*, 2004; D'Ascenzo *et al.*, 2007; Shigetomi *et al.*, 2008]. The average amplitude stated in the literature ranges between 29 and 182 pA, rise time between 27 and 135ms and decay time between 121 and 608 ms [Parri *et al.*, 2001; Angulo *et al.*, 2004; Fellin *et al.*, 2004; Perea & Araque, 2005; Fellin *et al.*, 2006; Xu *et al.*, 2007; Navarrete & Araque, 2008; Shigetomi *et al.*, 2008]. Variability in the SIC magnitude and kinetics is thought to arise from multiple release sites from one or several astrocytes contacting the same neuron [Angulo *et al.*, 2004; Fellin *et al.*, 2004; Haydon & Carmignoto, 2006]. Different diffusion distances in extracellular space and size of the glutamate releasing vesicles may also contribute to the variability [Angulo *et al.*, 2004; Fellin *et al.*, 2004; Haydon & Carmignoto, 2006].

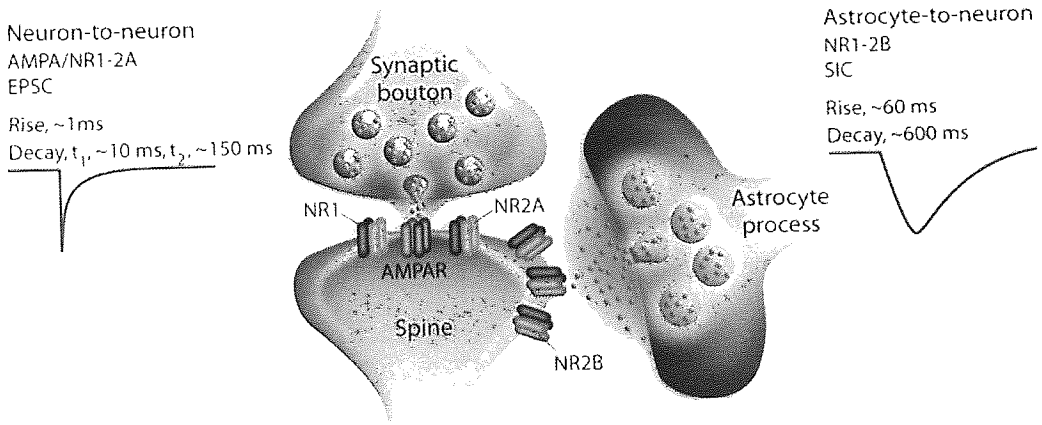

Figure 1.4: Slow Inward Currents. Astrocytes release glutamate that targets extrasynaptic NMDA-receptors containing the NR2B subunit. SICs are characterised by their extremely slow kinetics and are orders of magnitude larger than synaptic EPSCs in hippocampus (Figure is from Haydon & Carmignoto, 2006).

SICs can occur spontaneously or be evoked by various methods that induce astrocytic Ca^{2+} increases [Parri *et al.*, 2001; Angulo *et al.*, 2004; Fellin *et al.*, 2004; Perea & Araque, 2005; Fellin *et al.*, 2006; Kozlov, 2006; D'Ascenzo *et al.*, 2007; Xu *et al.*, 2007; Navarrete & Araque, 2008; Shigetomi *et al.*, 2008]. A number of studies have shown direct evidence that astrocytic Ca^{2+} increases coincide with neuronal SIC [Parri *et al.*, 2001; Fellin *et al.*, 2004; Perea & Araque, 2005; Narravete & Araque, 2008]. Astrocytic Ca^{2+} dependent vesicular release of glutamate has been directly linked to the generation of SICs and, indeed, such

astrocytic vesicles have been located opposite to extrasynaptic NMDA-receptors [Araque *et al.*, 2000; Bezzi *et al.*, 2004; Xu *et al.*, 2007].

Spontaneous SICs occur at very low frequencies *in vitro*, mean frequency ranging between 0.05 and 1.8 SICs/min corresponding to ~0.001–0.03 Hz [Fellin *et al.*, 2004; Angulo *et al.*, 2004; Perea & Araque, 2005; Fellin *et al.*, 2006; Kozlov *et al.*, 2006; D'Ascenzo *et al.*, 2007; Navarrete & Araque, 2008; Shigetomi *et al.*, 2008]. Most studies have used Mg-free medium to enhance the detection of NMDA-mediated events, however SICs do occur in normal aCSF containing Mg^{2+} albeit at ;ower frequencies [Fellin *et al.*, 2004; Perea & Araque, 2005; D'Ascenzo *et al.*, 2007]. Furthermore, although most studies have used young animals (5-23 PN days), SICs have been observed up to the age of 6 weeks with no significant differences in their prevalence [Angulo *et al.*, 2004; Kozlov *et al.*, 2006; D'Ascenzo *et al.*, 2007].

Even though astrocyte mediated neuronal depolarization can be large enough to cause neuronal firing, initially shown by Hassinger and colleagues [1995], the purpose of SICs is not fully understood. It has been shown that SICs are not necessary for the modulation of synaptic transmission as it can be modulated in the absence of SICs, or SIC can be detected without the modulation of synaptic transmission [Araque *et al.*, 1998; D'Ascenzo *et al.*, 2007; Jourdain *et al.*, 2007]. However, in paired recordings, populations of SICs have been shown to occur in synchrony and to elicit robust bursts of action potentials indicating that SICs may participate in neuronal synchronization [Angulo *et al.*, 2004; Fellin *et al.*, 2004; Fellin *et al.*, 2006; D'Ascenzo *et al.*, 2007]. Furthermore, as SICs have been shown to induce neuronal Ca^{2+} elevations [Parri *et al.*, 2001], it can be expected that SICs participate in biochemical processes involving Ca^{2+} entry and subsequent activation of second messenger pathways and gene transcription [Shepherd, 1994].

1.2.2.6 NMDA-receptors: target for astrocytic glutamate release

Ionotropic glutamatergic NMDA-receptors (*N*-methyl *D*-aspartate) consist of combinations of different NR1/NR2A-D subunits with distinct kinetics [Cull-Candy *et al.*, 2001]. For example, application of glutamate onto NR1/NR2A assemblies generate a macroscopic current with deactivation time constant of tens of milliseconds compared to several seconds for NR1/NR2D receptors [Cull-Candy *et al.*, 2001]. NMDA-receptors are characterised by voltage-dependent Mg^{2+} block and require glycine or D-serine as a co-agonist [Cull-Candy *et*

al., 2001]. These receptors have a high Ca^{2+}/Na^{+} permeability ratio and are strong implicated in synaptic plasticity as well as in excitoxicity [Shepherd, 1994; Simon *et a* 1984; Cull-Candy *et al.*, 2001; Wittmann *et al.*, 2004].

Subunit expression varies both temporally and spatially [Wenzel *et al.*, 1996; 1997; Cul Candy *et al.*, 2001]. In the rat thalamus, for example, NR2B and NR2C subunit expression weak during the first post-natal week but increases after P10 [Wenzel *et al.*, 1997 Functionally, the synaptic NMDA-receptor is composed of NR2B subunits at early post-nat age but reduces its sensitivity around second post-natal week whilst the NR2A become dominant in the VB thalamus [Liu *et al.*, 2004; Arsenault & Zhang, 2006]. Expression c NR2B at extrasynaptic location has been shown to be weak in the thalamus throughout th first 3 PN weeks [Liu *et al.*, 2004]. NR2D subunit, which is shown to be expresse exclusively at extrasynaptic sites, is abundant at early stages but absent in the VB complex b P21 [Wenzel *et al.*, 1997; Liu *et al.*, 2004].

1.2.2.7 Dysfunction of glia and unbalanced glia-neuron glutamate signalling

Glutamate is the main excitatory neurotransmitter in the brain, however, in excess it can be potential neurotoxin [Olney, 1969; Simon *et al.*, 1984; Shepherd, 1994]. Astrocyti dysfunction and unbalanced glia-neuron glutamate homeostasis in the CNS has bee associated with many pathological conditions such as epilepsy, amytrophic lateral sclerosis stroke and ischemia [Aschner *et al.*, 2002; Seifert *et al.*, 2006]. Interestingly, two recen studies linked astrocytic $[Ca^{2+}]_i$ increases and subsequent glutamate release to generation o seizure activity [Kang *et al.*, 2005; Tian *et al.*, 2005]. In these studies, SICs were shown t generate neuronal paroxysmal depolarizations resembling those typical of intericta epileptiform acitivity. In contrast, two other studies showed that increased astrocytic Ca^{2-} signalling was more of a result of the preceding epileptic activity than a cause for it [Fellin *e al.*, 2006; Ding *et al.*, 2007]. However, the authors did not exclude the possibility tha astrocytic glutamate release may modulate the intensity of seizure-like events. Furthermore this astrocytic glutamate release was implicated as a critical signalling element tha contributes in the induction neuronal death [Ding *et al.*, 2007].

1.3 The ventrobasal thalamus and its connections

The thalamus lies deep in each side of the cerebral hemispheres of the forebrain. It is thought to have multiple functions and different parts of the thalamus are engaged with sensory (e.g. lateral geniculate nucleus for optic tract) or motor systems (ventrolateral nuclei for cerebellar afferents) [Shepherd, 1994; Shepherd, 2004]. One of the major roles of the thalamus is to process and relay sensory, excluding olfactory, information from the periphery to the neocortex [Tanabe *et al.*, 1975; Sherman & Guillery, 1996; Jones, 1998; Castro-Alamancos, 2004]. In this thesis, my particular interest is in the thalamic ventrobasal (VB) nucleus and in its connections. In rodents the VB complex relays sensory information from the vibrissae (tactile information from whiskers) to the cortex via the medial lemniscal tract [Woolsey & Van der Loos, 1970; Killackey *et al.*, 1995; Castro-Alamancos, 2004]. The thalamus is also involved in regulating sleep and wakefulness as well as levels of arousal via the corticothalamic feedback loop and brain stem connections [Steriade, 1994; Steriade *et al.*, 1996; Contreras *et al.*, 1997].

1.3.1 Anatomical connections of the thalamus

Thalamic nuclei are divided into two functionally distinct groups: the first group contains first order relay cells transferring information between periphery and cortex and the second group contains higher order relay cells conveying information between cortex and thalamus as well as between different thalamic nuclei [Guillery, 1995; Shepherd, 2004].

Ventrobasal thalamus (VB complex). The ventrobasal thalamus (also known as primary somatosensory thalamus or somathetic relay nuclei) consists of ventroposterior medial (VPm) and lateral (VPl) nuclei [Guillery, 1995; Shepherd, 2004]. It is classified as a first order nucleus (primary relay) and is the primary thalamic nucleus of the somatosensory system [Guillery, 1995; Shepherd, 2004]. The major VB connections include glutamatergic corticothalamic afferents (CT input), thalamocortical efferents (TC output) and primary sensory afferents via the medial lemniscal tract (Sen input) [Guillery, 1995; Shepherd, 2004]. The VB nucleus is highly interconnected with neocortex and also between different thalamic nuclei [Guillery, 1995; Shepherd, 2004; Crabtree & Isaac, 2002]. Figure 1.5 outlines the basic circuitry.

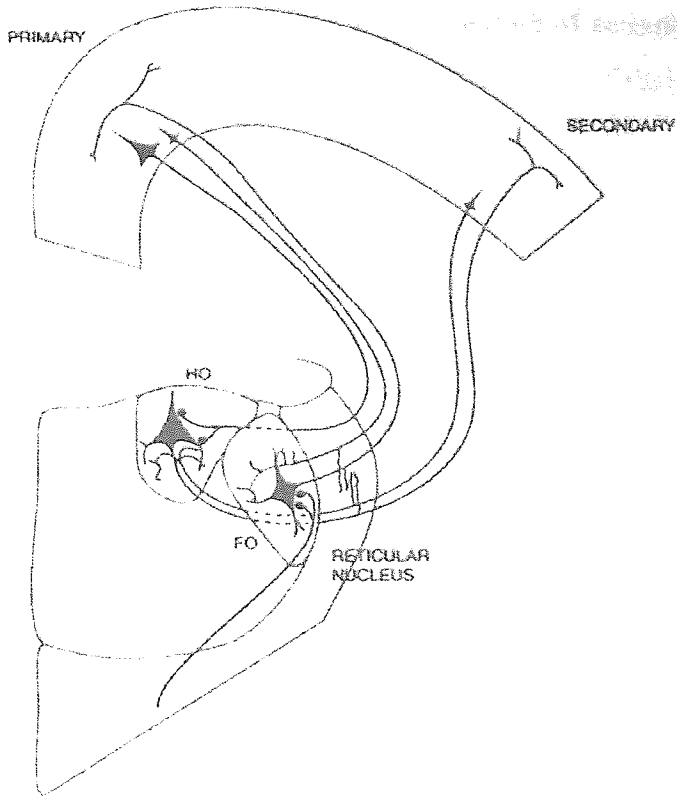

Figure 1.5: Thalamocortical circuitry. Schematic of the thalamic nuclei and their connections. The first order (FO) nuclei, such as VB complex, receive input from the periphery (blue track at the bottom). The first order relay cells (TC neurons) project to cortical layer IV (primary). The FO receive feedback connections from the cortical layer VI through the reticular nucleus of thalamus (nRT). The nRT also sends GABAergic projections to the FO. Higher order (HO) nuclei convey information between cortex and different thalamic nuclei. (Figure from Guillery, 1995).

The vibrissae system. Sensory input from visual, somatosensory and auditory afferents form topographic maps in the thalamus and cortex [Killackey *et al.*, 1995]. In rodents, each whisker is mapped in the same order in the VB nuclei and somatosensory cortex giving a rise to the vibrissae system [Woolsey & Van der Loos, 1970; Killackey *et al.*, 1995; Shepherd, 2004]. Within this vibrissae system, tactile information is processed at three levels: The first level of information processing from mechanoceptors occurs in the trigeminal complex in the brainstem, where generally one whisker forms one cluster i.e. barrelettes. The trigeminal axons, forming the lemniscal pathway, innervate the second level barreloids in VPm, where each cluster of cells represents the same principal whisker. Finally the axons from barreloids innervate the barrels in layer IV in the cortex giving rise to the thalamocortical pathway [Castro-Alamancos, 2004, Shepherd, 2004].

CT loop. The thalamus relays sensory information to layer IV of the somatosensory (S1) cortex via thalamocortical efferents and receives feedback from corticothalamic afferents originating in cortical layer VI forming the corticothalamic loop. CT afferents are the most abundant input to the VB thalamus, and are twice as large as the thalamocortical output or lemniscal input, but have smaller postsynaptic densities [Castro-Alamancos, 2004; Shepherd, 2004]. The functional role of this feedback system is not completely understood but it is

thought to be involved in the processing of sensory information, synchronisation of thalamic firing and transitions in the response mode of thalamic relay cells [Castro-Alamancos, 2004; Alexander & Godwin, 2005; Pinault *et al.*, 2006].

nRt. The nucleus reticularis (nRt) of the thalamus lies in the path of the thalamocortical and corticothalamic collaterals lateral to dorsal thalamus. This thin layer of cells projects GABAergic input to the VB complex and is thought to provide an important regulatory input since in rodents, the VB complex lacks interneurons and recurrent axon collaterals between them [Barbaresi *et al.*, 1986; Gentet & Ulrich, 2002; Castro-Alamancos, 2004; Shepherd, 2004; Blethyn *et al.*, 2006].

Other afferents. Other afferents arising from brainstem and basal forebrain include cholinergic neurons of the parabrachial region, noradrenergic neurons of the locus coeruleus and serotonergic neurons of the dorsal raphe nucleus. Histaminergic and GABAergic input arise from hypothalamus and basal forebrain respectively [Castro-Alamancos, 2004; Shepherd, 2004]. The latter one does not directly innervate the VB but influences relay properties of the nRt cells [Castro-Alamancos, 2004; Shepherd, 2004].

1.3.2 Synaptic transmission in the VB thalamus

1.3.2.1 Firing modes of the TC neurons

Thalamocortical (TC) neurons are traditionally thought to operate in two different modes depending on behavioural state: These are *tonic firing* and *bursts firing* [Jahnsen & Llinas, 1984; Sherman, 2001; Shepherd, 2004]. At hyperpolarised potentials sufficiently large and fast depolarising currents lead to burst firing whereas at more depolarised potentials (positive to -55mV) these cells relay information in tonic firing mode both *in vivo* and *in vitro* [Shepherd, 2004; Llinas & Streriade, 2006]. In general burst firing occurs during drowsiness and/or slow wave sleep, and tonic firing during wakefulness and arousal [Shepherd, 2004]. It is now known however that TC neurons can exhibit a range of firing modes [Li *et al.*, 2003; Hughes *et al.*, 2004; Crunelli *et al.*, 2006; Lörincz *et al.*, 2008]. These include high threshold bursting, tonic firing, slow (<1Hz) oscillations and burst firing/delta oscillations [Crunelli *et al.*, 2006].

1.3.2.2 Sensory afferents and synaptic transmission

Lemniscal (sensory input) terminals form glutamatergic specialised synapses (glomeruli) with the soma and/or proximal dendrites of the TC neurons in the VB [Castro-Alamancos, 2004; Miyata, 2007]. The sensory synapse has multiple release sites and exhibits highly secure all-or-none responses arising from single axonal contact [Arsenault & Zhang, 2006; Miyata & Imoto, 2006]. The excitatory input is high in amplitude, fast firing and has short latency compared to corticothalamic inputs and indeed Lemniscal EPSCs are largely mediated by AMPA receptors [Castro-Alamancos, 2002; 2004; Miyata, 2007].

During arousal and active exploration TC neurons are in relay mode [Castro-Alamancos, 2002; 2004]. During active exploration rodent whiskers vibrate at frequencies between 4-12 Hz which can rise to several hundred Hertz when a rat whisks over an object [Moore, 2004]. During quiescence vibrissae typically stay almost still vibrating at frequencies below 1 Hz [Moore, 2004]. Only low frequencies, below 2 Hz, are relayed during quiescent states and *in vitro* studies have shown that lemniscal input is suppressed at frequencies above 2 Hz [Castro-Alamancos, 2002; 2004]. This can be altered by increased levels of ACh and NA (from brainstem and basal forebrain afferents) during arousal, when the postsynaptic depolarization they produce on TC neurons brings the depressed Lemniscal EPSPs close to firing threshold [Castro-Alamancos, 2002].

1.3.2.3 Corticothalamic afferents and synaptic transmission

The glutamatergic synapses of CT afferents target the distal parts of the dendritic processes of the TC neurons with a single release site [Liu *et al.*, 1995; Castro-Alamancos, 2004]. The corticothalamic EPSP is relatively small in amplitude and slower in kinetics compared to lemniscal input possibly due to a higher ratio of NMDA-, kainate- and mGlu- receptors to Lemniscal synapses [Miyata, 2007]. CT synapses also display strong synaptic facilitation. This corticothalamic LTP is input-specific, NMDA-receptor independent and reversible, and its induction is entirely presynaptic and Ca^{2+} dependent [Castro-Alamancos & Calcagnotto, 1999]. Neurotransmitter release probability rises greatly at frequencies above 5 Hz and, in contrast to lemniscal input ACh and NA depress the efficacy of CT synapses [Castro-Alamancos, 2004].

The thalamocortical network undergoes distinct functional changes between sleep and arousal. During sleep, cortex and thalamus are engaged in low frequency oscillations whereas in wakefullness they are engaged, for example, in α-rythms (8-13Hz) or high frequency gamma oscillations at 20-60 Hz or [Steriade *et al.*, 1996; Castro-Alamancos, 2004; Hughes *et al.*, 2004]. Synchronised fast oscillations (20-60 Hz) can appear spontaneously during activated states as well as over the depolarization phase of slow wave sleep oscillations in thalamocortical networks [Steriade *et al.*, 1996]. During sleep, there are three major types of oscillations present in the thalamus including the VB complex [Steriade, 1994; Marks, 1996; Hughes *et al.*, 2002; Zhu *et al.*, 2006]: Spindles (7-14 Hz) are generated in the thalamus and blocked by ACh; Delta oscillations (1-4 Hz) are generated by thalamic neuronal and CT afferent interplay and are suppressed with ACh and NA; Slow wave oscillations (<1 Hz) are generated in the cortex and thalamus and are also blocked by ACh and NA.

1.3.2.4 Pathological frequencies engaging thalamic circuits

Absence seizures (3-4Hz) and sleep spindles (7-14Hz) are hypothesized to engage the same pathways between cortex and thalamus including the VB complex [Pinault *et al.*, 1998; Blumenfeld & McCormick, 2000; Crunelli & Leresche, 2002; Meeren *et al.*, 2002; Pinaults *et al.*, 2006; Steriade, 2006]. In ferret brain slices, for example, single CT stimuli generated sleep spindles at 6-10 Hz in the thalamus whereas high frequency (600 Hz) burst resembling seizures lead to paroxysmal oscillations at 3-4Hz [Blumenfeld & McCormick, 2000]. On the other hand, CT oscillations at 5-9 Hz have shown to be more pro-epileptogenic compared to physiological 7-14 Hz sleep spindles in some epilepsy model types [Pinault *et al.*, 2006].

In addition, infraslow oscillations (0.02-0.2 Hz), which may involve inputs from subcortical structures, have been recorded from the cortex during sleep [Vanhatalo *et al.*, 2004]. These infraslow oscillations were strongly synchronised to faster activities as well as interictal epileptic events and K complexes [Vanhatalo *et al.*, 2004]. Interestingly, it has been shown that neurons and glia respond coherently to cortical stimuli and that they oscillate together during slow sleep oscillations and spike-and-wave seizures [Amzica & Steriade, 2000].

1.3.3 Developmental issues of the thalamus

During development, the topographic maps in the thalamus and cortex emerge sequentially from periphery to the cortex [Killackey *et al.*, 1995]. In rats the topographic order of afferents in the VB can be first detected in embryonic day 16 (E16) with more discrete partitioning occurring during birth (P0) [Killackey *et al.*, 1995]. The formation of the cortical pattern is complete by postnatal day 7 (P7) [Killackey *et al.*, 1995]. These early postnatal days are considered as a "critical period" during which vibrissal damage alters the cytoarchitectonic patterns, and the thalamic critical period ends about two days before that in the cortex (around P5) [Woolsey *et al.*, 1979; Arsenault & Zhang, 2006]. The development of corticothalamic projections occurs later: retrograde labelling is detected for the first time at birth, with a sudden increase in projections at P7 [Miller *et al.*, 1993].

The continuing developmental remodelling of the cells and synapses and proliferation of CT afferents in the VB nucleus occur most prominently during the first two postnatal weeks, being completely formed by the end of third week [Ivy & Killackey, 1981; Matthews *et al.*, 1977; Arsenault & Zhang, 2006; Mooney & Miller, 2007]. Developmental remodelling also includes death of the postmigratory neurons and selective elimination and reinforcement of synaptic connections [Katz & Shatz, 1996; Mooney & Miller, 2007]. Neuronal number decreases during the first postnatal week but increases 2-fold over the next 3 weeks [Mooney & Miller, 2007]. This postnatal nonhierarchical neurogenesis is intrathalamic and matches changes in neuromodulatory systems and the arrival of corticothalamic afferents [Mooney & Miller, 2007]. The total volume of the VB increases 10-fold during the first postnatal month whilst the neuronal density decreases [Mooney & Miller, 2007].

Extensive refinement of the sensory (lemniscal) synapses occurs during the second postnatal week. During the first 2 weeks, VPm neurons receive sensory inputs from many axons and reach the adult state at P16 when most neurons show all-or-none responses suggesting they receive input from a single axon [Arsenault & Zhang, 2006]. Increase in AMPA and decrease in NMDA components as well as replacement of synaptic NR2B with NR2A subunits occurs during this time period [Arsenault & Zhang, 2006]. The maximal rate of synaptogenesis appears at second PN week. At P7 VB contains only a moderate number of synaptic complexes [Matthews *et al.*, 1977]. Several fundamental changes appear by P12 and evident mature synaptic glomeruli can be seen at P15 [Matthews *et al.*, 1977].

The electrophysiological membrane properties of rat TC neurons have been shown to reach mature characteristics after P12 when the spike bursts riding on the low threshold calcium spikes appear, consistent with the emergence of synchronised thalamocortical oscillations [Mares *et al.*, 1982; Velazquez & Carlen, 1996]. The resting membrane potential becomes more negative during maturation (-60mV at P13-50) whilst input resistance decreases (~300MΩ at P6-11 and 150MΩ at P13-50) [Velazquez & Carlen, 1996].

1.4. The aims of the project

This study examines relationships between astrocytes, neurons and synaptic stimulation in the rodent VB thalamus and whether this signalling is related to postsynaptic modulation and outputs from the thalamus. A particular aim is to find factors that increase this type of signalling.

Acutely prepared brain slices containing the VB thalamus are used to model the phenomena for several reasons: Firstly, acute slice preparations preserve intact anatomical relations. Secondly, it is known that spontaneous astrocyte-neuron signalling occurs here [Parri *et al.*, 2001; Parri & Crunelli, 2003] and the astrocytic calcium signals can be evoked by synaptic stimulation [Parri, unpublished data]. Thirdly, this brain area has an interesting functional role since it relays sensory information from the periphery to the cortex and is also involved in the regulation of sleep and awakening allowing us to relate possible neuron-astrocyte-neuron signalling to functional roles of the thalamus. We will use standard methods as described in the literature to study astrocyte-neuron signalling. Therefore, fluorescence imaging approaches will be used to study the astrocytic Ca^{2+} responses, and electrophysiological voltage clamp recordings will be used to investigate the properties of the type of activity that can lead to an increase in astrocyte mediated SICs recorded from the TC neurons. Pharmacological studies will be used to support the experiments and provide additional information on which receptors and neuroactive substances are involved. Figure 1.6 illustrates a simplified model for the working hypothesis.

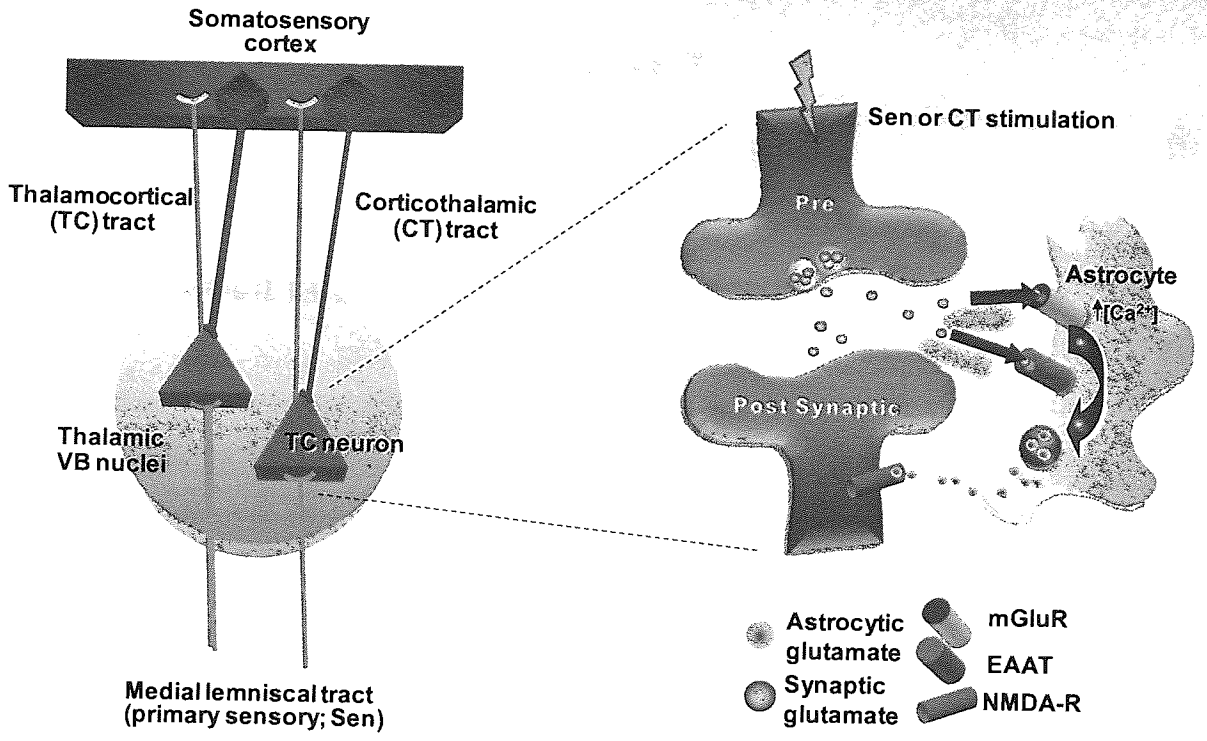

Figure 1.6: Schematic of the working hypothesis. In the VB thalamus, astrocytes exhibit spontaneous $[Ca^{2+}]_i$ signalling which leads to glutamate release and subsequent NMDA-receptor mediated SICs recorded from the TC neurons. Thalamic astrocytes also respond to a synaptic stimulation by elevating their $[Ca^{2+}]_i$. Therefore, we propose that in response to a stimulation of the Corticothalamic and/or Sensory afferents, astrocytes respond with $[Ca^{2+}]_i$ rises via mGluRs that lead to glutamate release and feedforward signalling onto TC neurons manifesting as SICs. We propose that the functional link between synaptic input and astrocytic output is dependent on the type of stimulation such as stimulus frequency or duration of the activity.

Chapter 2

Materials and Methods

2.1 Preparation and maintenance of brain slices

Experimental animals and ethics. Animals used for this study were male Wistar rats aged between 6 and 23 post-natal (PN) days. Care was taken in planning the experiments to minimize the number of animals needed. All procedures were in accordance of UK Home Office legislation and Animals (scientific procedure) Act 1986. Animals were placed in the inhalation incubator and deeply anaesthetized with isoflurance (Fig. 2.1). Loss of pain reflex was tested by tail- and toe- pinch test. Animals were killed by a Schedule 1 method in accordance with the Animals (scientific procedure) Act 1986. This was either cervical dislocation of the neck or overdose of anaesthetics. Complete cessation of blood circulation and respiratory function was checked before decapitation and removal of the brain.

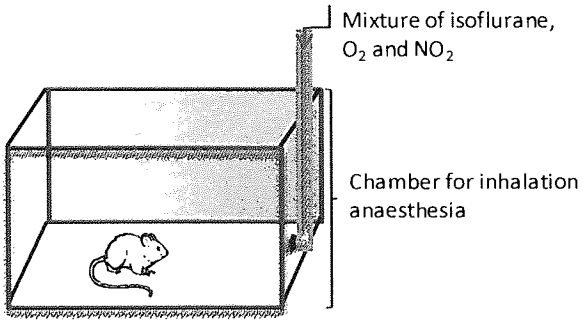

Figure 2.1: Anesthesia incubator.

Preparation of acute brain slices. Acute brain slice preparations [Edwards *et al.*, 1989] were used for this study. After decapitation the brain was rapidly (<60s) removed and placed in ice-cold **artificial cerebrospinal fluid (aCSF)** for cutting and storage, consisting of **(in mM): 126 NaCl, 26 $NaHCO_3$, 1 KCl, 1,25 KH_2PO_4, 5 $MgSO_4$,1 $CaCl_2$, 10 Glucose, 5 pyruvate, 0.3 ascorbic acid and 0.045 indomethacin**. Final osmolarity of the cutting/storage aCSF was approximately 305 mOsm and pH 7.3-7.4. The solution was oxygenated with a mixture of 95% O_2 / 5% CO_2. Slices were prepared using DTK-1000 Microslicer (Dosaka, Japan) or HM 650 V Vibration Microtome (Microm International GmbH, Germany). Within couple of minutes post decapitation, the brain was fixed to the slicing stage with cyanoacrylate adhesive and placed into the slicing chamber containing the same aCSF solution as described above. Solution was

maintained at +3° Celsius and continuously bubbled with 95% O_2 / 5% CO_2. When the region of interest was reached, the speed of cutting was adjusted to ≤0.5mm/sec, frequency to 90 Hz and amplitude to 0.8mm. 300-350 μm thick slices of the VB thalamus containing sensory and corticothalamic inputs were prepared in horizontal plane [Castro-Alamancos, 2002] as shown in figure 2.2. Brain slices were moved onto petri dish containing same ice-cold cutting solution, and smaller sections (mini-slices) containing the VB and afferents were dissected out. The isolation and cutting of the brain slices was carried out within 30 minutes.

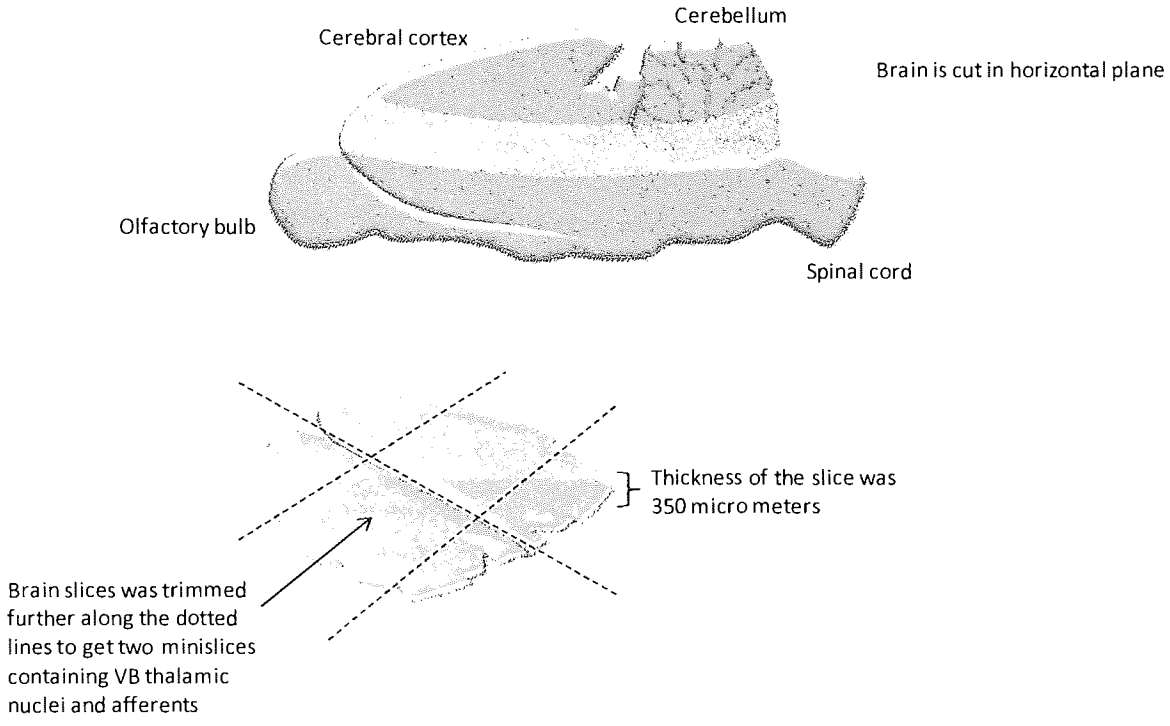

Figure 2.2: Brain tissue slicing. Top picture illustrates the brain and orientation for cutting. Slices were cut in horizontal plane and trimmed from the top to bottom to reach the area of interest. Slice below shows the preparation of mini-slices containing the VB thalamus in the middle.

Maintenance of brain slices. Immediately after dissection, slices were transferred into a storage chamber and kept in submerged conditions at room temperature (~25°C) for up to 8 hours (Fig. 2.3). Storage aCSF had the same composition as cutting aCSF excluding indomethacin, and was continuously bubbled with 95% O_2 / 5% CO_2. The bubbler was placed so that it was not causing movement for the slices resting on a mesh but was sufficient to keep the aCSF oxygenated and circulating. Figure 2.4 shows DIC images of slice preparations.

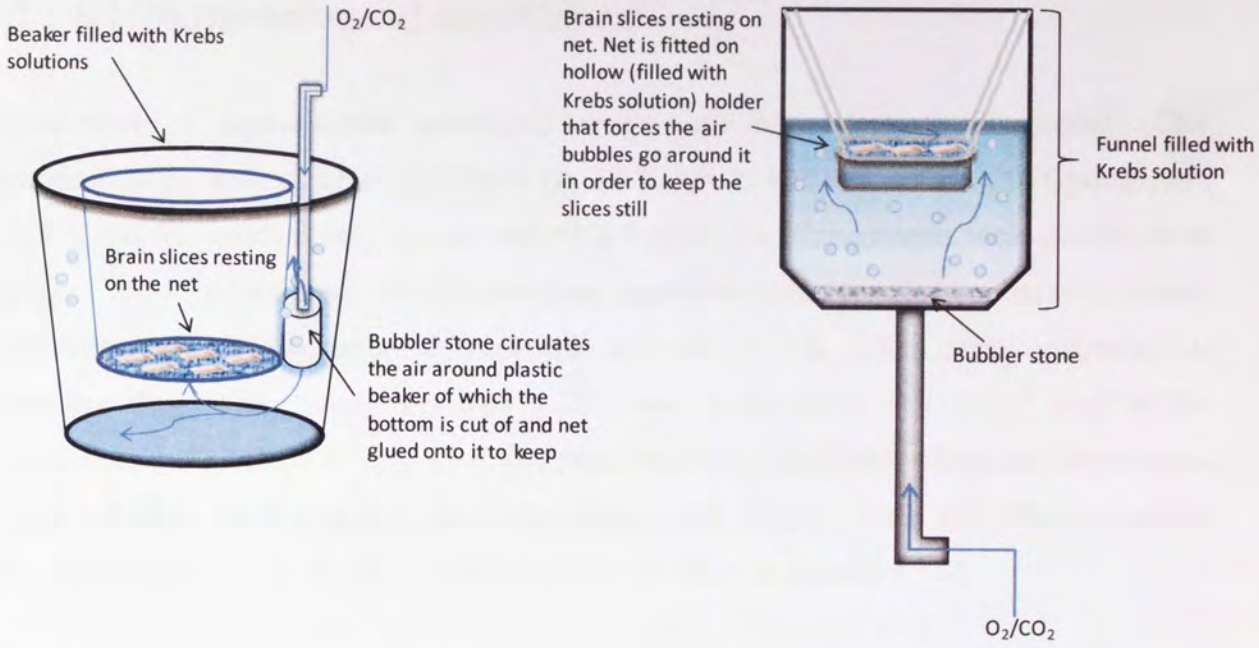

Figure 2.3: Storage of slices. Two different storage models were used with different volumes (Beaker ~200ml/Buchner Flask ~500ml). Beaker was used for the pre-incubation experiments.

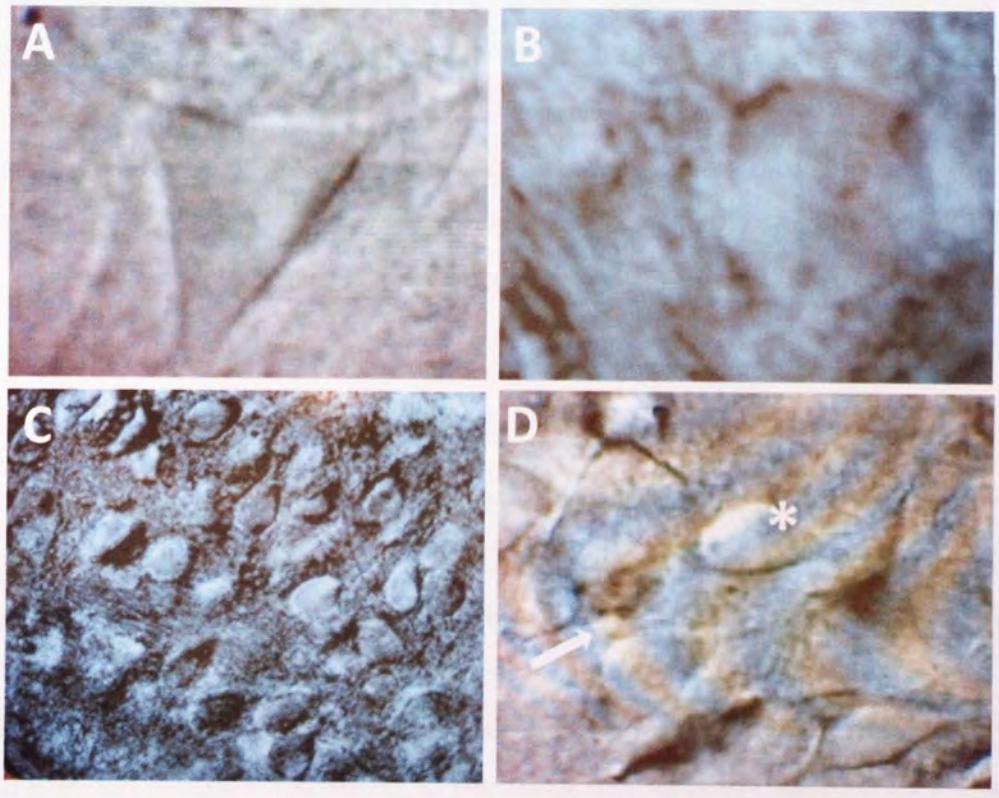

Figure 2.4: DIC images of TC neurons. (A) Healthy TC neuron of 2 weeks old animal is smooth with clear outline. **(B)** Dead TC neuron with round swollen cell body and visible nuclei. **(C)** Lots of healthy TC neurons in a slice of post-natal week 1 animal. **(D)** Healthy TC neurons (*) from post-natal week 2 animal. Smaller cells are probably glia (→).

2.2 Electrophysiological experiments

Preparation of experimental solutions, drugs and bio-chemicals. Recording aCSF comprised of **(in mM): 126 NaCl, 26 $NaHCO_3$, 2.5 KCl, 1.25 KH_2PO_4, 2 $CaCl_2$, 10 Glucose (and 1 Mg^{2+})**, and was continuously gassed with 95% O_2/5% CO_2. Experiments were performed in Mg-free aCSF to enhance NMDA-receptor mediated events unless otherwise stated. Osmolarity was approximately 300 mOsm and pH 7.3-7.4. When small quantities of expensive drugs were used, recording aCSF was re-circulated. All drugs used in the experiments were diluted at least 1000-fold from stocks and applied by drug delivery system. Stocks solutions were prepared when appropriate with distilled water (dH_2O) or dimethyl sulfoxide (DMSO)[7]. All drugs used for the thesis are listed in appendix 1.

Electrophysiological recordings and patch clamp set-up. The method used in these experiments was the "whole-cell" patch clamp configuration in voltage clamp mode [Hamill *et al.*, 1981]. The establishment of whole cell recording and the basic patch clamp circuitry are summarised in figure 2.5. The set-up consisted of the basic electrophysiological devices required for visualised patch clamping (Fig. 2.6). Slices were viewed with an upright microscope (Olympus, UK) equipped with water immersion lens of x40 magnification, attached to charge-coupled device (CCD) camera (Olympus U-CMAD-2, Japan) for differential interface contrast (DIC) image. The microscope and a movable top plate platform (MP MTP-01, Scientifica, UK) were mounted on the air-table (Melles Griot, UK). The recording chamber and micromanipulators (PatchStar, Scientifica, UK) were mounted on the platform.

Slices were allowed to recover for at least 1 hour prior to experimenting. In the recording chamber, slices were kept in submerged conditions and continuously perfused with recording aCSF at +32°C or at room temperature (+25°C) with flow rate of 2-3 ml/min (Fig. 2.7). Low resistance (3-5MΩ) patch microelectrodes using borosilicate GC120F-10 glass micropipettes (1.2mm O.D. x 0.69 I.D, Harvard apparatus Ltd, UK), were pulled with a P-97 Flaming/Brown micropipette puller (Sutter instrument Co, Novato, CA). The electrodes were filled with **internal solution consisting of (in mM): 120 $KMeSO_4$, HEPES 10, 4 Na_2ATP, 0.5 GTP and 0.1 EGTA.** Internal solution pH was adjusted to 7.3 with KOH. Osmolarity was adjusted with KCl if necessary and aimed approximately 10-20 mOsm below recording aCSF

[7] DMSO is a polar aprotic and miscible solvent that means it mixes in all proportions forming homogenous solutions

osmolarity. The current signal was sampled at 10 kHz (interval 100 µs) with analog-to-digital-converter Digidata 1200/1440A interface (Axon Instruments, Union City, CA) and filtered at 1 kHz (low-pass Bessel 80dB)[8] with Axopatch-200B amplifier (Molecular Devices, Sunnyvale, CA) or computer controlled MultiClamp 700A (Molecular Devices). Amplifier output gain was set to x20 for the optimal detection of SICs and adjusted if required. Data were acquired and viewed online using computer software PClamp 9.2 (Molecular Devices) for Axopatch-200B amplifier or Axoscope 10.0 (Molecular Devices) for MultiClamp 700A amplifier. Resting membrane potential (*RMP*) and ability to fire action potentials was assessed soon after establishing the whole cell configuration, and cells were then clamped at -60mV. Membrane potential (V_m), series resistance (R_S), input resistance (R_I) and holding current (I_h) were monitored throughout the experiments. If *Vm* was more positive than -40mV, $R_S > 20M\Omega$ or $I_h > -200pA$, cells were discarded.

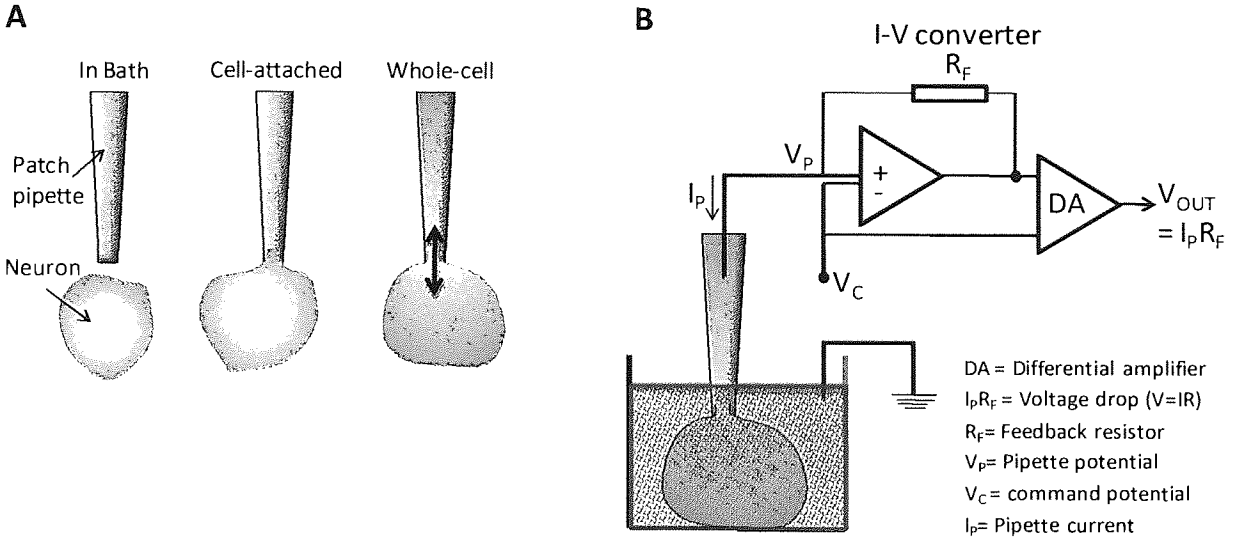

Figure 2.5: Whole cell patch clamp. A) Applying negative pressure to the patch pipette leads to "cell-attached" configuration and formation of giga-seal (resistance ≥1GΩ) between the patch pipette and cell membrane. Sharp suction ruptures the membrane at the patch leading to low resistance "whole-cell" configuration. Cell cytoplasm content is exchanged with the pipette solution within a few minutes. **B)** Basic circuitry consists of current-to-voltage converter with feedback resistor and differential amplifier. Pipette attached to the headstage functions as sensor of the original signal source. If the cell is clamped at desired potential, I-V converter forces the pipette potential to follow command potential. The recorded pipette current flows through the feedback resistor producing a voltage drop that is a sum of command potential and voltage drop. DA subtracts the command potential giving an output signal of $V_{OUT}=I_P R_F$. After signal conditioning by amplifier, the signal can be read by the digitizer that converts the analog voltage signal to a digital signal for the computer processing (Figure modified from Safronov & Vogel, 1999).

[8] Low-pass Bessel filter attenuates frequencies above the cut-off frequency

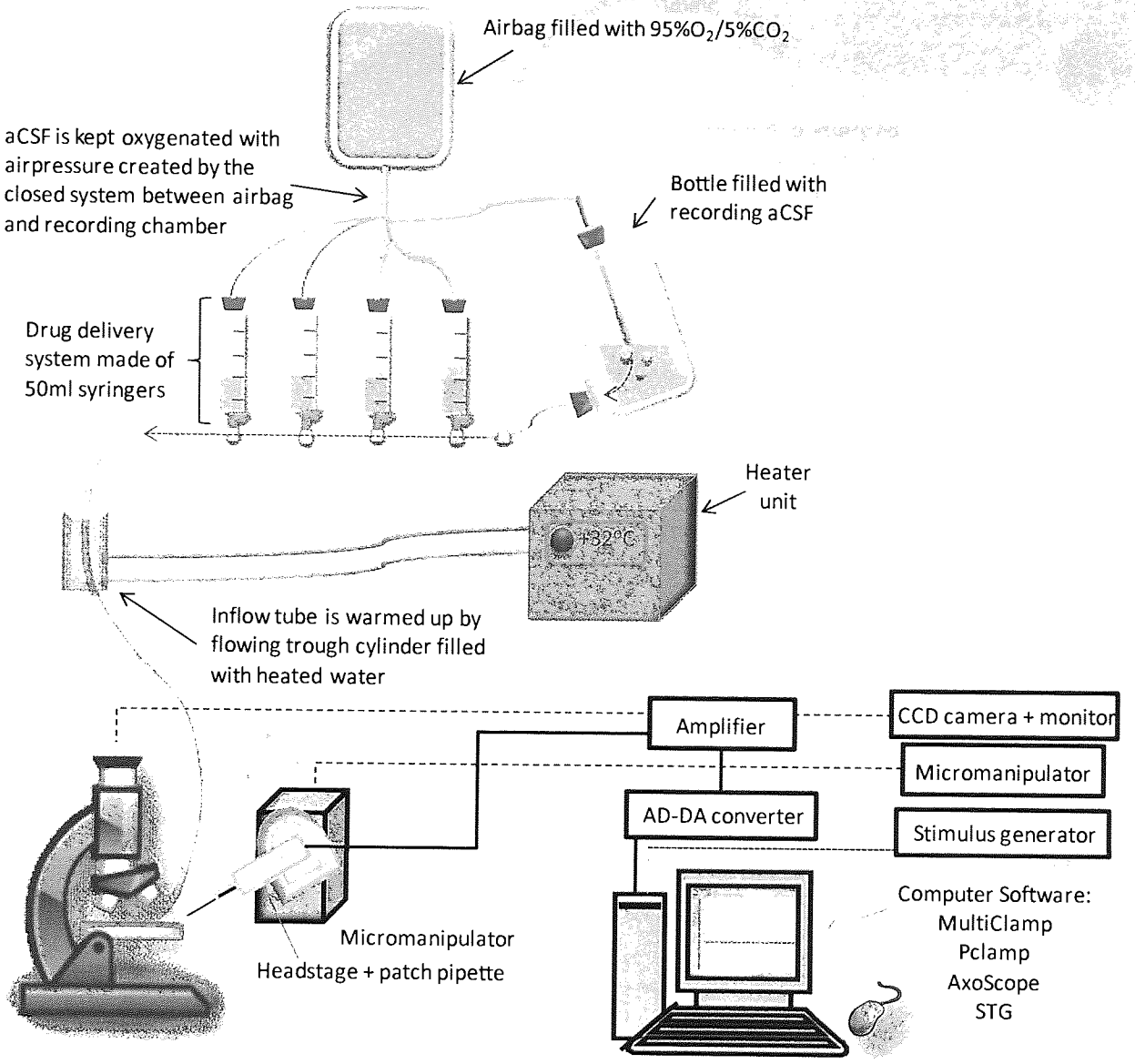

Figure 2.6: Patch-clamp set-up. Perfusion for the set-up consisted of closed circuit system where oxygenation is maintained by pressure from the air-bag filled with $95\%O_2/5\%CO_2$. The aCSF flows to the recording chamber by gravity and is heated by circulating through cylinder filled with hot water. Drugs were delivered to the recording chamber from syringes. The recording parts for the set-up include amplifier that is connected to the headstage and patch pipette, and analog-to-digital (AD-DA) converter (digitizer) combined with computer software to acquire and control data. Additional hardware for the set-up included separate stimulation generator, motorised micromanipulators, CCD camera and a monitor.

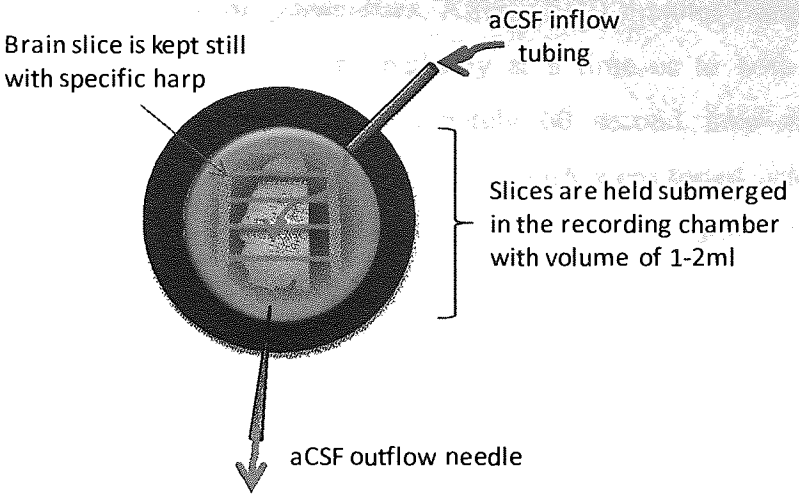

Figure 2.7: Submerged recording chamber. The flow through the recording chamber was approximately 2-3ml/min and the slices were stabilised with specific harp-shaped weight made of platinum wire and nylon strings.

2.3 Synaptic stimulation protocols

Bi-polar stimulating electrodes (Harvard apparatus) were placed on the primary sensory and corticothalamic afferents and responses were recorded from the TC neurons (Fig. 2.8). Computer controlled 2-channel stimulus generator STG1002 (Multichannel systems, Germany) or Master-8 (Intracell, UK) was used to program different constant current stimulation protocols.

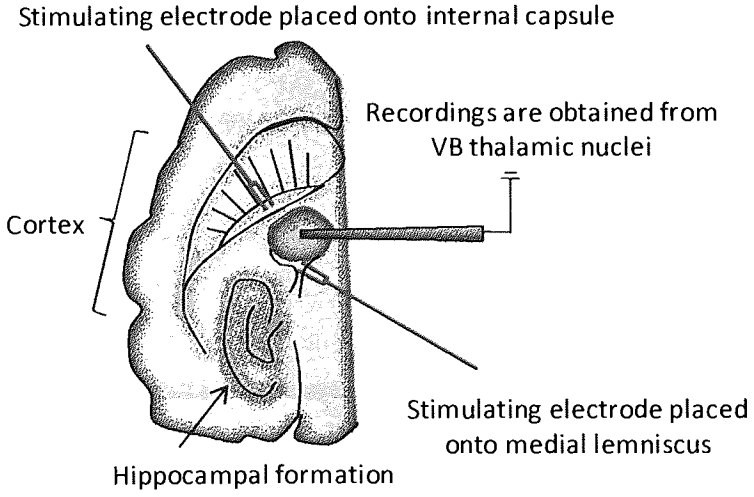

Figure 2.8: Orientation of the VB thalamus and electrodes. Figure illustrates schematic of horizontal slice preparation showing one hemisphere containing the VB thalamic nucleus, which was clearly visible in the slice as darker opal area. Stimulating electrodes were places as indicated in the figure, onto medial lemniscus to stimulate sensory afferents and onto internal capsule to stimulate corticothalamic fibers. Recordings were aimed to obtain from the middle of the VB nuclei.

Protocols for different stimulation parameters. After a 5-10 minutes baseline recording, a stimulation protocol was delivered to one pathway at a time or to both simultaneously. Stimulus episodes were separated by approximately 60 second inter-stimulus-intervals. Different stimulus amplitudes ranging from 0.1mA to 3mA were tested using trains of 2ms pulses for 1 second at 50 Hz in randomised order. Different stimulus durations ranging between 2ms and 10s were tested at 50Hz by changing the number of pulses within the train (using sub-maximal stimulus amplitude determined from the evoked EPSC, I_{75}). Different frequencies were tested by generating trains of pulses at frequencies between 1Hz and 500Hz using constant number of stimuli with I_{75} stimulus amplitudes. Figure 2.9 illustrates how the frequency and duration protocols were composed. If R_S and I_{hold} were stable, subsequent protocols or their combinations were applied.

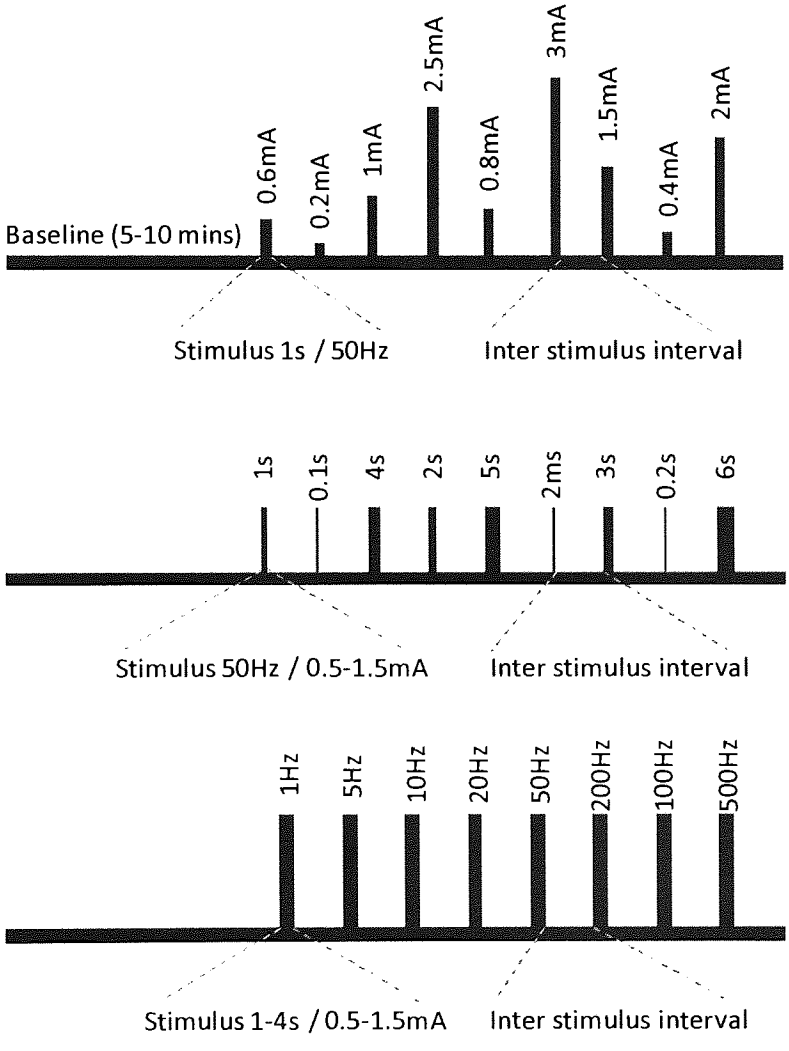

Figure 2.9: Stimulation protocols for different frequencies and durations. (Top) Protocol for different stimulus intensities ranging from 0.2mA to 3mA. **(Mid)** Protocol for different stimulus durations. Duration was altered by increasing/decreasing the number of pulses within the stimulus. **(Bottom)** Protocol for different stimulus frequencies. Number of pulses was kept constant (50 pulses) and the pulse interval was changed.

Long term stimulation protocol A and B. Long term stimulation (LTS) experiments consisted of at least 30 minutes long continuous stimulation burst episodes. Each episode consisted of 10/20 pulses at 50 Hz repeated every 5-10s with approximate I_{75} stimulus intensity. Two protocols were applied: **A)** Sen and CT were stimulated separately whilst recording neuronal activity (Fig. 2.10A), or **B)** both afferents were stimulated simultaneously and neuronal activity was recorded after ceasing the stimulation (Fig. 2.10B). A stimulus was delivered onto each afferent separately prior to spontaneous recording to check the presence of synaptic inputs. Control slices were exposed to the same conditions in the absence of stimulation for 60 minutes prior to recording.

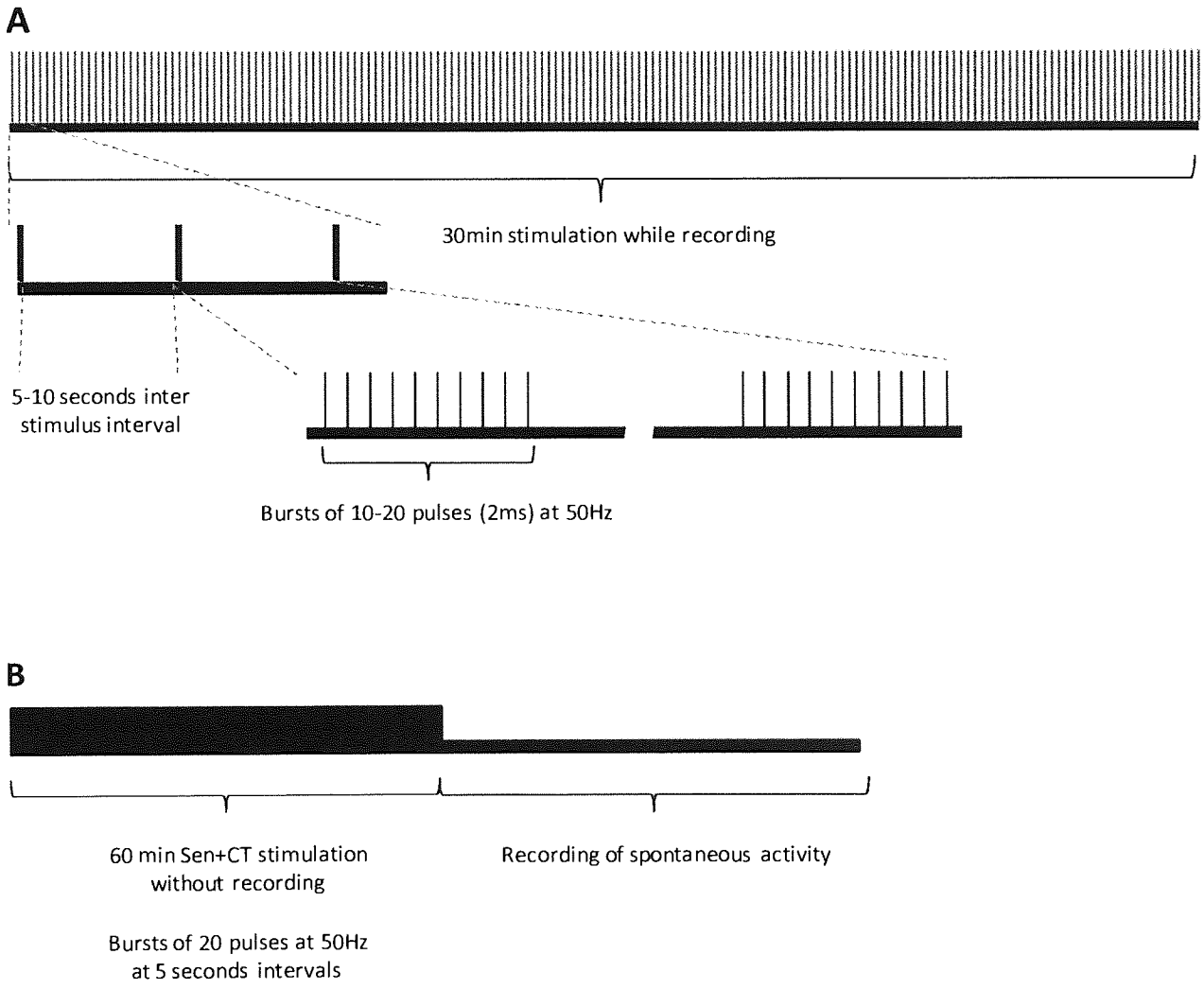

Figure 2.10: Long Term Stimulation protocols. (A) Protocol for long term stimulation (LTS) of either Sensory or CT afferents while recording neuronal activity and SIC incidence. **(B)** LTS protocol of Sen and CT afferents stimulation for 60 minutes prior to patching a cell.

Sleep spindle protocol. A single "spindle stimulation pattern" (SSP) described by Rosanova & Ulrich [2005] consisted of 22 spikes in duration of 728ms (Fig. 2.11). Mean spike rate was 30 Hz, grouped to initial 10 Hz bursts followed by tail of decreasing tonic frequency. In some experiments the SSP was repeated 30 times every 0.6 Hz to mimic the grouping of spindles by the slow (0.6-0.8 Hz) oscillation [Rosanova & Ulrich, 2005].

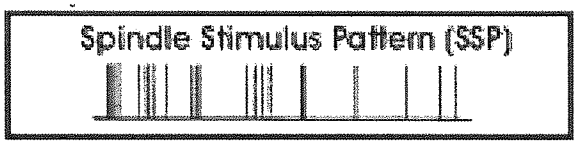

Figure 2.11: SSP protocol. (Figure from Rosanova & Ulrich, 2005).

2.4 Electrophysiological data analysis

Slow Inward Currents. Clampfit 9.2 software (pClamp 9.2, Molecular Devices) Event Detection function was used for SIC analysis. Data were filtered off-line using Notch[9] (Center frequency at 50 Hz and / -3dB width at 10 Hz) and Low-pass Bessel 8-pole (-3dB cut-off at 100 Hz) filtering. Threshold search function settings for SICs were as follows: Trigger at -20pA, re-arm at -10pA, min allowed duration 50ms and noise rejection 10ms). For this project, **inward currents with ≥20ms rise time measured according to the set threshold criterions and amplitude >20pA were accepted as SICs.** SICs with <20ms rise time were accepted in cases where the total duration of the inward current exceeded >100ms. Figure 2.12 illustrates the measurements used for SIC characterisation. Data were transferred into SigmaPlot 9.0 (Systat Software Inc. USA) or Office Excel 2007 (Microsoft, USA) for further analytical evaluations. Frequency or incidence was normalised to number of SICs per 60 seconds. Cells with ≥1 SICs during a minimum of 10 minutes recording time were counted as "cells with SICs".

Evoked neuronal post-synaptic currents. Evoked excitatory PSC (eEPSC) amplitude was measured from the peak in respect to baseline level (Clampfit 9.2/AxoScope 10.0). Rise time was taken from the onset of stimulus to the peak amplitude. Area of the eEPSC was measured by using the Statistics function (Clampfit) and converted into charge (Q) and expressed as milli-coulombs (mC).

[9] Notch filter passes through all other frequencies expect those centred on a centre frequency.

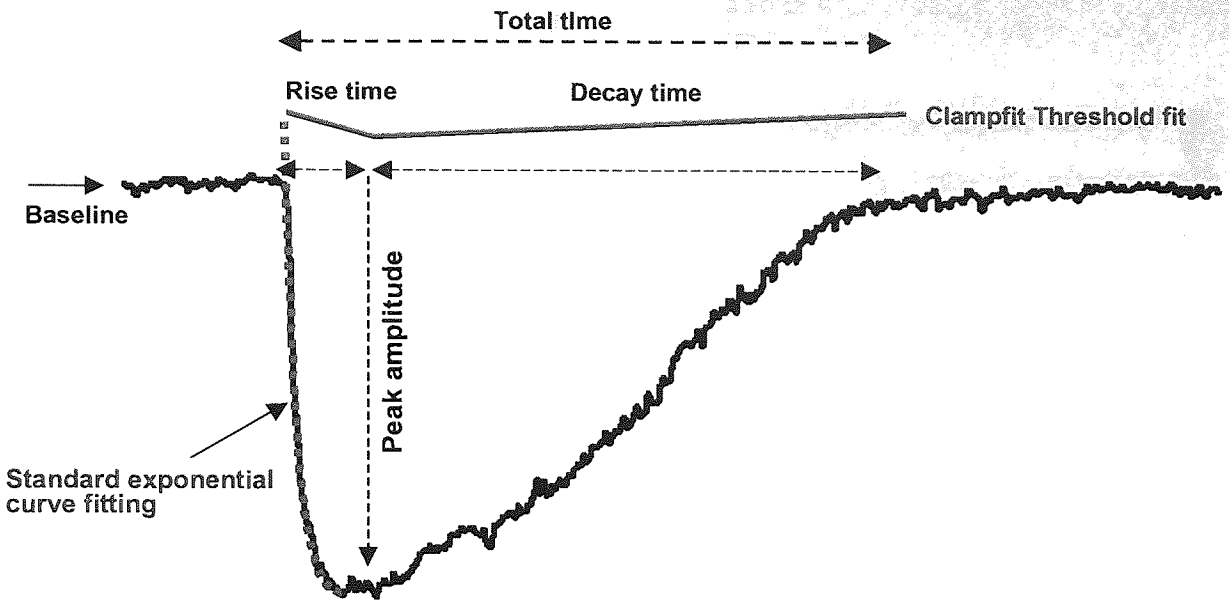

Figure 2.12: Acceptance criterion for SICs. Peak amplitude over 20pA, rise time (time to peak) over 20ms and total duration (total time from peak to anti-peak) of the current over 100ms were set as criterion for acceptance as SICs.

Data presentation. Numerical data is presented as mean ± S.E.M unless otherwise stated. Data were normalised to 100% of control when appropriate. Regression (r^2) line was used to describe the scatter of data correlation. Box plot[10] was used to compare the spread and symmetry of variables and population distribution was assessed using cumulative probability graphs when appropriate.

Statistical analysis. For looking at changes in the data, paired or unpaired Student's *t*-test (SigmaPlot), and Mann-Whitney test (Clampfit) were used as appropriate. Student's one-tail *t*-test (Excel) was used to assess changes in a particular direction. Kolmogorov-Smirnoff (Clampfit) test was used when appropriate for testing significance in population distribution. Pearson's correlation coefficient was used to test whether r^2 value was significantly correlated (Clampfit). The statistical significance in figures is presented as $p<0.05$ *, $p<0.01$ ** or $p<0.005$ ***.

[10] Box plot is used to summarise following statistical measures: median (line in the box), upper and lower quartiles (the box contains the middle 50% of the data, upper hinge indicates the 75 and lower hinge the 25 percentaile of the data). Box plot also shows the minimum and maximum data values (ends of the vertical lines) unless outliers are present (points outside the ends of the vertical lines)

2.5 Calcium imaging experiments

The calcium sensitive dye Fluo4-AM[11] (Molecular Probes, Eugene, Or., USA) was used to detect changes in the $[Ca^{2+}]_i$ levels by measuring the fluorescence intensity, whereas the astrocyte-specific fluorescent dye Sulforhodamine (SR101) was used to identify astrocytes [Nimmerjahn *et al.*, 2004; Kafitz *et al.*, 2008]. The principle of fluorescence imaging and the characteristic spectra for excitation and emission wavelengths for Fluor4 and SR101 are shown in figure 2.13.

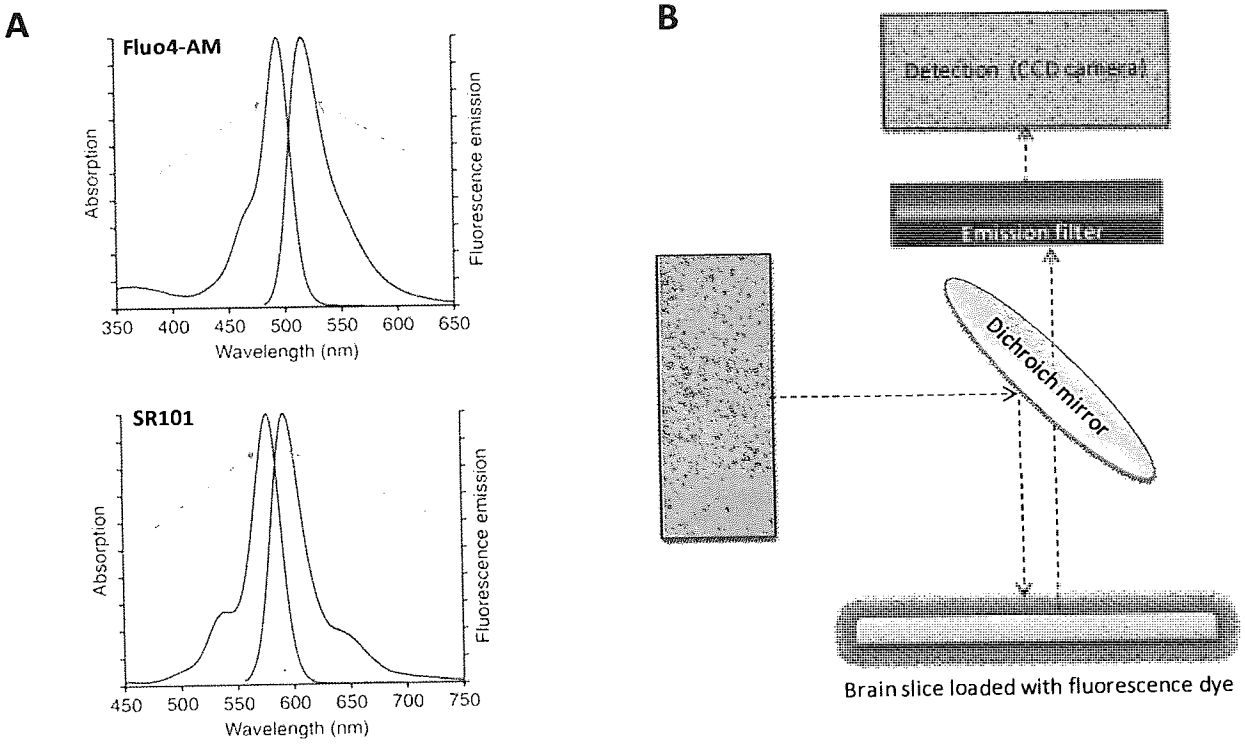

Figure 2.13: Fluorescence imaging method. A) Diagrams showing the characteristic excitation and emission wavelengths for Fluo4 (top) and SR101 (bottom). (Images are from www.invitrogen.com). **B)** Schematic of the main components for fluorescence detection in our system. A monchromator is the source for the light. The dichroic mirror (filter) splits the light on the basis of wavelength. For Fluo4, wavelengths below 510 are reflected on the sample to excite the fluorescence dye. Emitted light with wavelength above 510 is transmitted through the dichroich mirror. The emission filter is an optical filter that transmits specific wavelengths and eliminates background noise and focuses that to the photosensitive array of the CCD camera.

[11] Acetoxymethyl ester (-AM) attached to the dye aids loading as it is cell permeable but becomes trapped inside the cell due to cleavage by intracellular esterase

Dye loading. Slices were prepared as described earlier and allowed to recover for at least 30 minutes in storage chamber. 0.001% Pluronic acid and SR101 (final conc. 1μM) were mixed with cutting/storage aCSF. Fluo-4 was first dissolved in DMSO and then added to the solution containing aCSF/pluronic acid/SR101. Final Fluo-4 concentration was 10 μM. Three slices at a time were transferred to the dye containing beaker that was kept in a heated water bath at +32°C for at least one hour (Fig. 2.14). For the last 20 minutes heat was increased to +37°C to assist SR101 loading.

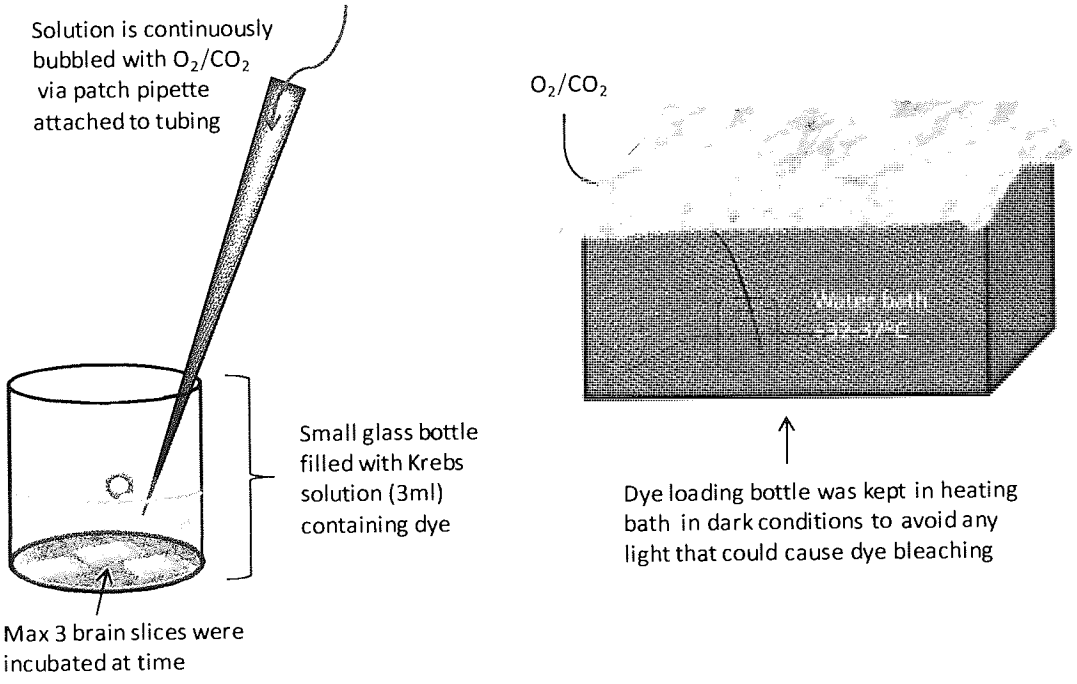

Figure 2.14: Dye loading. Slices were loaded in small volume of aCSF mixed with Fluo4, SR101 and Pluronic acid. Dye container was kept in dark water bath at +32°C for at least one hour prior to imaging.

Imaging set-up. The imaging part of the set-up consisted of an upright Nikon FN1 microscope (Japan) fitted with specific filter cubes (Chroma VT, USA) for Fluo4 and SR101 dyes (Molecular Probes), water immersion lens (NA=0.8) with x20 magnification, Optoscan monochromator (Cairn, UK), Ocra CCD camera (Hamamatsu, Japan) and computer controlled acquisition software Simple PCI (Compix, Cranberry Township, PA) as illustrated in figure 2.15. The microscope (Hamamatsu) and remotely movable bridge (Luigs and Neumann, Germany) were mounted on an air-table (TMC, USA). Submerged recording chamber and micromanipulators (Luigs and Neumann) were mounted on the bridge. The aCSF was continuously bubbled with 95%O_2/5%CO_2, and the inflow and outflow was adjusted and controlled by peristaltic pump (Watson-Marlow Bredel, UK).

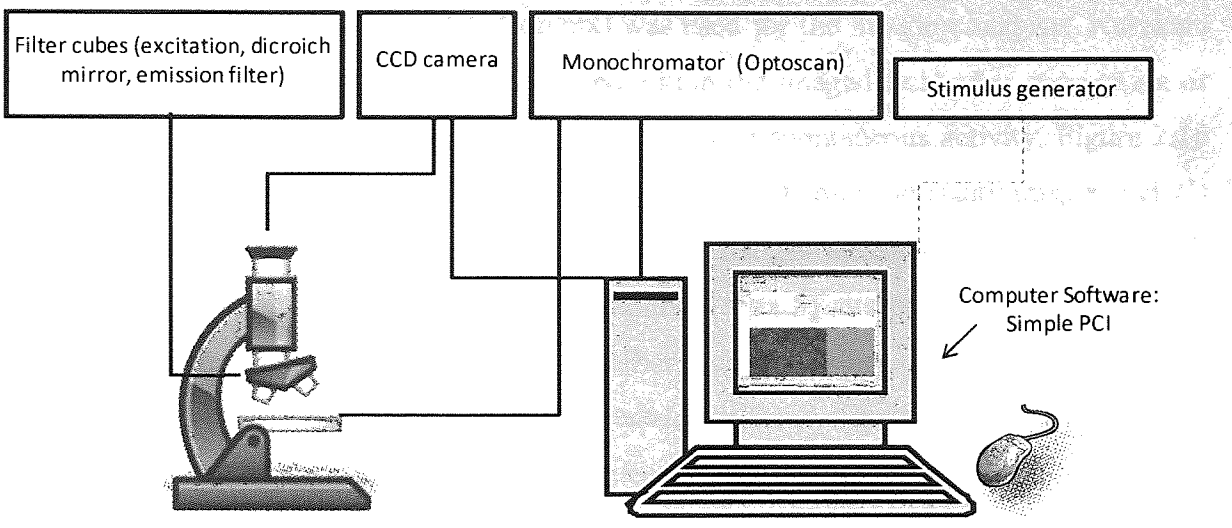

Figure 2.15: Generalized scheme for imaging set-up. The imaging part consisted of microscope fitted with CCD camera for data acquisition, filter cubes for Fluo4 and SR101 fluorescence, monochromator to excite the fluorescence dyes and computer software for controlling the data acquisition. Other parts of the set-up (not shown in figure) consisted of the same basic elements that are used for patch clamping from acute brain slices.

Fluorescence imaging. All imaging experiments were performed in aCSF containing Mg^{2+} (1mM). Slices were imaged just below the surface from the image field size of 444μm x 341μm. Fluo4 dye was excited at wavelengths within 460-490nm using the Optoscan monochromator. Images were acquired for a duration of 0.05-0.1s every 5s (spontaneous recording) or 2s (short stimulation protocol) using Orca CCD camera (Hamamatsu). Acquisition was controlled by Simple PCI software (Compix). For optimal image quality, black level was aimed to keep ~255 and gain adjusted to lowest possible. SR101 imaging was acquired by changing the focal plane in small steps up or down the slice at each 5s frame length giving overall image in depth of the astrocytes. SR101 dye was excited at wavelength range 560-570 nm.

Experimental protocols. Spontaneous Ca^{2+} signals were recorded for 15 minutes in presence of TTX (1μM). The short stimulation protocol consisted of trains of 2ms pulses for 1-2 second at 50 Hz delivered on Sen or CT. Responses were recorded for at least 1 minute post stimulation. For long term stimulation experiments, the same LTS protocol was used as described in Fig. 2.10B. After ceasing the stimulation, TTX (1μM) was bath applied and images were acquired for 15 minutes. Control slices were exposed to the same conditions in absence of stimulation for 60 minutes prior to imaging.

Analysis of Ca^{2+} signals. Simple PCI (Compix) was used for the imaging analysis. Numbers of cells with fluorescence changes were counted within the imaged field after stimulation or during the whole recording time for experiments assessing spontaneous activity. Figure 2.16 illustrates an example of fluorescence intensity changes in 3D colour intensity images and 2D graph of fluorescence changes over time. Fluorescence changes were accepted as Ca^{2+} signal-events if they returned back to baseline and amplitude was 5x the noise level. Simple PCI analysis was transferred into SigmaPlot for further analysis. When necessary, the relative intensity change ($\Delta F\%$) of the Ca^{2+} signal was used to quantify the increase in fluorescence and was calculated by dividing the fluorescence change by the basal x100%. Frequency was counted as number of Ca^{2+} rises per cell over 15 minutes normalised to mean number of Ca^{2+} peaks per 60s. In stimulation experiments, latency was measured from the onset of stimulus to the peak of the calcium response.

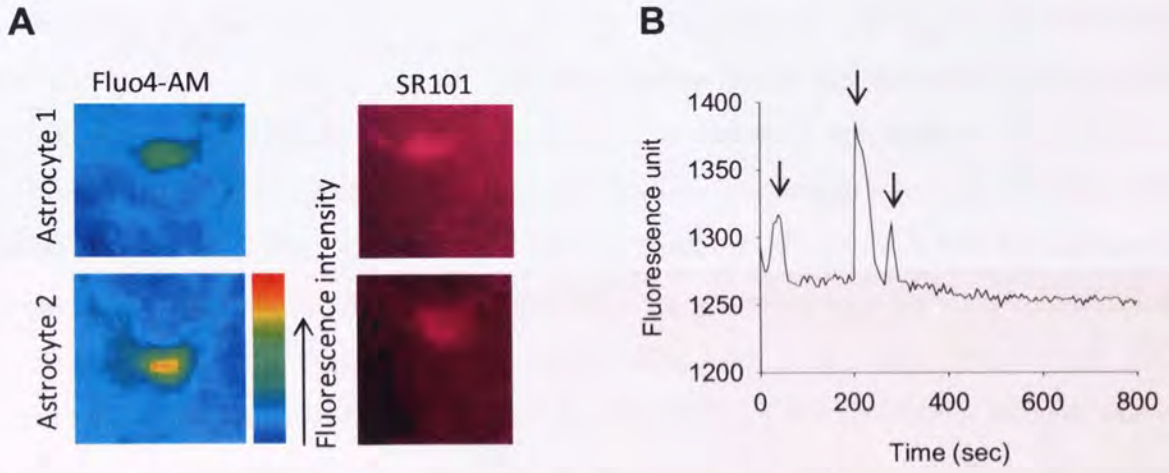

Figure 2.16: Calcium imaging analysis. A) Fluo-4 intensity changes were detected using the pseudocolour images (left). Color chart (middle) is indicative of the fluorescence intensity. The identity of astrocytes was detected by SR101 staining using Magenta images (right). **B)** Graph showing examples of accepted calcium intensity changes (indicated with arrows). The duration and magnitude of fluorescence unit varied and were accepted as events if 5x the noise level and returned back to baseline.

Data presentation and statistical analysis. Images for figures were reconstructed by averaging chosen frames. Correction for dye bleaching was considered when presenting data by subtracting the bleaching factor from the original trace. Bleaching factor was calculated using the Sigmaplottransform "*Col(Y)=Col(ΔF)+(Col(time) x bleach factor)*", where Y is the ΔF after bleach factor subtraction. Numerical data were expressed as mean ± S.E.M. Paired or unpaired Student's *t*-test was used for the statistical evaluations and the significance is presented as $p<0.05$ *, $p<0.01$ ** or $p<0.005$ ***.

Chapter 3

Spontaneous astrocyte to neuron communication in the Ventrobasal thalamus

We first characterised the properties of the spontaneous SICs and astrocytic $[Ca^{2+}]_i$ elevations in the Ventrobasal thalamus. Although SICs are known to occur at extremely low frequencies as well as to vary in amplitude and kinetics [Parri *et al.*, 2001; Angulo *et al.*, 2004; Fellin *et al.*, 2004; Perea & Araque, 2005; Fellin *et al.*, 2006; Xu *et al.*, 2007; Navarrete & Araque, 2008; Shigetomi *et al.*, 2008], extensive characterisations of their properties have not been published. Therefore, in order to understand any effects of synaptic stimulation on SIC prevalence and properties, it is helpful to assess the profile of spontaneous SIC activity.

As described in the introduction chapter, the VB thalamus undergoes developmental remodelling until the end of the 3rd post-natal week when the thalamus shows mature anatomical and physiological characteristics. Previous studies on spontaneous astrocytic Ca^{2+} signalling in the VB showed a developmental profile suggesting a role in the maturation process [Parri *et al.,* 2001]. However, the developmental profile of SICs was not assessed in that study. As many studies have shown that SICs are generated by a Ca^{2+} dependent release of glutamate from the astrocytes [Araque *et al.*, 2000; Parri *et al.*, 2001; Bezzi *et al.*, 2004; Fellin *et al.*, 2004; Perea & Araque, 2005; Xu *et al.*, 2007], it is of particular interest whether the decrease in spontaneous Ca^{2+} signalling is associated with a decrease in the spontaneous astrocyte to neuron communication.

3.1 SICs may be classified by their size and kinetics

In our experimental conditions, inward currents with peak amplitude over 20pA, rise time over 20ms and decay time over 100ms were accepted as SICs in agreement with the acceptance criteria in the field in general [Araque *et al.*, 1998; Angulo *et al.*, 2004; Fellin *et al.*, 2004]. Here, spontaneous excitatory currents that did not meet our acceptance criteria were observed occasionally. These currents resembled spontaneous and miniature thalamic EPSCs shown in two previous studies [Pfrieger *et al.*, 1992; Gil *et al.*, 1999], and were therefore quantified for comparison with SICs.

Figure 3.1A shows an example of a recording with an average frequency of 5.5 inward currents per minute (~0.1Hz). Of the total of 198 events, four were accepted as SICs (~0.002Hz). Mean amplitude of these SICs was 108.1±43pA compared to 37.8±1.1pA of the smaller currents considered as EPSCs. Mean rise and decay time for SICs was 48.7±9.5ms and 207.2±34.05ms respectively, whereas for EPSCs they were 10.4±0.4ms and 69.7±3.03ms. The mean values are listed in table 3.1. Box plots in figure 3.1B demonstrate the spread of amplitude, area, rise time and decay time between the currents accepted as SICs (n=211 events; 98 cells) and currents considered as EPSCs (n=211 events; 24 cells). As expected, all parameters for SICs were notably greater than those not meeting the criteria (Student's t-test $p<0.005$; all parameters). We chose the SIC acceptance criterion to exclude events that may not be SICs to avoid contamination of SIC analysis, and the distinct properties of these spontaneous EPSC-like events and putative SICs confirm the validity of my method.

	Amplitude (pA)		Rise time (ms)		Decay time (ms)		Area (pA*ms)	
	SIC	EPSC	SIC	EPSC	SIC	EPSC	SIC	EPSCs
Mean	98.40	39.86	176.56	10.6241	738.50	58.17	52390.49	1852.00
Median	64.73	35.89	67.00	11.1250	226.20	52.13	12401.38	1516.06
Std.Dev	95.52	14.17	397.54	4.0781	1760.31	30.63	135606.49	958.21
Std.Err	6.58	0.95	27.37	0.2920	121.18	2.06	9357.74	64.46

Table 3.1: SIC versus EPSCs. SICs were notably greater than EPSC-like currents ($p<0.005$, all parameters).

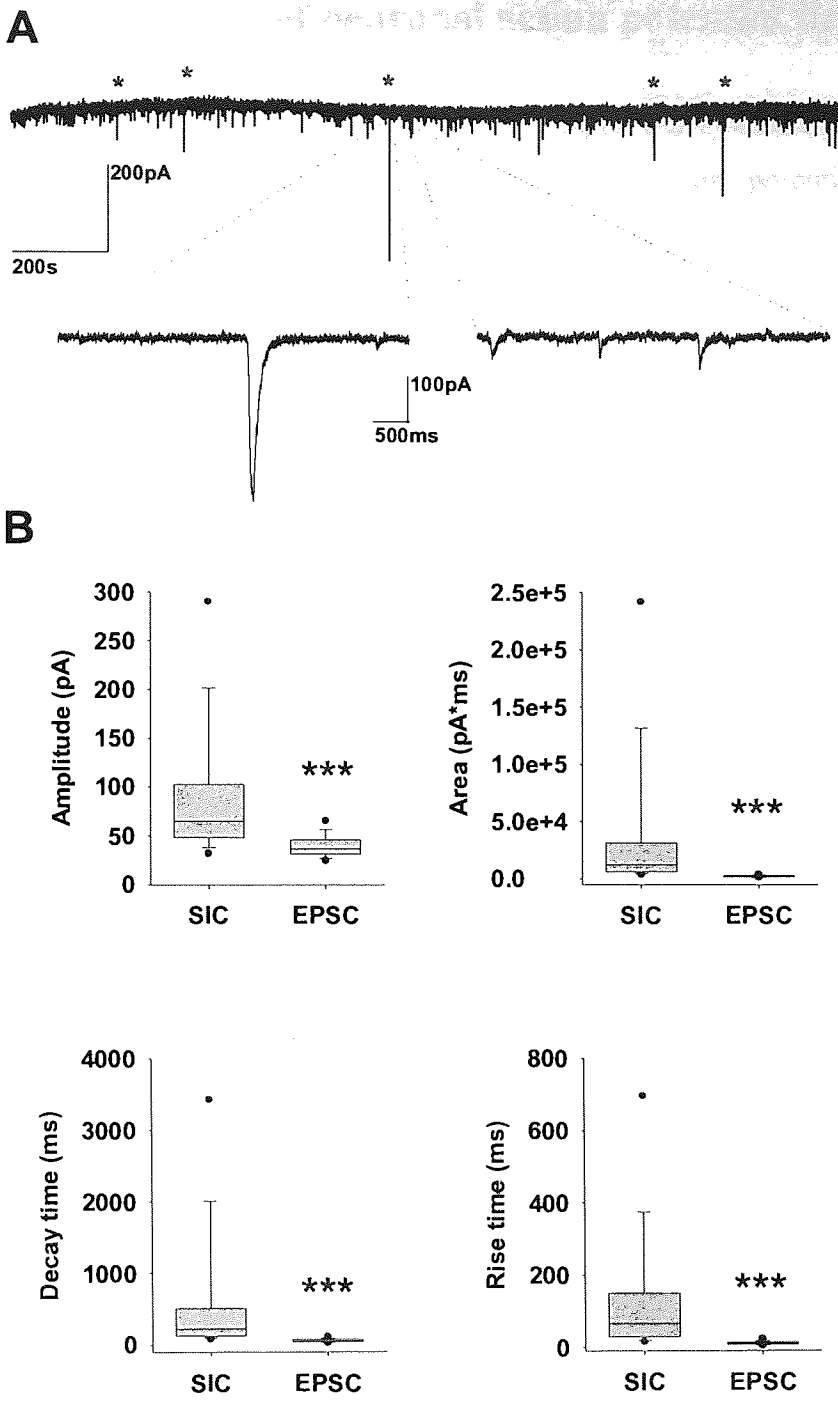

Figure 3.1: SICs are classified by their very slow kinetics. A) An example of a recording with a high number of excitatory inward currents. Currents accepted as SICs are marked with red asterisks. Expanded sections of the recording beneath shows an example of a SIC on the left and example of currents not meeting the SIC criteria on the right. **B)** Box plots illustrate the scatter of amplitude, area, rise time and decay time for SICs compared to the group of currents considered as EPSCs. The statistical difference is presented as $p<0.05$*, $p<0.01$** or $p<0.005$***.

3.2 SICs are independent of neuronal action potential firing

To assess the SIC dependency on continuing neuronal synaptic transmission, we added TTX (1μM) to the recording medium to block Na^+-dependent action potential firing and neurotransmitter release. Only data arising from cells where TTX blocked the sodium current when the cells were step depolarised to -30mV were included. Figure 3.2A shows a representative recording of the SICs in the presence of TTX whilst the spontaneous synaptic currents were abolished. Average frequency of SICs did not change in the presence of TTX (Ctrl 0.27±0.085 SICs/min; TTX 0.23±0.12 SICs/min; paired Student's t-test p=0.7; n=9 cells). SIC properties did not change largely as summarised in figure 3.2B. Amplitude was reduced in TTX from 120.45±30.73 pA to 80.86±16.84 pA (Ctrl n=14 SICs; TTX n=23 SICs; 9 cells; Paired Student's t-test p=0.02) which results from one unexpectedly active cell which SIC frequency increased 2-fold during TTX wash-on and these SICs were of much lower amplitude. Rise time, decay times and area were not different (Paired Student's t-test p>0.05, all parameters).

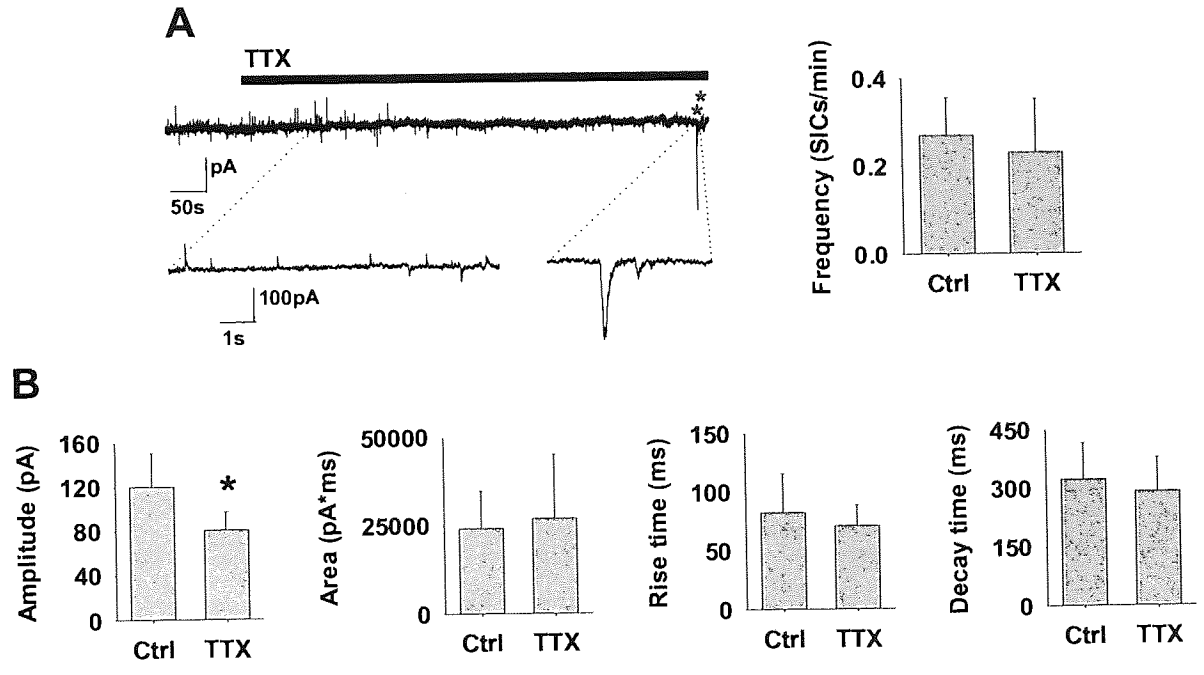

Figure 3.2: SICs are independent of neuronal activity. A) Trace showing spontaneous activity before and during TTX application (1μM). Spontaneous synaptic IPSCs and EPSCs (expanded beneath, left) were abolished within few minutes whereas SICs (indicated by red asterisks and expanded beneath) remained intact. Bar graph on the right summarises the mean SIC frequency in control and presence of TTX. **B)** Bar graphs summarise the mean amplitude, area, rise time and decay time for SICs before and during TTX.

3.3 SICs exhibit large variability in occurrence and magnitude

Presence of spontaneous SICs varies across the data as shown in examples in figure 3.3.1A. Average SIC frequency over the three weeks post-natal period was 0.093±0.019 SICs/min (0.0015Hz) which equal to 1 SIC during 10 minutes recording (n=98 cells). 43.9% of the TC neurons did not show SICs at all, and 65.3% had frequency less than 0.05 SICs/min (Fig. 3.3B). Average inter event interval (IEI) in recordings with ≥2 SICs was 4.41±0.51 minutes (range 0.007-29.8 min; n=157 IEIs from 34 cells). Frequency histogram in figure 3.3.1C shows the spread of IEI.

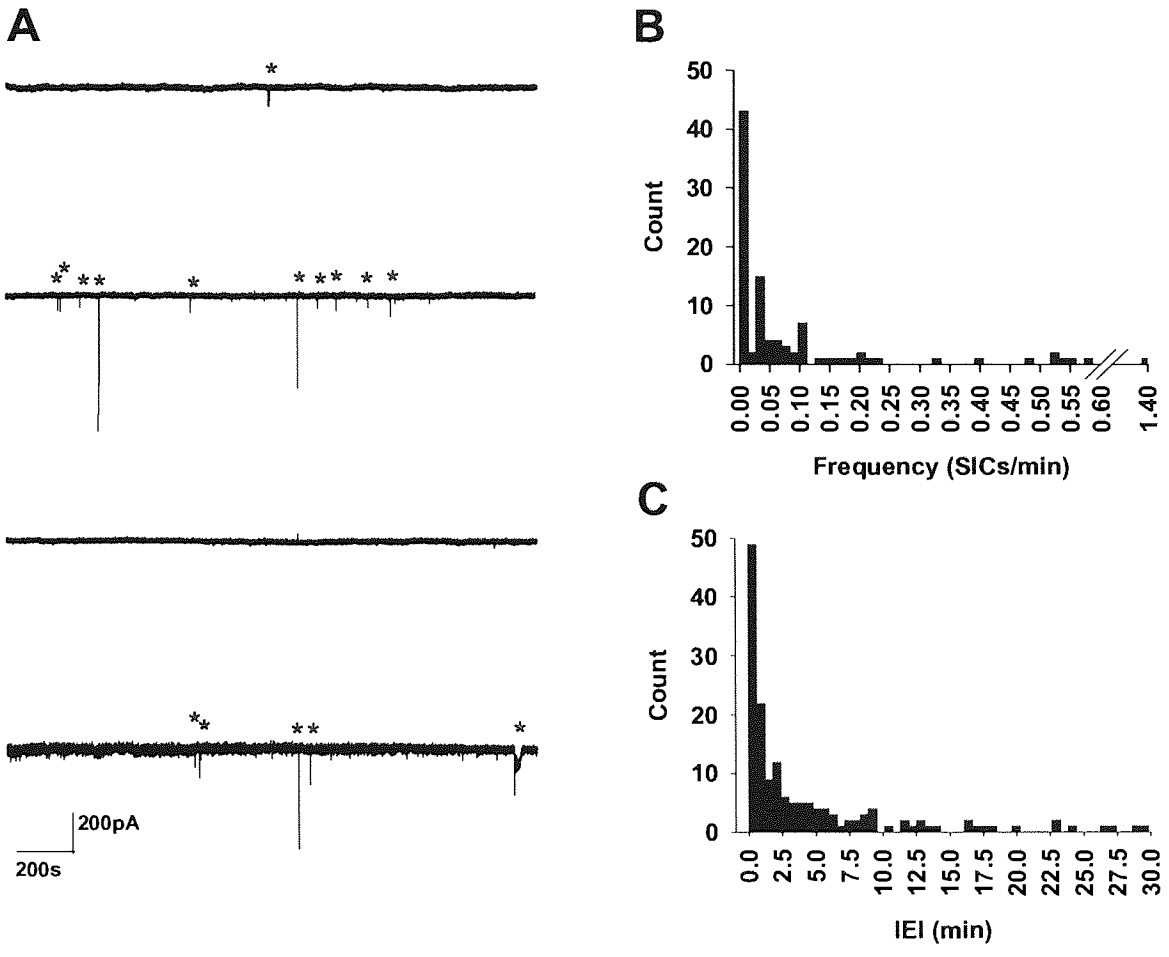

Figure 3.3.1: SIC prevalence varies across the cell population. A) Traces showing low and high SIC prevalence (SIC marked with red asterisk) from four different cells over a 30 minute's recordings. **B)** Frequency histogram shows the distribution of SIC prevalence as a function of SICs/minute (range: from 0 to 1.4 SICs/min). **C)** Frequency histogram for IEI from recordings showing ≥2 SICs (range: 0.007-29.8 min).

In addition to the variability in frequency, the size of SICs was very heterogeneous as seen in examples in figure 3.3.2A. The spread of the parameters are illustrated in the histograms in figure 3.3.2B. Amplitude ranged between 24.4pA and 689.5pA, rise time between 10.5ms and 3.9s, decay time between 62.1ms and 6.6s, and area between 1810.2 and 1165315pA*ms (n=211 SICs). As described in materials and methods, SICs with rise time >10ms were only accepted if the overall duration exceeded 100ms.

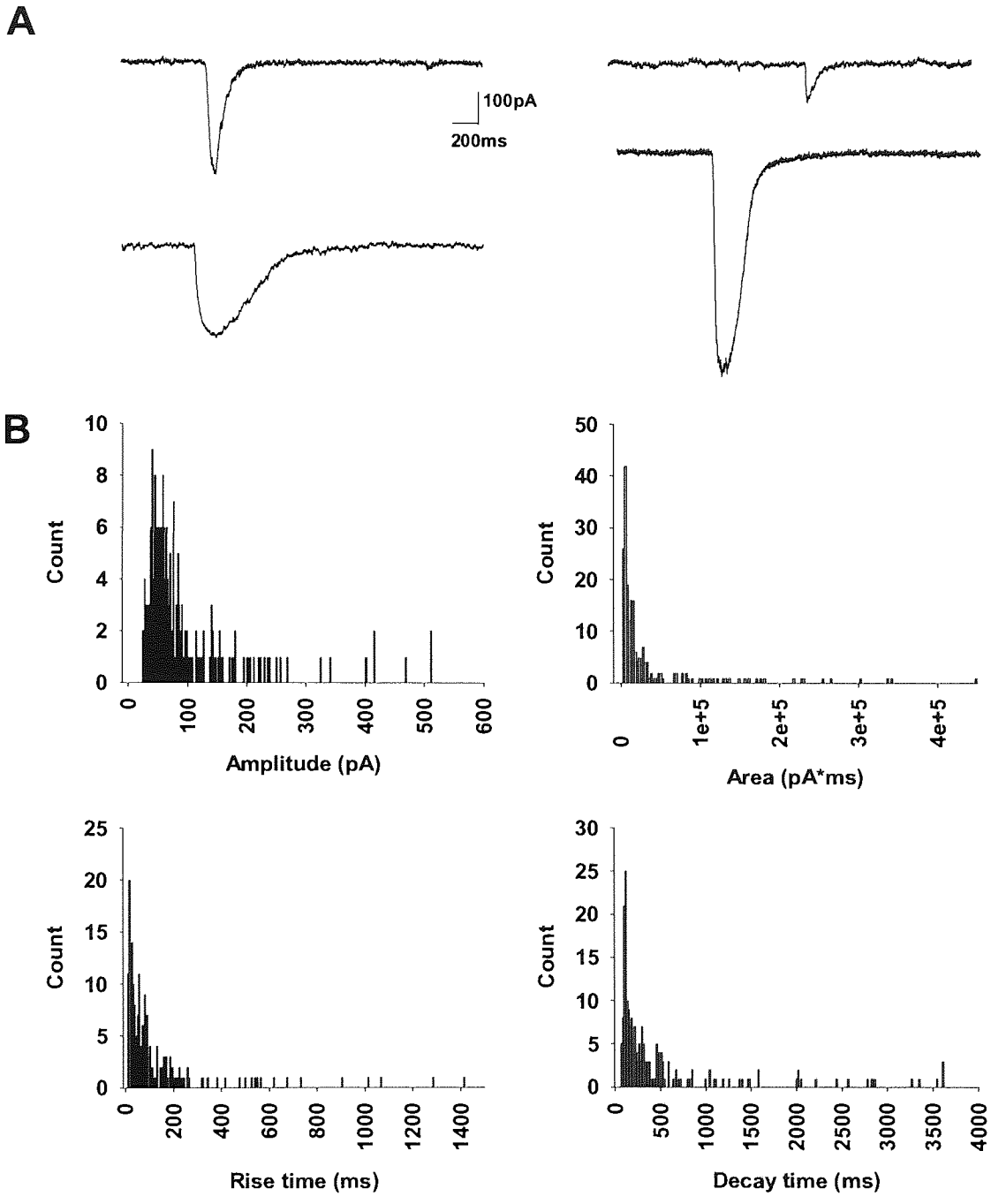

Figure 3.3.2: SIC amplitude and kinetics are variable. A) Four examples of SICs of different magnitudes. **B)** Frequency histograms for SIC amplitude, area, rise and decay times. Amplitudes over 600pA not shown in the graph (1 SIC). Rise times longer than 1.5s are not shown in the graph (4). Decay times longer than 4s are not shown in the graph (6) and areas greater than 450000pA*ms are not shown in the graph (4).

3.4 SICs are NMDA-receptor mediated

Non-specific NMDA-receptor antagonist D-AP5 (50μM) blocked SICs (Ctrl 0.24±0.04 SICs/min; AP5 0.01±0.01 SICs/min; paired Student's t-test p=0.005; n=5 cells) consistent with previous studies. Of 11 SICs in control condition, one SIC was still detected in the presence of D-AP5. Figure 3.4 summarises the effect of D-AP5.

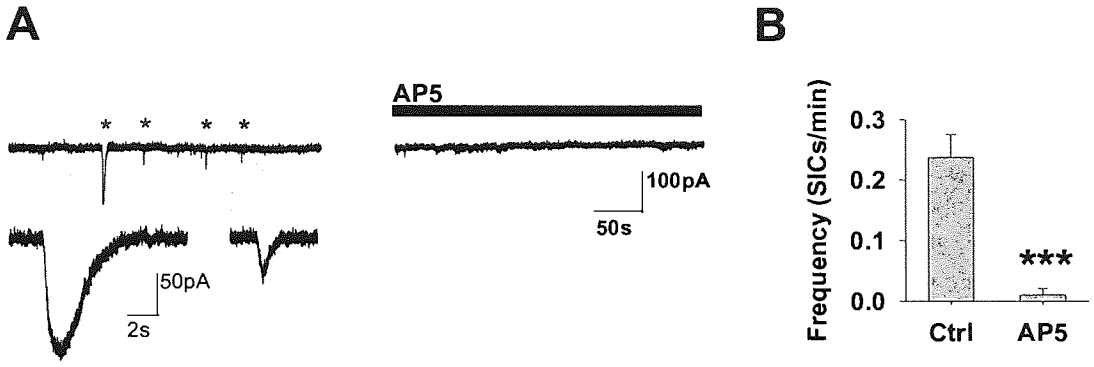

Figure 3.4: SICs are NMDA-receptor mediated. A) Top traces showing SIC prevalence before (left) and during (right) D-AP5 (50μM) application. SICs from control trace are marked with asterisks and two of them expanded beneath. **B)** Mean SIC frequency in control and in presence of D-AP5.

The NMDA-receptor NR2B subunit specific antagonist, ifenprodil (10μM), also reduced the number of SICs from 21 to 4 in three cells tested (19% of control; n=2 from P12, 1 from P20). However, the mean frequency difference was not significant (Ctrl 0.37±0.12 SICs/min; Ifen 0.09±0.03 SICs/min; paired Student's t-test p=0.2; data not shown). The magnitude of the SICs were reduced in the presence of ifenprodil (Amplitude from 116.0±27.1pA to 77.4±23.8pA; rise time from 103.1±23.4ms to 39.36±9.1ms; decay time from 340.9±102.2 to 185.5±45.7ms; Area 35053±12408 pA*ms to 9378.9±2273.1 pA*ms; Student's t-test p>0.2 all parameters; n=21, 4 respectively).

3.5 Spontaneous SICs are detected in presence of Mg^{2+}

Because NMDA-receptors are characterised by voltage-dependent Mg^{2+} block, most experiments were done using 0-Mg^{2+} aCSF to enhance the detection of NMDA-receptor mediated events. Therefore, in order to assess SICs prevalence in more physiological conditions, spontaneous activity was recorded from TC neurons in normal aCSF containing Mg^{2+} (1mM) and compared to SICs recorded in 0-Mg^{2+}. As anticipated from previous studies [Fellin *et al.*, 2004; Perea & Araque, 2005; D'Ascenzo *et al.*, 2007], SIC frequency was significantly higher in Mg-free medium as shown in figure 3.5A (Mg^{2+} 0.019±0.007 SICs/min; Mg-free 0.069±0.013 SICs/min; Student's *t*-test p=0.04; n=11; 35 cells respectively). Box plots (shown as 5^{th}/95^{th} percentile for rise and decay times and area) illustrate the spread of the data between the two groups (Fig. 3.5B). Mean values are listed in table 3.5. None of the mean parameters were significantly different (Student's t-test p>0.1, all parameters; Mg^{2+} n=10; 0-Mg^{2+} n=105 SICs). However, with Mg-free medium, SICs with very large amplitude (shown in the box plot as potential outliers) were observed more often (Fig. 3.5B).

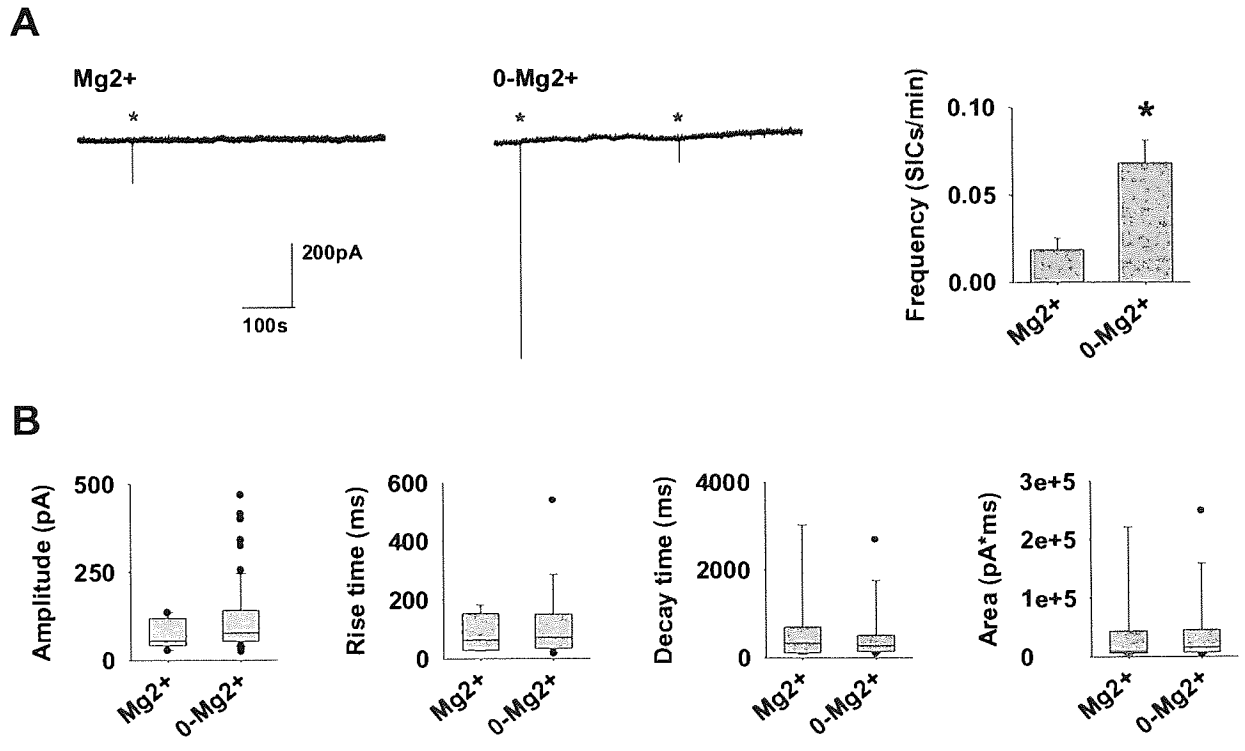

Figure 3.5: Spontaneous SIC prevalence is enhanced in Mg-free aCSF. A) Trace on the left shows a representative recording of a spontaneous SIC (red asterisk) in normal aCSF containing 1mM Mg^{2+}. Trace on the right shows an example recording in 0-Mg^{2+} aCSF. Bar graph on the right summarises mean frequency. **B)** Box plots compare the parameters for both conditions.

	Amplitude (pA)		Rise time (ms)		Decay time (ms)		Area (pA*ms)	
	Mg^{2+}	0-Mg^{2+}	Mg^{2+}	0-Mg^{2+}	Mg^{2+}	0-Mg^{2+}	Mg^{2+}	0-Mg^{2+}
Mean	74.31	124.31	81.15	139.76	636.51	753.16	40301.80	66805.84
Median	53.61	76.82	62.16	73.13	329.61	268.63	9393.06	15883.09
Std.Dev	41.23	118.55	63.07	232.41	957.01	2109.31	72213.40	170012.43
Std.Err	13.04	11.57	19.94	22.68	302.63	205.85	22835.88	16671.09

Table 3.5: SIC properties in Mg^{2+} vs. 0-Mg^{2+}. Mean values were not statistically different ($p>0.1$).

3.6 SIC frequency and post-natal development

The VB thalamus undergoes developmental remodelling until the end of the 3rd post-natal week. Therefore, spontaneous SIC prevalence during this period was assessed by comparing the data from 3 different post-natal weeks (PN wk1 P6-7, wk2 P10-15 and wk3 P19-22). Figure 3.6 shows representative traces for each group and summarises the data. During the 2nd PN week, 77.2% of the TC neurons exhibited ≥1 SICs (n=35 cells), whereas during the 1st and 3rd PN week, SICs were recorded in less than half of the cells (42.4% and 46.7%; n=33, 30 respectively; Fig 3.6B). The overall frequency did not change between the groups (Wk1 0.094±0.03 SICs/min; Wk2 0.069±0.013 SICs/min; Wk3 0.12±0.05 SICs/min; Student's t-test $p>0.2$; all groups compared; Fig 3.6C). However, if the mean frequency was calculated only from the cells that showed SICs, there was a significant decrease in the frequency during the 2nd PN week compared to the 1st and 3rd week (0.22±0.06>0.089±0.015<0.25±0.099 SICs/min respectively; Student's t-test $p<0.03$; all groups compared). Furthermore, IEI from data with ≥ 2 SICs per recording showed significant increase during the 2nd PN week as shown in figure 3.6D (wk2 6.3175±0.7985 min, n=17 cells, 79 SICs, compared to wk1 2.2200±0.6339 min n=8/39 and wk3 2.7263±0.9353 min, n=9/39; K-S test $p<0.001$ for both; wk1 compared to wk3 $p=0.15$).

SIC amplitude during the 2nd PN week was significantly higher compared to the 1st and 3rd week as seen in figure 3.6E (Student's t-test $p\leq0.02$, all groups compared). Rise time, decay time and area were not significantly changed (rise time $p>0.3$; decay time $p>0.6$; area $p>0.2$). Tables 3.6.1 and 3.6.2 list the mean values.

Amplitude (pA)	Wk1	Wk2	Wk3	Area (pA*ms)	Wk1	Wk2	Wk3
Mean	84.08	**124.31**	61.40	Mean	36156.76	65309.71	43273.30
Median	62.71	**76.82**	52.90	Median	7136.23	15651.98	12440.94
Std.Dev	68.50	**118.55**	32.98	Std.Dev	81175.00	170598.39	94792.75
Std. Err	9.41	**11.57**	4.53	Std. Err	11150.24	16728.55	13020.79

Table 3.6.1: SIC amplitude and area during maturation. Wk1 n=53; Wk2 n=105 and Wk3 n=53 SICs. Wk2 amplitude was significantly higher (**bold**) compared to wk1 and wk3 ($p \leq 0.02$).

Rise time (ms)	Wk1	Wk2	Wk3	Decay time (ms)	Wk1	Wk2	Wk3
Mean	185.47	139.76	240.55	Mean	781.89	753.16	666.08
Median	30.31	73.13	82.31	Median	153.69	268.63	269.75
Std.Dev	441.62	232.41	572.88	Std.Dev	1522.19	2109.31	1136.16
Std. Err	60.66	22.68	78.69	Std. Err	209.09	205.85	156.06

Table 3.6.2: SIC kinetics during maturation. Mean values were not statistically different ($p>0.1$).

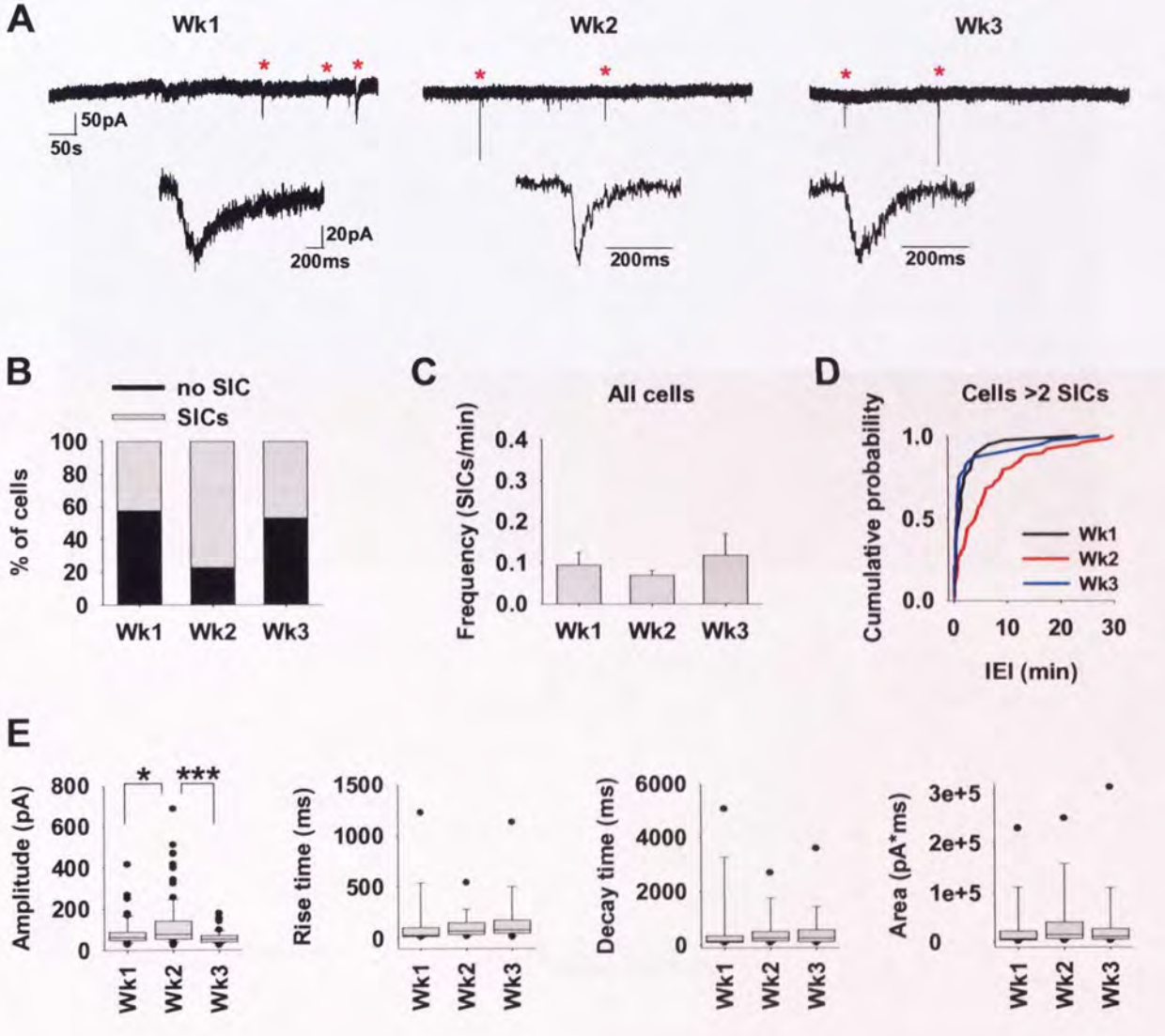

Figure 3.6: Spontaneous SICs show developmental differences. A) Example recordings during different PN weeks. SICs are marked with asterisks and examples expanded beneath. **B)** Stacked bar graph on the left shows the percentage of TC neurons exhibiting SICs. **C)** Bar graph summarise the mean frequency of all cells shown in B. **D)** Cumulative probability graph showing the IEI distribution between each group from cells with ≥2 SICs. **E)** Box plots showing the scatter of SIC parameters.

3.7 Glutamate induces astrocytic $[Ca^{2+}]_i$ elevations

Previous studies on spontaneous astrocytic Ca^{2+} signalling in the VB showed a developmental profile [Parri *et al.*, 2001]. Here, we assessed the frequency and prevalence of spontaneous astrocytic $[Ca^{2+}]_i$ activity in P10-12 slices in our experimental conditions. Spontaneous astrocytic $[Ca^{2+}]_i$ increases were recorded over a 15 minute period in normal aCSF containing TTX (1μM). Consistent with previous data, spontaneous activity manifested in various profiles as illustrated in figure 3.7.1. Cell 3 showed oscillation, whereas cells 1 and 5 exhibited only a couple of small peaks. Cell 4 showed a Ca^{2+} peak as well as Ca^{2+} plateau. Cells 2 and 6 showed multiple peaks of larger magnitude. Mean frequency for these cells was 0.22 peaks/min (range: 0.067-0.47 peaks/min).

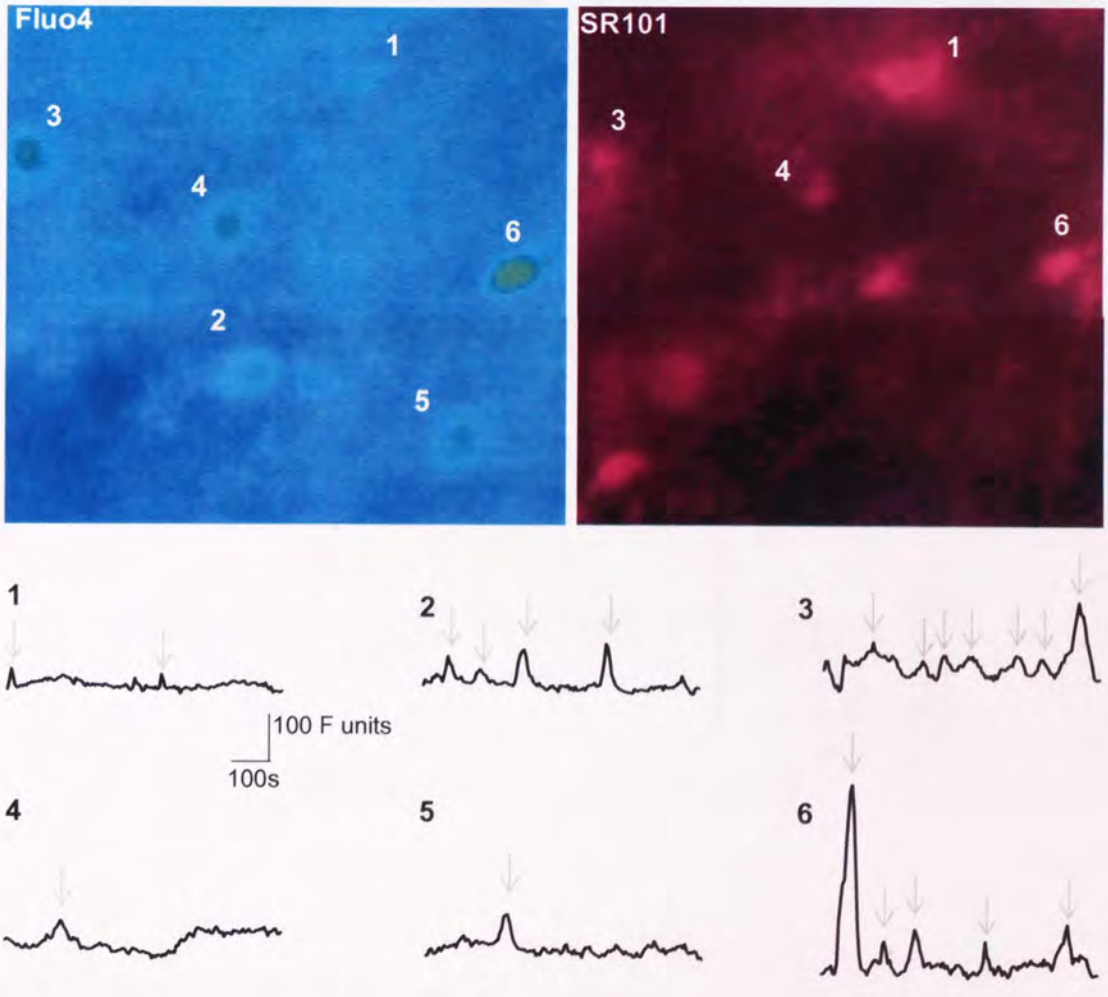

Figure 3.7.1: Spontaneous $[Ca^{2+}]_i$ signalling show variable profiles. Top left panel shows Fluo4 loaded cells with fluorescence increases (numbered) of selected area of the whole image field. Panel on the right shows same area for SR101 staining, demonstrating that the numbered cells were astrocytes. SR101 staining for cells 2 and 5 was not detected and could have been out of the SR101 detection focus. Traces below show Ca^{2+} increases over time (indicated with arrows) for the numbered cells.

As described in the introduction, astrocytes express glutamate receptors and can exhibit Ca^{2+} elevations in response to external glutamate application or glutamate released from synaptic terminals. Our primary aim in this thesis was to investigate the effects of synaptic stimulation on astrocytic signalling onto neurons. Therefore, astrocytes ability to respond to glutamate was assessed after quantification of spontaneous activity. Glutamate (200μM) was washed on for 1 minute in the presence of TTX and the number of active astrocytes per image field increased significantly from 25.4±7.9 cells to 44.6±10.5 (n=5 slices; paired Student's t-test p=0.026). Figure 3.7.2 summarises the responses.

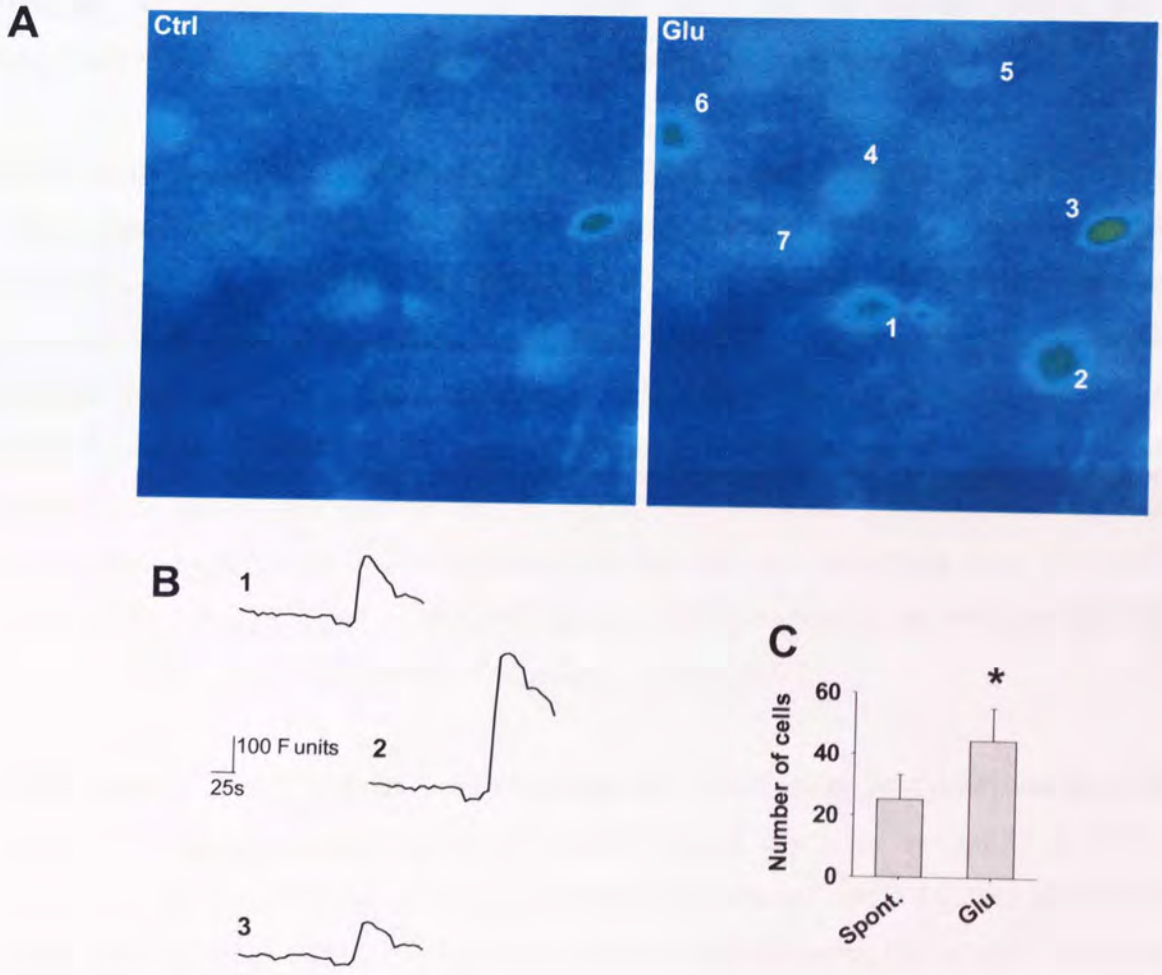

Figure 3.7.2: Astrocytes respond to glutamate. A) Pseudocolour images from selected area showing the astrocytic Ca^{2+} intensity changes before and during Glu (200μM) application. Astrocytes are circled and most of them are showing increase in fluorescence intensity in response to glutamate. **B)** Three examples of the glutamate responses from numbered cells. **C)** Mean bar graph showing the overall number of astrocytes in spontaneous recordings versus in response to glutamate application.

3.8 Discussion

These results show that two distinguishable populations of spontaneous excitatory currents, SICs and EPSC-like events, exist in the VB thalamus. SICs could be distinguished by their extremely slow kinetics, insensitivity to TTX and sensitivity to NMDA-receptor antagonists. To clarify, recording aCSF did not include TTX or any antagonists to block spontaneous EPSCs, IPSCs or slow outward currents (SOCs; see Kozlov *et al.*, 2006) unless otherwise stated, therefore these currents were often observed throughout the experiments presented later on. As the aim of this project was to study the modulation of astrocyte mediated SICs, properties or modulation of any other currents than those meeting the criteria for SIC acceptance in our experimental conditions were not investigated further.

SICs were present in aCSF containing Mg^{2+}, albeit of reduced prevalence consistent with the voltage-dependent Mg^{2+} block of NMDA-receptors that mediate SICs. Consistently, SICs were blocked by the wide spectrum NMDA-receptor antagonist D-AP5 and the results are in agreement with previous work done *in situ* [Parri *et al.*, 2001; Fellin *et al.*, 2004; Angulo *et al.*, 2004; Perea & Araque, 2005; Fellin *et al.*, 2006; Kozlov *et al.*, 2006; D'Ascenzo *et al.*, 2007]. The number of SICs was reduced by application of selective antagonist of NR2B containing receptors, although the lack of significance in overall frequency/size differences may be due to the rarity of spontaneous events and age variability (wk 2-3). Indeed, extrasynaptic NR2D subunit [Cull-Candy *et al.*, 2001] expression is stronger than NR2B expression during the 2^{nd} PN week [Wenzel *et al.*, 1996; 1997].

The variability in SIC kinetics points towards the involvement of extrasynaptic receptors [Haydon & Carmignoto, 2006]. Here, we have shown extensive variability in both SIC prevalence and magnitude recorded from different TC neurons. If the kinetics and amplitude differences arise from different release sites and diffusion distances, the synaptic structure and degree of glial coverage is expected to have major impact. Indeed, the degree of glial coverage of neurons has been shown to influence synaptic efficacy [Oliet *et al.*, 2001], but specific effects at the extrasynaptic locations are still unknown. Nevertheless, we know that at least two different forms of glial coverage of synapses exist in the VB thalamus: sensory synapses termed as "glomeruli" that are completely covered by glial sheet, and cortical synapses with smaller synaptic boutons [Matthews *et al.*, 1977; Castro-Alamancos, 2004]. Furthermore, the degree of glial coverage of synapses has been estimated in barrel cortex in

the work by Genoud *et al.* [2006]. They demonstrated that spines in barrel columns show a large diversity in the portion of their surface that contacts astrocytes: some showed almost complete astrocytic coverage, whereas others were completely devoid of contact [Genoud *et al.*, 2006]. Since the primary somatosensory cortex of small rodents is an isomorphic representation of the body surface and parallel representations are characteristic of the subcortical pathways [Killackey *et al.*, 1995], similar diversity of astrocytic contacts with synapses and cells could exist in the VB thalamus. Thus, it can be speculated that the large variability in SIC frequency and magnitude presented here arise from the heterogeneity of glial contact with neurons creating uneven extracellular spaces for glutamate diffusion. Diversity in size of SICs could also arise from astrocytic release of vesicles of variable sizes. Indeed, astrocytic processes opposing neuronal extrasynaptic receptors have been shown to have vesicles containing glutamate which may be enlarged in response to glutamate, though different research groups have reported large variability in the size of these vesicles (diameter ranging from 30nm to 7μm) [Bezzi *et al.*, 2004; Chen *et al.*, 2006; Xu *et al.*, 2007].

On the other hand, as roughly 40% of the total of 98 TC neurons did not show SICs at all, it may reflect contact with different astrocyte populations possessing distinct physiological functions regarding astrocyte to neuron communication. Interestingly, reactive astrocytes have been shown not to exhibit spontaneous astrocytic $[Ca^{2+}]_i$ increases [Aguado *et al.*, 2002]. Whether the absence of SICs results from damage to the astrocytes nearby the recorded neurons or different subpopulations would need further investigations.

Spontaneous $[Ca^{2+}]_i$ signalling in slice preparations from P10-12 was also assessed. Astrocytes exhibited variable forms of spontaneous signalling as seen in previous work done in the VB thalamus as well as in other brain areas [Parri *et al.*, 2001; Aguado *et al.*, 2002; Nett *et al.*, 2002]. Interestingly, the frequency and magnitude of Ca^{2+} peaks appeared to vary greatly. Furthermore, even within the six astrocytes shown in figure 3.7.1, the mean frequency of the Ca^{2+} peaks (0.004Hz) appeared higher than average SIC frequency (0.0015Hz). Assuming that SICs are due to Ca^{2+}-dependent glutamate release from the astrocytes, it is possible that only Ca^{2+} peaks achieving certain threshold in magnitude are capable of inducing glutamate release. This may therefore explain the diversity observed in SIC frequency. In addition, analysis of the IEI distribution demonstrated that most of the SICs occurred at short intervals. This combined with extremely low overall frequency suggests that SICs occur in periods of higher and lower probability.

The data also revealed distinct differences in the SIC prevalence at different post-natal weeks. The mean SIC frequency was not different between the PN groups. However, a notably larger population of TC cells exhibited SICs during the 2nd PN week compared to 1st and 3rd week, and SICs during the 2nd week were also larger in amplitude. However, surprisingly, the average SIC frequency of any active cells was lower during the 2nd week compared to 1st and 3rd. This observation is difficult to explain but it is important to remember that the VB thalamus undergoes most profound remodelling during the 2nd PN week. For example, a sudden increase in CT afferent proliferation takes place at the end of the 1st PN week and the maximal rate of synaptogenesis and synaptic remodelling occur during the second week [Matthews *et al.*, 1977; Miller *et al.*, 1993; Arsenault & Zhang, 2006]. Furthermore, post-natal maturation of neurons and their connectivity is accompanied with developmental changes in astrocytes. In the VB thalamus, the dramatic decrease of radial glia has been shown to occur during the first post-natal week, whilst GFAP staining becomes visible during the 2nd PN week [Frassoni *et al.*, 2000]. In the hippocampus, astrocytic morphology is highly heterogenous after birth, but becomes consistent by the end of the 2nd week [Bushong *et al.*, 2004]. During the first two postnatal weeks, astrocytes were shown to extend overlapping filopodial processes, whilst fine spongiform processes resulting in the development of boundaries between neighbouring astrocyte domains appeared during the third week [Bushong *et al.*, 2004]. In view of this, differences in SIC prevalence and properties may reflect functional importance during maturation. Alternatively, it could be a passive outcome resulting from physical changes in the reorganization of the TC neurons and synapses.

Developmental changes in spontaneous Ca^{2+} signalling were not investigated here, but previous studies have suggested developmental roles during maturation as the number of spontaneous Ca^{2+} signalling events appeared to decrease during maturation [Parri *et al.*, 2001; Aguado *et al.*, 2002]. Consequently, the observation that SIC frequency did not decrease during maturation, raises questions. One possible explanation for this difference is that in the previous studies, the actual loading of Ca^{2+} dye into the astrocytes decreased when the cells became more mature as suggested by Aguado *et al.* [2002]. An increase in connective tissue may also reduce the ability to detect Ca^{2+} signals. It is noteworthy that not all SICs observed in previous studies were associated with Ca^{2+} increases in astrocytes. For example in the VB thalamus, approximately 20% of the SICs were uncorrelated with astrocytic Ca^{2+} increases [Parri *et al.*, 2001]. As the SIC frequency appeared lower than the frequency of Ca^{2+} peaks, it is therefore possible that whilst the overall frequency of Ca^{2+} decreases, the proportion of Ca^{2+} peaks leading to glutamate release remains unaltered.

Finally, the most interesting question remains: What is the purpose of these extremely rare events occurring on average once every 10 minutes (0.0015 Hz) with approximately 40% of the TC neurons not receiving them at all? The low frequency and slow kinetics of SICs suggests contribution in slow physiological events such as biochemical processes involving Ca^{2+} rather than a role in fast synaptic transmission. Taken together, we showed that SICs were present throughout the three post-natal weeks at low frequencies and that astrocytic $[Ca^{2+}]_i$ signals were increased by application of exogenous glutamate indicating existence of functional glutamate receptors. These results form the basis for the hypothesis that glutamate released during synaptic stimulation elicits astrocytic $[Ca^{2+}]_i$ increases and potentially modulates the prevalence of SICs. Assessing a variety of different stimulation parameters may reveal conditions under which SICs are induced helping to understand their physiological role.

Chapter 4

Effect of synaptic stimulation on SIC incidence

As spontaneous astrocytic Ca^{2+}-elevations can lead to SICs in TC neurons and because astrocytes have been demonstrated to express functional glutamate receptors in the VB [Parri *et al.*, 2001; Chapter 3], we hypothesised that stimulation of the corticothalamic (CT) and/or sensory (Sen) afferents leads to SICs in TC neurons.

Synaptic stimulation of afferents has been shown to increase SIC frequency in other brain regions by approximately 5-fold [Fellin *et al.*, 2004; D'Ascenzo *et al.*, 2007]. A number of previous studies have shown that astrocytes showed a dependency on stimulation parameters exhibited as a potentiation of frequency and magnitude of Ca^{2+} responses by increasing the afferent stimulation intensity, frequency or duration [Porter & McCarthy, 1996; Pasti *et al.*, 1997; Araque *et al.*, 2002; Perea & Araque, 2005; Beierlein & Regehr, 2006]. Most interestingly, whisker stimulation at 5Hz has been shown to be the most effective at evoking Ca^{2+} responses in the barrel cortex *in vivo*, whilst 1Hz and 10Hz were least effective [Wang *et al.*, 2006]. If SICs, in response to synaptic stimulation, are generated by Ca^{2+} dependent glutamate release, the magnitude of Ca^{2+} increases in astrocytes may influence glutamate release. Indeed, it has been shown that SICs which did not correlate with astrocytic Ca^{2+} increases were approximately 40% smaller [Parri *et al.*, 2001] whilst another study reported weak correlations with SIC amplitude and magnitude of Ca^{2+} signals [Perea & Araque, 2005].

Taken together and bearing in mind that the thalamus can operate at distinct frequencies and firing modes depending on the state of arousal, we hypothesised that the astrocytic feedforward signalling may be recruited by particular stimulus frequencies or durations. The post-synaptic neuronal current is taken as an indication of pre-synaptic glutamate release that we assume also activates the perisynaptic astrocytes. Given that SICs are generated spontaneously in the VB thalamus at low frequencies, with tendency to periods of higher and lower incidence probability (Chapter 3), establishing differences in spontaneously occurring and synaptically evoked SICs is important. This could be achieved, for example, by ***1)*** comparing average SIC incidence before and after stimulation, ***2)*** looking at correlation between latencies of delayed SICs and delayed astrocytic Ca^{2+} responses, ***3)*** looking at specific peaks in latencies of post stimulus SICs, and ***4)*** by looking at any particular

differences in the nature of spontaneous and delayed SICs. "Delayed" refers to the time delay between onset of synaptic stimulation and the beginning of SIC or peak of Ca^{2+} response.

4.1 Most TC neurons receive both sensory and CT input

TC neurons in the VB receive synaptic inputs from sensory and CT afferents which have different characteristics (see introduction). In addition, previous studies have shown that less than 20% of the TC neurons receive both sensory and CT inputs [Miyata & Imoto, 2006]. Therefore, as our aim was to assess the effects of synaptic stimulation and potential function as coincidence detectors of simultaneous synaptic activity, we determined the properties and percentage of TC neurons receiving both sensory and CT inputs in our experimental conditions.

Sensory and CT afferents were stimulated in P10-19 at 50Hz for 1 second at different intensities. Figure 4.1A shows the placement of stimulating electrodes and recording electrode. Here, 73.3% (11/15) of TC neurons received both inputs. Evoked post-synaptic current (PSC) peak amplitude and rise time were measured. Sen and CT alone did not differ from each other (Student's t-test, $p=0.26$). Simultaneous Sen and CT stimulation evoked significantly larger currents than Sen alone, whereas currents during CT stimulation did not differ from the combined stimulation ($p=0.02$ and $p=0.2$, respectively). Increase in PSC amplitude was correlated with an increase in stimulus intensity (Sen $r^2=0.97$, Pearson's correlation $p<0.005$; CT $r^2=0.8$, $p=0.002$; Sen+CT $r^2=0.82$, $p=0.002$; Fig. 4.1B), whereas rise time was not ($r^2<0.007$, $p>0.5$; all groups). The lack of all-or-none response to sensory stimulation and high percentage of neurons receiving both inputs indicate that our stimulation parameters activate most of the afferents even at the lowest stimulus intensity. This is, however, expected as these were relatively intense stimulation parameters and as sensory input does not acquire the all-or-none response until after the second PN week.

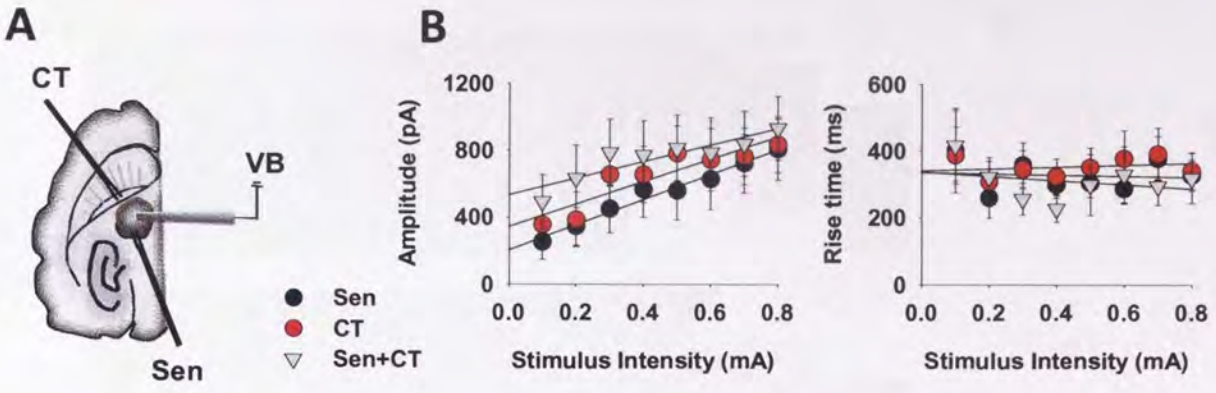

Figure 4.1: TC neurons receive both inputs. A) Schematic of the slice preparation showing the orientation of stimulating electrodes and recording electrode. **B)** Scatter plot on the left shows the mean amplitude of evoked excitatory PSCs versus stimulus intensity for Sen, CT and simultaneous stimulation. There was a positive correlation between stimulus intensity and amplitude. Scatter plot on the right shows the mean rise time with no correlations.

4.2 Astrocytes respond to synaptic stimulation with $[Ca^{2+}]_i$ elevations

The ability of synaptic inputs to elicit astrocytic $[Ca^{2+}]_i$ elevations and the potential for Ca^{2+} dependent glutamate release was assessed in P10-12 slices. Stimulations of sensory and CT inputs at 50Hz of 1-2s duration elicited Ca^{2+} elevations as shown in figure 4.2.1A. Co-loading of SR101 confirmed the astrocytic identity of the responsive cells. Figure 4.2.1B shows averages of 33 sensory and 16 CT evoked responses. On average 24.5±2.87 astrocytes responded to sensory afferent stimulation (n=4 slices) and 24.25±4.65 (n=8) to CT stimulation within the imaged area of 444μm x 341μm (Fig 4.2.1C). Stimulation for 1 or 2 seconds did not change the number of responsive astrocytes significantly (1s 29.8±4.9; 2s 20.4±3.7; n=5, 7 respectively; Student's t-test $p>0.1$; Fig. 4.2.1D).

The number of astrocytes responding to short stimulation (including Sen and CT) was compared to the data presented in the previous chapter (Fig. 3.7.2). The average number of astrocytes displaying $[Ca^{2+}]_i$ elevations in response to synaptic stimulation was not different to the average number of astrocytes showing them spontaneously (Spont 25.6±7.8; Stim 24.33±3.1; n=5, 12 slices respectively; Student's t-test $p=0.9$). The number of responsive astrocytes during glutamate application was significantly higher than in response to afferent stimulation (Glu 44.6±10.6, n=5; Student's t-test $p=0.03$), suggesting that synaptically released glutamate concentration may not be as potent and/or glutamate application also activates astrocytes not activated by synaptic stimulation.

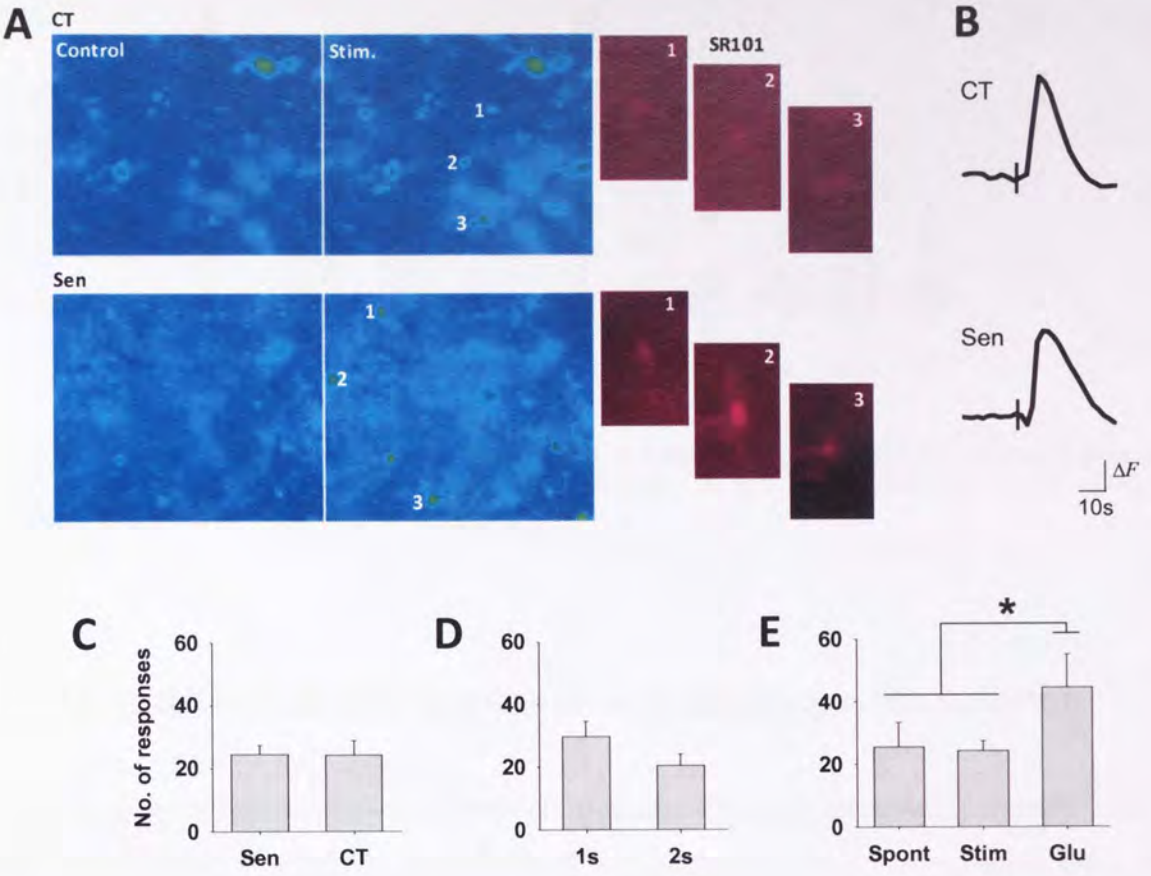

Figure 4.2.1: Synaptic stimulation evokes astrocytic $[Ca^{2+}]_i$ elevations. A) Pseudocolour images of slices loaded with Fluo-4 before (control) and following (stim) stimulation. Astrocytic Ca^{2+}-responses are seen as an increase in the fluoresce (change from blue to green). Three responding cells are numbered and the co-loading with SR101 (magenta images on the right) confirmed the astrocytic identity. **B)** Traces showing averages of 33 Sensory and 16 CT evoked responses to the afferent stimulation. **C)** Bar graph showing the mean number of astrocytes responding to Sen or CT afferent stimulation. **D)** Mean number of responses following stimulation for 1 or 2 seconds at 50Hz. **E)** Bar graph showing the mean number of spontaneously active astrocytes and in response to synaptic stimulation or glutamate application. (Statistical significance is presented as $p<0.05$ *, $p<0.01$ ** or $p<0.005$ ***).

Following stimulation, the average latency to peak was 6.89±0.17s (n=12 slices, 293 astrocytes) following stimulation. Time to peak was on average 1.5s longer in response to sensory stimulation (Sen 7.86±0.3s; CT 6.39±0.18s; n=99, 194 astrocytes respectively; Student's t-test p=0.00004; Fig. 4.2.2A). The relative intensity change of the Ca^{2+} fluorescence shown in figure 4.2.2B did not differ between sensory and CT stimulation (Sen 112.04±0.97ΔF%; CT 110.7±0.4ΔF%; n=99, 194 responses respectively; Student's t-test p=0.14) nor between 1s and 2s long stimulation (1s 111.53±0.58ΔF%; 2s 110.8±0.6ΔF%; n= 149, 144 respectively; Student's t-test p=0.4).

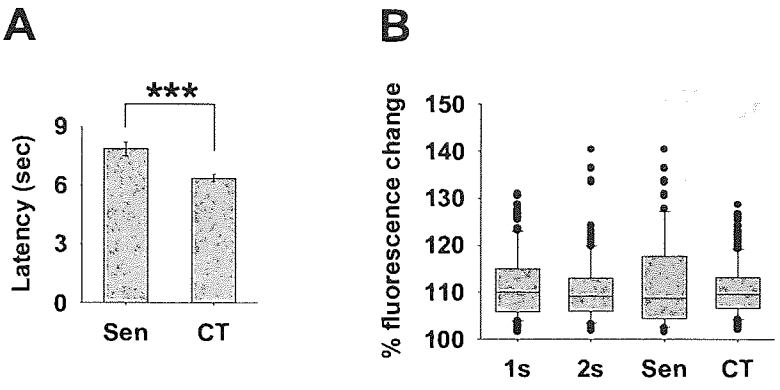

Figure 4.2.2: Latency and fluorescence change of the $[Ca^{2+}]_i$ responses. A) Bar graph showing the mean time delay between stimulation and the peak of the Ca^{2+} responses. **B)** Box plot showing the scatter of relative intensity changes between different stimulations.

4.3 SIC incidence is not increased with moderate stimulation

Above we showed that astrocytes do respond to synaptic stimulation reliably at least with the given parameters. Therefore, to investigate if any particular pattern of synaptic input may recruit astrocyte mediated neuronal SICs, stimulation protocols consisting of varying frequencies and durations were applied. Spontaneous SICs were observed in 40 of 76 (52.6%) recordings with a mean frequency of 0.16±0.03 SICs/min over a 5-10 minutes control period. The incidence of SICs after each stimulus episode was calculated and compared to the pooled spontaneous incidence.

Stimulus frequency protocol. The protocol comprised episodes with different frequencies (range 1-500Hz). For sensory input 61% of cells expressed SICs during stimulation (n=21 cells), whereas 53% of cells (n=30) expressed SICs with CT input. Figure 4.3.1A shows an example of a control recording following CT stimulation. SIC incidence was not significantly increased by varying the frequency for either sensory (Student's *t*-test for each stimuli $p>0.1$) or CT input ($p>0.6$) as shown in figure 4.3.1B. Furthermore, there was no correlation between increasing stimulus frequency and SIC incidence (Sen $r^2=0.02$, Pearson's correlation $p=0.45$; CT $r^2=0.4$, $p=0.1$; linear fit not shown).

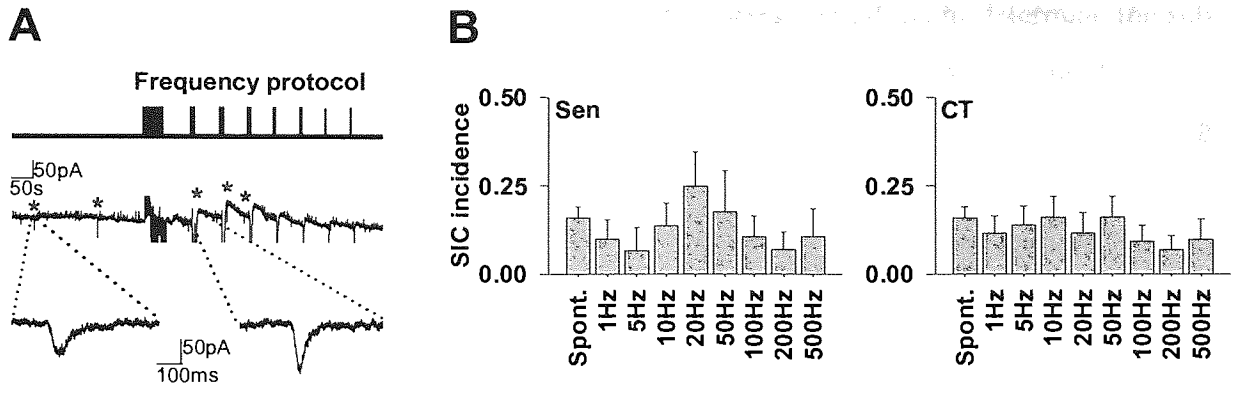

Figure 4.3.1: SIC incidence is not dependent on stimulus frequencies. A) Protocol (top) illustrating pattern of episodes of 50 stimuli delivered at different frequencies (1-500Hz) to CT input. The responses of the TC neuron are shown in the example trace below, with SICs indicated by asterisks. The neuronal post synaptic current and stimulation artefacts (vertical lines) are truncated for clarity. Expanded example SICs are shown beneath. **B)** Bar graphs show the relationship of mean incidence of SICs (SICs/min) to different stimulus frequencies for the sensory and CT inputs.

Stimulus duration protocol. Stimulus durations varied between 2ms – 10s as shown in the example in figure 4.3.2A. Of 24 cells, 45% expressed SICs during sensory stimulation, whereas 27% SICs occurred during CT stimulation (n=40). The incidence of apparent evoked SICs for any particular stimulus was either less than the level of spontaneous activity as shown in figure 4.3.2B (Sen: 2ms, 0.1s, Student's t-test $p<0.05$; CT: 2ms, 1-6s $p<0.05$) or unaltered ($p>0.1$ for the rest). For sensory input, a weak correlation was detected between increasing stimulus duration and SIC incidence ($r^2=0.4$, $p=0.06$). No correlation was observed between increasing CT stimulus duration and SIC incidence ($r^2=0.2$, $p=0.18$).

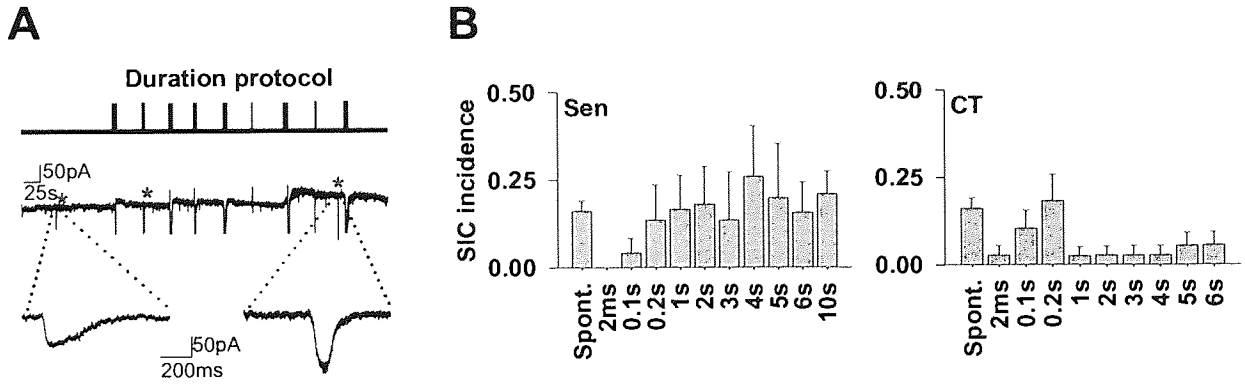

Figure 4.3.2: SIC incidence is not dependent on stimulus duration. A) Protocol (top) illustrating pattern of stimulation delivered at different duration (2ms-6s) to CT input. The responses of the TC neuron are shown in the example trace below, with SICs indicated by asterisks and examples are expanded beneath. **B)** Bar graphs summarising the mean incidences.

Stimulus intensity protocol. Stimulus intensity experiments were done to determine the sub-maximal (75%) stimulus intensity for each individual neuron for the experiments that were presented above. SIC incidence following these stimulations was assessed in addition (Fig. 4.3.3A). Sensory and CT afferents were stimulated for 1s at 50Hz whilst changing intensity between 0.1-3mA. SIC followed sensory and CT stimulation in 28% and 44% of the cells tested (n=25, 28 respectively), but did not increase incidence (Sen: 1-1.5mA and 2.5mA less than control, $p<0.03$, rest $p>0.2$; CT: 0.1mA and 3mA less than control, $p=0.02$ 0; rest $p>0.2$; Fig. 4.3.3B). Increase in stimulus intensity was not correlated with an increase in SIC incidence (Sen $r^2=0.07$, $p=0.5$; CT $r^2=0.008$, $p=0.8$).

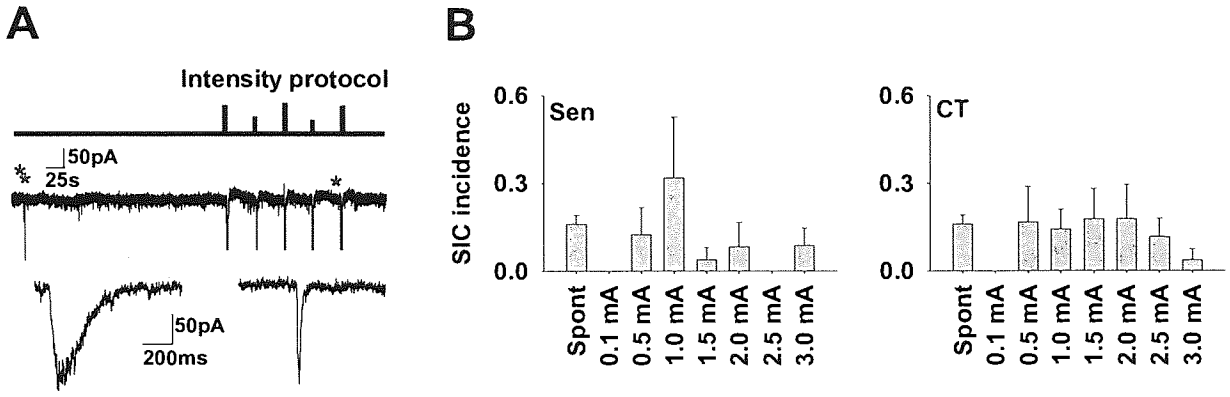

Figure 4.3.3: SIC incidence is not dependent on stimulus intensity. A) Protocol (top) illustrating pattern of stimulation delivered at different intensities (0.5-3mA) to CT input. The responses of the TC neuron are shown in the example trace below, with SICs indicated by asterisks. The neuronal post synaptic current is curtailed for clarity. Expanded example SICs are shown beneath. **B)** Bar graphs show the relationship of mean incidence of SICs to stimulus different stimulus durations.

Mean SIC incidence during the stimulation phase from the above protocols was pooled together and compared to the mean spontaneous incidence in order to assess the overall effect of stimulation on astrocytic signalling. Overall there was a 27.1% decrease in the SIC incidence during stimulation (Spont. 0.16±0.03 SICs/min; Stim. 0.12±0.02 SICs/min; Student's t-test $p=0.22$, $n=76$). Data were further divided into subsequent control for sensory and CT. No significant difference was observed during sensory stimulation (Ctrl. 0.1458±0.0472 SICs/min; Stim. 0.1341±0.0395 SICs/min; paired Student's t-test, $p=0.8$). However, SIC incidence decreased by 40.7% during CT stimulation (Ctrl. 0.1736±0.0385 SICs/min; Stim. 0.1029±0.0246 SICs/min, $p=0.05$). Figure 4.3.4 summarises the data.

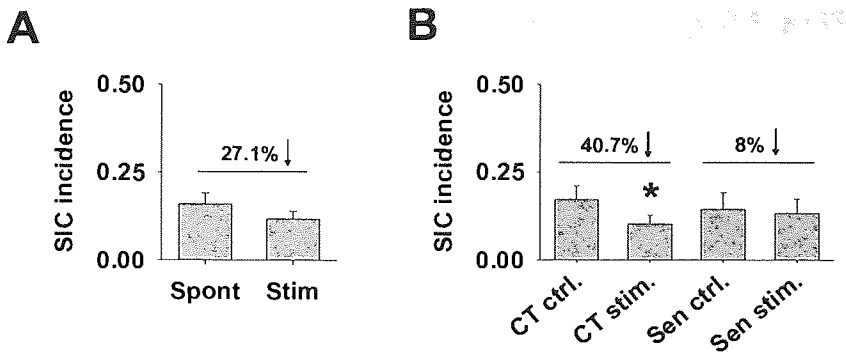

Figure 4.3.4: SIC incidence decrease during stimulation. A) Mean SIC incidence (SICs/min) comparing the overall effect of pooled control versus stimulation data. **B)** Overall incidence change between control and Sen or CT inputs.

The above stimulus frequency and duration protocols compared SIC incidence with stimulation patterns rather than with changes in PSC amplitude elicited by different stimulus frequencies and durations. Thus, SIC incidence was plotted against the mean amplitude of evoked PSC per stimulus type. As shown in figure 4.3.5, SIC incidence was not correlated with an increase in PSC amplitude consistent with the data from the stimulus intensity protocol.

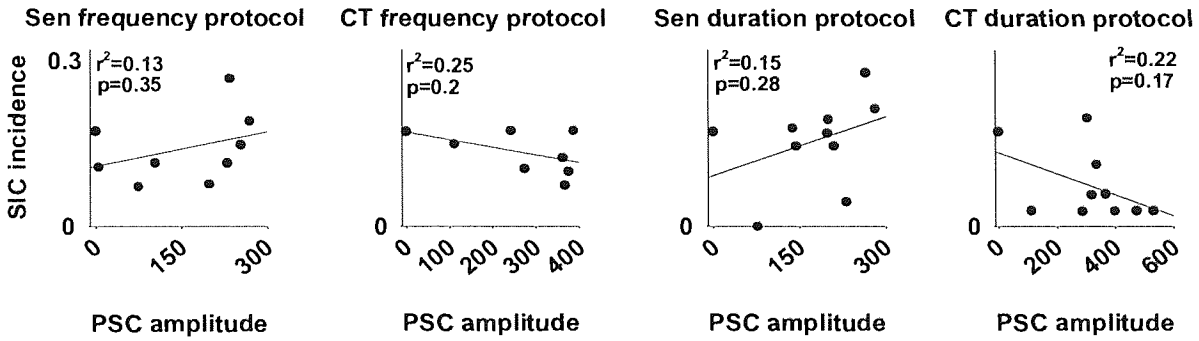

Figure 4.3.5: SIC frequency is not dependent on PSC amplitude. Mean SIC incidence was plotted against the mean post-synaptic current (PSC) peak amplitude per type of stimuli within each protocol. Y-axis scale on the right is same for all graphs.

Because of the developmental changes in the thalamus during the first three post-natal weeks, SIC incidence was compared with the post-natal age. Figure 4.3.6A compares PN age with the overall SIC incidence data from spontaneous control period and following stimulation protocols (n=76 cells). There was no significant correlation between the age and SIC incidence in either category, although a trend towards a decrease with maturation was seen during the stimulation protocols (Spont. r^2=0.0001, Pearson's correlation p=0.9; Stim. r^2=0.04, p=0.07). Correlation was also tested between the two inputs (Fig. 4.3.6B). SIC

incidence during sensory stimulation was not changed (r^2=0.01, p=0.5, n=35) whilst during CT stimulation a decrease with age was observed (r^2=0.18, p=0.03, n=41).

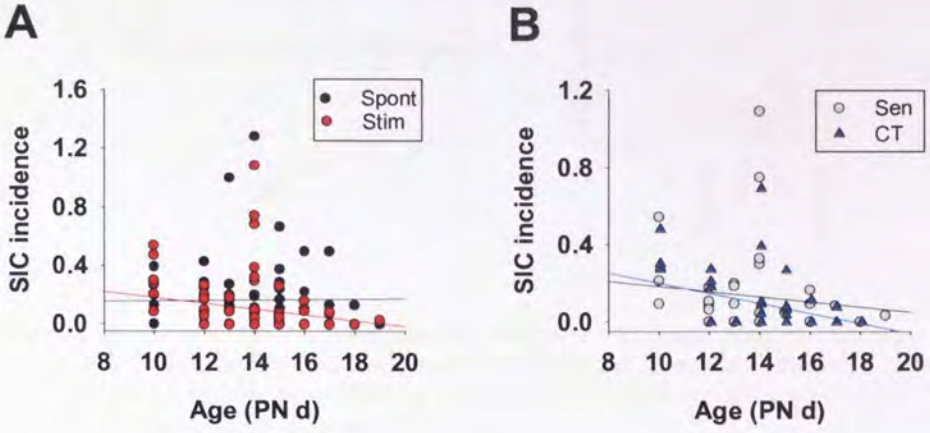

Figure 4.3.6: Post-natal age versus SIC incidence. A) Scatter plot showing SIC incidence before and during stimulation protocols against PN day. **B)** Scatter plot showing SIC incidence during Sen and CT stimulation protocols against PN day.

4.4 Astrocytes do not function as coincidence detectors

Perea & Araque [2005] speculated that astrocytes function as coincidence detectors as Ca^{2+} responses were potentiated during simultaneous Schaffer collateral and alveus stimulation, particularly at theta frequencies. Here, the possibility that astrocytes act as co-incidence detectors of simultaneous sensory and CT input was tested by combining apparent optimal parameters from the above data to their respective inputs, first separately and then simultaneously. By "apparent optimal" stimulation parameters I mean that SICs were most often, even if not significantly, detected after particular stimulation parameters. Thus the parameters for sensory input were 10s stimuli at 20Hz and for CT input 0.2s at 50Hz (each combination repeated four times). If SIC incidence was modulated by the apparent optimal parameters, repeated stimulation by these combinations would be expected to increase the overall SIC incidence with respect to spontaneous events. Although 85% of the cells (n=27) expressed SICs during the stimulation protocols, mean SIC incidence was not significantly increased either with the apparent optimal stimulation parameters or during simultaneous stimulation (Spont. 0.142±0.026 SICs/min; Sen 0.136±0.041 SICs/min, Student's t-test p=0.9; CT 0.204±0.049 SICs/min, p=0.2; and Sen+CT 0.116±0.027 SICs/min, p=0.6). This supports the above results that SIC frequency is not increased by acute synaptic stimulation neither do astrocytes function as coincidence detectors. Figure 4.4 summarises the results.

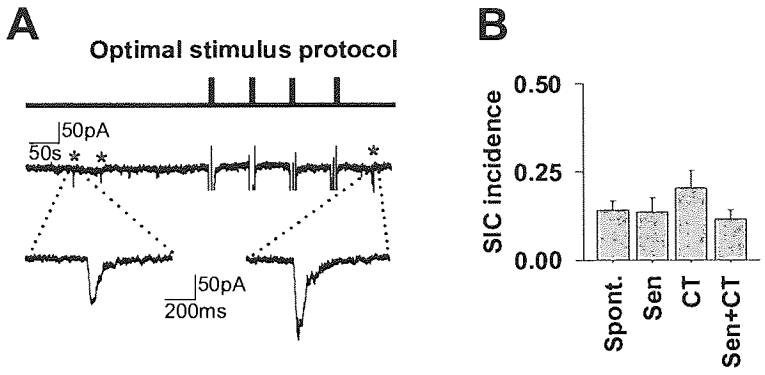

Figure 4.4: Astrocytes do not act as co-incidence detectors. A) Each vertical bar (top) represents a simultaneous Sen and CT stimulus episodes combined of the optimal parameters. Below is an example trace showing synaptic responses (vertical lines represent stimulus artefacts and inward currents) and SICs (marked with red asterisks). **B)** Bar graph summarises the SIC incidence.

4.5 Physiological state dependent stimulation does not increase SIC prevalence

Considering the nature of the thalamic network, neuromodulators involved in regulation of sleep and arousal could be critical. As described in the introduction, the thalamocortical network undergoes distinct functional changes: during sleep, cortex and thalamus are engaged in low frequency oscillations whereas in arousal they may be engaged in high frequency gamma oscillations [Steriade *et al.*, 1996; Castro-Alamancos, 2004]. We therefore tested more physiological stimulation patterns. These included stimulation of CT afferents with patterns resembling sleep spindles and slow oscillations as described by Rosanova & Ulrich [2005] (see materials and methods) and bath application of the cholinergic receptor agonist carbachol (CCh) and the β-adrenoceptor agonist isoproterenol (Isop.) in conjunction with afferent stimulation to mimic the release of ACh and NA from the brain stem afferents during arousal.

Sleep spindle stimulation was delivered via CT afferents either as a single SSP stimulation (Fig. 4.5.1A), or a train of 30 SSPs repeated four times (SSPx30x4; Fig 4.5.1B). SSP stimulation did not increase SIC incidence significantly (Ctrl 0.21±0.098 SICs/min; SSP 0.39±0.14 SICs/min; paired Student's t-test p=0.4, n=6 cells). Nor did trains of SSP; 47% of cells showed SICs following the SSPx30x4 protocol with an average SIC incidence of 0.076±0.024 SICs/min compared to spontaneous 0.109±0.039 SICs/min (Paired Student's t-test p=0.53; n=17).

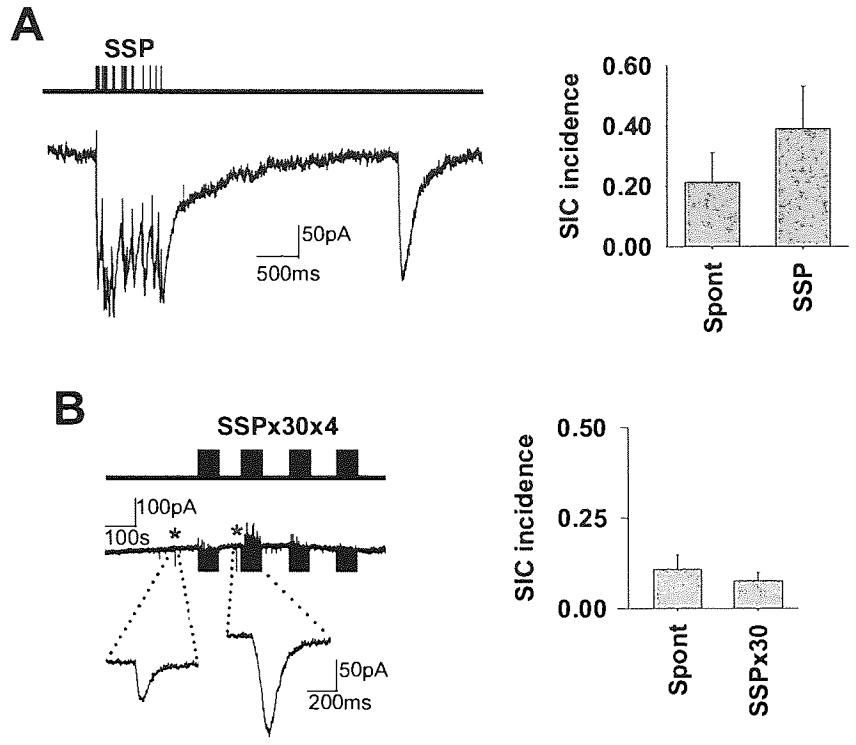

Figure 4.5.1: SIC incidence is not increased during "sleep" activity. A) Vertical bars at the top represent the SSP stimulation pattern. Trace below shows the post synaptic current in response to SSP stimulation (left) following with delayed SIC (right). Bar graph on the far right summarises the mean frequency before and after SSP stimulation. **B)** Stimulus protocol at the top and trace below with stimulus responses (black vertical bars) and SICs (asterisked and expanded beneath). Bar graph on the right shows the mean SIC incidence before and during protocol.

The cholinergic and noradrenergic inputs from the brain stem afferents depolarise thalamic neurons, allowing switching of the thalamus into active relay mode [McCormick, 1992; Castro-Alamancos, 2002]. Figure 4.5.2A summarises the hypothesis that depolarising TC neurons with ACh- and NA- receptor agonists would increase the SIC detection or synergistically activate astrocytes. Indeed, it has been reported that ACh and NA elicit $[Ca^{2+}]_i$ responses in the VB astrocytes [Parri & Crunelli, 2001]. Following the stimulation protocol, CCh (50μM), Isoproterenol (50μM) or both were applied and stimulation was repeated. SIC incidence was then compared to the preceding control period. All procedures, however, failed to increase the SIC incidence as summarised in figure 4.5.2B (Spont 0.066±0.037 SICs/min vs. Stim 0.13±0.037 SICs/min, paired Student's t-test p=0.1, n=12; CCh ctrl 0.04±0.04 SICs/min vs. CCh stim 0.036±0.036 SICs/min, p=0.9, n=5; Isop ctrl 0.0±0.0 vs. Isop stim 0.064±0.064 SICs/min, p=0.4, n=3 and CCh+Isop ctrl 0.13±0.054 SICs/min vs CCh+Isop stim 0.1514±0.0849 SICs/min, p=0.8, n=8). SIC incidence during stimulation with CCh/Isoproterenol was not significantly different to the spontaneous incidence either (p>0.3).

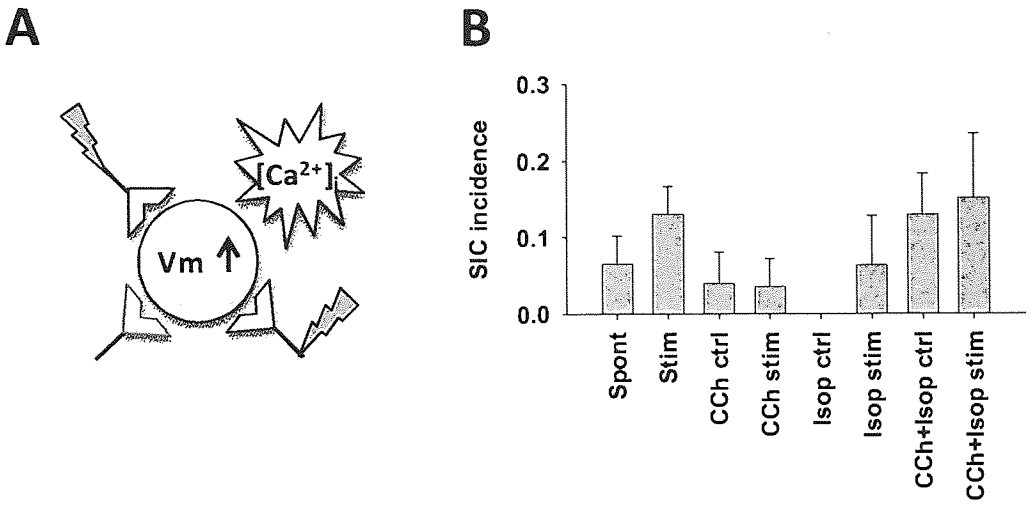

Figure 4.5.2: Stimulation with neuromodulators does not increase SIC incidence. A) Schematic of the hypothesis for using neuromodulators during stimulating Sen and CT inputs (lightning bolt). Pink synapse mimics the activation of brain stem afferents (not preserved in the slices preparation) by applying exogenous CCh (50μM) and Isop (50μM). This can change neuronal properties to detect SICs due to depolarization effect or enhance astrocytic responses **B)** Bar graph summarising the SIC incidence for each stimulation trial.

4.6 SIC incidence is not affected by the absence of action potential dependent neurotransmitter release

Abolition of delayed astrocytic Ca^{2+} responses in the presence of TTX and Cd^{2+} has been previously linked to neurotransmitter release from synaptic terminals [Perea & Araque, 2005; D'Ascenzo, 2007]. Furthermore, Xu *et al.* [2007] showed that SIC frequency was increased by methods that enhanced presynaptic glutamate release. This increase in SIC frequency was inhibited by TTX, suggesting that direct AP dependent glutamate release is involved. Here, after a control stimulation protocol, TTX (1μM) was bath applied and the protocol was repeated. Synaptic inward currents were completely blocked by TTX (Ctrl 570.5±49.3pA; TTX 0pA; paired Student's t-test, p=0.00008, n=10, data not shown) as illustrated in figures 4.6 A and C. However, SICs were unaffected: mean SIC incidence during stimulation in the absence of action potential dependent glutamate release was not changed (Ctrl 0.067±0.03 SICs/min; TTX 0.05±0.02 SICs/min; paired Student's t-test p=0.5; n=10; Fig. 4.6D). Consistent with the lack of effect of any stimulation protocol shown above, this supports the findings that even though afferent stimulation elicited astrocytic Ca^{2+} increases in the VB, the spontaneous SIC activity is unaffected in our experimental conditions.

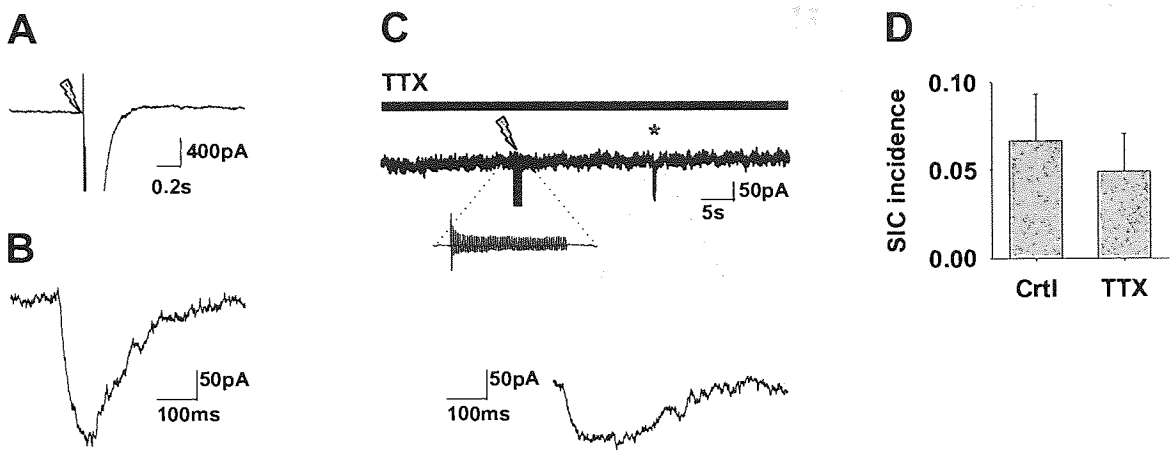

Figure 4.6: SIC incidence is not affected by absence of AP induced Glu release. A) Example of the postsynaptic inward current in response to stimulation indicated by lightning bolt. Excitatory inward current is shown partially. **B)** SIC from the same recording. **C)** In presence of TTX, inward current was abolished (same neuron), indicating blockage of action potential mediated transmitter release whereas SICs were still detected. Black vertical bar indicates stimulation artefact (expanded beneath). SIC is indicated with an asterisk and expanded beneath. **D)** Mean SIC incidence during control stimulation and in presence of TTX.

4.7 SIC incidence was not increased by inhibition of astrocytic Glu-Gln cycle

Next we investigated whether increasing cytosolic glutamate concentration in astrocytes would enhance SIC generation. Glutamate which escapes the synaptic cleft during action potential firing is cleared by astrocytic transporter uptake and recycled back to neurons via the glutamate-glutamine cycle (see introduction). Previous studies have shown that by inhibiting the conversion of glutamate into glutamine, the subsequent accumulation of glutamate inside the astrocytes resulted in increased SIC frequency [Takano *et al.*, 2005; Xu *et al.*, 2007]. We investigated whether this would work in our experimental conditions as outlined in figure 4.7A. The glutamine synthetase inhibitor MSO (2-5mM) was bath applied and SIC incidence was compared before and after stimulation. Surprisingly, this treatment also failed to increase SIC incidence (MSO Ctrl 0.1757±0.0856 SICs/min; MSO stim. 0.1555±0.0903 SICs/min, paired Student's t-test, p=0.9, n=7; Fig. 4.7B). Compared to average spontaneous SIC frequency, MSO treatment did not change the SIC incidence significantly either (Spont. 0.09±0.02; MSO 0.17±0.06; Student's t-test p=0.2; n=98, 13 respectively).

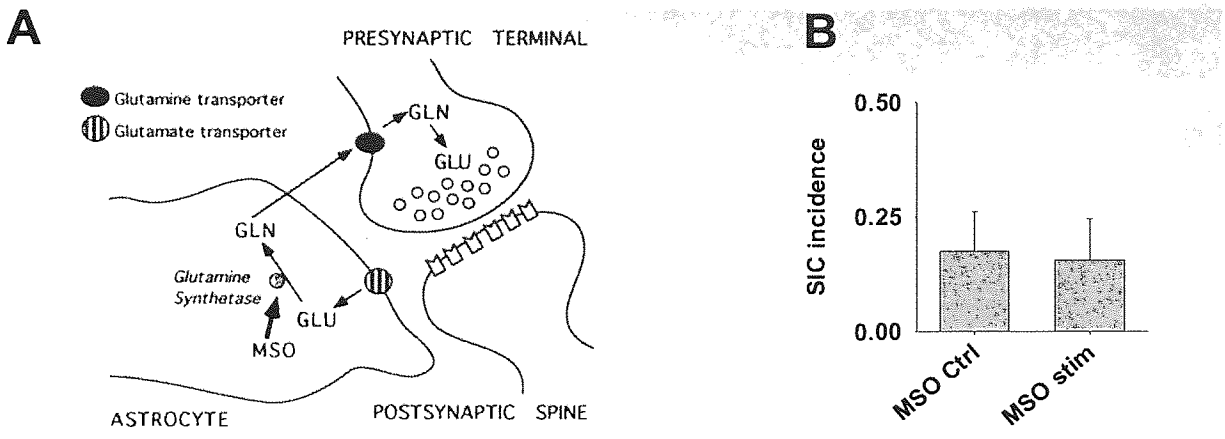

Figure 4.7: SIC incidence is not affected by accumulating cytosolic glutamate. A) MSO inhibits the conversion of glutamate (Glu) into glutamine (Gln). As a consequence, Glu released during synaptic stimulation accumulates into the astrocytes, which is then expected to enhance the chances for astrocytic glutamate release. [Figure from Bacci *et al.*, 2002]. **B)** Bar graph summarising the effect of MSO before and after stimulation.

4.8 SIC properties show some differences during stimulation

SIC amplitude, rise time, decay time and area were compared before and during stimulation protocols. Spontaneous SICs were compared to pooled data for Sen, CT and simultaneous stimulation from experiments including different stimulus frequencies, durations, intensities and optimal parameters. Data are summarised in figure 4.8.1 and the mean values are listed in tables 4.8.1 and 4.8.2. SICs were significantly increased in amplitude during sensory stimulation (Student's t-test, $p<0.005$). Rise time and area during CT stimulation were also significantly increased ($p=0.03$ and $p=0.05$, respectively). Decay time was slightly increased during CT stimulation ($p=0.07$). Changes during CT stimulation are most likely due to few large outliers in the data as seen in figure 4.8.1. Other parameters were not significantly different ($p>0.05$).

Amplitude (pA)	Spont	Sen	CT	Sen+CT	Area (pA*ms)	Spont	Sen	CT	Sen+CT
Mean	143.30	**317.47**	172.95	101.56	Mean	26752.66	62173.418	**122687.2**	12163
Median	100.70	**178.62**	109.05	80.32	Median	12110.95	26166.8	**18067.31**	9283
Std.Dev	127.68	**308.74**	170.66	63.82	Std.Dev	50217.75	201992.62	**512014.7**	8832
Std.Err	11.70	**32.37**	15.98	15.95	S.E.M	4682.83	21411.175	**49731.26**	2280

Table 4.8.1: SIC amplitude and area during stimulation. (n=SICs: Spont 119, Sen 91, CT 114, Sen+CT 16). Significantly different values are highlighted in **bold** (amp. $p<0.005$, area $p=0.05$).

Rise time (ms)	Spont	Sen	CT	Sen+CT	Decay time (ms)	Spont	Sen	CT	Sen+CT
Mean	61.49	63.34	**189.67**	51.61	Mean	307.72	422.18	880.10	184.60
Median	40.50	34.84	**42.99**	36.36	Median	217.31	231.91	234.11	166.25
Std.Dev	49.31	73.31	**652.96**	34.88	Std.Dev	272.89	758.02	3435.00	78.09
Sts.Err	4.54	7.69	**61.16**	8.72	S.E.M	25.23	79.46	321.72	19.52

Table 4.8.2: SIC kinetics during stimulation. Significantly different values are highlighted in bold (p=0.03).

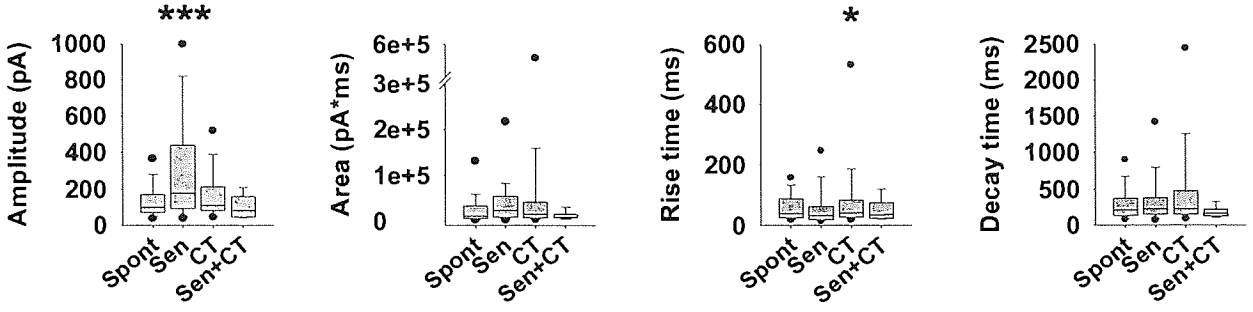

Figure 4.8.1: SIC parameters versus stimulus. Box plots show the scatter of data between different inputs. (Statistical significance is presented as $p<0.05$ *, $p<0.01$ ** or $p<0.005$ ***).

SIC from SSP, MSO, CCh and isoproterenol stimulation experiments were compared to spontaneous SICs as shown in the previous paragraph (n=119 SICs). Data are summarised in figure 4.8.2 and mean values listed in tables 4.8.3 - 4.8.5. SSP stimulation did not change SIC properties compared to spontaneous (Student's t-test p>0.1, all parameters, n=26 SICs). For experiments including treatment with exogenous agents, SICs from control and during stimulation were pooled together and compared to previous spontaneous SICs in order to see the overall effect of these agents on SIC size. CCh and Isoproterenol (50μM) had no effect on SIC size (p>0.1, n=18), neither did MSO (2-5mM; p>0.1, n=30).

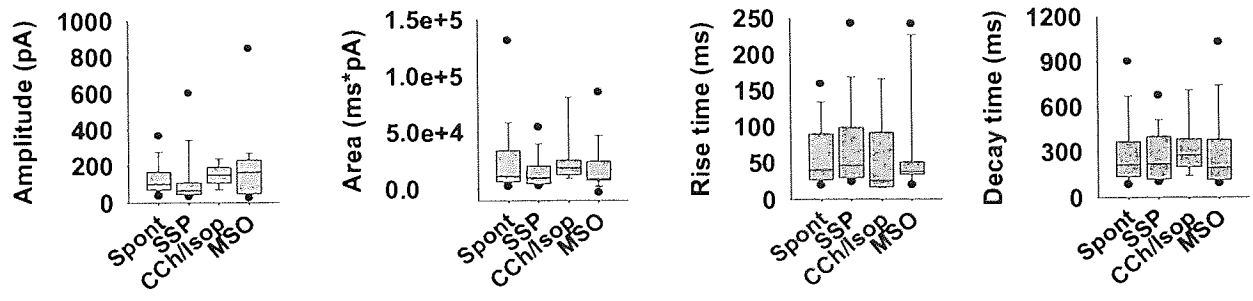

Figure 4.8.2: SIC parameters during specific stimulus protocols. Box plots show the scatter of data between different stimulation groups compared to spontaneous SICs.

SSP	Amplitude (pA)	Rise time (ms)	Decay time (ms)	Area (pA*ms)
Mean	118.341	72.9915	273.4873	15470.44
Median	65.2642	46.4531	221.5	9689.6
Std.Dev	147.5877	61.9108	174.6528	14438.88
Std.Err	28.9443	12.1417	40.0681	2887.777

Table 4.8.3: SIC parameters during SSP stimulation protocol. No significant differences were found.

CCh/Isop.	Amplitude (pA)	Rise time (ms)	Decay time (ms)	Area (pA*ms)
Mean	162.7475	59.094	371.7343	25702.19
Median	152.4589	25.5406	281.8495	18611.52
Std.Dev	102.4445	56.3456	394.752	25632.22
Std.Err	24.1464	13.2808	93.0439	6041.571

Table 4.8.4: SIC parameters during CCh/Isoproterenol treatment. No significant differences were found

MSO	Amplitude (pA)	Rise time (ms)	Decay time (ms)	Area (pA*ms)
Mean	168.3	63.2288	298.2175	17318.3074
Median	142.7974	38.2002	194.141	9108.9575
Std.Dev	213.7024	66.5569	267.4518	21855.8191
Std.Err	39.0165	12.1516	48.8298	3990.3084

Table 4.8.5: SIC parameters during MSO treatment. No significant differences were found.

4.9 SIC timing is independent of synaptic stimulation

Astrocytic Ca^{2+} responses were shown to occur with an average 6.89±0.17s (n=12 slices, 293 astrocytes) delay from the onset of stimulation. A peak in the delayed SIC timing at a particular latency to Ca^{2+} responses would suggest a presence of synaptically evoked, astrocyte mediated SICs. Time delay was measured from the onset of the stimuli as indicated in figures 4.9 A and B. SIC latencies were pooled from all the stimulation experiments, excluding SSPx30x4 and experiments treated with TTX, CCh, Isoproterenol and MSO, and compared with astrocytic Ca^{2+} responses (Fig. 4.9 C and D). Time delay of SICs following sensory stimulation ranged from 0.37 to 173.3 seconds. Delay after CT stimulation ranged between 0.85 and 100.7s, and 4.8-150.9s following simultaneous stimulation. The astrocytic Ca^{2+} elevations ranged from 2 to 20 seconds during sensory stimulation and from 2 to 18 seconds during CT stimulation. On average SICs occurred 26.1 seconds later than Ca^{2+} responses. However, the overlapping frequency histograms showed a clear peak for the Ca^{2+} responses, but, it failed to reveal any relevant peak for the SIC latencies.

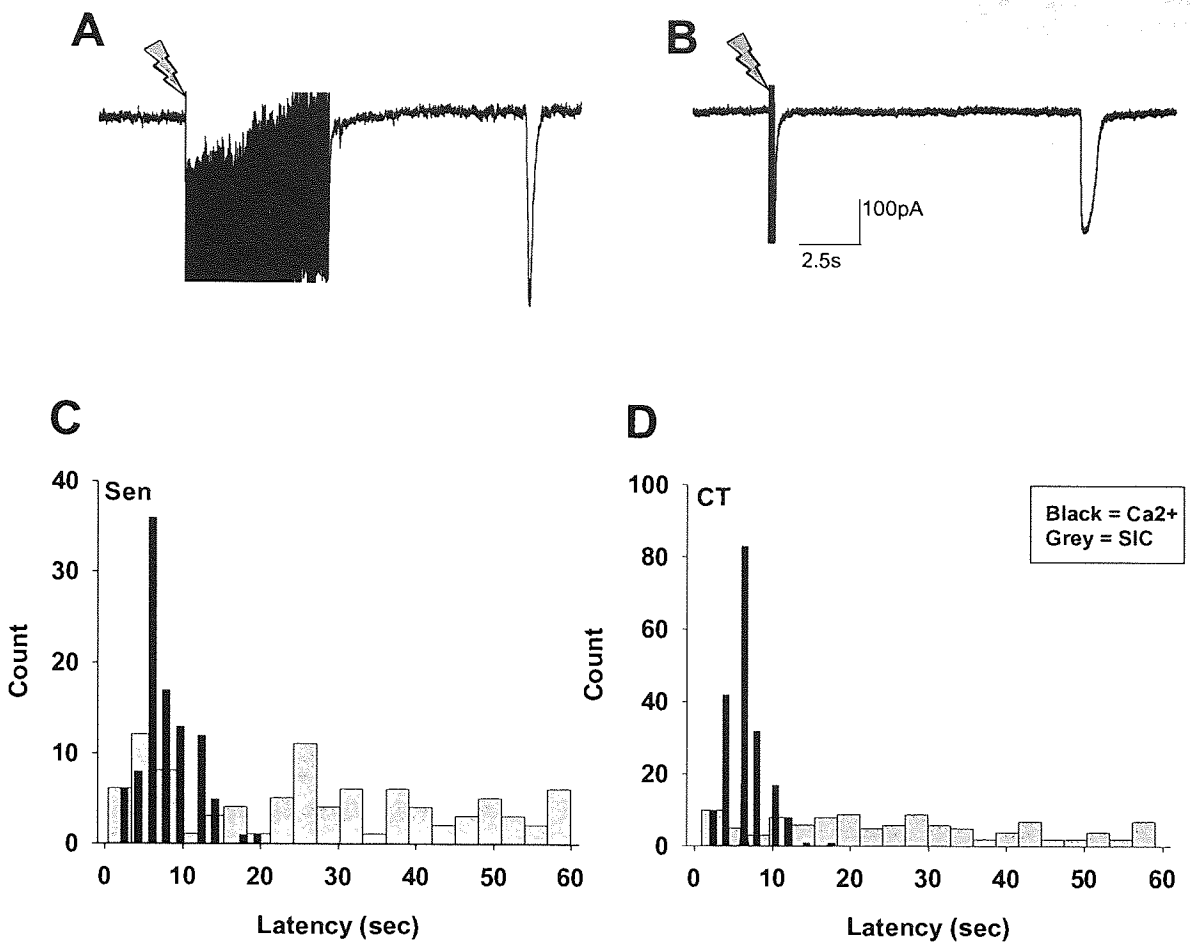

Figure 4.9: SIC timing is independent of synaptic stimulation. A) Example of 5s long stimulus at 50Hz delivered on sensory afferents. Stimulus onset is indicated with lightning bolt followed by an inward current and stimulus artefacts. A SIC was observed within few seconds from the onset of stimuli. **B)** Example of 0.2s long stimulus at 50Hz delivered on CT afferent with a SIC following within few seconds. **C)** Frequency histogram showing the distribution of SIC latencies (grey bars) and Ca^{2+} delays (black bars) during sensory stimulation. **D)** Frequency histogram of latencies during CT stimulation.

As expected for the average of 60 seconds time window, mean SIC latency was 31.1±2.6s for Sen (n=100 SICs), 32.2±2.2 for CT (n=137) and 45.3±7.5s after simultaneous Sen and CT stimulation (n=21) (data not shown). Sen and CT latencies were not different from each other (Student's t-test p=0.7), but SICs following simultaneous stimulation had significantly longer delays compared to stimulation of individual inputs (p=0.0036 and p=0.0032, respectively). The difference is most likely due to the range in stimulus length itself as latencies were measured from the onset of stimuli and Sen+CT experiments only comprised optimal stimulus parameters of overall stimulus duration of 10s. Measuring SIC latency from the stimulus offset instead of from the onset did not change the latency histogram scatter (data not shown), and is therefore unlikely to contribute to the lack of peak for SIC latencies presented here.

4.10 SICs are not predictable

It has been shown previously that stimulation of afferents with the same parameters can evoke SICs repeatedly [Fellin *et al.*, 2004]. In addition, latencies following the first stimulation can predict the latency of the next response [Fellin *et al.*, 2004]. We therefore quantified how often SIC followed the same stimulus using data from the optimal stimulus parameter experiments where the same stimulus was repeated four times for each pathway or simultaneously. Reproducibility was quantified by using index where SIC following 1 out of 4 stimulations equals to 0.25 and SICs following each of the four stimulations (4/4) equals 1. In this index, reproducibility would be signified by an index of 0.5 or greater. The data are summarised in figure 4.10A-B. During sensory stimulation 44.4% of the cells exhibited SICs. Within these cells, the average reproducibility index was 0.31±0.03 (Fig. 4.10B). During CT stimulation, 48% of the cells exhibited SICs with reproducibility index of 0.46±0.06. Simultaneous sensory and CT stimulation exhibited SICs in 44.4% of the cells with index of 0.28±0.02. Within the data with index of ≥0.5 (n=13), no correlation was detected between the first and second responses (r^2=0.008, Pearson's correlation p=0.8; Fig. 4.10C), suggesting that the SIC did not occur in response to that particular stimulus.

A

Index	Sen	CT	Sen+CT
0	15	14	15
0.25	9	5	10
0.5	3	6	2
0.75	0	1	0
1	0	1	0

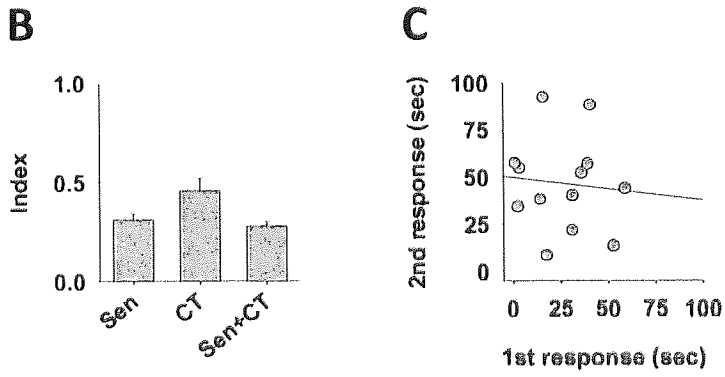

Figure 4.10: SICs are not predictable. A) Table showing the number of recordings against the index value of how often SICs followed the same stimulation. **B)** Mean index value for recordings with index ≥0.25. **C)** Scatter plot showing the latency of SICs following the first stimuli compared to latency in response to second stimuli.

4.11 Discussion

Here, we have shown that in the VB thalamus, synaptic stimulation elicits astrocytic Ca^{2+} increases, yet did not lead to an increase in SIC incidence. This was shown by a series of experiments testing various stimulation parameters, including more physiological scenarios

using sleep spindle stimulations as well as neuromodulators mimicking ACh and NA release from brain stem afferents during arousal. As several previous studies have provided evidence that astrocytic Ca^{2+} increases were accompanied by glutamate release and synaptic modulation as discussed in the introduction, the lack of effect here points towards different mechanisms.

It must be noted that the increase in SIC frequency in response to afferent stimulation seen by other groups occurred only in about 27-43% of the cells [Fellin *et al.*, 2004; D'Ascenzo *et al.*, 2007]. Furthermore, more robust methods that elicit astrocytic Ca^{2+} increases such as agonist application, direct mechanical stimulation or UV-photolysis of Ca^{2+}, also evoked SICs only in about half of the cells (28-83%) [Araque *et al.*, 2000; Fellin *et al.*, 2004, 2006; D'Ascenzo *et al.*, 2007]. The increase was often stated only for the responding cells. Therefore, the lack of effect here could reflect different analytical methods. Here, it was also noticeable that higher SIC incidence during spontaneous control period was followed with lower SIC incidence during stimulation protocols, whilst absence of SICs during control was accompanied with significantly increased chances of detecting SICs during stimulation protocols (data were not shown). This pattern seems to fit with the profile of spontaneous SIC appearance at low frequencies with a tendency to periods of higher and lower probability (chapter 3). SIC incidence after stimulation only for these responding cells (SICs occurring during stimulation protocols) was therefore checked, and this did not change the result outcome (data were not shown). Thus, these alternative data analysis only support the lack of effect by acute synaptic stimulation.

Some variation in SIC properties was observed. For example, SICs following sensory stimulation protocols were shown to be higher in amplitude. This may reflect that a small population of SICs during sensory stimulation was influenced by the synaptic stimulation, however not strongly enough to be picked up by analysing the mean incidence changes relative to spontaneous activity. If this was true, we would expect to see the same changes by sensory afferent stimulation in the future experiments. However, considering the unpredictable nature regarding the prevalence and magnitude of spontaneous SICs as outlined in chapter 3, it is not surprising that some variation existed. Nonetheless, the lack of significance in most SIC parameter comparisons only further supports the general lack of effect of synaptic stimulation.

Even though astrocytes have been shown to respond to increases in stimulus strength by an increase in the magnitude of the $[Ca^{2+}]_i$ elevations, we did not assess the Ca^{2+} responses for more than 1-2s long stimulations at 50Hz. It is worth noting that in our experiments, relatively large postsynaptic currents were observed even with the lowest stimulation intensities and shorter durations, thus we would expect astrocytes to detect most of them. The increase in the postsynaptic current amplitude in response to increase in stimulus intensity and duration in our experiments, was not generally correlated with the SIC incidence, suggesting that SICs were not dependent on the amount of glutamate detected by the postsynaptic neuron and presumably by the synaptically associated astrocytes. Saying that, it is tantalising to speculate, that the *weak* correlation with the increase in SIC incidence by increasing stimulus duration during sensory stimulation was real, as SICs were never observed after 2ms stimulation and single shots to afferents have been shown ineffective at eliciting astrocytic Ca^{2+} increases [Beierlein & Regehr, 2006].

The finding that overall SIC frequency often decreased following stimulation rather than increased (Fig. 4.3.4), adds complexity to the interpretation of the results. The reason for an apparent decrease in SIC incidence following stimulation episodes is unclear. However, due to the method of calculating SIC incidence in the 60s after stimulation episodes, it may be expected that some episodes would have low values for SIC incidence. However, what is clear is that there is no increase in SIC incidence following synaptic stimulation. In concern that we should not only focus on the increase in incidence in respect to spontaneous activity, we looked at the patterns within the stimulation protocols. As shown for example in figure 4.3.2 for different stimulus durations delivered on CT afferents, SICs were most often seen after 0.2s stimulation and a weak trend was seen with increasing the stimulus duration during sensory stimulation. However, even after several repeated stimulations by these apparent optimal parameters, the overall SIC incidence was not increased.

In conclusion, these results seem to be in agreement with Beierlein & Regher [2006], Fiacco *et al.* [2007], Petravicz *et al.* [2008] and Shigetomi *et al.* [2008] who all reported that increase in astrocytic Ca^{2+} elevations was not accompanied with modulation of synaptic transmission or generation of SICs. The fact that SICs occur at extremely low frequencies in general makes the evaluation more difficult. Whether acute synaptic stimulation decreased the SIC incidence by unknown mechanisms or whether the decrease occurred by chance, requires further, alternative experiments, preferably in preparations with already enhanced spontaneous SIC activity.

Chapter 5

Effect of prolonged synaptic stimulation on SIC frequency

In the *in vivo* situation, the thalamus would be expected to receive continual sensory and CT input in both awake and sleep states [Steriade, 2006]. Since moderate stimulation was not able to increase SIC incidence, we tested whether SIC incidence can be modified with prolonged synaptic activity. *In vivo* studies in the cerebral cortex have shown a higher percentage of active astrocytes than in brain slice preparations, and that increased neuronal activity was associated with increased astrocytic Ca^{2+} signalling [Hirase *et al.*, 2004]. Additionally, continuing neuronal activity may increase the glutamate supply at the synapse. In support for this hypothesis is one previous study where spontaneous SICs started to emerge only after repeated glutamate exposure [Xu *et al.*, 2007]. The authors demonstrated that this was due to an emergence of larger glutamate vesicles with increased probability of Ca^{2+} dependent exocytosis in response to repeated exposure to glutamate.

Considering these data, we proposed the hypothesis that continuing neuronal activity enhances astrocytic Ca^{2+} signalling, which then lead to SIC generation (Fig. 5.0). To investigate this, two approaches were applied; firstly we record the SIC frequency whilst stimulating to monitor both neuronal and astrocyte mediated changes; secondly we stimulated the slice for a prolonged period and recorded spontaneous activity, both astrocytic Ca^{2+} signals and SICs, after ceasing the stimulation.

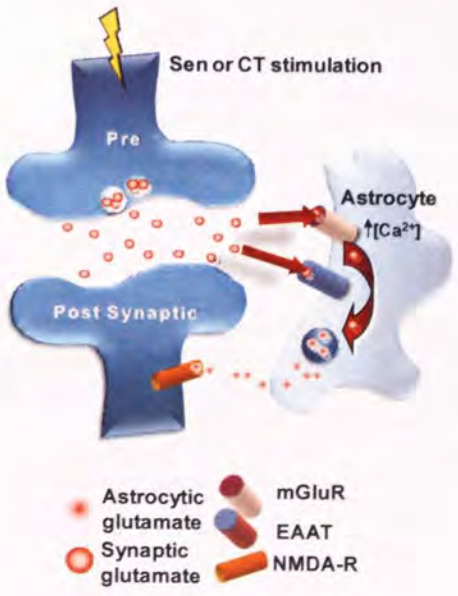

Figure 5.0: Long term stimulation model. Enhanced astrocyte-to-neuron signalling may be recruited by stimulations that mimic continuous neuronal activity *in vivo*. Long term stimulation may increase the frequency of astrocytic $[Ca^{2+}]_i$ elevations via enhanced mGluR activation, thus increasing subsequent glutamate release and SIC generation. Alternatively, increased glutamate supply and possible accumulation into astrocytes via excitatory amino acid transporters (EAATs) can increase the glutamate concentration available in astrocytes for the, presumably, Ca^{2+} dependent vesicular release.

5.1 Long term stimulation increases SIC incidence over time

First we assessed the effect of long term stimulation (LTS) whilst recording from TC neurons. LTS consisted of bursts of 10 pulses at 50Hz delivered to sensory or CT input every 10s for up to 30 minutes in P10-15 slices. This revealed an increase in the incidence of SICs over the course of stimulation as show in the example on figure 5.1.1A. The raster plot shows the SIC occurrence over time for each TC neuron (Fig. 5.1.1B). Number of SICs in the first 10 minutes for sensory stimulation was 0.6±0.22 and in the last 10 minutes 1.9±0.6 (Paired Student's t-test p=0.02, n=10). Numbers for CT stimulation were 0.38±0.18 and 1.5±0.65 respectively (p=0.1, n=8). Histograms in figure 5.1.1C show the increase in number of SICs over time: During sensory stimulation, SIC incidence was positively correlated with increased time stimulated (r^2=0.8, Pearson's correlation, p=0.008; linear fit not shown) whereas increase during CT stimulation was not significant (r^2=0.4, p=0.07).

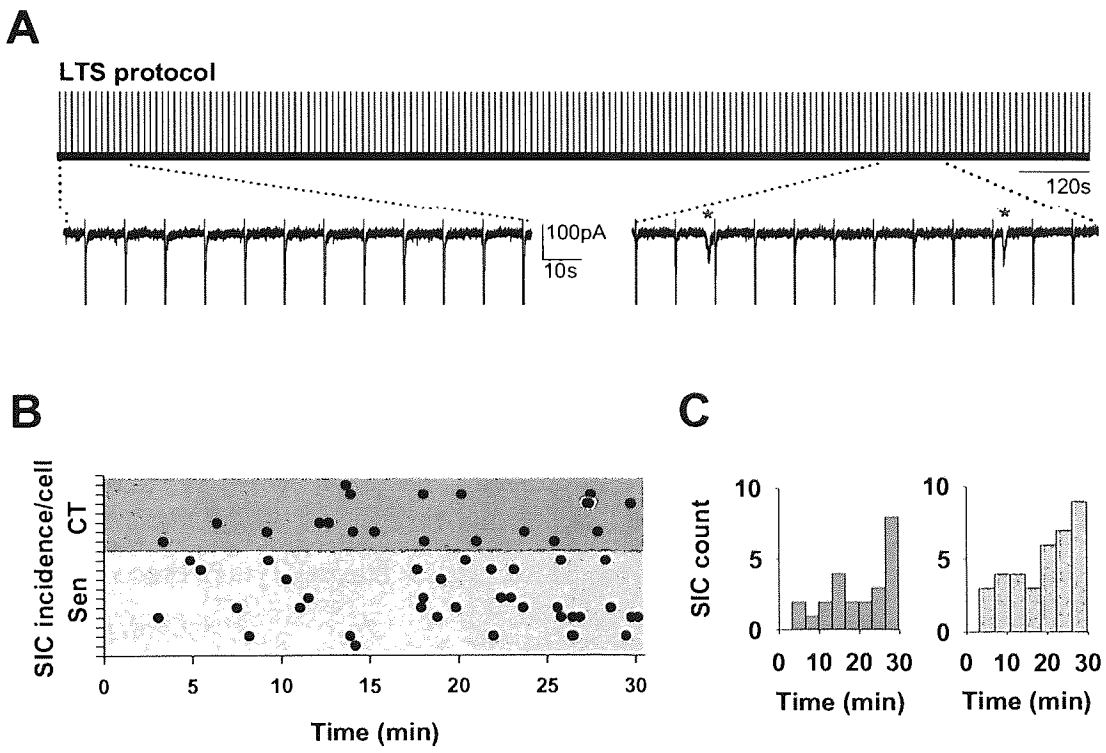

Figure 5.1.1: LTS stimulation increases SIC incidence over time. A) Top bar shows the 30 minute long LTS protocol. Below are two examples of 2 minute sections from the first 10 minutes of stimulation (left) and from the final 10 minutes (right) during which SICs were observed (red asterisk). **B)** Raster plot displays the data for SIC incidence (black dots) during a 30 minute LTS protocol for CT (dark grey) and Sen inputs (light grey). White circle indicate a point of 6 events overlapping. **C)** Histograms for SIC incidence during CT (dark grey) and Sen (light grey) inputs over time.

We took this opportunity to measure SIC amplitude during sensory stimulation since in chapter 4 SICs occurring during moderate sensory stimulation were significantly higher in amplitude. Here, SICs during long term stimulation of sensory afferents were compared to spontaneous SICs at the same age group. SIC amplitude was not different (Spont. 124.3±11.6pA; Sen 91.2±22pA; Student's t-test p=0.2; n=105, 38 respectively; data not shown), suggesting that the increase in amplitude with sensory stimulation presented in chapter 4 was not due to the synaptic stimulation effect. SIC amplitude during CT input (112.1±2pA, n=24) was not different to spontaneous SICs or to the ones occurring during sensory stimulation ($p>0.6$, both comparisons).

With the hypothesis that long term stimulation enhances SIC frequency, which the above data suggests, it is important that the synaptic glutamate release is maintained. Therefore we assessed the stability of postsynaptic current during LTS protocol by measuring the peak amplitude at 5 minutes intervals. Interestingly, neurons exhibited either facilitation or depression in the PSC amplitude as shown in figure 5.1.2A. As shown in figure 5.1.2B, synaptic efficacy was at least maintained if not increased (Sen r^2= 0.7 Pearson's correlation p=0.02; CT r^2=0.3, p=0.05). Strong facilitation occurred in 4 out of 10 cells during sensory stimulation and in 3 out of 8 cells during CT stimulation, while depression occurred in 6/10 and 5/8 cells respectively. The average facilitation was 584.3±309.2% for Sen and 275.7±69.6% for CT, whereas depression was 56.9±12% and 50.8±11.8% of the controls respectively (Fig. 5.1.2C). The reason for such strong facilitation during sensory stimulation is difficult to explain as only CT synapses have been reported to express strong facilitation [Castro-Alamancos & Calcagnotto, 1999]. Whether the depression was due to depletion of synaptic glutamate stores and facilitation due to changes in input resistance, residual post stimulation potentiation [Diamond & Jahr, 2000] or real facilitation requires further studies.

The overall SIC incidence over the 30 minutes LTS protocol was also compared to the percentage change of the PSC amplitude. As shown in figure 5.1.2D, SIC incidence was not correlated with the changes in PSC amplitude (Sen r^2=0.075, Pearson's correlation p=0.54; CT r^2=0.05, p=0.51). Furthermore, SIC amplitude was not increased over the course of stimulation as shown in figure 5.1.2E (r^2=0.008, p=0.5).

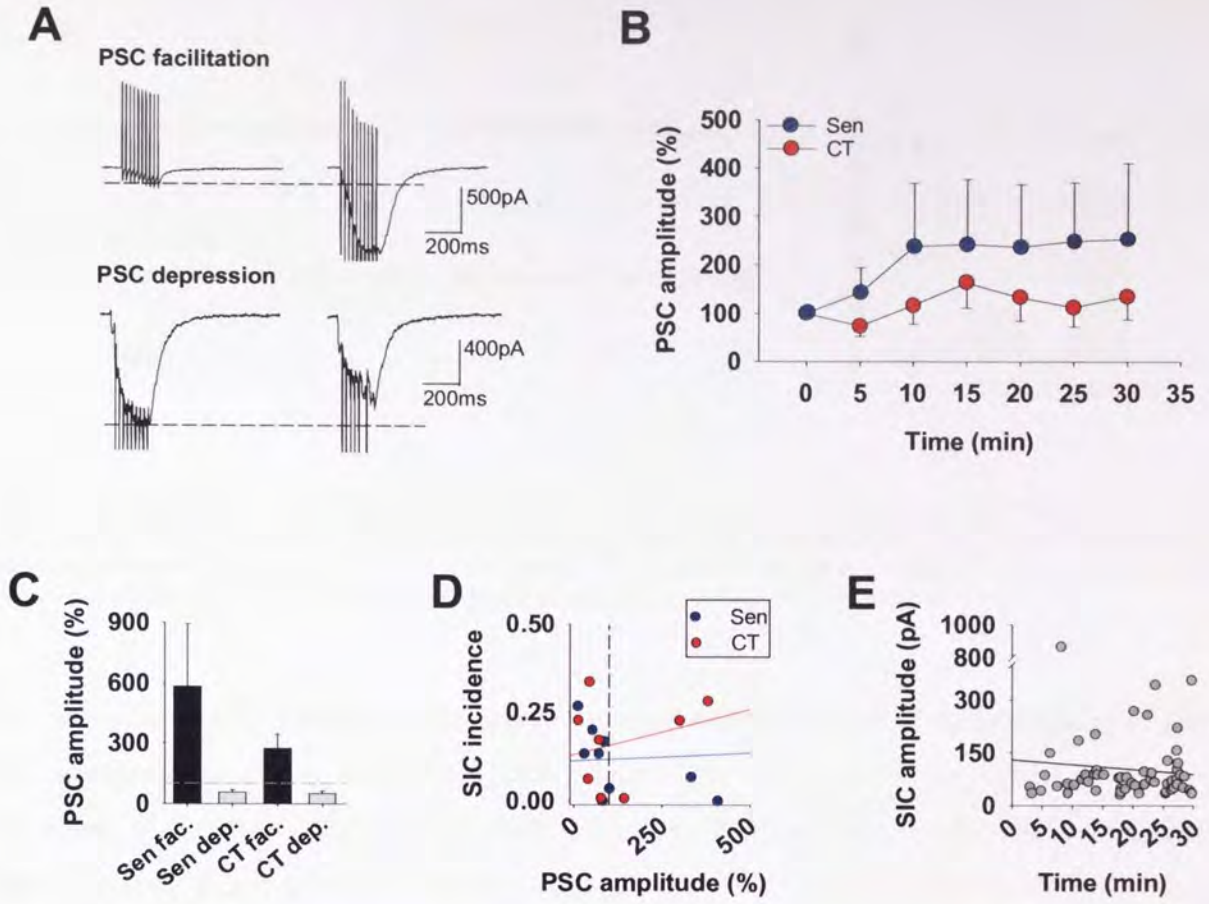

Figure 5.1.2: Post-synaptic current during LTS and SIC incidence. A) Top trace shows example of PSC facilitation. Trace on the left is the PSC at the beginning of LTS, and on the right after 30 minutes stimulation. Below is example of PSC depression. **B)** Mean scatter plot showing the amplitude change over the 30 min LTS protocol for Sen (blue) and CT (red) inputs. **C)** Average percentage change of facilitation (black) and depression (grey) for Sen and CT. Dashed horizontal line marks the 100% control. **D)** Scatter plot showing Sen (blue) and CT (red) PSC amplitude as % change against the SIC incidence. Dashed vertical line represents the 100% control: facilitated values are to the right and depressed values to the left. One outliner for Sen is not shown in the graph (PSC 1491% of control vs. 0.23 SICs/min). **E)** Scatter plot showing the SIC amplitude against the course of stimulation.

5.2 LTS induces Long Term Enhancement of SIC frequency

To assess whether the SIC frequency increase was due to an emergence of evoked responses or changes in the glutamate release properties of the astrocytes, a modified LTS protocol (20 pulses every 5s) was applied to both sensory and CT inputs for up to 60 minutes, and recordings were then made after ceasing the stimulation. Figure 5.2.1A shows two examples of control recordings (non-stimulated) and two examples after the 60 minutes LTS protocol. The average frequency of all control slices was compared to stimulated slices. This revealed a significant 265% increase in the post LTS SIC frequency (Ctrl 0.086±0.01 SICs/min; post LTS 0.314±0.06 SICs/min; Student's t-test $p=0.0001$; M-W test $p<0.005$; $n=73$, 53 respectively; Fig. 5.2.1B).

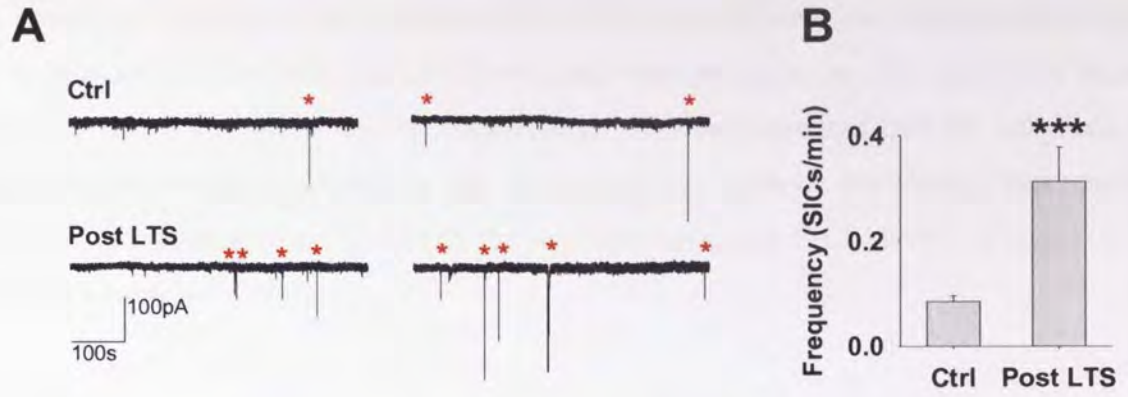

Figure 5.2.1: LTS increases SIC frequency. A) Traces at the top show 10 minute representative recordings of SIC activity in non-stimulated slices (SICs indicated with red asterisks). The two traces below show representative recordings after a 60 min LTS protocol. **B)** Mean SIC frequency from control versus post LTS stimulated slices. (Statistical significance is presented as $p<0.05$ *, $p<0.01$ ** or $p<0.005$ ***).

The increase in SIC frequency was due to an increased population of cells showing higher SIC incidence as shown in figure 5.2.2A (range: Ctrl 0-0.36 SICs/min; post LTS 0-2.84 SICs/min; K-S test $p<0.005$; n=73, 53 respectively). 75.5% of the post LTS cells exhibited SIC frequency that was above a control value of mean+S.E.M (higher than 0.096 SICs/min). 16.4% of the control recordings showed no SICs at all, whereas after LTS 5.7% of the cells did not exhibit SICs. Furthermore, inter event interval was calculated for the cells with ≥2 SICs (Fig. 5.2.2B). In control slices, 56.2% (41/73) of cells had an average IEI of 5.55±0.45 minutes, and for post LTS cells 86.8% (46/53) had an average IEI of 2.14±0.16 minutes (Range: Ctrl 0.016-33.77min, n=192; Post LTS 0.006-18.8min, n=439; K-S test $p<0.005$).

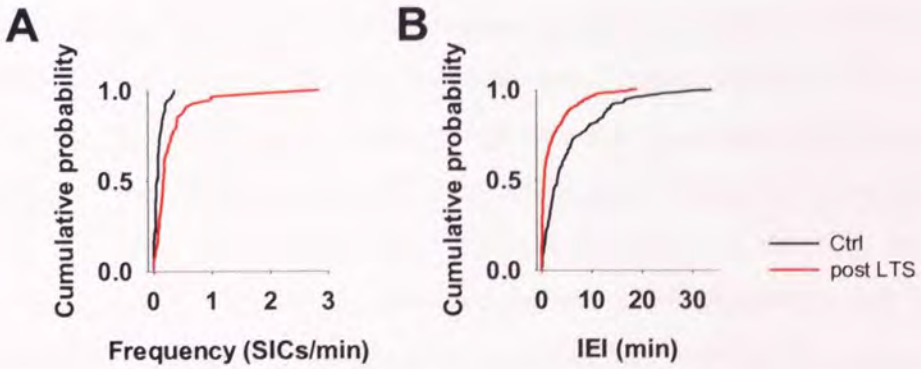

Figure 5.2.2: LTS leads to increase in SIC frequency and decrease in IEI. A) Cumulative probability distribution of average SIC frequency per cell (K-S test $p<0.005$). **B)** Cumulative probability distribution of IEI for cells with ≥2 SICs ($p<0.005$).

To assess the stability of the enhancement, SICs were analysed according to their time of emergence in 5 minute bins, and all control slices were compared to LTS stimulated slices as shown in figure 5.2.3A (n=73, 53 respectively). This demonstrated that the enhanced SIC frequency persisted for over an hour after the cessation of synaptic stimulation, thus revealing a Long Term Enhancement (LTE) of the astrocyte mediated SICs shown in figure 5.2.3B (Student's t-test p=0.0005).

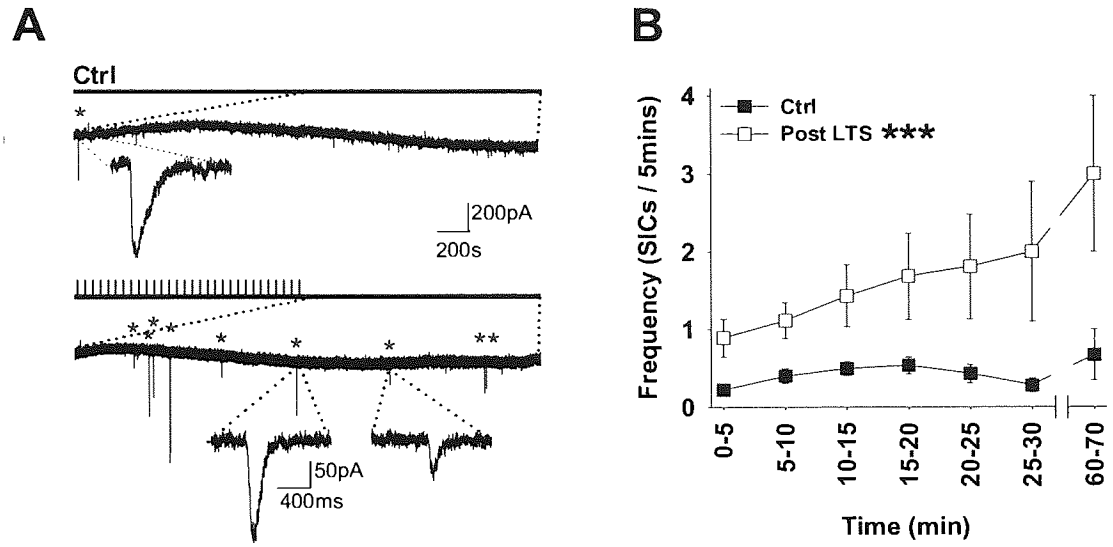

Figure 5.2.3: LTS induces Long Term Enhancement. A) Top: Example of protocol and trace from a control experiment where the slice remains unstimulated for 1 hour before recording. SIC is indicated with red asterisks and expanded beneath. Bottom: Example of LTS protocol (black bar with vertical lines) and a trace recorded following 1 hour stimulation. **B)** Mean scatter plot illustrating control (■) and post LTS (□) SIC frequency in 5 minute bins over a 70 minute period.

To investigate whether basal level of SIC frequency affected the amount LTE that could be induced, different recording aCSF compositions were tested. Firstly, LTS protocol was induced by using Mg-free aCSF in order to replicate the recording conditions used during stimulations in earlier experiments (Ctrl n=35 cells; post LTS n=13). The second group included Mg-free recording medium with additional glutamine (2mM) to increase synaptic glutamate supply (n=11, 11). Thirdly, we used normal aCSF containing Mg^{2+} (1mM) and glutamine (n=12, 11). The aCSF composition modified the level of basal/spontaneous SIC frequency, but the magnitude of LTE induction was not affected as shown in figure 5.2.4 (Mg-free Ctrl 0.069±0.013 SICs/min, post LTS 0.14±0.03, Student's t-test p=0.01; Mg-free+Gln Ctrl 0.19±0.03, post LTS 0.51±0.15, p=0.05; Mg^{2+}+Gln Ctrl 0.07±0.02, post LTS 0.24±0.08, p=0.045), thus verifying the reliability of the LTS protocol in enhancing the SIC frequency.

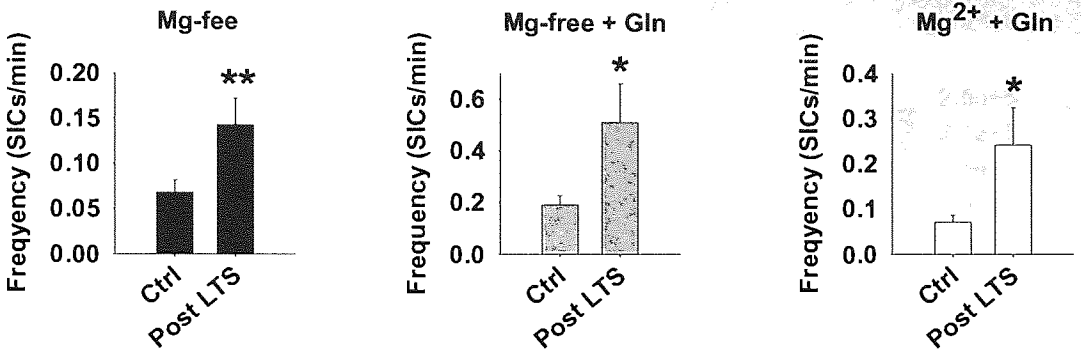

Figure 5.2.4: LTE induction is reliable. Recording aCSF composition was varied in order to investigate whether basal level of SICs affects the amount of LTE that could be induced by LTS stimulation. Control slices were exposed to the same aCSF composition, in absence of stimulation, for 60 minutes prior to recording. Bar graphs show the mean average SIC frequency for control and post LTS cells according to the aCSF composition.

5.3 Properties of LTE SICs are not different to spontaneous SICs

SICs from all control experiments and post LTS experiments were pooled together. Box plots show the spread of the data in figure 5.3A and the mean values are listed in table 5.3. Mean values were not significantly different (Ctrl n=252; post LTS n=489; Student's t-test, $p>0.1$, all parameters). Testing differences in the cumulative probability distributions using K-S test, significant differences between control and post LTS SICs were detected ($p<0.03$, all parameters). This suggests that after LTS, SICs with lower amplitude and slower kinetics were seen more often even though the average SIC magnitude remained the same.

	Amplitude (pA)		Area (pA*ms)		Rise time (ms)		Decay time (ms)	
	Ctrl	Post LTS	Ctrl	Post LTS	Ctrl	Post LTS	Ctrl	Post LTS
Mean	162.1	147.3	194152.6	50940.3	121.2	125.9	864.2	459.1
Median	105.6	91.0	14657.6	19350.4	50.0	71.8	220	309.2
Std.Dev	156.3	158.9	2229104	106775.2	351.1	142.5	5663.1	532.6
Std.Err	9.8	7.2	140699.8	4833.5	22.1	6.4	356.7	24.1

Table 5.3: Spontaneous vs. LTE SIC parameters. Mean SIC parameters were not significantly different ($p>0.1$). (Ctrl n=252; post LTS n=489 SICs)

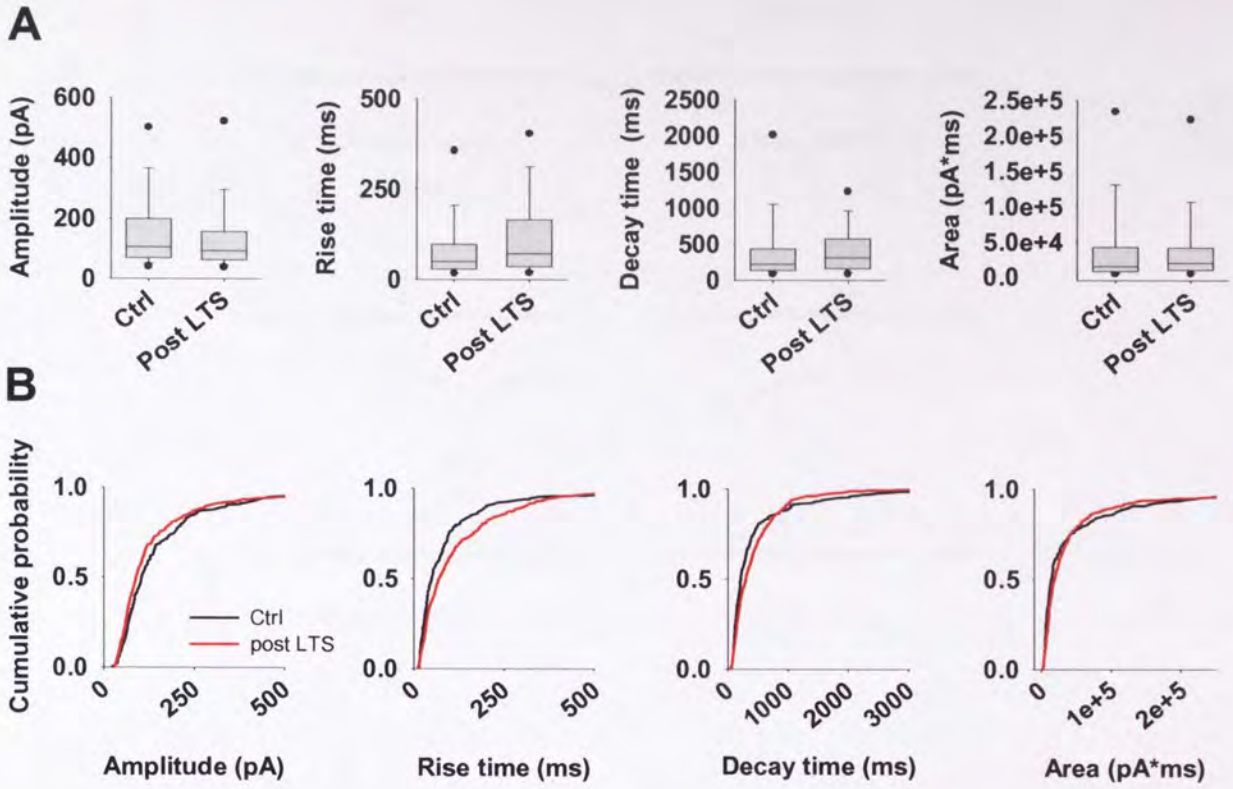

Figure 5.3: Post LTS SIC properties. A) Box plots show the spread of data for control and post LTS slices. Mean values were not significantly different. **B)** Cumulative probability graphs shows the distribution probability for control versus post LTS. Scale on the x-axis is adjusted not to show the whole range. K-S test $p<0.03$ for all parameters.

5.4 LTE induction shows developmental profile

Due to the developmental changes within the first three post-natal weeks, and the differences in spontaneous SIC activity presented in chapter 3, we studied LTE induction separately at different ages using aCSF containing Mg^{2+} (1mM) and Gln (2mM). Spontaneous SICs occurred throughout the period, however the degree of LTE that could be induced changed during maturation as show in figure 5.4.1A. Figure 5.4.1B summarises the mean data. No significant LTE was seen in week 1 (Ctrl: 0.17±0.04 SICs/min, n=17, post LTS: 0.27±0.05, n=13, 1-tail Student's t-test p=0.1), whilst LTE was induced in postnatal week 2 (Ctrl: 0.07±0.01, n=12, post LTS., n=11: 0.24±0.08, p=0.02) and in postnatal week 3 (Ctrl: 0.12 ±0.028, n=15, post LTS: 0.95± 0.41, n=21, p=0.049). Overall, from weeks 1-3, the LTE SIC frequency was increased by an average 50%, 240% and 750% respectively.

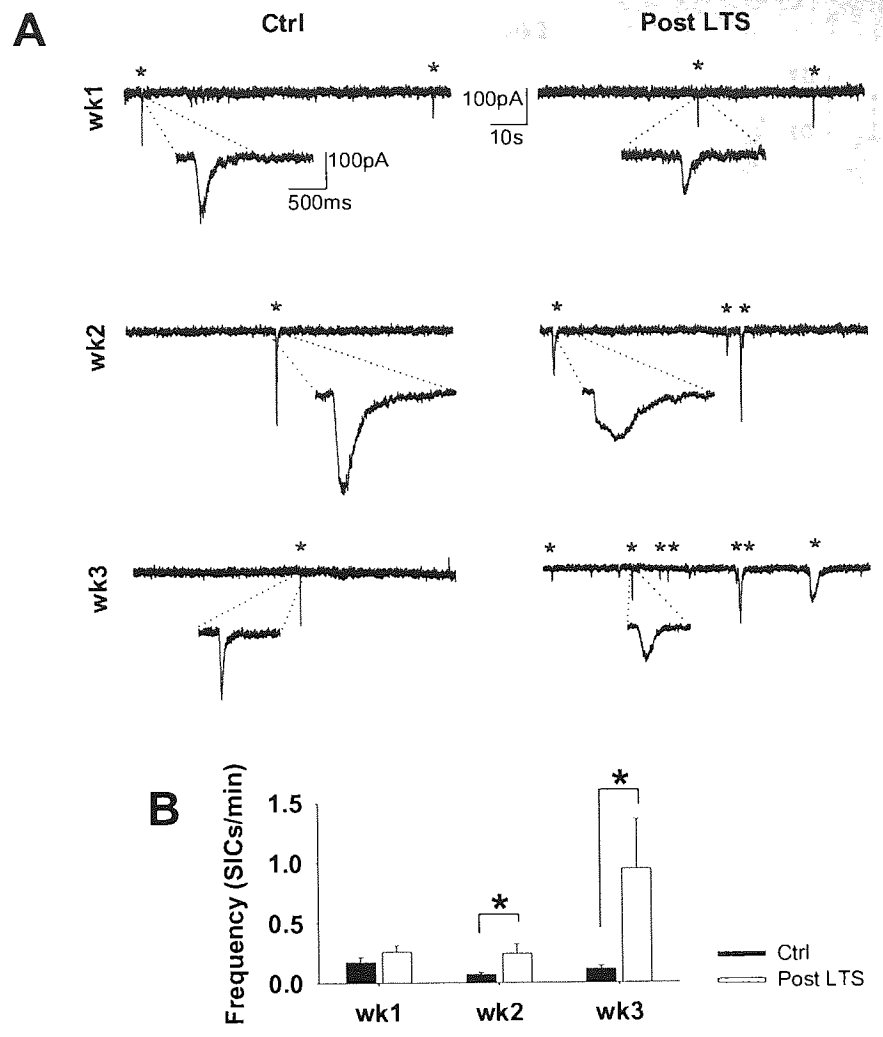

Figure 5.4.1: Developmental profile of LTE. A) Example traces from all different age groups. Representative traces of control recordings are presented on the left and traces from post LTS slices are presented on the right. PN week is indicated on the far right next to the control recordings. **B)** Bar graph shows the mean SIC frequency in control conditions compared to post LTS conditions for each PN week.

The inter event interval was calculated in control and post LTS cells with ≥2 SICS. Mean IEI during week 1 was 2.29±0.3 minutes in control (range 0.021-10.39, n=51 IEIs, 10 cells) and 2.82±0.4 minutes for post LTS (range 0.049-12.96, n=49 IEIs, n=12 cells). During the 2nd week, the mean IEI for control was 6.7±1.54 minutes (range 0.016-16.5, n=15 IEIs, n=7 cells) and 3.22±0.6 minutes post LTS (range 0.03-12.1, n=30 IEIs, n=8 cells). During the 3rd week, control IEI was 5.1±1.1 minutes (range 0.16-13.1, n=17 IEIs, 7 cells) and 0.99±0.15 minutes post LTS (range 0.004-12.89, n=203 IEIs, 18 cells). Overall, the decrease in IEI after LTS during the 2nd and 3rd week was significant (Student's t-test $p=0.014$ and $p<0.005$, respectively), whereas the IEI was not different in week 1 ($p=0.29$). Figure 5.4.2 summarises the data.

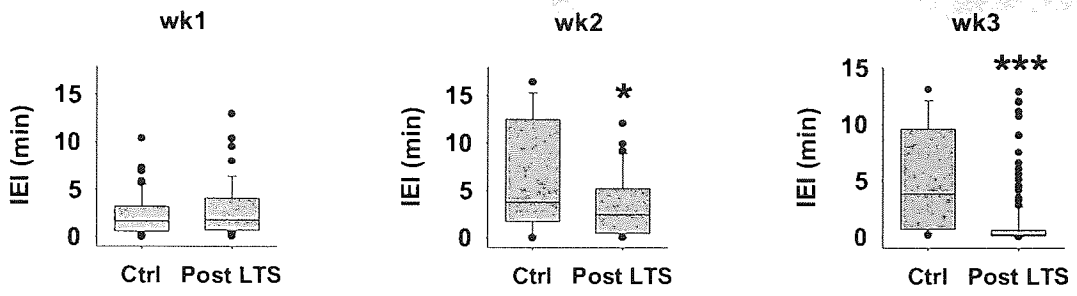

Figure 5.4.2: IEI for LTE SIC during maturation. Box plots show the spread of IEI in control and post LTS slices for each age group. (Statistical significance is presented as $p<0.05$ *, $p<0.01$ ** or $p<0.005$ ***).

The control values reflect consistency with spontaneous SIC frequencies presented in chapter 3 where cells during week 2 were shown to exhibit the lowest rate of SICs. While week 1 cells presented a higher degree of heterogeneity regarding the SIC frequency both in control and post stimulated slices (range: Ctrl 0-0.703 SICs/min; post LTS 0-0.77 SICs/min), cells during the 2nd week showed more reliable LTE induction (range: Ctrl 0-0.2 SICs/min, post LTS 0-0.99 SICs/min). During week 3, the post LTS neurons could be divided into lesser affected and highly enhanced (range: Ctrl 0-0.32, post LTS 0-7.51 SICs/min), which is also evident from the spread of the IEI data in figure 5.4.2 shown as large number of potential outliers; 4 out of 21 cells had frequency above 1 event per minute, which was 19% of all wk3 post LTS cells. During wk1 46.2% of the cells were above the mean control value ± S.E.M (0.22 SICs/min). During wk3 57.1% were above 0.14 SICs/min, whereas during wk2 72.7% were above 0.087 SICs/min. This suggests that although PN wk3 shows highest overall percentage increase, the induction of LTE during week 2 is most reliable.

We then tested whether the increase in LTE induction could be explained by an increase in glutamate input during maturation. As a measurement of this, we took the postsynaptic charge (PSQ) during Sen+CT stimulation to give an indication of the sum of the excitatory input onto each neuron. The PSQ did not significantly increase in the same way as the LTE induction as show in figure 5.4.3A (wk1 0.37±0.12 mC, n=13; wk2 0.43±0.13 mC, n=11; wk3 0.49±0.08 mC, r^2=0.02, Pearson's correlation p=0.35). In addition, LTE SIC frequency was not correlated to PSQ for individual cells (r^2=0.025, Pearson's correlation p=0.4, n=39 recordings) consistent with previous results that SIC incidence was not related to PSC amplitude.

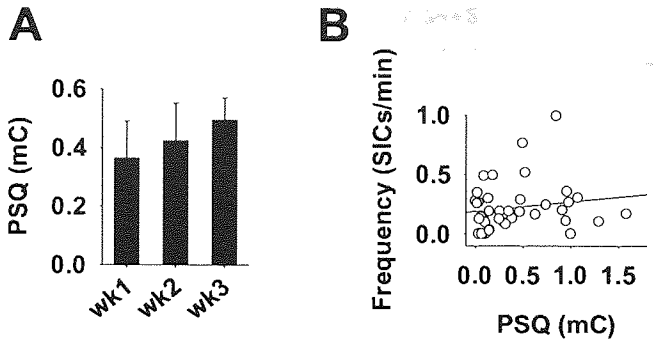

Figure 5.4.3: LTE is not related to PSQ. A) Bar graph showing the mean post-synaptic charge for each age group. **B)** Scatter plot showing SIC frequency against post-synaptic charge.

In general, control SICs were not different from post LTS SICs within any age group (wk1 ctrl n=65 SICs, post LTS n=61 SICs; wk2 n=25/40, wk3 n=26/221; Student's t-test p>0.1). However, reduced post LTS amplitude in PN wk3 was observed in comparison to wk3 control SICs (Ctrl 128.6±23.7pA, post LTS 84.0±3.3pA, p=0.0004). This is evident in figure 5.4.1 where SIC frequency was notably higher after LTS compared to control frequency: many of these post LTE SICs were low in amplitude. The data are shown in figure 5.4.4 and mean values for amplitude, rise time,decay time and area are listed in tables below.

	Amplitude (pA)		Rise time (ms)		Decay time (ms)		Area (pA*ms)	
Wk1	**Ctrl**	**Post LTS**	**Ctrl**	**Post LTS**	**Ctrl**	**Post LTS**	**Ctrl**	**Post LTS**
Mean	119.45	96.3	191.6	109.1	785.8	393.9	31131.6	23101.8
Median	87.9	81.1	50.8	41.6	164.1	151.3	9299.2	8806.2
Std.Dev	111.0	60.2	614.0	189.9	2855.5	1166.5	68744.2	52719.3
Std.Err	13.8	7.7	76.2	24.3	354.2	149.4	8593.0	6750.0

Wk2	**Ctrl**	**Post LTS**	**Ctrl**	**Post LTS**	**Ctrl**	**Post LTS**	**Ctrl**	**Post LTS**
Mean	125.6	99.1	62.0	69.7	268.4	255.7	23271.2	16984.2
Median	97.8	71.6	36.7	63.6	213.0	174.8	10014.3	9777.0
Std.Dev	89.4	71.8	52.2	47.9	197.6	206.5	26892.0	17594.0
Std.Err	17.9	11.4	10.4	7.6	39.5	32.6	5378.4	2781.9

Wk3	**Ctrl**	**Post LTS**	**Ctrl**	**Post LTS**	**Ctrl**	**Post LTS**	**Ctrl**	**Post LTS**
Mean	128.6	**84.0**	46.6	158.1	235.7	370.5	19175.9	33321.9
Median	80.8	**72.9**	34.0	58.3	159.6	167.5	9430.4	10536.6
Std.Dev	120.7	**48.8**	31.5	527.9	186.0	1003.4	23245.1	137209.7
Std.Err	23.67	**3.3**	6.2	35.5	36.5	67.5	4558.7	9229.7

Table 5.4: LTE SIC parameters during development. Significantly different values are **highlighted** (p=0.0004).

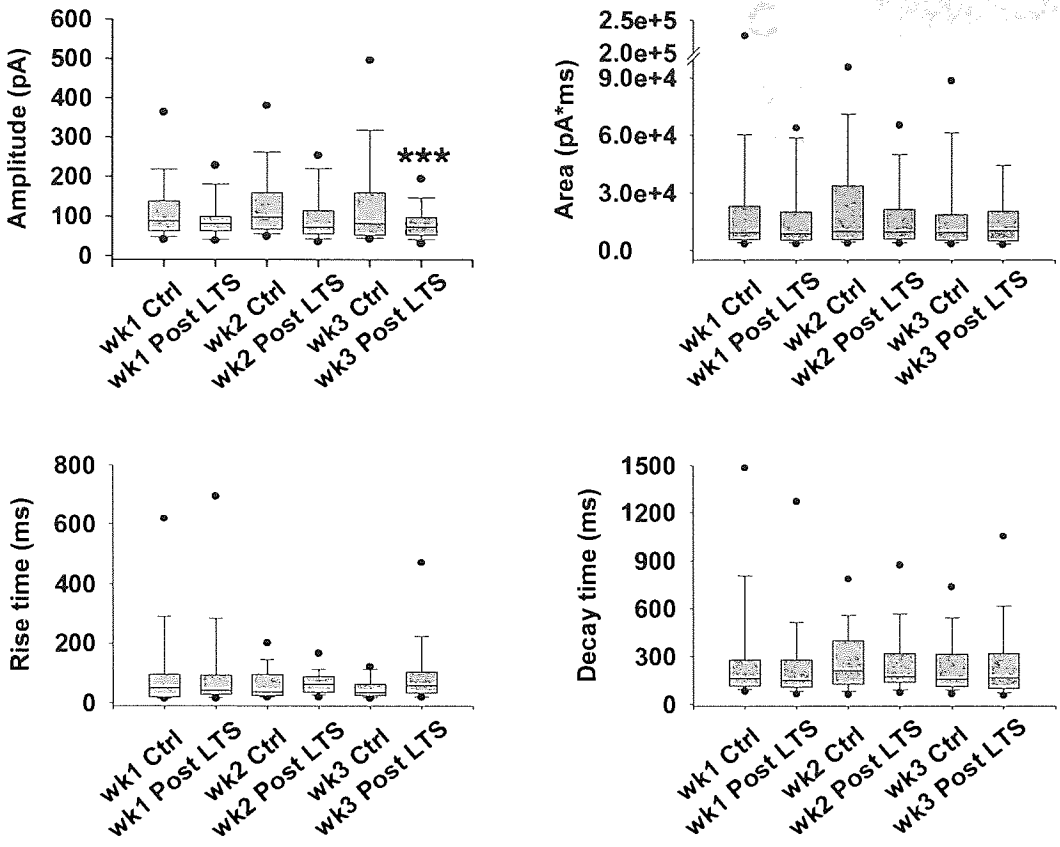

Figure 5.4.4: Control versus LTE SICs during development. Box plots show spread of SIC properties between controls and post LTS cells for each PN group. (Statistical significance is presented as $p<0.05$ *, $p<0.01$ ** or $p<0.005$ ***).

5.5 LTE SICs are not dependent on continuing neuronal activity

To rule out the possibility that LTE SICs are due to changes in spontaneous neuronal firing properties, TTX (1μM) was applied after a control period of LTE SICs including all age groups. Afferents were stimulated before and during TTX application to confirm the block of action potential dependent neurotransmitter release as shown in figure 5.5.1A. Figure 5.5.1B shows the LTE SICs before and during TTX application of the same cell. The frequency of LTE SICs was not reduced by the presence of TTX (Post LTS 1.94±1.1 SICs/min; post LTS/TTX 3.99±2.34 SICs/min, paired Student's t-test p=0.16, n=7; Fig. 5.5.1C).

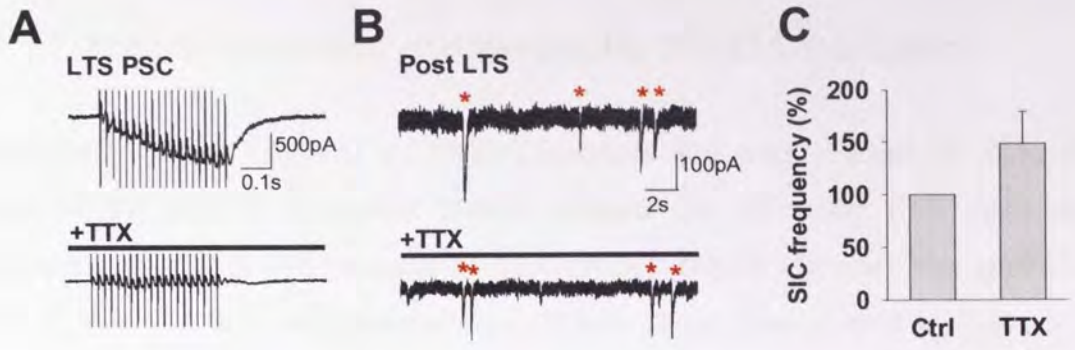

Figure 5.5.1: LTE SICs persist in TTX. A) Top trace shows PSC after LTS protocol, below PSC in presence of TTX that was applied after control period of post LTS SICs in B. **B)** Post LTS SICs (marked with red asterisks) before (top) and during TTX (1μM, below). **C)** Bar graph showing the percentage change of SIC frequency in the presence of TTX compared to control.

LTE SIC properties were compared before and during TTX application. Figure 5.5.2 shows the cumulative probability distribution for amplitude, rise time, decay time and area in control and TTX (n=102, 107 SICs, respectively). Amplitude, rise time and area were not different (K-S test $p>0.3$, each category), but decay time was differently distributed in control versus TTX (K-S, $p=0.0005$); Mean control decay time was 280.2±89.15 and during TTX, 195.4±13.5 (Paired Student's t-test, $p=0.2$).

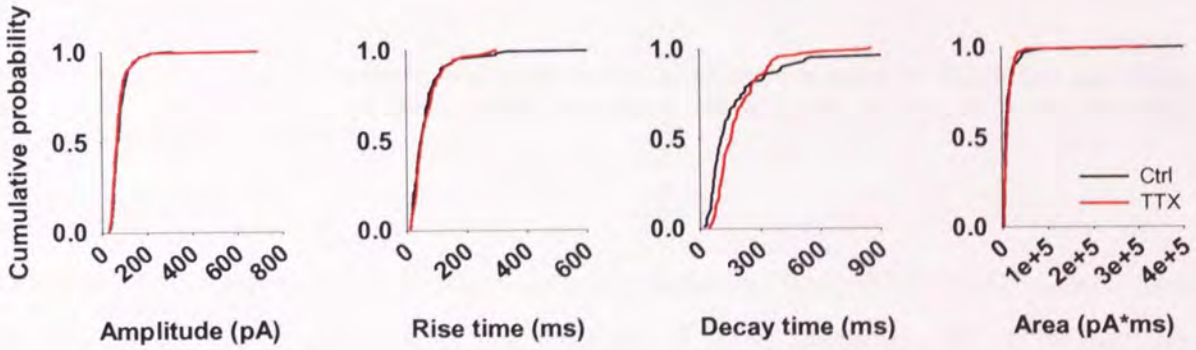

Figure 5.5.2: LTE SIC properties in TTX. Cumulative probability graphs show the distribution of LTE SICs before and during TTX (1μM) application. K-S test $p>0.3$ for amplitude, rise time and area; decay time $p=0.0005$.

5.6 LTE targets neuronal extrasynaptic NMDA-receptors

Spontaneous SICs are mediated by NMDA-receptors and were reduced by 96% in the presence of the NMDA antagonist D-AP5 (chapter 3). After the LTS protocol and establishment of LTE in the presence of TTX (1μM), D-AP5 (50 μM) was applied. The number of observed SICs was reduced from 178 to 18 as demonstrated in figure 5.6.1A. Overall, the LTE SIC frequency reduced to 14.5±5% of the control as shown in figure 5.6.1B (Ctrl 0.86±0.43 SICs/min; AP5 0.13±0.07 SICs/min; paired Student's t-test p=0.00001; n=6). Depression in SIC frequency was reversed by D-AP5 wash-out (wash 1.27±0.17, n=2). The remaining 18 SICs were only slightly reduced in size: amplitude reduced from 76.5± 4.7 to 61.9±9.1pA, rise time from 181.8±11.1ms to 163.3±31.5ms and decay time from 504.2±23.4ms to 422.6±90.9ms (Student's t-test p>0.2, all parameters; data not shown).

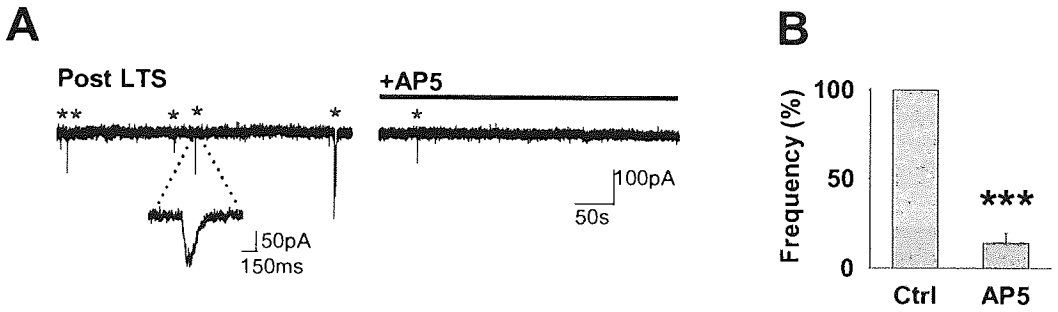

Figure 5.6.1: LTE SICs are mediated by NMDA-receptors. A) Example of post LTS SICs before and during D-AP5 (50μM) application. SICs are indicated with red asterisks. **B)** Bar graph showing the mean percentage decrease of SIC frequency (SICs/min).

In addition, we used the selective NR2B subunit antagonist Ifenprodil (10μM) in three post LTS cells of 3rd PN week. Here, in the presence of TTX, ifenprodil did not reduce the frequency as shown in figure 5.6.2A (Ctrl 6.45±3.2 SICs/min; Ifenp. 4.98±2.5 SICs/min; paired Student's t-test p=0.5; n=3).

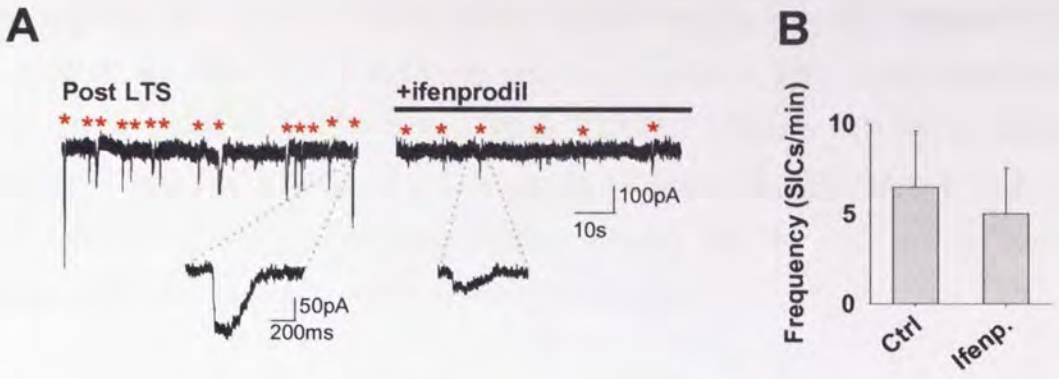

Figure 5.6.2: LTE SIC and Ifenprodil. A) Example of post LTS SICs before and during ifenprodil (10μM) application. SICs are indicated with red asterisks and examples expanded beneath. **B)** Bar graph showing the mean frequency in ctrl and in presence of ifenprodil.

However, ifenprodil caused a 40% reduction in the magnitude of the LTE SICs. Mean amplitude reduced from 76.0±2.8pA to 56.2±1.7pA (Student's t-test $p<0.005$; n=178, 184 SICs, respectively), decay time from 187.1±11.3ms to 146.9±7.3ms ($p=0.003$) and area from 12744.1±942.2pA*ms to 7549.7±429.9pA*ms ($p<0.005$). Rise time was not affected by Ifenprodil (Ctrl 67.3±4.3ms; Ifenp. 64.4±5.6ms; $p=0.7$). Figure 5.6.3 shows the cumulative population distribution graphs for amplitude (K-S test $p<0.005$), rise time ($p=0.4$), decay time ($p=0.02$) and area ($p=0.0004$).

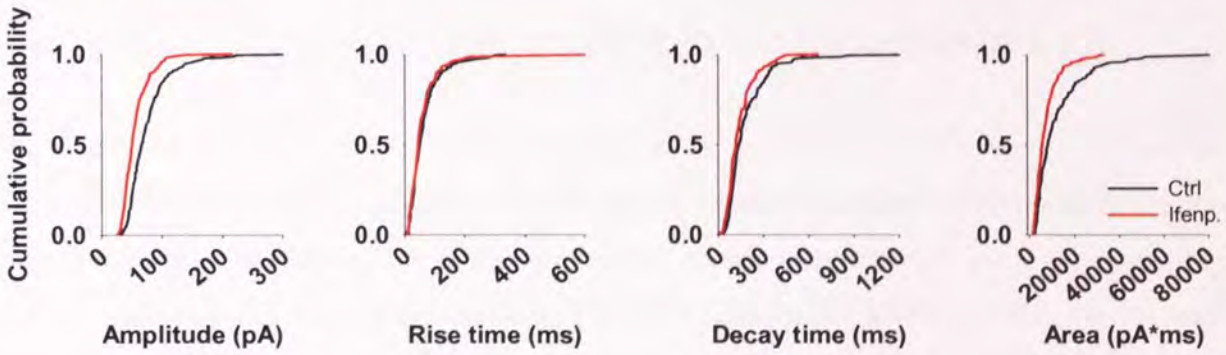

Figure 5.6.3: Magnitude of LTE SICs reduced by Ifenprodil. Cumulative probability distribution graphs of post LTS SICs in control period and in the presence of Ifenprodil (10μM). K-S test; amplitude ($p<0.005$), rise time ($p=0.4$), decay time ($p=0.02$) and area ($p=0.0004$).

To further probe the possible extrasynaptic location of LTE SICs via NR2B containing NMDA-receptors, the effects of D-AP5 (50μM) and ifenprodil (10μM) were assessed on evoked neuronal PSCs. Figure 5.6.4 summarises the data. D-AP5 reduced the PSC amplitude significantly both during sensory (from 588.8±145.1pA to 205.8±79.2pA, paired Student's t-test $p=0.024$; n=5) and CT stimulation (from 573.9±187.2pA to 114.3±68.4pA; $p=0.048$;

n=7). These were 23% and 31% of the control respectively. In contrast, Ifenprodil did not have any significant effect on PSCs. During sensory stimulation, PSC during ifenprodil was 90.7% of the control (Ctrl 377.8±48.0pA; Ifenp. 370.8±163.1pA; p=0.7; n=5). During CT stimulation PSC was 95% of the control in presence of Ifenprodil (Ctrl 253.1±40.6pA; Ifenp. 240.9±64.3pA, p=0.8; n=7). These data together suggest that the SICs are mediated via extrasynaptic NMDA-receptors containing the NR2B-subunit.

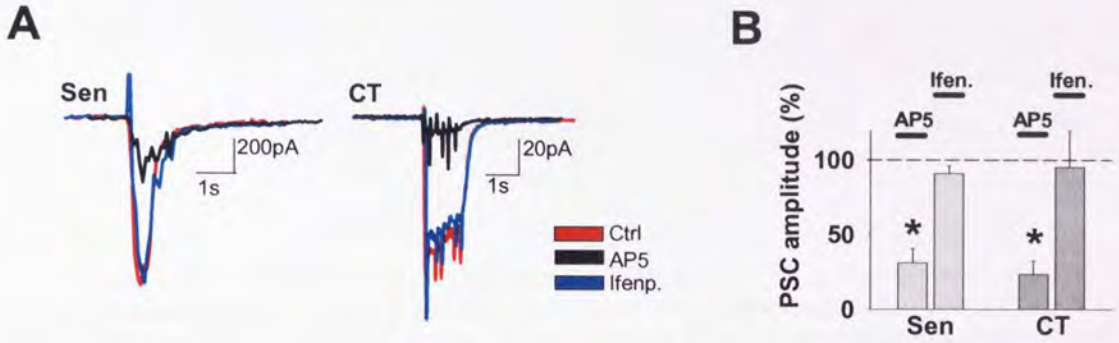

Figure 5.6.4: Evoked synaptic current not affected by Ifenprodil. A) Example traces of PSC from the same in response to Sen and CT stimulation in control and in presence of AP5 (50μM) and Ifenprodil (10μM). **B)** Bar graph summarises the effects of the NMDA antagonists on PSC for both inputs. Dashed line represents the 100% control.

5.7 Glutamate uptake is not involved in the induction of LTE

We next studied the mechanism of LTE induction. Both sensory and CT inputs to the VB thalamus are glutamatergic, therefore, we first asked whether increased synaptic activity was accompanied by an increase in glutamate uptake which consequently could increase the cytosolic glutamate in astrocytes over time. The EAAT blocker DL-TBOA (100-150μM) was included in the recording aCSF during the LTS induction protocol. The post LTS data were compared to LTS experiments using Mg-free aCSF with glutamine. The LTS protocol with TBOA increased the SIC frequency similarly to LTS protocol (post LTS 0.51±0.15; post LTS/TBOA 0.47±0.12 SICs/min; Student's t-test, p=0.9; n=11, 10, respectively) and was significantly increased compared to control (Ctrl 0.19±0.03; LTS+TBOA 0.47±0.12 SICs/min; p=0.03) as summarised in figure 5.7. These data suggest that the LTE induction mechanism involves neurotransmitter receptors activation rather than glutamate uptake.

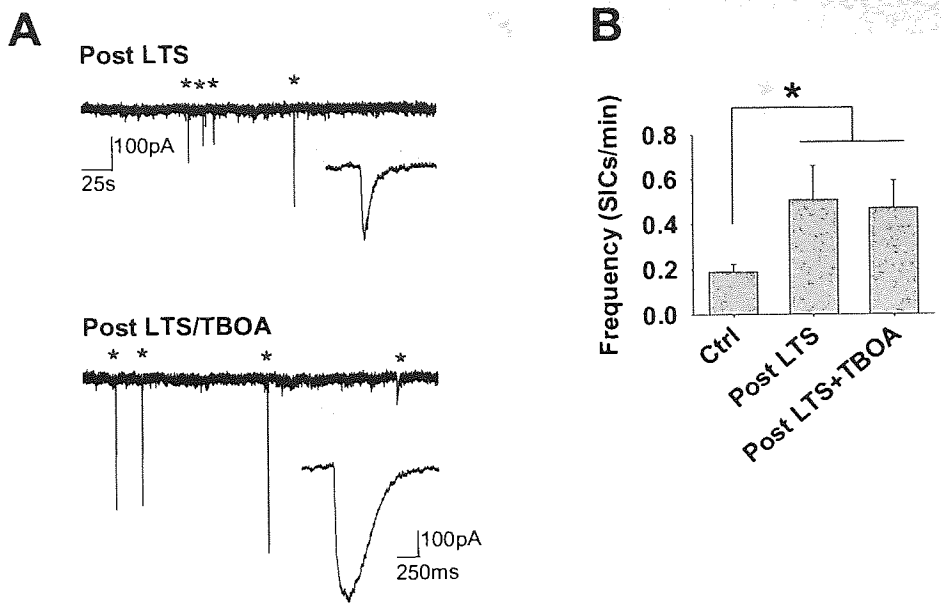

Figure 5.7: EAATs are not involved in LTE induction. A) Top trace shows an example after post LTS. SICs are indicated with asterisks and expanded beneath. Trace below shows an example from post LTS with TBOA (100-150μM). **B)** Bar graph comparing the mean SIC frequency in control (non-stimulated), post LTS and post LTS with TBOA.

5.8 Ionotropic Glu receptors are not involved in induction of LTE

As discussed in the introduction, astrocytes express both ionotropic and metabotropic glutamate receptors and both types can induce astrocytic Ca^{2+} responses and potential glutamate release [Cornell-Bell *et al.*, 1990; Parpura *et al.*, 1994; Parri *et al.*, 2001; Serrano *et al.*, 2006]. We next applied glutamatergic antagonists in the aCSF during the LTE induction protocol period in order to identify the receptor subtypes involved in the induction mechanism. LTE induction was not affected by the broad spectrum ionotropic glutamate receptor (iGluR) antagonist kynurenic acid (2mM) as shown in figure 5.8 (Ctrl 0.06±0.01 SICs/min; post Kyn LTS 0.22±0.08 SICs/min; Student's t-test p=0.03; n=15, 8, respectively) indicating that ionotropic NMDA and AMPA receptor activation is not necessary for LTE induction.

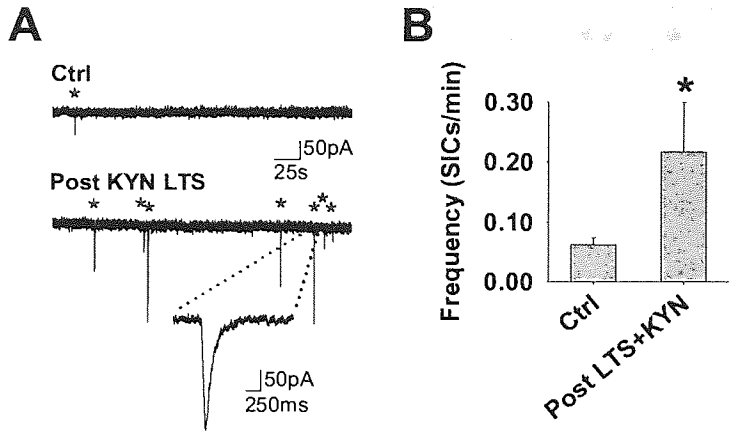

Figure 5.8: LTE does not involve iGluRs. A) Top trace shows example of control recording exposed to Kynurenic acid (2mM) in absence of stimulation. SICs are indicated with red asterisks. Trace below shows an example after LTS protocol including kynurenic acid. **B)** Bar graph shows the mean SIC frequency for control and post LTS protocol including Kynurenic acid.

5.9 LTE is induced via group I mGluR

Since group I mGluR activation elicits astrocytic $[Ca^{2+}]_i$ elevations and subsequent glutamate release in the VB thalamus [Parri *et al.*, 2001], we then tested the potential role of group I mGluRs in LTE using the mGluR5 antagonist MTEP (50μM) and mGluR1 antagonist CPCCOEt (200μM). Experiments were compared to spontaneous SIC frequency and post LTS SIC frequency, revealing that the presence of mGluR antagonists during LTS prevents LTE induction as shown in figure 5.9.1. The LTS protocol induced a significant increase in SIC frequency compared to spontaneous frequency (Spont 0.069±0.013 SICs/min, n=35; post LTS: 0.14±0.03 SICs/min; Student's t-test p=0.01; n=35, 13, respectively). In contrast, SIC frequency after the LTS protocol with MTEP and CPCCOEt was 0.056±0.02 SICs/min (n=8). This was not increased above normal spontaneous SIC frequency (Student's t-test p=0.7), and was significantly less compared to the LTS protocol without the mGluR blockers (p=0.04). LTE induction therefore requires mGluR activation.

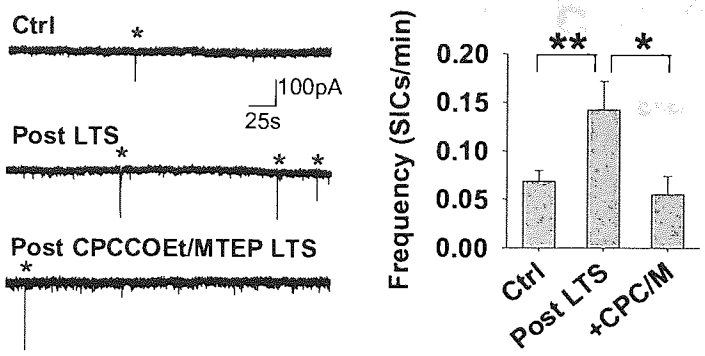

Figure 5.9.1: Group I mGluR receptors are involved in LTE induction. A) Top trace shows normal spontaneous activity. Middle trace shows a SIC prevalence after LTS protocol. Bottom traces shows SIC frequency after LTS protocol with group I mGluR antagonists CPCCOEt (200μM) and MTEP (50μM). SICs are indicated with asterisks. **B)** Bar graph comparing the mean SIC frequency in spontaneous, post LTS and post LTS with CPCCOEt (CPC) and MTEP (M).

To confirm the role of group I mGluRs, slices were exposed to the selective agonist DHPG (100μM) for 60mins in the absence of synaptic stimulation. Recordings made after DHPG wash-out showed that this treatment also resulted in significant increase in SIC frequency as shown in figure 5.9.2A-B (Ctrl 0.06±0.01 SICs/min; post DHPG 0.25±0.11 SICs/min; 1-tail Student's t-test p=0.04; n=15, 13, respectively). Furthermore, analysis of the time span for the post DHPG induced SIC enhancement confirmed that group I mGluRs play a role in LTE as the increased frequency was maintained for up to an hour as shown in figure 5.9.2C.

The previous study in the VB thalamus used acute bath application of group I/II agonist 1S,3R-ACPD that was shown to elicit astrocytic Ca^{2+} increases and SICs [Parri *et al.*, 2001]. Here, prolonged exposure to ACPD (100μM), however, did not induce LTE (Ctrl 0.06±0.01 SICs/min; post ACPD 0.061±0.03; 1-tail Student's t-test p=0.5; n=15, 10 respectively). Whilst DHPG increased SIC frequency above control mean+S.E.M (0.073) in 53% of the cells, only 50% of the cell post ACPD exhibited SICs at all (data not shown).

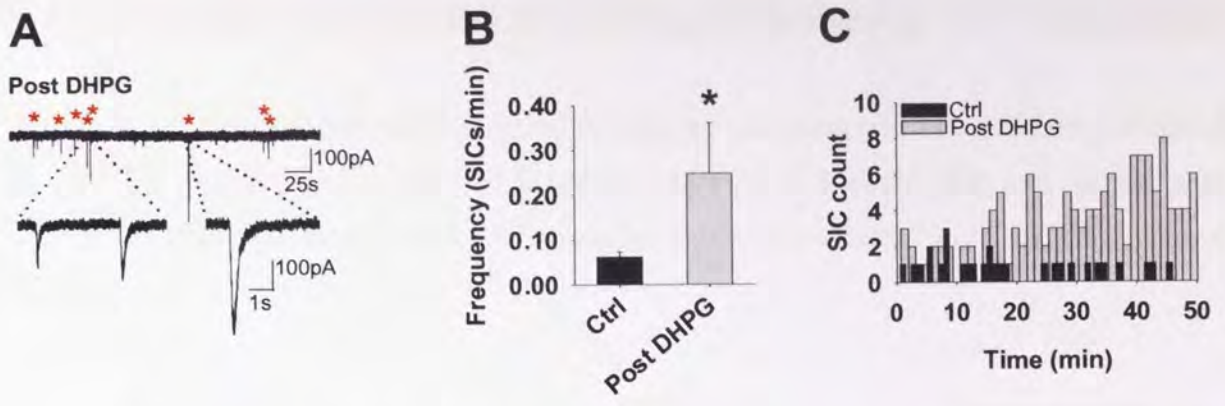

Figure 5.9.2: Group I mGluR activation leads to LTE. A) Representative trace showing SICs (asterisked and few of them expanded) in slices treated with DHPG (100μM) for an hour in absence of synaptic stimulation. **B)** Bar graph showing the mean SIC frequency in controls and after DHPG treatment. **C)** Frequency histogram comparing SIC prevalence over a 50 minutes recording time for control and post DHPG cells.

To assess whether SICs induced by group I mGluR activation were different to spontaneously occurring SICs, post DHPG SIC (n=161) properties were compared to control SICs from LTE experiments presented above (P10-15; n=251). Figure 5.9.3 summarises the data. Mean amplitude was significantly reduced in post DHPG SICs compared to control SICs (Ctrl 162.1±9.8pA; post DHPG 99.1±3.9pA; Student's t-test $p<0.005$). Cumulative probability distribution analysis also showed significant changes towards lower amplitudes in the post DHPG SICs (K-S test $p=0.0002$). Mean area was not reduced (Student's t-test $p=0.4$) but small distributional changes were significant, consistent with amplitude change (K-S $p=0.009$). Kinetics were not different (t-test $p>0.1$; K-S $p>0.05$). This supports the observation that DHPG mediated events were SICs, rather than direct neuronal events, as the slow kinetics were indistinguishable from spontaneous and LTE SICs.

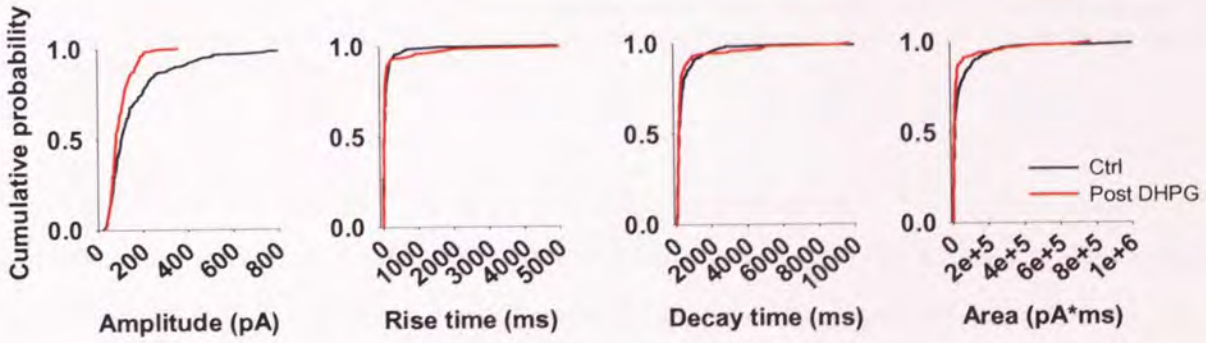

Figure 5.9.3: DHPG induced LTE SICs. Cumulative probability distribution graphs show that group I mGluR agonist DHPG induced long term enhancement of SICs that were kinetically not different ($p>0.05$) from spontaneous SICs albeit lower in amplitude ($p=0.0002$).

5.10 LTS does not alter the frequency of astrocytic Ca^{2+} elevations

Since astrocytic mGluR activation is linked to calcium signalling and SIC generation [Parri *et al.*, 2001] we imaged Ca^{2+} elevations in control and post LTS slices. Both control and post LTE slices exhibited spontaneous Ca^{2+} elevations of variable profiles as shown in figure 5.10.1.

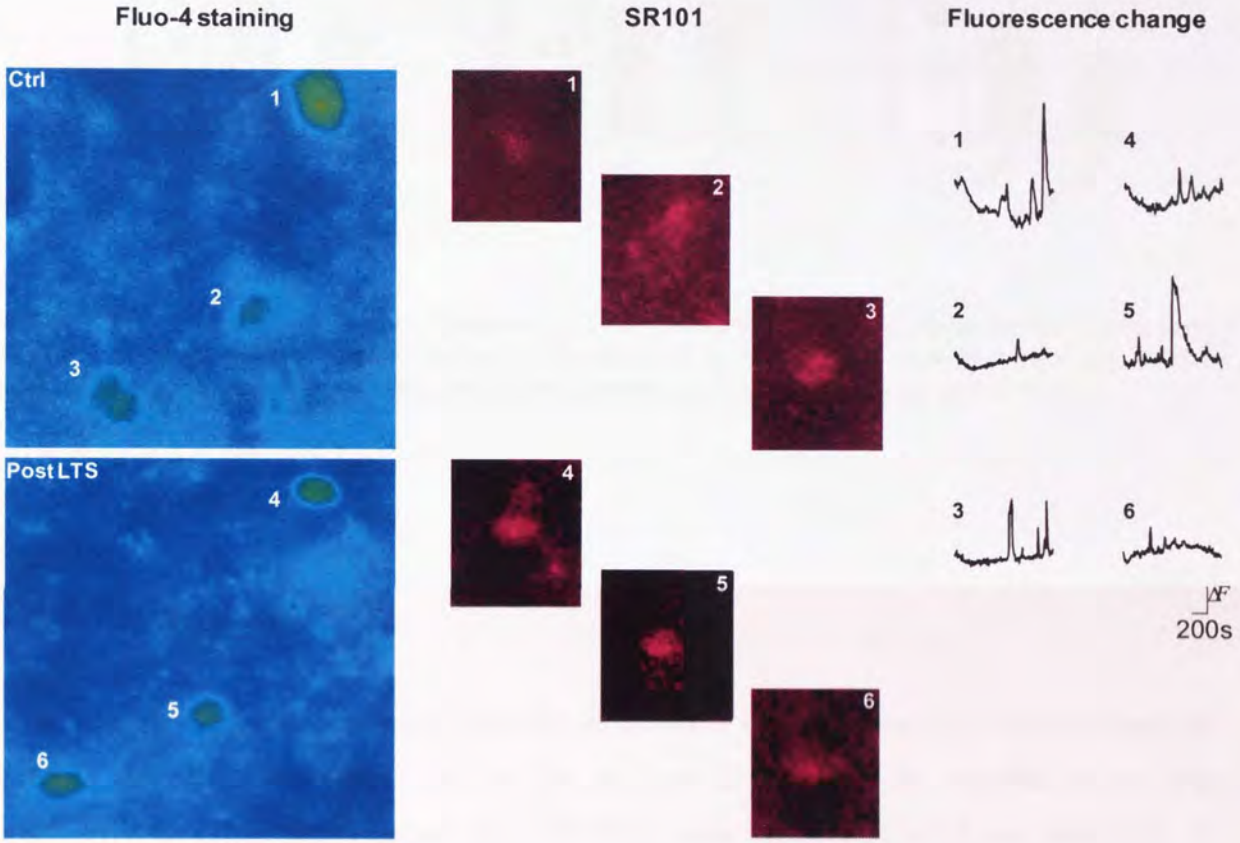

Figure 5.10.1: Spontaneous astrocytic $[Ca^{2+}]_i$ elevations in control and post LTS slices. Pseudocolour panels on the left show Fluo-4 staining in active astrocytes in control (top) and post LTS (bottom) slices. Example astrocytes are numbered (Ctrl 1-3; post LTS 4-6). Middle panels show magenta images for SR101 staining for corresponding astrocytes numbered. Traces on the right show the fluorescence change over 15 minutes recording for the corresponding astrocytes.

Surprisingly, the increase in LTE SICs was not accompanied by an increased number of spontaneously active astrocytes (Ctrl 29.8±7.5 astrocytes; post LTS 24±2.0 astrocytes, Student's t-test p=0.5; n=6 slices for both) nor by increased frequency of astrocytic calcium oscillations as shown in figure 5.10.2 (Ctrl 0.29±0.016 events/min; post LTS 0.31±0.02 events/min, Student's t-test p=0.5). Qualitative assessment of the 178 Ca^{2+} peaks in control slices and 142 Ca^{2+} peaks in post stimulated slices did not show any clear differences in the

appearance of the Ca^{2+} peaks between the groups. The proportion of Ca^{2+} peaks of ≥ 5 fluorescence (F) units out of the total number of peaks per astrocyte was assessed: no difference was found between the control and post stimulated slices (Ctrl 33.8±5%; Post LTS 28.2±5.7%; Student's t-test p=0.2; Fig. 5.10.2C).

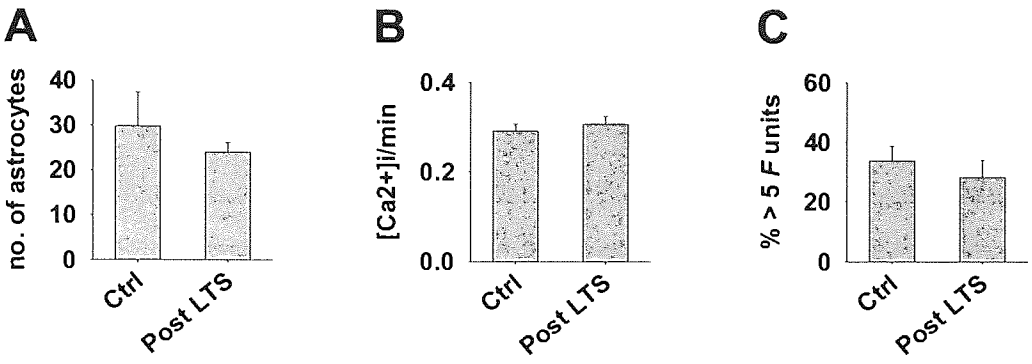

Figure 5.10.2: LTS does not increase frequency of $[Ca^{2+}]_i$ elevations. A) Bar graph shows the mean number of active astrocytes within the imaged field in control and post LTS slices. **B)** Bar graph shows the mean number of $[Ca^{2+}]_i$ elevations per minute. **C)** Bar graph shows proportion of Ca^{2+} peaks over 5F units.

5.11 Discussion

Here, we showed that prolonged synaptic stimulation induced long term enhancement of SICs. This enhancement was sustained for an hour after ceasing the stimulation and was insensitive to TTX demonstrating that LTE SICs were neither mediated nor dependent on ongoing neuronal activity. LTE induction required group I mGluR activation and targeted extrasynaptic NMDA-receptors. In addition, it was shown that LTE has a developmental profile.

In contrast to moderate synaptic stimulation (Chapter 4), LTE was reliably induced by prolonged synaptic stimulation. Stimulation of just one afferent pathway was sufficient to elicit the increase in SIC incidence: Sensory stimulation showed stronger enhancement as measured by the increase in incidence over the course of stimulation. This may be related to the differential architecture of the sensory synapse (glomeruli) where astrocytes form more intimate contact with the synapse. Stronger LTE during sensory stimulation may therefore have important functional roles.

Consistent with spontaneous SICs shown in Chapter 3 (Fig. 3.4), LTE SICs were inhibited by NMDA-receptor antagonists. Previous studies demonstrated that SICs were mediated by extrasynaptic NMDA-receptors containing NR2B subunit [Fellin *et al.*, 2004; D'Ascenzo *et al.*, 2007; Shigetomi *et al.*, 2008], and indeed NMDA-receptors in the hippocampus are composed almost exclusively of NR2A and NR2B subunits [Wenzel *et al.*, 1997]. Here, ifenprodil reduced the LTE SIC amplitude significantly, whilst neuronal PSC was not affected, demonstrating that SICs in the VB thalamus target NMDA-receptors at extrasynaptic locations as well. However, 75% of the SIC current still persisted which may reflect the presence of other subunits with slow kinetics such as NR2C that is abundantly expressed in the thalamus by P21 [Wenzel *et al.*, 1997]. The fact that SICs displayed similar properties to spontaneous SICs indicates that induction of LTE does not require a new signalling source but an actual increase in SIC frequency.

The LTE induction mechanism involved presynaptic glutamate release acting on, presumably astrocytic, group I mGluRs. This was proved by several experiments. First of all, presynaptic glutamate release was sufficient to induce the LTE, as in the presence of broad spectrum iGluR antagonist Kynurenic acid, postsynaptic current was completely abolished thus preventing any secondary glutamate release from the postsynaptic neurons (data were not shown). LTE induction however was unaffected demonstrating that iGluRs on astrocytes were not involved. An increase in glutamate uptake appeared not to play a major role either as in the presence of broad spectrum transporter inhibitor TBOA, LTE induction was not affected. LTE induction was mimicked by long term exposure to group I agonist DHPG but prevented in the presence of group I antagonists MTEP and CPCCOEt. Group I mGluR includes two subtypes: mGluR1 and mGluR5. To distinguish whether there was difference between activation of these two receptors will require further experiments, but mRNA expression studies have shown pronounced expression of mGluR5 on thalamic astrocytes and only weak expression of mGluR1 [Biber *et al.*, 1999], suggesting mGluR5 may play more profound role.

An involvement of group I mGluR is in agreement with many previous studies showing that agonist application increased SIC frequency, and antagonist application during stimulation prevented it [Parri *et al.*, 2001; Angulo *et al.*, 2004; Fellin *et al.*, 2004; D'Ascenzo *et al.*, 2007]. The difference is that these studies showed the effect with acute application whereas here, mGluR activation required at least 30 minutes of stimulation. Most surprisingly, LTE was not accompanied by enhanced astrocytic Ca^{2+} signalling as shown in the previous studies

using acute agonist application. Neither the number of active astrocytes nor the frequency of each astrocyte was affected. Several explanations could account for this:

First of all, the resolution of the imaging method means that detected Ca^{2+} elevations are most likely somatic in origin. Therefore, Ca^{2+} elevations occurring in processes may go undetected. Astrocytic vesicles containing glutamate are shown to be located at the processes in close proximity to neuronal synapses [Bezzi *et al.*, 2004; Montana *et al.*, 2004; Jourdain *et al.*, 2007; Xu *et al.*, 2007]. Combining this with the studies showing higher frequency of Ca^{2+} increases in processes relative to soma and that Ca^{2+} propagation into processes coincide with SICs [Pasti *et al.*, 1997; Fellin *et al.*, 2004], suggest that the signalling in processes may be the crucial factor where glutamate release is concerned. Furthermore, whisker stimulation evokes group I mGluR mediated Ca^{2+} elevations in the barrel cortex and increases in the processes occurred approximately 1s earlier than in soma [Wang *et al.*, 2006]. Therefore, the fact that SIC frequency was increased without a change in somatic Ca^{2+} may reflect a greater degree of Ca^{2+} signalling in processes which do not propagate to the soma. Alternatively, as spontaneous Ca^{2+} increases have been shown to propagate into processes with a delay compared to soma [Parri *et al.*, 2001], higher proportions of somatic Ca^{2+} increases may have propagated into processes to induce vesicle release in post LTS slices. It is also possible that glutamate release may not be dependent on Ca^{2+} *per se*. Even if the glutamate was released from the synaptic vesicles, a recent study by Holt *et al.* [2008] suggests that synaptic vesicles are active fusion machines needing only synaptoprevin for activity. In addition, they demonstrated that the fusion was not accelerated but rather slowed by Ca^{2+}.

Furthermore, alternative glutamate release mechanisms to Ca^{2+} dependent/independent vesicle release should be considered. As described in the introduction, several mechanisms for gliotransmission exist such as swelling induced release. For example, mGluR stimulation may lead to depolarisation of the astrocyte membrane with resultant K^+ efflux and Na^+ influx [Hansson & Rönnbäck, 1995]. Accumulation of extracellular K^+ can then lead to neuronal depolarization and additional glutamate release. The secondary glutamate release and increase in extracellular K^+ causes K^+ accumulation in astrocytes leading to swelling and possible swelling induced glutamate release. The mGluR dependent swelling of astrocytes has also been reported elsewhere [Yuan & Wang, 1996].

Increases in SIC frequency may also be due to extension of astroglial filopodia in response to glutamate stimulation as occurs in cultures [Cornell-Bell *et al.*, 1990]. Interestingly, synaptically released glutamate in response to whisker stimulation has been shown to increase astrocytic coverage of the synaptic bouton-spine interface in the cortex *in vivo* [Genoud *et al.*, 2006]. Therefore, it is possible that long term stimulation causes astrocytic processes to adopt more intimate contact with synapses *in situ*. In support for this is the observation that even though LTE SICs on average were not changed in amplitude or kinetics, which suggest an increase in the properties of GT release rather than changes in neurons, the cumulative population distribution analysis revealed a higher proportion of smaller SICs after LTS. Considering that glutamate may be released from multiple sites and diffuses variable distances across the extracellular space, a decrease in diffusion distances due to increased physical contact with the synapse [Piet *et al.*, 2004] might account for increased detection of lower amplitude SICs.

The developmental profile of LTE induction may reflect the physical changes, such as changes in the synaptic structures and afferent connections, occurring during the first 3 PN weeks in the VB thalamus. Therefore, more mature connectivity will have a stronger impact on neuron-to-astrocyte signalling and *vice versa*. As discussed in the chapter 3, astrocytes themselves also undergo developmental changes. Therefore, astrocytes may acquire the facility to express LTE during maturation. The fact that the degree of LTE increased regardless of the change in postsynaptic charge is consistent with previously shown data (chapter 4) that SIC frequency was not dependent on PSC amplitude. Taken together, these findings suggest that long term enhancement of gliotansmitter signalling may have important physiological roles in the functioning adult brain.

In conclusion, we have shown an increase of astrocyte mediated signalling that far outlasts the inducing stimulus and thus represents a glial "memory" of previous neuronal synaptic activity. Previously, an increase in SICs has been only shown to occur for a maximum of 5 minutes post stimulation [Fellin *et al.*, 2004; D'Ascenzo *et al.*, 2007]. However, astrocytic Ca^{2+} signalling has been demonstrated to undergo plasticity and long lasting (>3h) increase in Ca^{2+} oscillation frequency after repetitive episodes of neuronal stimulation and mGluR activation [Pasti *et al.*, 1997]. This was also proposed to represent astrocytic memory of previous neuronal activity and may therefore be related to the findings presented here if any future experiments will reveal an increase in Ca^{2+} signalling in the astrocytic processes following LTE induction.

Chapter 6

Effect of glutamate exposure on SIC generation

Next we asked whether SIC frequency and LTE were dependent on glutamate supply and/or time exposed to increased glutamate concentration at the synapse. As long term stimulation led to a significant group I mGluR mediated increase in SIC frequency over time, we reasoned that the difference between ineffective moderate stimulation and LTS could be an increase in glutamate levels at the synapse over time [Diamond and Jahr, 2000]. In other words, after prolonged stimulation glutamate accumulation may overcome the glutamate-transporter efficacy and *enhance* the activation of mGluRs on the perisynaptic astrocytes. Previous results (chapters 4 and 5) however do not completely support this since SIC frequency was never correlated with an increase in PSC amplitude/charge suggesting that increase in Glu supply *per se* is not sufficient to elicit an increase in SIC frequency. Furthermore, moderate synaptic stimulation was sufficient to elicit astrocytic $[Ca^{2+}]_i$ elevations. If the increase in SIC frequency during LTS was due to *increased glutamate supply* at the synapse *over time*, exposure to external glutamate for prolonged periods would be expected to have similar effects as LTS and the mGluR agonist DHPG. In addition, by increasing external glutamate concentration, astrocytic glutamate stores may be enlarged [Xu *et al.*, 2007] via Glu uptake, which could then enhance spontaneous SICs generation. The experimental approach is outlined in figure 6.0.

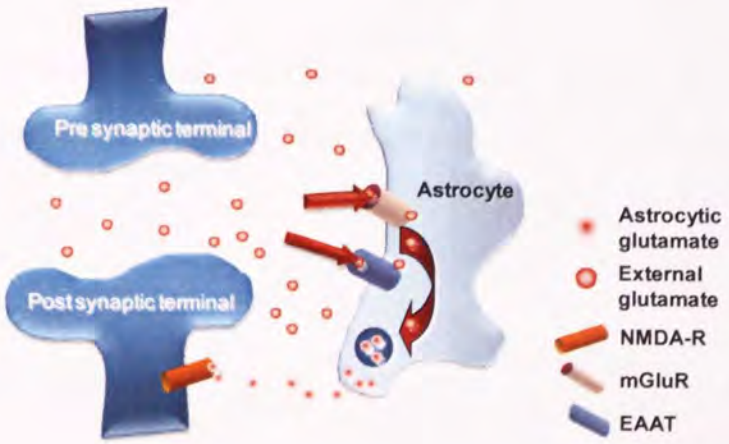

Figure 6.0: Long term Glu exposure model. By pre-incubating slices in glutamate, we can further study the time dependency of the LTE, as it is often not practical to stimulate slices for hours. Furthermore, Glu pre-incubation will provide information whether Glu loading into astrocytes plays a role in LTE.

6.1 Increasing cytosolic Glu does not increase SIC frequency

Before testing the effect of external glutamate application, we first assessed whether increasing astrocytic glutamate levels by accumulating glutamate within the slices into astrocytes would enhance SIC frequency. Considering that LTS led to LTE over a 30 minute time period, and that inhibiting glutamate conversion into glutamine with MSO during moderate synaptic stimulation did not affect SIC frequency (Fig. 4.7), a longer time may be required to increase cytosolic Glu concentrations. Therefore, slices were exposed to MSO (1.5-5mM) for ≥60 minutes prior to experimenting. As shown in figure 6.1, this led to a small, although not significant, increase in the SIC frequency compared to spontaneous P10-15 slices (Spont 0.069±0.013 SICs/min; MSO 0.14±0.06 SICs/min; Student's t-test p=0.1; n=35, 6 respectively). The increase in frequency was not dependent on the MSO concentration (r^2=0.01, Pearson's correlation p=0.8; data not shown). These results suggest that in absence of continuing synaptic activity or external mGluR activation, there is not enough glutamate present in astrocytes/slices to increase spontaneous SIC frequency.

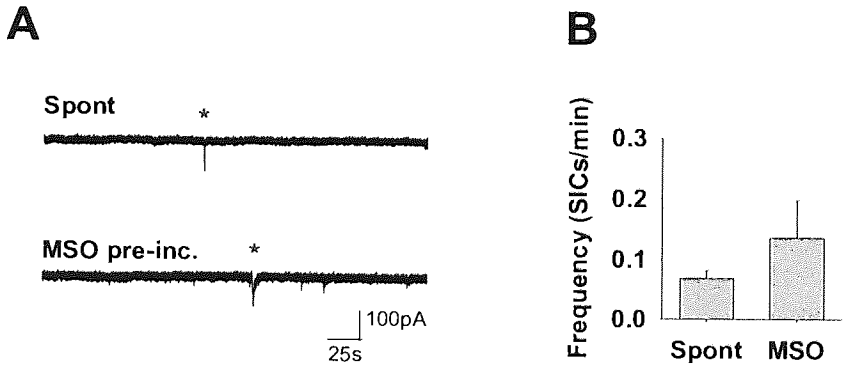

Figure 6.1: Prolonged MSO treatment slightly increases SIC frequency. A) Top trace shows normal spontaneous recording and trace below shows recording after pre-incubation in MSO (2.5mM). SICs are indicated with red asterisks. **B)** Bar graph comparing mean SIC frequency in spontaneous control slices and after MSO pre-incubation.

6.2 Long term exposure to Glu leads to "chemical" form of LTE

We next exposed the slices to external glutamate (Glu) by pre-incubating them in 200μM Glu for ≥60 minutes prior to experimenting. Kyn (2mM) was included in the pre-incubation medium to protect against tonic NMDA-receptor activation without preventing glutamate induced mGluR activation. Kyn pre-incubation alone did not have any effect on the spontaneous SIC frequency (Spont. 0.069±0.013 SICs/min {P10-15}; Kyn 0.062±0.01 SICs/min, Student's t-test p=0.75; n=35, 15 cells, respectively). Therefore spontaneous and Kyn data were pooled together and used as control. As shown in figure 6.2.1, pre-incubation with glutamate led to a substantial increase in spontaneous SIC frequency: The average SIC frequency after pre-incubation was increased by 1800% compared to control SIC frequency (Ctrl 0.066±0.01 SICs/min; Glu 1.26±0.2 SICs/min; Student's t-test p<0.005; n=50, 25 cells respectively).

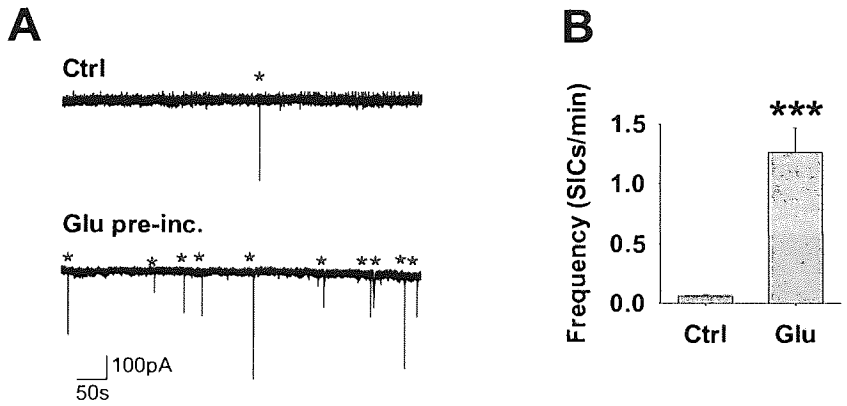

Figure 6.2.1: Glutamate pre-incubation increases SIC frequency. A) Top trace showing representative recording from a control slice (Kyn pre-incubated) and the trace below shows a recording from Glu (200μM) pre-incubated slice. SICs are indicated with red asterisks. **B)** Bar graph showing the mean SIC frequency in control and Glu (200μM) pre-incubated slices. (Statistical significance is presented as $p<0.05$ *, $p<0.01$ ** or $p<0.005$ ***).

The stability of Glu pre-incubation induced SIC enhancement was then analysed in the same way as SIC frequency in post LTS slices. SIC frequency from control slices (n=50) was compared to SIC frequency from pre-incubated slices (n=25) in 5 minutes bins over a 30 minute recording period. As seen in figure 6.2.2, Glu pre-incubation also induced a long lasting increase in SIC frequency, thus revealing a "chemical" form of LTE (Student's t-test p<0.005).

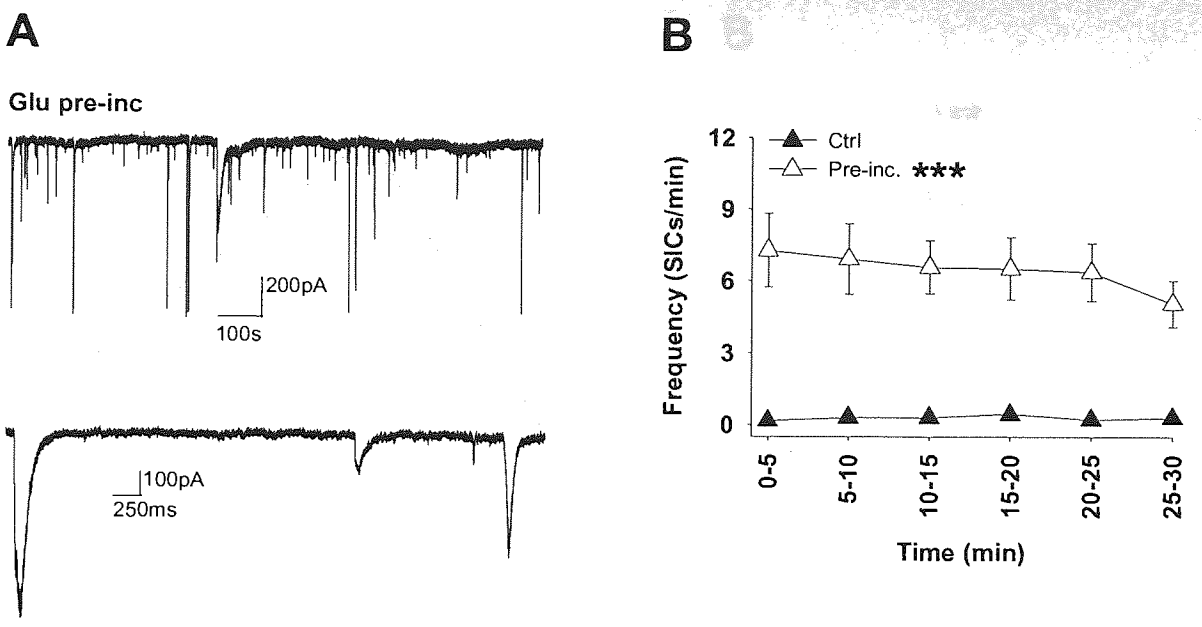

Figure 6.2.2: Glu pre-incubation induces "chemical" LTE. A) Recording from Glu pre-incubated slice showing high SIC frequency. Examples of 3 SICs are expanded beneath. **B)** Mean scatter plot illustrating SIC frequency in control (black) and Glu pre-incubated (white) slices in 5 minute bins over a 30 minute recording.

6.3 Glutamine pre-incubation also increases SIC frequency

As glutamine is converted to glutamate in neurons by glutaminase enzyme, we tested whether pre-incubating slices in glutamine (1mM) leads to an increase in SIC frequency. This may occur indirectly via enhanced spontaneous glutamate release from the neuronal presynaptic terminals [Szerb & O'Regan, 1984; 1985], which may then increase Glu supply at the synapse and consequently activate astrocytes. In addition, direct conversion of glutamine to glutamate may occur in astrocytes [Bowyer *et al.*, 1995] thus increasing the astrocytic glutamate stores. As shown in figure 6.3, pre-incubating slices in just glutamine did, indeed, increase the SIC frequency compared to Kyn pre-incubated control slices (Ctrl 0.06±0.01 SICs/min; Gln 0.5±0.2 SICs/min; Student's t-test p=0.0007; n=15, 4 cells respectively). This together with Glu pre-incubation results suggest that increase in glutamate supply leads to enhancement of spontaneous astrocytic gliotransmission release.

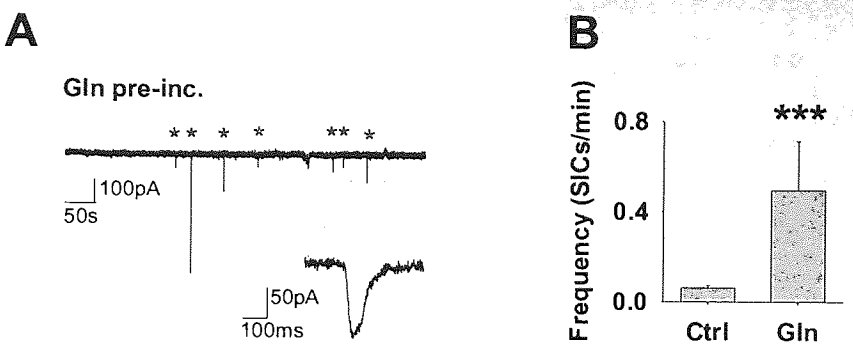

Figure 6.3: Glutamine pre-incubation increases SIC frequency. A) Recording from a Gln (1mM) pre-incubated slice. SICs are indicated with red asterisks with an example expanded beneath. **B)** Bar graph showing the mean SIC incidence in control and Gln pre-incubated slices.

6.4 "Chemical" LTE SICs are similar to spontaneous SICs

We then compared SICs induced by Glu pre-incubation with the spontaneous control SICs to assess if their properties and behaviour were similar. After a control recording period, TTX (1μM) was bath applied. As expected, SICs were insensitive to TTX (Ctrl 0.85±0.24; TTX 0.69±0.17; paired Student's t-test p=0.3; n=5 cells, Fig. 6.4.1).

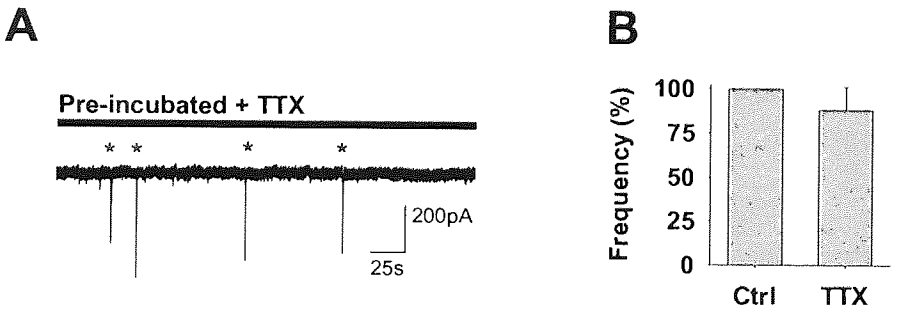

Figure 6.4.1: "Chemical" LTE SICs are TTX insensitive. A) Recording from pre-incubated slice showing insensitivity to TTX (1μM). SICs are indicated with red asterisks. **B)** Bar graph showing the percentage change of SIC frequency in presence of TTX in respect to control.

Cumulative probability distribution graphs in figure 6.4.2 show that SICs from Glu and Gln pre-incubated slices were often larger in amplitude and slower in kinetics (Ctrl n=134, Glu n=948 SICs; K-S test p<0.001, all parameters). The mean values are listed in table 6.4.2: mean amplitude was significantly increased in pre-incubated slices (Student's t-test p<0.005), whereas other mean parameters were not different (p>0.06).

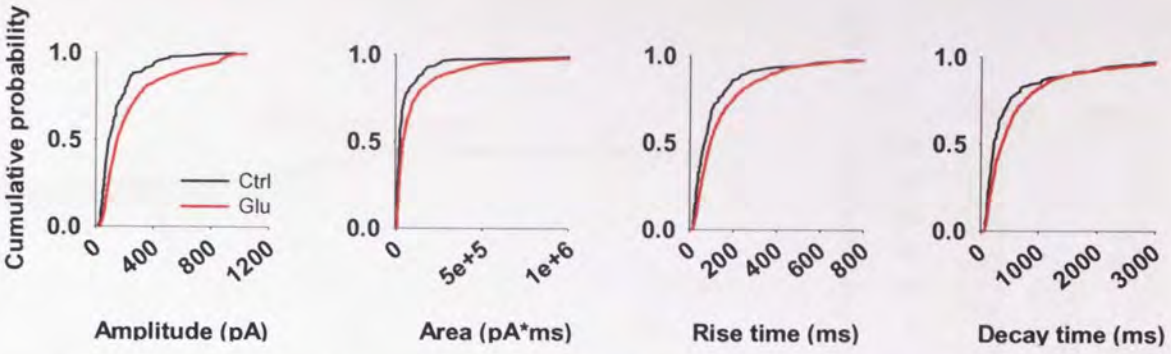

Figure 6.4.2: Cumulative probability distribution of ctrl and "chemical" LTE SICs. K-S test was significant for all parameters ($p<0.001$) (ctrl n=134; Glu n=948).

	Amplitude (pA)		Area (pA*ms)		Rise time (ms)		Decay time (ms)	
	Ctrl	Glu	Ctrl	Glu	Ctrl	Glu	Ctrl	Glu
Mean	149.5	**243.4**	328665.7	136456.8	165.4	172.4	1316.7	729.8
Median	94.7	**152.9**	16438.9	37683.4	68.0	94.5	231.6	366.6
Std.Dev	146.2	**227.4**	3060496.2	332704.7	469.0	241.4	7742.1	1254.9
Std.Err	12.6	**7.4**	265378.7	10805.7	40.5	7.8	668.8	40.8

Table 6.4.2: Mean SIC parameters of ctrl and "chemical" LTE. Amplitude was significantly different ($p<0.005$; **bolded**). Other parameters were not different ($p>0.06$).

The mean amplitude and rise time between Glu and Gln pre-incubated slices was also tested. This showed a significant difference (Amplitude: Glu 248.5±7.7pA, Gln 177.1±8.2pA, Student's t-test $p<0.005$; Rise time: Glu 161.1±23.4ms, Gln 98.2±20.7ms, $p=0.05$; n=892, 56 SICs respectively; data not shown), suggesting that pre-incubation directly in Glu increases the concentration in the astrocytic glutamate stores more efficiently.

"Chemical" LTE SICs were reversibly inhibited by the NMDA-receptor antagonist D-AP5 (50µM): Frequency was reduced from 1.3±0.5 SICs/min in control to 0.37±0.15 SICs/min (26.0% of control) during D-AP5 application (paired Student's t-test $p=0.0002$; n=6), returning to 0.86±0.38 SICs/min (53.0% of control) during D-AP5 wash-out ($p=0.02$). Figure 6.4.3 summarises the data. The remaining 40 SICs during D-AP5 application were significantly reduced in amplitude compared to 227 SICs in control conditions (Ctrl 231.0±14.7pA; AP5 142.1±27.3; Student's t-test $p=0.01$). Other parameters were not significantly changed ($p>0.07$). Mean values are listed in table 6.4.3. Presence of few SICs during D-AP5 application was probably due to incomplete antagonising effect.

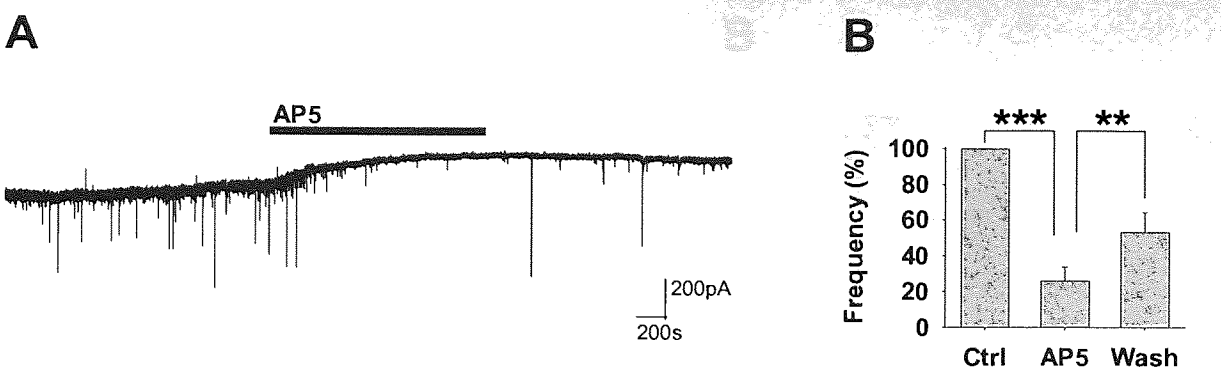

Figure 6.4.3: "Chemical" LTE SICs are inhibited by D-AP5. A) Recording from Glu pre-incubated slice showing high SIC frequency that is reversibly inhibited by D-AP5 (50μM). Shift in baseline in response to D-AP5 is due to tonic glutamate activation. **B)** Bar graph showing SIC frequency change during D-AP5 application and during wash-out in respect to control.

	Amplitude (pA)		Area (pA*ms)		Rise time (ms)		Decay time (ms)	
	Ctrl	AP5	Ctrl	AP5	Ctrl	AP5	Ctrl	AP5
Mean	231.0	**142.1**	115959.5	81105.5	159.0	225.0	618.7	738.1
Median	141.9	**78.0**	33020.4	28343.7	100.4	165.3	317.8	490.3
Std.Dev	220.9	**172.6**	243986.6	125600.8	217.5	208.8	894.4	803.6
Std.Err	14.7	**27.3**	16194.0	19859.2	14.4	33.0	59.5	127.1

Table 6.4.3: "Chemical" LTE SIC parameters for ctrl vs. D-AP5. Ctrl n=277 SICs; AP5 n=40 SICs. Amplitude p=0.01 (**bolded**), other parameters p>0.07.

Ifenprodil (10μM) also reduced both frequency and amplitude of SICs. Frequency was reduced to 47.2±8.5% of the control (Ctrl 1.83±0.87 SICs/min; Ifen. 0.8±0.4 SICs/min; paired Student's t-test p=0.025; n=3 cells). The remaining 24 SICs compared to 139 SICs during control period, were 64.4% smaller in amplitude (Student's t-test p=0.05), whilst other parameters were not different (p>0.1). Figure 6.4.4 summarises the frequency data and mean values for SIC parameters are listed in table 6.4.4.

	Amplitude (pA)		Area (pA*ms)		Rise time (ms)		Decay time (ms)	
	Ctrl	Ifen	Ctrl	Ifen	Ctrl	Ifen	Ctrl	Ifen
Mean	251.5	**89.6**	110305.2	28230.7	126.7	137.2	558.2	444.0
Median	100.7	**66.6**	26533.5	13427.7	99.2	93.9	333.3	350.9
Std.Dev	403.3	**63.5**	287902.1	28954.4	94.5	135.8	735.9	455.6
Std.Err	34.2	**13.0**	24419.5	5910.3	8.0	27.7	62.4	93.0

Table 6.4.4: "Chemical" LTE SIC parameters for ctrl vs Ifenprodil. Ctrl n=139 SICs; Ifen n=24 SICs. Amplitude p=0.05 (**bolded**), other parameters p>0.1.

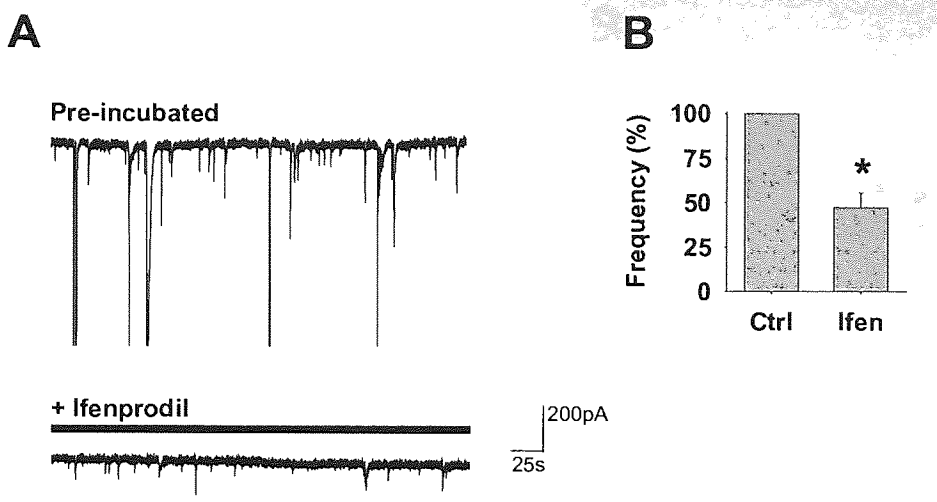

Figure 6.4.4: "Chemical" LTE SICs are inhibited by ifenprodil. A) Top traces shows recording from pre-incubated slice with high SIC frequency and below same TC neuron in presence of Ifenprodil (10μM) showing reduced SIC amplitudes. **B)** Bar graph showing the average frequency change in presence of Ifenprodil in respect to control.

6.5 The temporal profile of "chemical" LTE

Slices were pre-incubated for different durations prior to recording. As shown in figure 6.5.1, increase in SIC frequency was strongly correlated with the glutamate incubation time (r^2=0.3, Pearson's correlation p=0.003; n=25 cells). Mean SIC frequency in slices incubated for less than 2 hours was 0.43±0.1 SICs/min whereas after incubating for 5-6 hours, it was 2.68±0.1 SICs/min (Student's t-test p>0.000). In contrast, control slices incubated in Kyn (2mM) showed no change in SIC frequency as expected (r^2=0.06, p=0.4; n=15; Fig. 6.5.1).

In addition to increase in frequency, SIC kinetics became slower with longer incubation times as shown in figure 6.5.2 (Area r^2=0.9, Pearson's correlation p=0.0002; rise time r^2=0.85, p=0.0004; decay time r^2=0.8, p=0.001). Amplitude did not show significant correlation with the incubation time (r^2=0.3, p=0.1). In contrast, SICs in control conditions did not show any changes in SIC parameters (Ctrl amp r^2=0.1, p=0.6; rise r^2=0.06, p=0.8; area r^2=0.06, p=0.6; decay r^2=0.2, p=0.6).

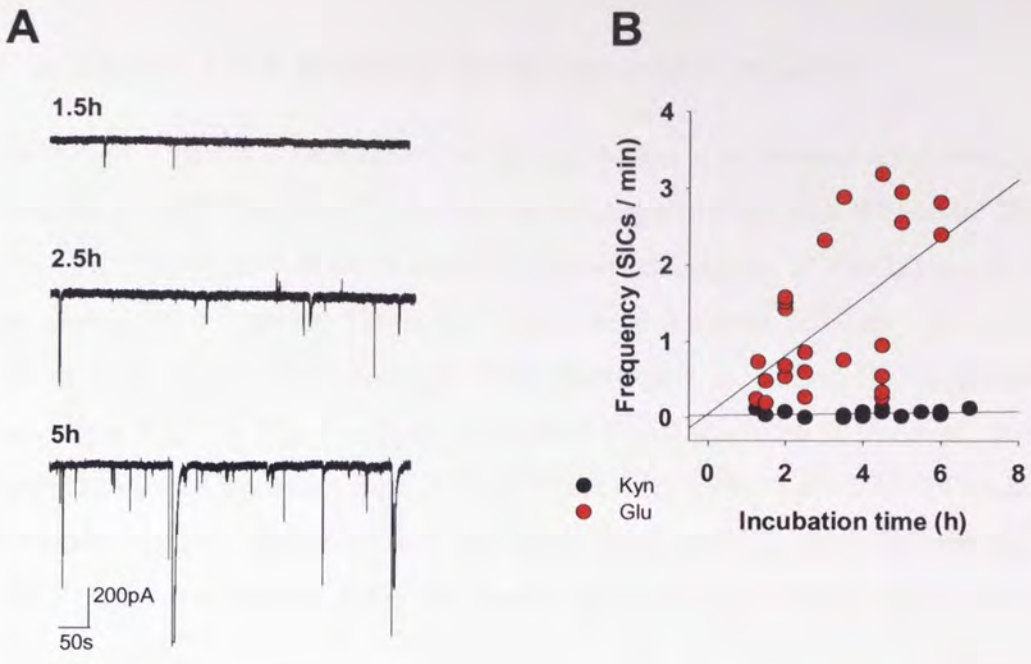

Figure 6.5.1: "Chemical" LTE shows temporal profile. A) Recordings from slices showing different SIC frequencies depending on the pre-incubation time (as indicated) in Glu (200µM) prior to experimenting. **B)** Scatter plot showing SIC frequency against the incubation time for control (Kyn) and Glu pre-incubated slices.

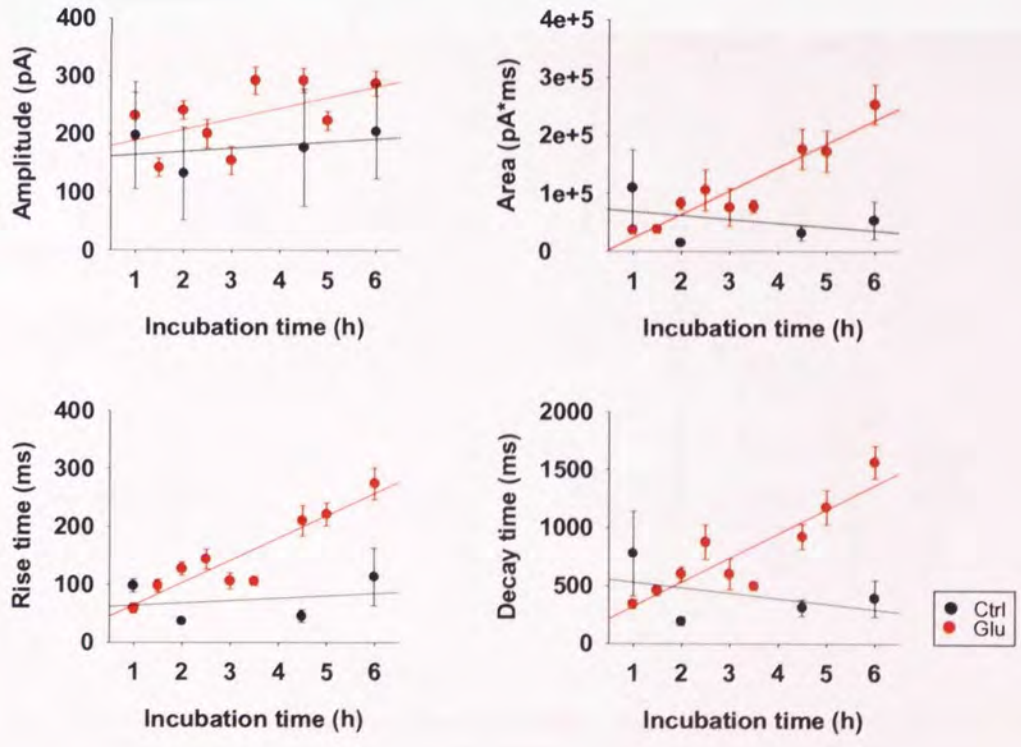

Figure 6.5.2: SIC magnitude increases with incubation time. Mean scatter plots showing amplitude, area, rise time and decay time in respect to Glu pre-incubation time (red) or control (black). Area, rise time and decay times showed positive correlation for Glu pre-incubation. Ctrl SICs did not show any correlation.

6.6 "Chemical" LTE displays developmental profile

The developmental profile of the effects of pre-incubation was assessed as shown in figure 6.6.1A-C. The overall frequency from Glu pre-incubated slices was 0.23±0.07 SICs/min during the 1st PN week (n=4 cells), 1.26±0.2 SICs/min during the 2nd (n=25) and 0.56±0.16 SICs/min during the 3rd (n=10) PN week. Significance between different age groups was compared from slices incubated between 3.5-5 hours only to control the incubation time dependent effect (Fig. 6.6.1D). Frequency of 0.23±0.07 SICs/min for 1st PN week (n=4) was significantly less than frequencies from 2nd and 3rd PN week (Wk2 1.67±0.38 SICs/min, n=10, Student's t-test p=0.04; Wk3 0.78±0.18 SICs/min, n=7, p=0.05). Although the frequency during the 2nd week was highest, it was not significantly different to the 3rd week (p=0.08).

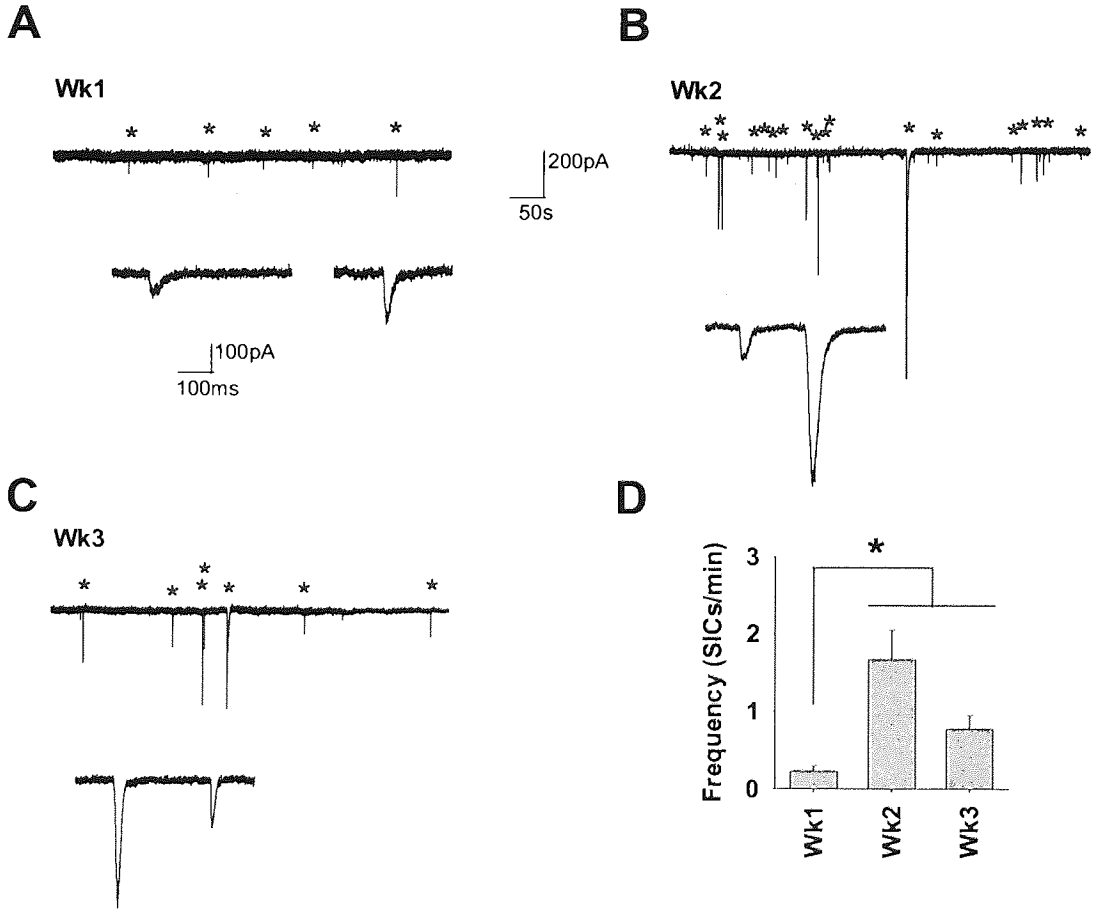

Figure 6.6.1: "Chemical" LTE shows developmental profile. A) Example trace from PN wk 1 pre-incubated slice. SICs are indicated with asterisks and expanded beneath. Scales are same for all traces (top scale for long recordings, bottom scale for SICs). **B)** Example from 2nd PN week pre-incubated slice. **C)** Example from 3rd PN week pre-incubated slice. **D)** Bar graph comparing the SIC frequency between age groups from slices incubated between 3.5-5 hours only.

Differences in SIC properties at different ages are illustrated in figure 6.6.2. Only SICs from slices incubated for 3.5-5h are included for comparison. The amplitude of the SICs was significantly higher during the 2nd PN week compared to the 1st and 3rd (wk1 127.3±27.1pA, n=29 SICs, Student's t-test p=0.002; wk2 265.3±11.7pA, n=420 SICs; wk3 114.0±10.1pA, n=72, p<0.005). SIC area during the 3rd week was significantly less (wk2 149547.1±19002.6 pA*ms; wk3 54818.7±10344.2 pA*ms, p=0.01). Other parameter were not significantly different (p>0.2).

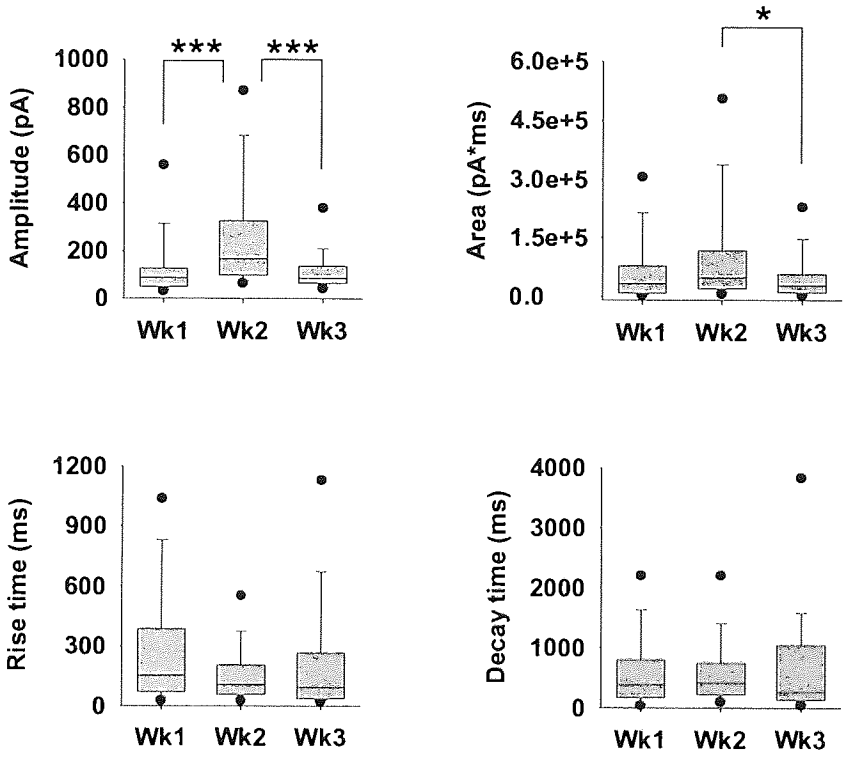

Figure 6.6.2: SIC properties vs. age for pre-incubated slices. SICs from experiments (Statistical significance is presented as $p<0.05$ *, $p<0.01$ ** or $p<0.005$ ***).

6.7 Group I mGluR antagonists do not inhibit "chemical" LTE

We then investigated the mechanism of Glu pre-incubation induced LTE. Since LTS induced SIC enhancement is via mGluRs, we first used the mGluR antagonists MTEP (20μM) and (s)-4-CPG (100-200μM) with Glu (200μM). Figure 6.7.1 summarises the results. The presence of MTEP and CPG during the pre-incubation period did not block the Glu incubation induced "chemical" LTE (Ctrl 1.04±0.45 SICs/min; MTEP+CPG 0.99±0.2 SICs/min; Student's t-test p=0.9; n=5, 6 cells respectively).

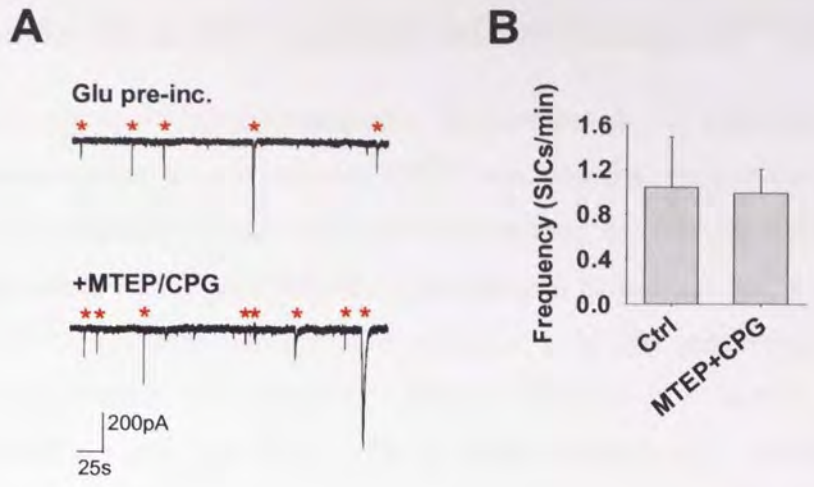

Figure 6.7.1: Group I mGluR antagonist does not inhibit "chemical" LTE. A) Top trace shows recording from Glu pre-incubated slice and trace below shows recording from Glu incubation in presence of group I mGluR antagonists MTEP (20μM) and CPG (200μM). SICs are indicated with red asterisks. **B)** Mean bar graph showing the SIC frequency in control (Glu pre-incubated) and pre-incubation in presence of mGluR antagonists.

Changes in SICs were assessed by comparing the two populations (Fig. 6.7.2). Rise times showed a significant difference in the cumulative population distribution (K-S test p=0.05) whereas other parameters did not (p>0.2). Mean ctrl amplitude was 267.9±20.9pA and in slices incubated with mGluR blockers and Glu it was 252.4±17.7pA (Student's t-test p=0.6; n=155, 192 SICs respectively). SIC area was 168612.2±25834.1 pA*ms for ctrl and 226002.5±34026.6 pA*ms for mGluR blockers (p=0.2). Rise time was 177.7±23.0ms for ctrl and 271.8±45.2ms for mGluR blockers (p=0.08). Mean decay time was significantly slower in slices pre-incubated with the blockers (Ctrl 946.5±102ms; MTEP/CPG 1315.4±137.4ms; p=0.04).

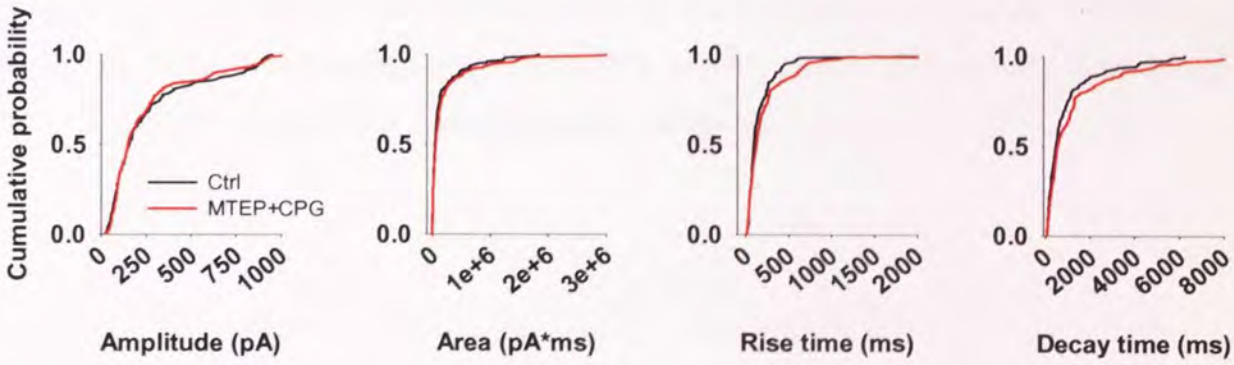

Figure 6.7.2: "Chemical" LTE SICs from ctrl vs. with mGluR antagonists slices. K-S test for rise time showed significant difference (p=0.05). Other parameters were not different.

6.8 Glu uptake via EAAT is required for "chemical" LTE

Next we studied glutamate uptake transporter involvement in the induction of "chemical" LTE. The broad-spectrum EAAT inhibitor TBOA was added to the pre-incubation medium together with Glu (200μM). Figure 6.8.1 summarises data for Glu pre-incubation and Glu incubation in presence of TBOA (300μM) in comparison to average SIC frequency in Kyn controls. In these experiments Glu incubation induced a 4670% increase in SIC frequency compared to spontaneous SIC frequency (Kyn 0.066±0.013 SICs/min; Glu 3.13±0.6 SICs/min; Student's t-test $p<0.005$; n=15, 6 cells respectively). TBOA significantly attenuated this Glu incubation induced increase in SIC frequency (Glu/TBOA 0.41±0.17 SICs/min; p=0.01; n=7). Glu incubation induced "chemical" LTE was not however completely inhibited and the SIC frequency remained significantly higher compared to Kyn controls (p=0.005) which may be attributable to mGluR activation.

The decrease in "chemical" LTE in the presence of TBOA showed concentration dependency as seen in figure 6.8.1C. In respect to mean SIC frequency in Glu pre-incubated slices (1.26±0.2 SICs/min; n=25 cells), TBOA at concentrations of 50μM (n=9) and 100μM (n=7) did not cause significant reduction (50μM 1.5219±0.4029 SICs/min, p=0.5; 100μM 0.75±0.49, p=0.3).

Mean SIC properties from Glu pre-incubated, and Glu pre-incubated in presence of 300μM TBOA were compared. Mean amplitude was significantly lower in TBOA treated slices (Ctrl 268.4±12.3pA; TBOA 154.3±19.2pA; Student's t-test $p<0.005$; n=334, 76 SICs respectively) although SIC area was not different (Ctrl 113107.1±15335.3 pA*ms; TBOA 96849.3±32250.3 pA*ms; p=0.6). On the other hand, TBOA treated slices had slower kinetics (Rise time: Ctrl 155.4±12.2ms, TBOA 250.3±76.8, p=0.03; Decay time: Ctrl 538.7±46.6ms, TBOA 812.2±175.4ms, p=0.04). Data is presented in figure 6.8.2.

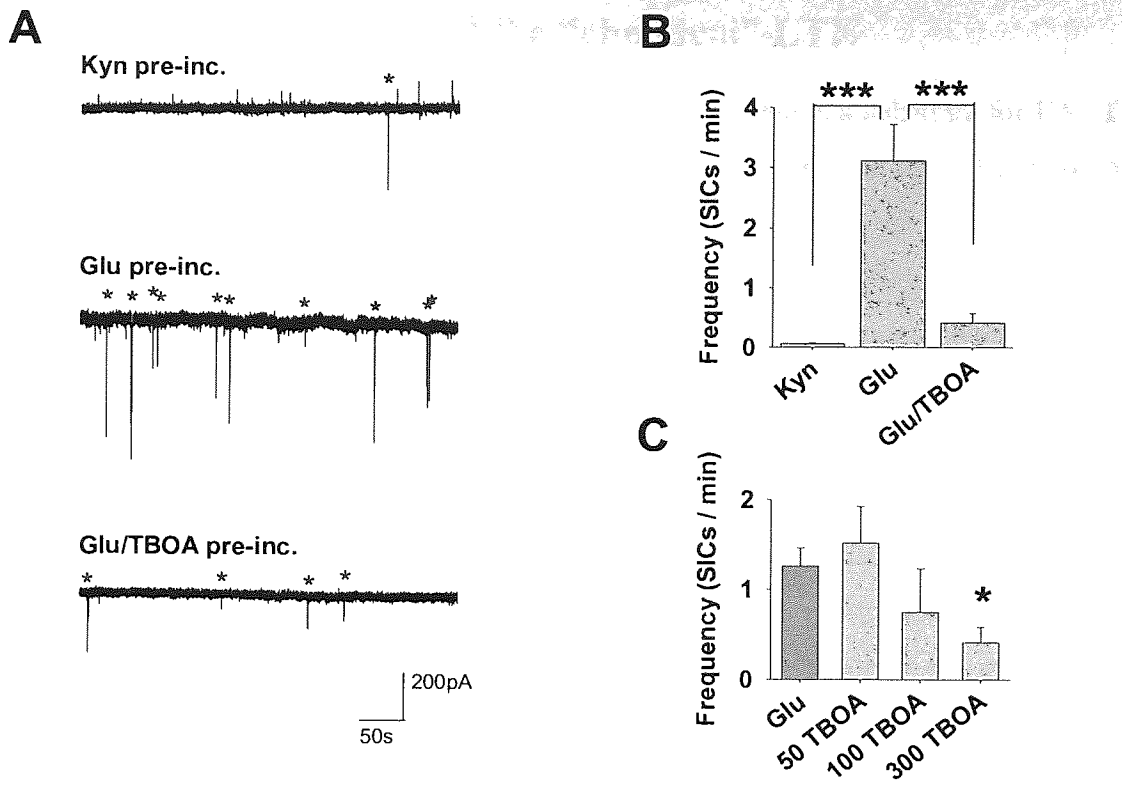

Figure 6.8.1: "Chemical" LTE is inhibited by TBOA. A) Top trace shows a control recording (pre-incubated in Kyn, 2mM). Middle trace shows a recording from Glu (200μM) pre-incubated slice and trace at the bottom shows recording from a slice incubated in Glu (200μM) and TBOA (300μM). **B)** Bar graph compares the mean SIC frequency from control slices (Kyn) to Glu pre-incubated and Glu/TBOA pre-incubated slices. **C)** Mean SIC frequency in Glu pre-incubated and in presence of different TBOA concentrations.

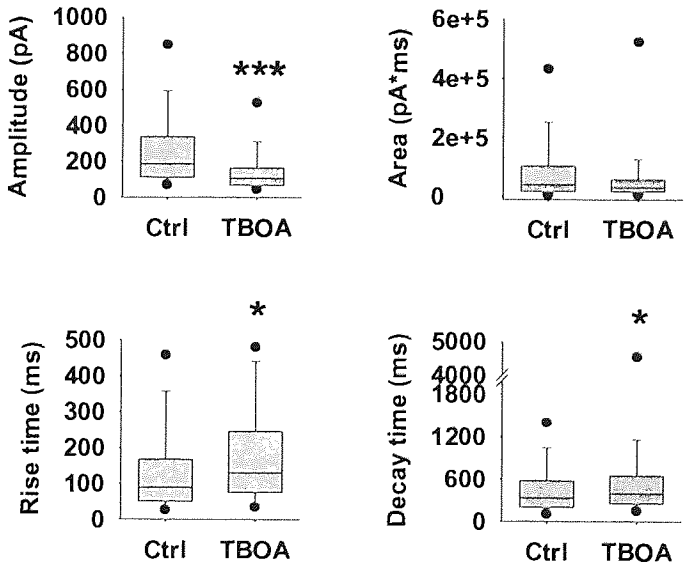

Figure 6.8.2: SIC properties in Glu vs Glu/TBOA pre-incubated slices. (Statistical significance is presented as $p<0.05$ *, $p<0.01$ ** or $p<0.005$ ***).

6.9 D-Aspartic acid reproduced the "chemical" LTE

Aspartic acid acts as a selective agonist for the NMDA-receptor and is a substrate for EAAT transporters (D'Aniello, 2007). Thus, D-Aspartic acid (D-Asp) (200μM) could be used to further examine the involvement of glutamate transporter activity in the pre-incubation induced LTE. As shown in figure 6.9.1, pre-incubation in D-Asp led to a similar "chemical" LTE as did pre-incubation in Glu (200μM). SIC frequency from D-Asp pre-incubated slices (0.74±0.23 SICs/min, n=10) was compared with controls (Kyn 0.062±0.01 SICs/min, n=15) and Glu pre-incubated slices (1.26±0.2 SICs/min, n=25). The D-Asp induced increase in SIC frequency was significantly higher than control slices (Student's t-test p=0.001), but insignificant to Glu induced LTE (p=0.15). Furthermore, the results showed similar incubation time dependent increase in SIC frequency as during Glu pre-incubation (r^2=0.76, Pearson's correlation p=0.001; Fig. 6.9.1C). Less than 2h pre-incubation (n=3) resulted in frequency of 0.14±0.02 SICs/min compared to 1.28±0.3 with over 3 hours pre-incubation (n=5).

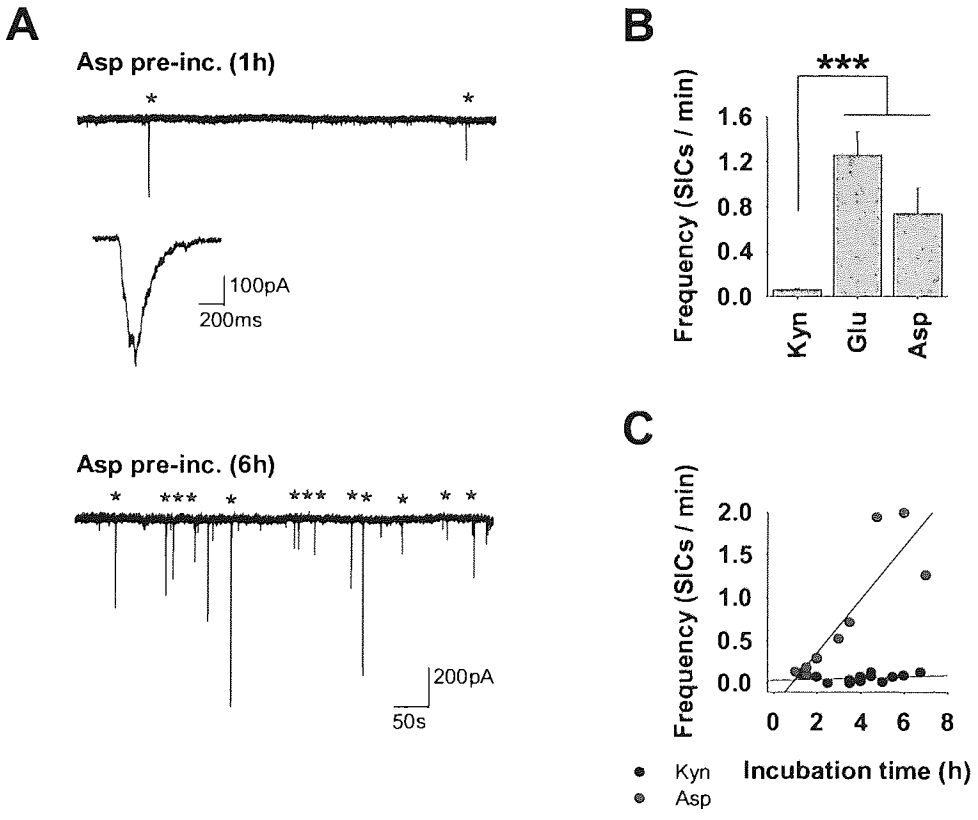

Figure 6.9.1: D-Asp mimics the Glu pre-incubation induced LTE. A) Top trace shows an example recording from a slice pre-incubated in D-Asp (200μM) for 1 hour. SICs indicated with red asterisks and example expanded beneath. Trace below shows an example recording from a slice incubated for 6h. **B)** Bar graph comparing the SIC frequency from control (Kyn pre-incubated, 2mM), Glu (200μM) pre-incubated and D-Asp pre-incubated slices. **C)** Scatter plot showing SIC frequency in respect to incubation time (hours) in control conditions and D-Asp pre-incubation.

D-Asp pre-incubation induced SICs (n=183) were characterised and compared to spontaneous control SICs (n=134). Mean values are listed in table 6.9.1. Amplitude was significantly higher after D-Asp pre-incubation (Student's t-test $p<0.005$). Other parameters were not significantly different ($p>0.1$).

	Amplitude (pA)		Area (pA*ms)		Rise time (ms)		Decay time (ms)	
	Ctrl	Asp	Ctrl	Asp	Ctrl	Asp	Ctrl	Asp
Mean	149.5	**255.8**	328665.7	116219.3	165.4	156.2	1316.7	553.8
Median	94.7	**155.0**	16438.9	42511.0	68.0	100.6	231.6	322.7
Std.Dev	146.2	**243.4**	3060496.2	226241.7	469.0	160.6	7742.1	787.8
Std.Err	12.6	**18.0**	265378.7	16724.3	40.5	11.9	668.8	58.2

Table 6.9.1: D-Asp incubation induced SIC parameters. Amplitude was significantly different ($p<0.005$; **bolded**), but other parameters did not differ significantly ($p>0.1$).

Furthermore, we assessed TTX insensitivity and the involvement of NMDA-receptors on the D-Asp induced SICs. Figure 6.9.2 summarises the data. As expected, TTX (1μM) did not have any effect on the frequency (Ctrl 1.28±0.3 SICs/min; Asp 1.04±0.3 SICs/min; paired Student's t-test $p=0.3$; n=5 cells) and SICs were reversibly blocked by D-AP5 (50μM). Frequency was reduced from 1.43±0.3 SICs/min to 0.36±0.15 SICs/min in presence of D-AP5 (Paired Student's t-test $p=0.01$; n=4), and returned to 0.66±0.2 SICs/min during D-AP5 wash-out ($p=0.02$). These results demonstrate that D-Asp induces SICs that express similar kinetics and properties to normal spontaneous and Glu incubation induced SICs.

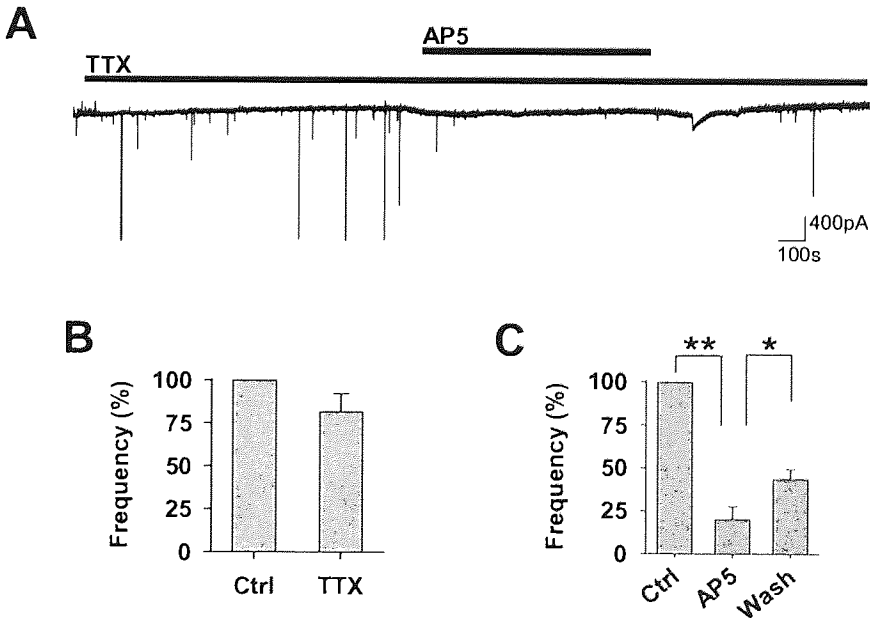

Figure 6.9.2: D-Asp induced SICs are TTX insensitive and NMDA-R mediated. A) Example recording from D-Asp pre-incubated slice showing that SIC were TTX insensitivite (1μM) but reversibly inhibited by D-AP5 (50μM). **B)** Bar graph showing mean SIC frequency in presence of TTX in respect to control. **C)** Bar graph showing mean SIC frequency in control, in D-AP5 and during wash-out.

6.10 D-Asp uptake confirms the role of EAAT in "chemical" LTE

To test whether D-Asp induced "chemical" LTE by uptake mechanism rather than direct action on NMDA-receptors, TBOA (150-300μM) was included in the pre-incubation medium (D-Asp, 200μM). As shown in figure 6.10, TBOA inhibited the "chemical" D-Asp LTE also in a concentration dependent manner. SIC frequency from slices treated with a ≥2 hour pre-incubation period in D-Asp (1.0±0.28 SICs/min; n=7) was compared to events from slices pre-incubated in the presence of TBOA. A concentration of 150μM did not inhibit the "chemical" LTE (0.91±0.26 SICs/min; Student's t-test p=0.8; n=3), whereas at concentration of 300μM, the frequency was decreased by approximately 85% (0.15±0.07 SICs/min; p=0.02; n=6) compared to D-Asp pre-incubation.

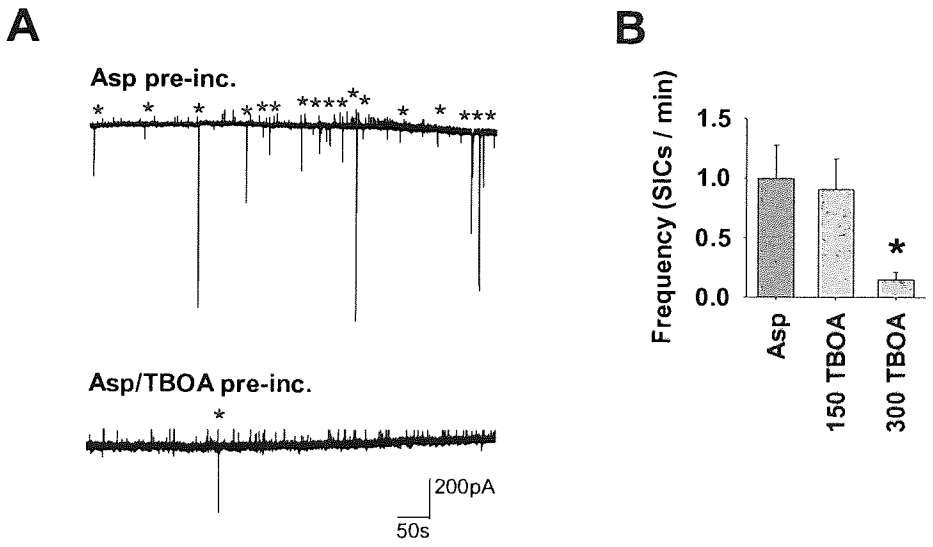

Figure 6.10: TBOA inhibits D-Asp induced "chemical" LTE. A) Top trace shows recording form a slice pre-incubated in D-Asp (200μM) and trace below shows a recording from slice incubated in D-Asp and TBOA (300μM). SICs are indicated with red asterisks. **B)** Bar graph showing the mean SIC frequency for slices incubated just in D-Asp or in presence of TBOA.

6.11 mGluR activation does not enhance D-Asp induced LTE

We showed previously that long term exposure to DHPG (100μM) mimicked the LTS induced LTE (Fig. 5.9.2). Since D-Asp acts on NMDA-receptors but not mGluRs, we next studied whether pre-incubation in D-Asp together with the mGluR agonist DHPG would further augment the "chemical" LTE. However, pre-incubation in D-Asp (200μM) with DHPG (100μM) did not further increase the SIC frequency as shown in figure 6.11, suggesting saturation of the system. Mean frequency after D-Asp/DHPG pre-incubation was 0.56±0.11 SICs/min (n=5) compared to 0.74±0.23 SICs/min with D-Asp alone (n=10; Student's t-test p=0.6).

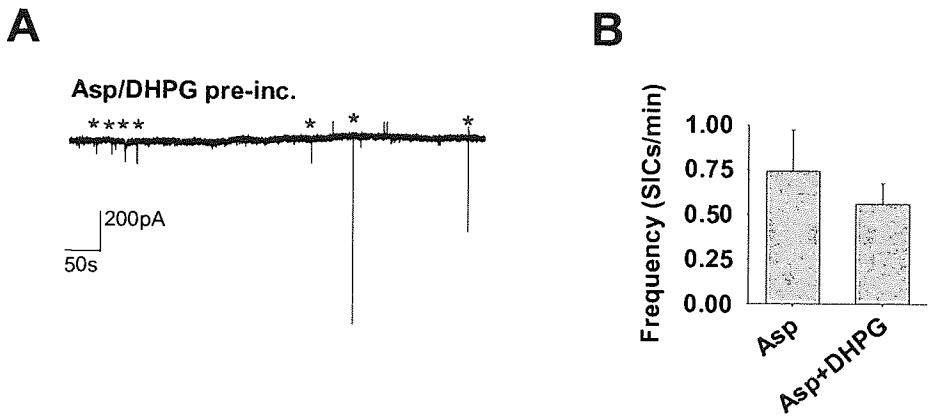

Figure 6.11: DHPG does not augment the D-Asp induced "chemical" LTE. A) Example recording from slice pre-incubated in D-Asp (200μM) with DHPG (100μM). **B)** Bar graph comparing the mean SIC frequency from D-Asp and D-Asp/DHPG pre-incubated slices.

To assess whether DHPG in addition to D-Asp had any effect on SICs, we compared SICs from D-Asp pre-incubation experiments with SICs from D-Asp/DHPG pre-incubated slices. Mean values are listed in table 6.11. Rise times were significantly longer after pre-incubation with D-Asp/DHPG (Student's t-test p=0.03; Asp n=183; Asp/DHGP n=83), but other parameters were not different (p>0.5).

	Amplitude (pA)		Area (pA*ms)		Rise time (ms)		Decay time (ms)	
	Asp	Asp/DHPG	Asp	Asp/DHPG	Asp	Asp/DHPG	Asp	Asp/DHPG
Mean	255.8	234.2	116219.3	149029.1	156.2	**231.3**	553.8	555.6
Median	155.0	146.4	42511.0	27180.7	100.6	**88.8**	322.7	279.7
Std.Dev	243.4	242.0	226241.7	493764.4	160.6	**405.0**	787.8	755.9
Std.Err	18.0	26.6	16724.3	54197.7	11.9	**44.5**	58.2	84.0

Table 6.11: Asp vs Asp/DHPG induced. Rise time was significantly different (p=0.03, **bolded**), whereas other parameters were not.

6.12 Discussion

Here, we showed that increasing extracellular glutamate concentration induces long term enhancement of SIC frequency, which was termed "chemical" LTE. This increase was attributable to glutamate uptake via EAAT. "Chemical" LTE SICs shared the same basic properties as spontaneous SICs presented in Chapter 3: they were similar in kinetics, insensitive to TTX and inhibited by the NMDA-receptor antagonist D-AP5.

Glutamate uptake into the astrocytes played the major role in "chemical" LTE as the broad spectrum EAAT antagonist TBOA significantly reduced it. It is noteworthy that SIC prevalence after Glu/TBOA incubation was still significantly higher than spontaneous frequency in control slices. Therefore, it is likely that a proportion of the "chemical" LTE was due to mGluR activation. D-Asp, which is a substrate for EAA transporter [D'Aniello, 2006], also induced "chemical" LTE, thus confirming the central role of EAA uptake into astrocytes. Presynaptic amino acid uptake and subsequent spontaneous release cannot be excluded, but it is unlikely as all chemically induced SICs shared the same properties as the well established SICs from non-neuronal origins (see introduction and chapter 3). Furthermore, as D-Asp is an agonist only for NMDA-receptors [D'Aniello, 2006], it confirms the central role of NMDA-receptors being the target for gliotransmission. Considering the slow variable kinetics of these SICs, they are most likely extrasynaptic as discussed before in chapter 3.

Surprisingly, the increase in SIC frequency by Glu/Asp pre-incubation exhibited strong temporal dependency. It may be that the time dependent increase was due to insertion of new EAA transporters which has been shown at least on cultured astrocytes in response to Glu exposure [Duan *et al.*, 1999]. This would increase uptake rate over time and potentially aid building up of cytosolic glutamate in astrocytes. Increase in surface expression of GLASTs was shown to be triggered by transporter activity itself rather than activation of glutamate receptors, which may explain why the results presented here as well as in the previous study were reproduced by D-Asp [Duan *et al.*, 1999].

The finding that D-Asp induces SICs adds even further complexity to the possible gliotransmitter release mechanism. As we showed in the previous chapter, LTE was surprisingly not accompanied with changes in astrocytic somatic Ca^{2+} elevations, thus questioning the consensus of Ca^{2+} dependent gliotransmission. D-Asp (and Glu) has been

shown to be released from astrocytes via P2X, hemichannels and swelling induced mechanisms, which all are considered as more pathological than physiological conditions [Rutledge & Kimelberg, 1996; Duan *et al.*, 2003; Ye *et al.*, 2003]. Furthermore, vesicular glutamate transporters have been shown not to transport aspartate [Fremeau *et al.*, 2001]. However, some evidence suggests that D-Asp is stored in synaptic vesicles-like structures at nerve endings in conjunction with other AAs [D'Aniello, 2006]. Therefore, SICs mediated via Ca^{2+} dependent/independent vesicle release in pre-incubated slices is not completely ruled out.

We also tested glutamine induced enhancement of glutamate release which has been previously shown in cell cultures and hippocampal slices [Szerb & O'Regan, 1984; 1985]. Here, glutamine incubation led to a significant increase in SIC frequency. However, the increase was not as intense as with Glu pre-incubation, rather it reached the same level as with the LTS protocol. This suggests that the SIC increase was due to an indirect enhancement of spontaneous presynaptic Glu release acting on astrocytic mGluRs or glutamate uptake, rather than directly in astrocytes. However, several Na^{+}-dependent glutamine transporter genes have been isolated and studies in rats indicate that ASCT2/ATB^{0}, for example, is expressed on glia [Bode, 2001; Heckel *et al.*, 2003]. Transporters have been shown to mediate both influx and efflux; therefore it is possible that astrocytic amino acid transporters are also involved in uptake of glutamine [Bröer *et al.*, 1999]. Indeed, some studies suggest that enzymatic conversion of glutamine to glutamate within glia may be an important factor in the glutamine-mediated elevation of extracellular glutamate levels [Bowyer *et al.*, 1995; Kvamme *et al.*, 2001]. The mechanism of Gln induced enhancement of SICs was not studied further at this point, but these results support the idea that increasing external glutamate supply directly or indirectly is a critical factor in enhancement of spontaneous SIC frequency.

The degree of "chemical" LTE varied across the developmental period; the 2nd PN week exhibited the most profound increase. Interestingly, SICs during this week were again higher in amplitude which is consistent with spontaneous SICs presented in chapter 3. Although more data will be needed to assess the degree of "chemical" LTE to its full extension, it is interesting to note that slices from the 1st PN week were hardly affected similarly to post LTS LTE presented in chapter 5. Moreover, even though the overall post LTS LTE was highest during the 3rd PN week, the second week appears to be most reliable. As discussed in chapter 3 and 5, this may be related to the developmental changes in the VB thalamus.

Chapter 7

Effect of synaptic stimulation on "Glu loaded" slices

The finding that overall SIC frequency often decreased following stimulation rather than increased as shown in chapter 4 (Fig. 4.3.4), added complexity to the interpretation of bi-directional signalling between neurons and astrocytes. The fact that SICs occur at extremely low frequencies in general made the evaluation more difficult whether acute synaptic stimulation decreased SIC incidence by an unknown mechanisms or occurred by chance. Since we have now discovered a method to increase the glutamate concentrations in astrocytes and SIC frequency, we took advantage of this to investigate the effects of acute synaptic stimulation modulating the SIC frequency (Fig. 7.0). If the lack of SICs occurring reliably after acute stimulation was due to insufficient Glu stores in astrocytes, stimulation of glutamate "loaded" astrocytes should give more insight to whether SICs can be evoked via the astrocytic mGluR pathway or whether spontaneous SICs are unresponsive to acute stimulation.

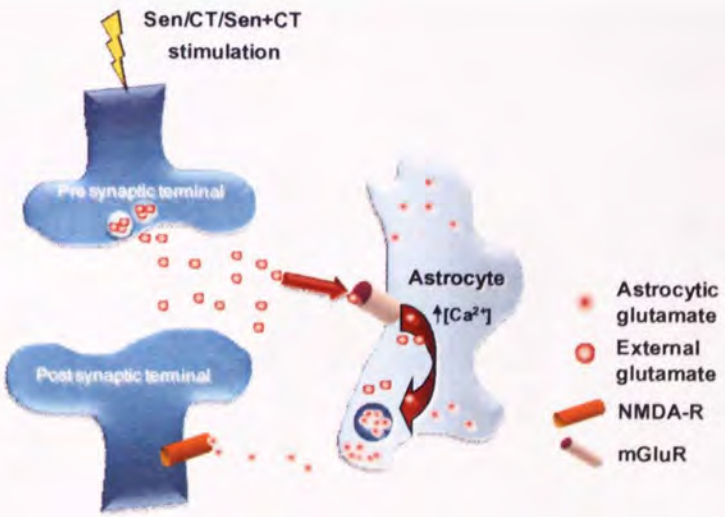

Figure 7.0: Synaptic stimulation on Glu "loaded" slices. Slices were first pre-incubated with Glu to "load" the astrocytes. Acute stimulations were then delivered onto Sen or CT or simultaneously to both inputs to assess the effect on SICs.

7.1 Stimulation at different frequencies and durations does not increase SIC frequency in pre-incubated slices

First, the effect of different stimulus durations and frequencies was assessed. Four different stimulus durations (0.2s, 3s, 6s, 10s) or frequencies (1Hz, 5Hz, 10Hz, 50Hz) were delivered on sensory or CT afferents after pre-incubating slices in Glu (200μM) for ≥2h to increase spontaneous SIC frequency. Sen and CT stimulation data were pooled together. Mean SIC frequency from the spontaneous control period was compared to mean SIC frequency over 60s after each stimulation. Figure 7.1 summarises the data. Apart from depression of SIC frequency following 1Hz stimulation (from 0.3231±0.0533 to 0.0769±0.0769 SICs/min; paired Student's t-test p=0.02; n=13 cells), neither different stimulus durations (n=15) nor different frequencies (n=13) had any effect on SIC frequency.

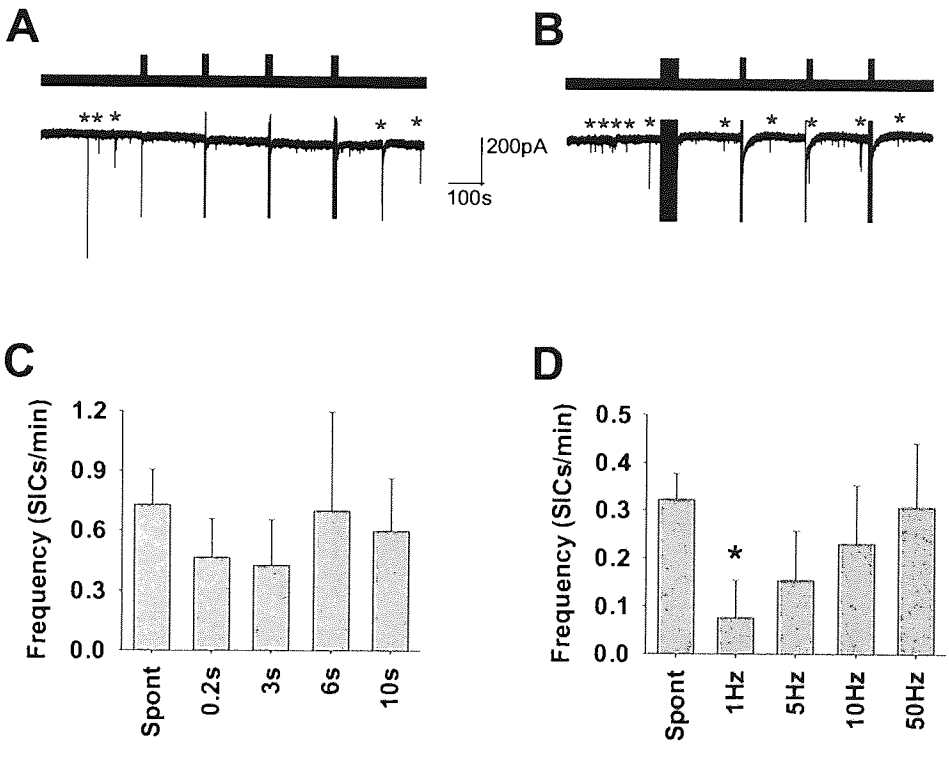

Figure 7.1: Different stimulus durations and frequencies on pre-incubated slices. A) Protocol (top) illustrating pattern of four different stimulus durations delivered to CT input. The responses are shown in the example trace below, with SICs indicated by red asterisks. **B)** Protocol (top) illustrating different stimulus frequencies pattern and below is an example trance of responses during Sen stimulation. **C)** Mean bar graph showing the SIC frequency from spontaneous control period and following different stimulus durations. **D)** Mean bar graph showing the SIC frequency from spontaneous control period and following different stimulus frequencies. (Statistical significance is presented as $p<0.05$ *, $p<0.01$ ** or $p<0.005$ ***).

7.2 Acute synaptic stimulation suppresses SIC activity

To assess the overall effect of stimulation on the SIC frequency, slices were first pre-incubated in Glu (200μM). We then applied the optimal stimulus protocol (shown in Fig. 4.4) first to their respective inputs (Sen 10s/20Hz; CT 0.2s/50Hz) and then simultaneously. The experiment was constructed so that spontaneous activity was recorded for 10 minutes before any stimulation period. Each stimulation period consisted of 4 stimulation episodes using the optimal stimulus parameters at 60s inter-stimulus-intervals. Mean SIC frequency of the 10 minutes spontaneous recordings between any stimulation period was compared to mean SIC frequency during each stimulation period. Interestingly, on average SIC frequency was depressed during stimulation periods whilst appearing increased during the 10 minutes silent periods between the stimulation episodes as shown in figure 7.2B. SIC frequency reduced from 0.92±0.2 SICs/min to 0.63±0.13 SICs/min during Sen stimulation (Paired Student's t-test p=0.04; n=11 cells), from 0.88±0.18 to 0.59±0.14 during CT stimulation (p=0.1; n=9) and from 0.83±0.2 to 0.35±0.13 during simultaneous stimulation (p=0.03; n=7). Overall there was a 40% reduction during stimulation periods.

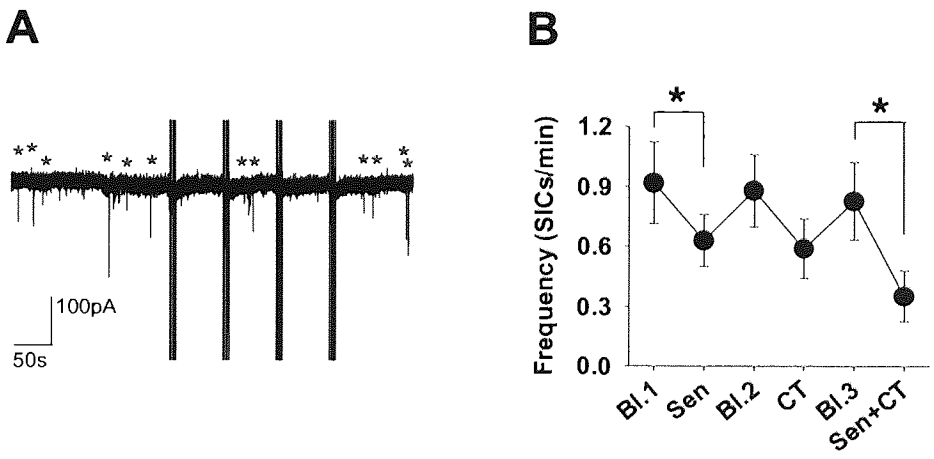

Figure 7.2: SIC frequency decrease during stimulation in Glu loaded slices. A) Example trace from Glu (200μM) pre-incubated slice showing baseline prior to CT stimulation (4 stimulation episodes of 5x0.2s/50Hz stimuli). SICs are indicated with red asterisks. Thick vertical bars indicate stimulation artefacts. SIC incidence over the 10 minutes silent period prior to the first stimulation was compared to the overall SIC incidence over the stimulation episodes (including all 4 stimulation shown in the figure and 60s after the last stimulation). **B)** Mean scatter plot showing the SIC frequency change during silent baseline (Bl.1-3) periods and stimulation episodes.

7.3 Stimulation suppresses SIC rather than enhances them

Next we focused on a single stimulation episode to assess what happens before and after stimulation. Slices were again pre-incubated in Glu (200μM) and then stimulated once either on sensory (10s at 20Hz/50Hz) or CT (0.2s or 10s at 50Hz) afferents. A minimum of 5 minutes was recorded before and after the stimulation. As shown in figure 7.3.1C-D, SIC amplitude was plotted against the time before and after stimulation to assess the change in SIC frequency and SIC properties at the same time. Specific attention was given to the period of 60s following synaptic stimulation as this corresponds to the typical inter-stimulus-interval used here and in Chapter 4 (grey shadowed area following stimulation marked with red line). After sensory stimulation (n=14), a slight decrease was observed in SICs prevalence after the stimulation, whereas after CT stimulation (n=21), the difference was not as obvious.

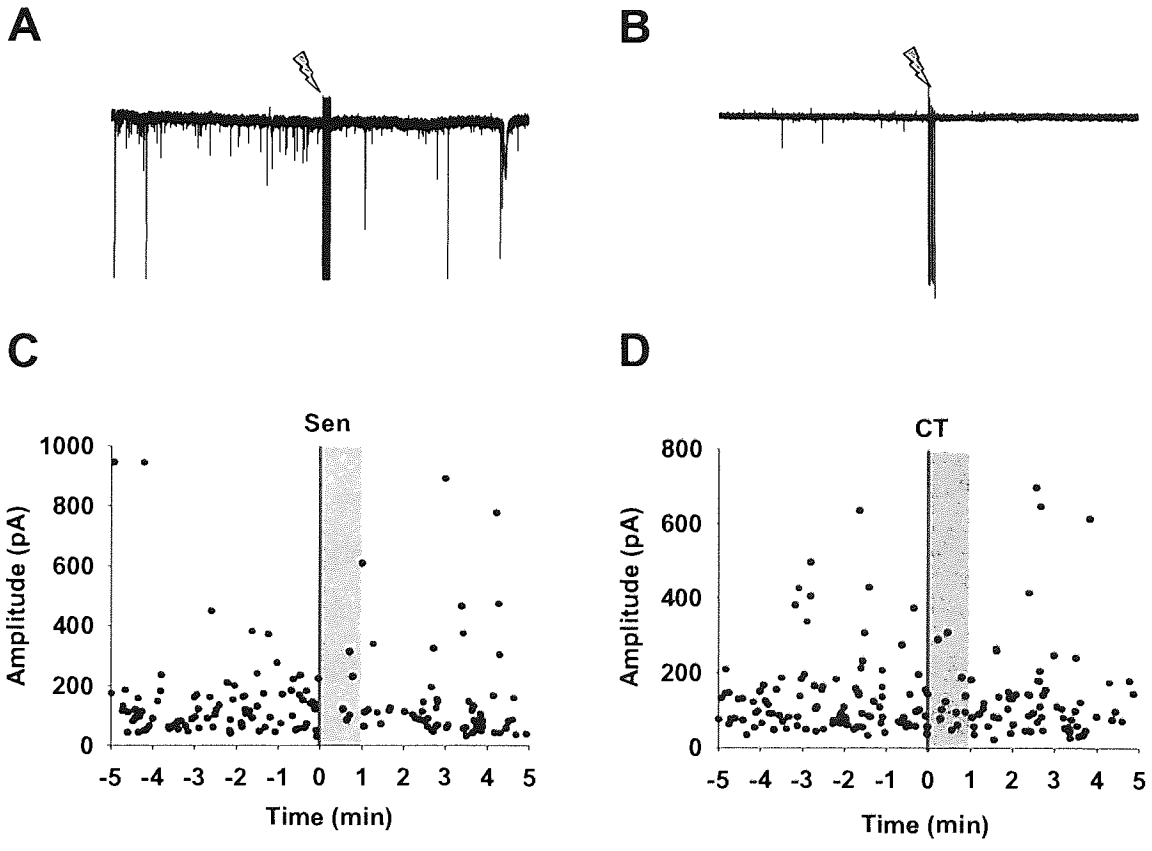

Figure 7.3.1: SICs pre and post stimulation in Glu incubated slices. A) Example of Sen stimulation on Glu (200μM) pre-incubates slices showing high SIC frequency. Lightning bolt indicates the stimulation (10s/20Hz). **B)** Example of CT stimulation (5x0.2s/50Hz) on pre-incubated slice showing SICs before but not after stimulation. **C)** Dot plot showing SIC amplitude against time before and after Sen stimulation. Red line at 0 time point indicates the stimulation time point. Grey area indicates an average inter-stimulus-interval period after the stimulus. **D)** SIC amplitude against the time before and after CT stimulation.

Mean SIC frequency was calculated 5 minutes before and after stimulation in 60 seconds bins as shown in figure 7.3.2. During both sensory and CT stimulation, mean SIC frequency appeared to be depressed for 1-2 minutes after the stimulation. This reduction, however, was not significant when comparing the frequency over 60 seconds before and after stimulation (Sen: pre stim. 1.43±0.7 SICs/min, post stim. 0.36±0.17 SICs/min, paired Student's t-test p=0.17, n=14; CT: pre stim. 1.0±0.2 SICs/min, post stim. 0.58±0.2 SICs/min, p=0.18, n=21).

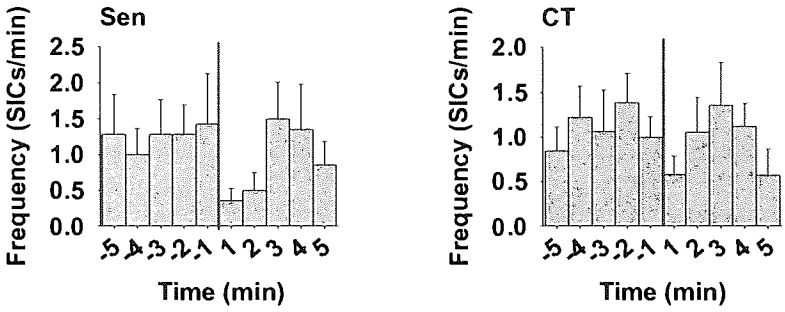

Figure 7.3.2: SIC frequency pre and post stimulation in pre-incubated slices. Mean SIC frequency was calculated for a each 60 minute time period 5 minutes before and after stimulation. Mean bar graph on the left shows data during sensory stimulation and on the right during CT stimulation.

7.4 Discussion

These results are in agreement with results shown in chapter 4 that despite evoking astrocytic Ca^{2+} elevations, synaptic stimulation does not evoke SICs. A trend towards a decrease in SIC prevalence after stimulation was even more profound here when using the "chemical" LTE slices. One possible explanation could be that the synaptically induced Ca^{2+} increases were above the threshold of feed forward signalling leading to an inhibition instead. As discussed in the introduction, Ca^{2+} propagation depends on Ca^{2+}-dependent autocatalysis at least in cell cultures, which means that at high $[Ca^{2+}]_i$ levels it can produce negative feedback [Bezprozvanny *et al.*, 1991; Kim *et al.*, 1994]. Therefore, high somatic Ca^{2+} level may actually inhibit Ca^{2+} dependent release in processes. Furthermore, recent studies suggesting that Ca^{2+} slows rather than enhances vesicle release [Holt *et al.*, 2008], could account for the reduction in SIC prevalence observed here after synaptic stimulation.

Chapter 8

Final discussion

The key findings in this thesis are that *1)* moderate synaptic stimulation evoked astrocytic $[Ca^{2+}]_i$ elevations which did not elicit SICs, *2)* long term synaptic stimulation induced an LTE of SICs that far outlasted that of neuronal activity, *3)* the degree of LTE showed a developmental profile, *4)* prolonged exposure to glutamate induced a "chemical" form of LTE and finally, *5)* moderate synaptic stimulation during "chemical" LTE induced depression of SIC frequency.

The functional importance of astrocyte to neuron signalling by synaptic stimulation in the VB thalamus appears more complex than shown in other brain areas [Fellin *et al.*, 2004; D'Ascenzo *et al.*, 2007]. First of all, moderate synaptic stimulation of varying frequencies and durations, including sleep patterns and neuromodulators, did not induce gliotransmission. Instead, LTE induction required sustained synaptic activity. It may therefore be predicted that LTE *in vivo* could be elicited by long lasting thalamocortical loop activity, and may indeed be dependent on the precise patterning of such activity in different arousal states. It is also noteworthy that LTE can be induced by input from a single pathway, so that sustained sensory input, such as from the vibrissae may induce enhancement of this form of non-synaptic astrocyte-neuron excitatory signalling.

The induction mechanism for synaptically induced LTE and "chemical" LTE was different: LTS induced LTE relied on prolonged mGluR activation whereas in "chemical" LTE, amino acid uptake played the major role. What was common to both of these induction mechanisms was that they exhibited a temporal profile. This was evident from experiments during stimulation showing that SIC frequency was not correlated with the increase in synaptic efficacy/charge, but showed a progressive increase during prolonged stimulation (chapter 5). "Chemical" LTE also showed a progressive increase in SIC frequency over time (chapter 6). Considering this time depedent profile, the possibility that LTE induction involves two phases, exists. Initially, both LTS and Glu pre-incubation induced LTE may be due to mGluR activation. This is supported by the observation that less than 2h Glu pre-incubation reached similar potentiation in SIC frequency as 60 minute LTS (0.43±0.1 SICs/min and 0.314±0.06 SICs/min respectively), whilst after pre-incubation in D-Asp, which is a substrate for EAATs

and NMDA-receptors, SIC frequency was still less than 0.2 SICs/min. The second phase occurring after prolonged period (>2h) may then involve EAA transporter uptake. As discussed in chapter 6, up-regulation of EAATs has been shown to occur in time dependent manner in response to glutamate exposure [Duan *et al.*, 1999] and may account for the 10-fold increase over several hours as more glutamate is continuingly taken up into astrocytes.

Normally, brain extracellular glutamate concentration is approximately 1-2μM [Benveniste *et al.*, 1984], whilst cytosolic concentration of Glu in neurons and astrocytes ranges between 1-10mM [Hertz *et al.*, 1988; Ottersen, 1989; Erecinska & Silver, 1990; Levi & Patrizio, 1992]. Upon synaptic activity, glutamate concentrations as high as several millimolar can be reached in the synaptic cleft (clearance is biphasic with time constants of approximately 100 μs and 2 ms) [Clements *et al.*, 1992; Clements, 1996; Diamond & Jahr, 1997]. Compared to this, a concentration of 200μM Glu during pre-incubation is relatively low. To what extent the actual amount of Glu plays a significant role in LTE during the LTS compared to the pre-incubation method, is difficult to estimate at this point. Further studies will be indeed needed to characterise the relationship and the temporal profile.

The properties of SICs presented here are consistent with previous work done in the VB thalamus and in other brain areas [Parri *et al.*, 2001; Fellin *et al.*, 2004; Angulo *et al.*, 2004; Perea & Araque, 2005; Beierlein & Regehr, 2006; Fellin *et al.*, 2006; Kozlov *et al.*, 2006; D'Ascenzo *et al.*, 2007; Ding *et al.*, 2007; Navarrete & Araque, 2008; Shigetomi *et al.*, 2008]. Regardless of whether they were spontaneous or synaptically/chemically enhanced, they had characteristic slow kinetics, were insensitive to TTX and targeted NMDA-receptors consistent with an astrocytic locus of modulation. SIC parameters, however, varied across the experiments to some extent. During moderate sensory stimulation, for example, SICs were increased in amplitude (chapter 4) but not during prolonged sensory stimulation (chapter 5). The significance of some of these changes is difficult to explain but may be attributable to the unpredictable nature of SICs as outlined in chapter 3. Some changes, such as an increase in amplitude after Glu pre-incubation can be related to the increased Glu uptake into astrocytes, as the broad-spectrum EAAT blocker TBOA prevented both the enhancement of frequency and increase in SIC amplitude. The mechanism of Glu release in both synaptically induced LTE and "chemical" LTE will also require further experiments. It is possible that they involve different mechanism, so that synaptic LTE recruits Ca^{2+} dependent/independent vesicle release whilst prolonged Glu/Asp pre-incubation may involve swelling induced release [Rutledge & Kimelberg, 1996; Duan *et al.*, 2003; Ye *et al.*, 2003].

The findings presented here describe two previously unrecognised forms of plasticity of glial-neuron signalling: a plasticity of glial output induced synaptically or chemically. For example, the synaptically induced enhancement far outlasts the inducing stimulus and so represents a glial "memory" of previous neuronal synaptic activity. "Chemical" LTE also outlasted the inducing period and may therefore represent a "memory" of previous Glu exposure. The physiological roles of LTE SICs may include, for example, involvement in synchronisation of TC neurons or induction of neuronal plasticity.

Single glial glutamate release events have been shown to induce synchronous SICs in neighbouring pairs of neurons, and to elicit action potential firing [Angulo *et al.*, 2004; Fellin *et al.*, 2004; Fellin *et al.*, 2006; D'Ascenzo *et al.*, 2007]. As TC neurons are coupled via gap-junctions [Hughes *et al.*, 2001], a single SIC may also promote synchronised firing in the VB thalamus by the propagation of elicited action potentials within small groups of neurons. Depression of SICs on chemical LTE slices following synaptic stimulation added more complexity to the interpretation of the functional roles, and further investigations into the mechanism of this depression are indeed required. However, as discussed in chapter 7, astrocytic $[Ca^{2+}]_i$ exceeding a certain threshold can in fact produce a negative feedback [Bezprozvanny *et al.*, 1991; Kim *et al.*, 1994; Holt *et al.*, 2008]. This may thus function as a gating mechanism that prioritises synaptic activity over extrasynaptic during specific short term input.

It is known that astrocytes contribute to neuronal plasticity and LTP either by releasing gliotransmitters or by changes in synaptic ensheathment [Yang *et al.*, 2003; Panatier *et al.*, 2006; Perea & Araque, 2007]. Signalling to glial cells can also undergo plasticity [Ge *et al.*, 2006] and the idea of glial cells showing plasticity similar to neuronal LTP was proposed almost a decade ago [Pasti *et al.*, 1995; 1997]. As SICs have been shown to elicit neuronal Ca^{2+} changes [Parri *et al.*, 2001], it can be expected that they participate in biochemical processes involving Ca^{2+} entry which can activate second messenger pathways and gene transcription [Shepherd, 1994]. Here, SICs were shown to target extrasynaptic receptors containing NR2B-subunits consistent with previous studies [Fellin *et al.*, 2004; D'Ascenzo *et al.*, 2007]. Interestingly, whereas synaptic NMDA-receptors are linked to LTP, the extrasynaptic NMDA-receptors containing NR2B and NR2D subunits have been shown to participate in LTD [Hrabetova *et al.*, 2000; Massey *et al.*, 2004; Duffy *et al.*, 2008]. Extrasynaptic NMDA-receptors have also been shown to participate in plasticity by inducing

a protein kinase C dependent switch in synaptic AMPA-receptors to the Ca^{2+}-impermeable subunit, thus suppressing synaptic LTP induction [Sun & Liu, 2007]. Gliotransmission targeting pre-synaptic sites is not completely excluded either, and may indeed account for the enhancement of PSC amplitude during LTS (chapter 5, section 5.1). Therefore, sustained LTE may be expected to impact on the processing of afferent synaptic signals to the thalamus by both presynaptic modulation of neurotransmitter release, and extrasynaptic excitation via NMDA-receptors, suggesting a distinct function of this excitation to synaptic input [Hrabetova *et al.*, 2000; Hardingham *et al.*, 2002; Massey *et al.*, 2004; Wittmann *et al.*, 2004; Ivanov *et al.*, 2006; Duffy *et al.*, 2008]. It is therefore possible that thalamic astrocytes have roles as "drivers" and "modulators" [Sherman & Guillery, 1998].

SIC frequency and properties showed developmental profiles in spontaneous (chapter 3), synaptically induced LTE (chapter 5) and chemically induced LTE (chapter 6) experiments. From weeks 1-3, the degree of SIC frequency was increased by an average 50%, 240% and 750% respectively. Interestingly, rats do not exhibit much whisking during the first PN week due to a lack of functional vibrissae [S Glazewski, personal communication], which would be consistent with the observed activity dependent mechanism of LTE. In addition, SICs during the second week displayed a tendency to be larger in amplitude. Furthermore, spontaneous SIC prevalence across the cell population (recorded neurons) as well as the induction of synaptic LTE and "chemical" LTE was most profound during the second PN week. Since the VB thalamus undergoes multiple developmental changes during the first three post-natal weeks, for example, the maximal rate of synaptogenesis and synaptic remodelling occur during the second week [Matthews *et al.*, 1977; Miller *et al.*, 1993; Arsenault & Zhang, 2006], these results may represent a previously unrecognised period of plasticity implicated in the development of the VB thalamus [Crair & Malenka, 1995; Lu *et al.*, 2001].

The possibility that both synaptically induced LTE and/or "chemical" LTE are recruited in pathological conditions *in vivo* still remains. Robust synchronized burst firing is a hallmark of epileptic activity [Najm *et al.*, 2001; Crunelli & Leresche, 2002]. As discussed in the introduction, previous brain slice studies have demonstrated increased SIC frequency and astrocytic Ca^{2+} signalling either as a cause or a result of epileptic activity [Kang *et al.*, 2005; Tian *et al.*, 2005; Fellin *et al.*, 2006; Ding *et al.*, 2007]. Fellin *et al.* [2006], for example, showed that epileptiform activity was associated with an increase in SIC frequency. Indeed, the LTS protocol partially resembles, for example, interictal-like activity in a way that it can also repeatedly synchronize a large population of TC neurons. Furthermore, SICs with sodium

currents as well as transient depolarisation with spontaneous spiking on top of them were resembling those that were suggested to induce epileptic discharges [Kang *et al.*, 2005], observed occasionally (data not shown).

Furthermore, 10-fold increases in extracellular EAA concentrations have been implicated in many pathological conditions such as ischemia and epilepsy [Benveniste *et al.*, 1984; Zhang *et al.*, 1995; Lipton, 1999; Chapman, 2000; Arundine & Tymianski, 2004; Seifert *et al.*, 2006]. Subsequently, Glu pre-incubation has been often used as a model to study such conditions, for example, primary hippocampal cultures were exposed to 5 μmol/L glutamate for various durations [Nonaka *et al.*, 1998; Sun *et al.*, 2001]. A 30 minute long exposure to 5 μmol/L glutamate produced a subset of neurons that died and a larger population of injured neurons that survived [Sun *et al.*, 2001]. In these pathological conditions, neurodegeneration, often characterized by a long delay between the insult and manifestation of major cell damage, is linked to increased NMDA-receptor activation [Simon *et al.*, 1984; Lipton, 1999; Cull-Candy *et al.*, 2001; Wittmann *et al.*, 2004]. Furthermore, as synaptic and extrasynaptic location of NMDA-receptors has been shown to promote neuronal survival and death respectively [Hardingham *et al.*, 2002; Vanhoutte & Bading, 2003; Wittmann *et al.*, 2004; Ivanov *et al.*, 2006], SICs that target extrasynaptic NMDA-receptors may therefore have a central role in pathological conditions.

In conclusion, these results showed that signalling between astrocytes and neurons in the VB thalamus is a complex phenomenon requiring future experiments. Nevertheless, the two previously unrecognised mechanisms of enhancing SIC frequency are of great importance in the field of glial signalling. The synaptically induced LTE represents a form of non-synaptic plasticity and a glial "memory" of previous synaptic activity whilst enhancement after prolonged Glu exposure may represent a pathological situation. Furthermore, these findings will provide new methods of studying the functional role of SICs in both physiological and pathological conditions.

References

Aguado F, Espinosa-Parrilla JF, Carmona MA and Soriano E. Neuronal activity regulates correlated network properties of spontaneous calcium transients in astrocytes in situ. *J Neurosci.* 2002; 22: 9430-9444

Alexander GM and Godwin DW. Presynaptic inhibition of corticothalamic feedback by metabotropic glutamate receptors. *J Neurophysiol.* 2005; 94: 163-175

Amzica F and Steriade M. Neuronal and glial membrane potentials during sleep and paroxysmal oscillations in the neocortex. *J Neurosci.* 2000; 20: 6648–6665

Anderson C and Swanson R. Astrocyte Glutamate transport: Review of properties, regulation, and physiological functions. *Glia.* 2000; 32: 1-14

Angulo MC, Kozlov AS, Charpak S and Audinat E. Glutamate released from glial cells synchronizes neuronal activity in the hippocampus. *J Neurosci.* 2004; 24: 6920-6927

Araque A, Parpura V, Sanzgiri RP and Haydon PG. Glutamate-dependent astrocyte modulation of synaptic transmission between cultured hippocampal neurons. *Eur J Neurosci.* 1998a; 10: 2129–2142.

Araque A, Parpura V, Sanzgiri RP and Haydon PG. Calcium elevation in astrocytes causes an NMDA receptor-dependent increase in the frequency of miniature synaptic currents in cultured hippocampal neurons. *J Neurosci.* 1998b; 18:6822–6829

Araque A, Parpura V, Sanzgiri RP and Haydon PG. Tripartite synapses: glia, the unacknowledged partner. *TINS.* 1999; 22:208–215

Araque A, Li N, Doyle RT and Haydon PG. SNARE protein –dependent glutamate release from astrocytes. *J Neurosci.* 2000; 20: 666-673

Araque A, Martin ED, Perea G, Arellano IJ and Buno W. Synaptically Released Acetylcholine Evokes Ca^{2+} Elevations in Astrocytes in Hippocampal Slices. *J Neurosci.* 2002; 22: 2443-2450

Arsenault D and Zhang Z-W. Developmental remodelling of the lemniscal synapse in the ventral basal thalamus of the mouse. *J Physiol.* 2006; 573: 121–132

Arundine M and Tymianski M. Molecular mechanisms of glutamate-dependent neurodegeneration in ischemia and traumatic brain injury. *Cell Mol Life Sci.* 2004; 61:657–668

Aschner M, Sonnewald U and Tan KH. Astrocyte modulation of neurotoxic injury. *Brain Pathol.* 2002; 12: 475-481

Auld DS and Robitaille R. Perisynaptic Schwann Cells at the Neuromuscular Junction: Nerve- and Activity-Dependent Contributions to Synaptic Efficacy, Plasticity, and Reinnervation. *Neuroscientist.* 2003; 9: 144-157

Bacci A, Sancini G, Verderio C, Armano S, Pravettoni E, Fesce R, Franceschetti S and Matteoli M. Block of glutamate-glutamine cycle between astrocytes and neurons inhibits epileptiform activity in hippocampus. *J Neurophysiol.* 2002; 88: 2302-2310

Ballanyi K, Grafe P and ten Bruggencate G. Ion activities and potassium uptake mechanisms of glial cells in guinea-pig olfactory cortex slices. *J Physiol.* 1987; 382:159–174

Barbaresi P, Spreafico R, Frassoni C and Rustioni A. GABAergic neurons are present in the dorsal column nuclei but not in the ventroposterior complex of rats. *Brain Res.* 1986; 382:305-26

Beierlein M and Regehr WG. Brief Bursts of Parallel Fiber Activity Trigger Calcium Signals in Bergmann Glia. *J Neurosci.* 2006; 26:6958-6967

Benveniste H, Drejer J, Schousboe A and Diemer NH. Elevation of the extracellular concentrations of glutamate and aspartate in rat hippocampus during transient cerebral ischemia monitored by intracerebral microdialysis. *J Neurochem.* 1984; 43:1369-74

Bellamy TC and Oqden D. Long-term depression of neuron to glial signalling in rat cerebellar cortex. *Eur J Neurosci.* 2006; 23: 581-6

Bergles DE and Jahr CE. Synaptic activation of glutamate transporters in hippocampal astrocytes. *Neuron.* 1997; 19:1297-308

Bernstein M, Behnisch T, Balschun D, Reymann KG and Reiser G. Pharmacological characterisation of metabotropic glutamatergic and purinergic receptors linked to Ca^{2+} signalling in hippocampal astrocytes. *Neuropharmacology.* 1998; 37: 169-178

Bezprozvanny I, Watras J and Ehrlich BE. Bell-shaped calcium-response curves of Ins(1,4,5)P3- and calcium-gated channels. *Nature.* 1991; 351: 751-754

Bezzi P, Gundersen V, Galbete JL, Seifert G, Steinhauser C, Pilati E and Volterra A. Astrocytes contain a vesicular compartment that is competent for regulated exocytosis of glutamate. *Nat Neurosci.* 2004; 6:613-620

Biber K, Laurie DJ, Berthele A, Sommer B, Tölle TR, Gebicke-Härter PJ, van Calker D and Boddeke HW. Expression and signaling of group I metabotropic glutamate receptors in astrocytes and microglia. *J Neurochem.* 1999; 72:1671-80

Blethyn KL, Hughes SW, Tóth TI, Cope DW and Crunelli V. Neuronal basis of the slow (<1 Hz) oscillation in neurons of the nucleus reticularis thalami in vitro. *J Neurosci.* 2006; 26:2474-86

Blomstrand F, Venance L, Sirén AL, Ezan P, Hanse E, Glowinski J, Ehrenreich H and Giaume C. Endothelins regulate astrocyte gap junctions in rat hippocampal slices. *Eur J Neurosci.* 2004; 19:1005-15

Bode BP. Recent Molecular Advances in Mammalian Glutamine Transport. *J Nutrition.* 2001; 131:2475-2485S

Bowyer JF, Lipe GW, Matthews JC, Scallet AC and Davies DL. Comparison of glutamine-enhanced glutamate release from slices and primary cultures of rat brain. *Ann N Y Acad Sci.* 1995; 765:72-85

Brockhaus J and Deitmer JW. Long-lasting modulation of synaptic input to Purkinje neurons by Bergmann glia stimulation in rat brain slices. *J Physiol.* 2002; 545: 581-93

Bröer A, Brookes N, Ganapathy V, Dimmer KS, Wagner CA, Lang F and Bröer S. The astroglial ASCT2 amino acid transporter as a mediator of glutamine efflux. *J Neurochem.* 1999; 73:2184-2194

Bröer A, Deitmer JW and Bröer S. Astroglial glutamine transport by system N is upregulated by glutamate. *Glia.* 2004; 48: 298-310

Blumenfeld H and McCormick DA. Corticothalamic Inputs Control the Pattern of Activity Generated in Thalamocortical Networks. *J Neurosci.* 2000; 20: 5153-5162

Bushong EA, Martone ME, Jones YZ and Ellisman MH. Protoplasmic Astrocytes in CA1 Stratum Radiatum Occupy Separate Anatomical Domains. *J Neurosci.* 2002; 22: 183–192

Bushong EA, Martone ME, Ellisman MH. Maturation of astrocyte morphology and the establishment of astrocyte domains during postnatal hippocampal development. *Int J Dev Neurosci.* 2004; 22:73-86

Carmignoto G, Pasti L and Pozzan T. On the Role of Voltage-Dependent Calcium Channels in Calcium Signaling of Astrocytes In Situ. *J Neurosci.* 1998; 18:4637-4645

Carmignoto G and Fellin T. Glutamate release from astrocytes as a non-synaptic mechanism for neuronal synchronization in the hippocampus. *J Physiol.* 2006; 99: 98-102

Castro-Alamancos MA and Calcagnotto ME. Presynaptic Long-Term Potentiation in Corticothalamic Synapses. *J Neurosci.* 1999; 19: 9090-9097

Castro-Alamancos MA. Properties of primary sensory (lemniscal) synapses in the ventrobasal thalamus and the relay of high-frequency sensory input. *J Neurophysiol.* 2002; 87: 946-953

Castro-Alamancos MA. Dynamics of sensory thalamocortical synaptic networks during information processing states. *Prog Neurobiol.* 2004, 74: 213-247

Chapman AG. Glutamate and epilepsy. *J Nutr.* 2000; 130:1043S-1045S

Chen XK, Xiong YF and Zhou Z. "Kiss-and-run" exocytosis in astrocytes. *Neuroscientist.* 2006; 12:375-8

Clements JD, Lester RA, Tong A, Jahr CE and Westbrook GL. The time course of glutamate in the synaptic cleft. *Science.* 1992; 258: 1498-1501

Clements JD. Transmitter time course in the synaptic cleft: its role in central synaptic function. *TINS.* 1996; 19: 163–171

Contreras D, Destexhe A, Sejnowski TJ and Steriade M. Spatiotemporal pattern of spindle oscillations in cortex and thalamus. *J Neurosci.* 1997; 17: 1179-1196

Cornell-Bell AH, Finkbeiner SM, Cooper MS and Smith SJ. Glutamate induces calcium waves in cultured astrocytes: long-range glial signalling. *Science.* 1990; 247: 470-473

Cornell-Bell AH, Thomas PG and Smith SJ. The excitatory neurotransmitter glutamate causes filopodia formation in cultured. *Glia.* 1990; 3: 322-34

Cotrina ML and Nedergaard M. ATP as a messenger in astrocyte-neuronal communication. *Neuroscientist.* 2000; 6: 120-126

Crabtree JW and Isaac JTR. New intrathalamic pathways allowing modulatory-related and cross-modality switching in the dorsal thalamus. *J Neurosci.* 2002; 22: 8754-8761

Crair MC and Malenka RC. A critical period for long-term potentiation at thalamocortical synapses. *Nature.* 1995; 375: 325-328

Crunelli V and Leresche N. Childhood absence epilepsy: Genes, channels, neurons and networks. *Nat Rev Neurosci.* 2002; 3: 371-382

Crunelli V, Cope DW and Hughes SW. Thalamic T-type Ca2+ channels and NREM sleep. *Cell Calcium.* 2006; 40: 175-190

Cull-Candy S, Brickley S and Farrant M. NMDA receptor subunits: diversity, development and disease. *Curr Opin Neurobiol.* 2001; 11: 327-335

D'Aniello A. D-Aspartic acid: An endogenous amino acid with an important neuroendocrine role. *Brain Res Rev.* 2007; 53: 215-234

D'Ascenzo M, Fellin T, Terunuma M, Revilla-Sanchez R, Meaney DF, Auberson YP, Moss SJ and Haydon PG. mGluR5 stimulates gliotransmission in the nucleus accumbens. *PNAS U S A.* 2007; 104: 1995–2000

Darby M, Kuzmiski JB, Panenka W, Feighan D and MacVicar BA. ATP Released From Astrocytes During Swelling Activates Chloride Channels. *J Neurophysiol.* 2003; 89: 1870-1877

Diamond JS and Jahr CE. Synaptically Released Glutamate Does Not Overwhelm Transporters on Hippocampal Astrocytes During High-Frequency Stimulation. *J Neurophysiol.* 2000; 83: 2835-2843

Diamond JS. Deriving the Glutamate Clearance Time Course from Transporter Currents in CA1 Hippocampal Astrocytes: Transmitter Uptake Gets Faster during Development. *J Neurosci.* 2005; 25: 2906-2916

Ding S, Fellin T, Zhu Y, Lee S-Y, Auberson YP, Meaney DF, Coulter DA, Carmignoto G and Haydon PG. Enhanced Astrocytic Ca^{2+} Signals Contribute to Neuronal Excitotoxicity after Status Epilepticus. *J Neurosci.* 2007; 27:10674-10684

Duan S, Anderson CM, Stein BA and Swanson RA. Glutamate Induces Rapid Upregulation of Astrocyte Glutamate Transport and Cell-Surface Expression of GLAST. *J Neurosci.* 1999, 19: 10193-10200

Duan S, Anderson CM, Keung EC, Chen Y, Chen Y and Swanson RA. $P2X_7$ Receptor-Mediated Release of Excitatory Amino Acids from Astrocytes. *J Neurosci.* 2003; 23:1320

Duffy S and MacVicar BA. Potassium-dependent calcium influx in acutely isolated hippocampal astrocytes. *Neuroscience.* 1994; 61: 51-61

Duffy S, Labrie V and Roder JC. D-Serine Augments NMDA-NR2B Receptor-Dependent Hippocampal Long-Term Depression and Spatial Reversal Learning. *Neuropsychopharmacology.* 2008; 33: 1004–1018

Edwards FA, Konnerth A, Sakmann B and Takahashi T. A thin slice preparation for patch clamp recordings from neurones of the mammali. *Pflugers Arch.* 1989; 414: 600-12.

Erecińska M and Silver IA. Metabolism and role of glutamate in mammalian brain. *Prog Neurobiol.* 1990; 35: 245-96

Fellin T, Pascual O, Gobbo S, Pozzan T, Haydon P and Carmignoto G. Neuronal synchrony mediated by astrocytic glutamate trough activation of extrasynaptic NMDS receptor. *Neuron.* 2004; 43: 729-743

Fellin T and Carmignoto G, Neurone-to-astrocyte signalling in the brain represents a distinct multifunctional unit. *J Physiol.* 2004; 559: 2-15

Fellin T, Pozzan T and Carmignoto G. Purinergic receptors mediate two distinct glutamate release pathways in hippocampal astrocytes. *J Biol Chem.* 2006; 281: 4274-4284

Fellin T, Gomez-Gonzalo M, Gobbo S, Carmignoto G and Haydon PG. Astrocytic Glutamate Is Not Necessary for the Generation of Epileptiform Neuronal Activity in Hippocampal Slices. *J Neurosci.* 2006: 26; 9312-9322

Feustel PJ, Jin Y and Kimelberg HK. Volume-Regulated Anion Channels are the Predominant Contributors to Release of Excitatory Amino Acids in the Ischemic Cortical Penumbra. *Stroke.* 2004; 35: 1164-1168

Fiacco TA and McCarthy KD. Intracellular Astrocyte Calcium Waves In Situ Increase the Frequency of Spontaneous AMPA Receptor Currents in CA1 Pyramidal Neurons. *J Neurosci.* 2004; 24: 722-32

Fiacco TA, Agulhon C, Taves S, Petravicz J, Casper K, Dong Xinzhong, Chen J and McCarthy KD. Selective stimulation of astrocyte calcium in situ does not affect neuronal excitatory synaptic activity. *Neuron.* 2007; 54: 611-626

Frassoni C, Amadeo A, Ortino B, Jaranowska A and Spreafico R. Organization of radial and non-radial glia in the developing rat thalamus. *J Comp Neurol.* 2000; 428: 527-542

Fremeau RT Jr, Troyer MD, Pahner I, Nygaard GO, Tran CH, Reimer RJ, Bellocchio EE, Fortin D, Storm-Mathisen J and Edwards RH. The Expression of Vesicular Glutamate Transporters Defines Two Classes of Excitatory Synapse. *Neuron.* 2001; 31: 247-260

Gabbott PL and Stewart MG. Distribution of neurons and glia in the visual cortex (area 17) of the adult albino rat: a quantitative description. *Neuroscience.* 1987; 21: 833-45

García-Marín V, García-López P and Freire M. Cajal's contributions to glia research. *TINS.* 2007; 30:479-87

Gardner-Medwin AR, Coles JA and Tsacopoulos M. Clearance of extracellular potassium: evidence for spatial buffering by glial cells in the retina of the drone. *Brain Res.* 1981; 209: 452-7

Ge WP, Yang XJ, Zhang Z, Wang HK, Shen W, Deng QD and Duan S. Long-term potentiation of neuron-glia synapses mediated by Ca2+-permeable AMPA receptors. *Science.* 2006; 312: 1533-7

Genoud C, Quairiaux C, Steiner P, Hirling H, Welker E and Knott GW. Plasticity of astrocytic coverage and glutamate transporter expression in adult mouse cortex. *PLoS Biol.* 2006: 4; e343

Gentet LJ and Ulrich D. Strong, reliable and precise synaptic connections between thalamic relay cells and neurones of the nucleus reticularis in juvenile rats. *J Physiol.* 2003; 546: 801-811

Gereau RW and Conn PJ. Multiple presynaptic metabotropic glutamate receptors modulate excitatory and inhibitory synaptic transmission in hippocampal area CA1. *J Neurosci.* 1995; 15:6879–6889

Giaume C and McCarthy KD. Control of gap-junctional communication in astrocytic networks. *TINS.* 1996; 19: 319-325

Giaume C and Venance L. Intercellular calcium signalling and gap junctional communication in astrocytes. *Glia.* 1998; 24: 50-64

Gil Z, Connors BW and Amitai Y. Efficacy of thalamocortical and intracortical synaptic connections: quanta, innervation, and reliability. *Neuron.* 1999; 23:385-97

Grafe P and Ballanyi K. Cellular mechanisms of potassium homeostasis in the mammalian nervous system. *Can J Physiol Pharmacol.* 1987; 65: 1038-42

Grosche J, Matyash V, Möller T, Verkhratsky A, Reichenbach A and Kettenmann H. Microdomains for neuron–glia interaction: parallel fiber signaling to Bergmann glial cells. *Nat Neurosci.* 1999; 2: 139-143

Guillery RW. Anatomical evidence concerning the role of the thalamus in corticocortical communication: a brief review. *J Anat.* 1995; 187: 583–592

Guthrie PB, Knappenberger J, Segal M, Bennett MVL, Charles AC and Kater SB. ATP released from astrocytes mediates glial calcium wave. *J Neurosci.* 1999; 19: 520-528

Hamill OP, Marty A, Neher E, Sakmann B and Sigworth FJ. Improved patch-clamp techniques for high-resolution current recording from cells and cell-free membrane patches. *Pflugers Arch.* 1981; 391: 85-100

Hansson E, Muyderman H, Leonova J, Allansson L, Sinclair J, Blomstrand F, Thorlin T, Nilsson M and Rönnbäck L. Astroglia and glutamate in physiology and pathology: aspects on glutamate transport, glutamate-induced cell swelling and gap-junction communication. *Neurochem Int.* 2000; 37: 317–329

Hansson E and Rönnbäck L. Astrocytes in glutamate neurotransmission. *FASEB J.* 1995; 9: 343-350

Hansson E and Rönnbäck L. Glial neuronal signalling in the central nervous system. *FASEB J.* 2003; 17: 341-348

Hardingham GE, Fukunaga Y and Bading H. Extrasynaptic NMDARs oppose synaptic NMDARs by triggering CREB shut-off and cell death pathways. *Nat Neurosci.* 2002; 5:405-14

Hassinger TD, Atkinson PB, Strecker GJ, Whalen LR, Dubek FE, Kossel AH and Kater SB. Evidence for glutamate mediated activation of hippocampal neurons by glial calcium waves. *J Neurobiol.* 1995; 28: 159-170

Hatton GI. Function-related plasticity in hypothalamus. *Annu Rev Neurosci.* 1997; 20: 375-97

Haydon PG and Carmignoto G. Astrocyte control of synaptic transmission and neurovascular coupling. *Physiol Rev.* 2006; 86: 1009-31

Hazell AS, Rao KVR, Danbolt NC and Pow DV. Butterworth R.F. Selective down-regulation of the astrocyte glutamate transporters GLT-1 and GLAST within the medial thalamus in experimental Wernicke's encephalopathy. *J Neurochem.* 2001; 78: 560-568

Heckel T, Bröer A, Wiesinger H, Lang F and Bröer S. Asymmetry of glutamine transporters in cultured neural cells. *Neurochem Int.* 2003; 43: 273

Hermans E and Challiss RAJ. Structural, signalling and regulatory properties of the group I metabotropic glutamate receptors: prototypic family C G-protein-coupled receptors. *Biochem. J.* 2001; 359: 465–484

Hertz L, Murthy CRK and Schousboe A. Metabolism of glutamate and related amino acids. The Biochemical Pathology of Astrocytes. Norenberg MD, Hertz L and Schousboe A (Eds.). 395–406. Alan R. Liss, 1988, New York

Hirase H, Qian L, Bartho P and Buzsaki G. Calcium dynamics of cortical astrocytic networks in vivo. *PLOS Biology*. 2004; 2: 494-499

Holt M, Riedel D, Stein A, Schuette C and Jahn R. Synaptic Vesicles Are Constitutively Active Fusion Machines, Which Function Independently of Ca^{2+}. *Curr Biol*. 2008; 17:715-722

Houades V, Koulakoff A, Ezan P, Seif I and Giaume C. Gap Junction-Mediated Astrocytic Networks in the Mouse Barrel Cortex. *J Neurosci*. 2008; 28: 5207-5217

Hrabetova S, Serrano P, Blace N, Tse HW, Skifter DA, Jane DE, Monaghan DT and Sacktor TC. Distinct NMDA receptor subpopulations contribute to long-term potentiation and long-term depression induction. *J Neurosci*. 2000; 20:RC81

Huang YH and Bergles DE. Glutamate transporters bring competition to the synapse. *Curr Opin Neurobiol*. 2004; 14:346-352

Hughes SW, Blethyn KL, Cope DW and Crunelli V. Properties and origin of spikelets in thalamocortical neurones in vitro. *Neuroscience*. 2001; 110: 395-401

Hughes SW, Cope DW, Blethyn KL and Crunelli V. Cellular mechanisms of the slow (<1 Hz) oscillation in thalamocortical neurons *in vitro*. *Neuron*. 2002; 33:947-58

Hughes SW, Lörincz M, Cope DW, Blethyn KL, Kekesi KA, Parri HR, Juhasz G and Crunelli V. Synchronised oscillations at α and Θ frequencies in the lateral geniculate nucleus. *Neuron*. 2004; 42: 253-268

Ivanov A, Pellegrino C, Rama S, Dumalska I, Salyha Y, Ben-Ari Y and Medina I. Opposing role of synaptic and extrasynaptic NMDA receptors in regulation of the extracellular signal-regulated kinases (ERK) activity in cultured rat hippocampal neurons. *J Physiol*. 2006; 572:789-98

Ivy GO and Killackey HP. Ontogenetic changes in the projections of neocortical neurons. *J Neurosci*. 1981; 2: 735-743

Jahnsen H and Llinas R. Electrophysiological properties of guinea-pig thalamic neurones: an in vitro study. *J Physiol*. 1984; 349: 205-226

Jones EG. A new view of specific and nonspecific thalamocortical connections. *Adv Neurol*. 1998; 77: 49-71

Jourdain P, Bergersen LH, Bhaukaurally K, Bezzi P, Santello M, Domercq M, Matute C, Tonello F, Gundersen V and Volterra A. Glutamate exocytosis from astrocytes controls synaptic strength. *Nat Neurosci*. 2007; 10: 331-9

Kafitz KW, Meier SD, Stephan J and Rose CR. Developmental profile and properties of sulforhodamine 101--Labeled glial cells in acute brain slices of rat hippocampus. *J Neurosci Methods*. 2008; 169: 84-92

Kang J, Jiang L, Goldman SA and Nedergaard M. Astrocyte-mediated potentiation of inhibitory synaptic transmission. *Nat Neurosci*. 1998; 1: 683-692

Kang N, Xu J, Xu Q, Nedergaard M and Kang J. Astrocytic Glutamate Release-Induced Transient Depolarization and Epileptiform Discharges in Hippocampal CA1 Pyramidal Neurons. *J Neurophysiol*. 2005; 94: 4121-4130

Katz LC and Shatz CJ. Synaptic Activity and the Construction of Cortical Circuits. *Science*. 1996; 274: 1133 – 1138

Killackey HP, Rhoades RW and Bennett-Clarke CA. The formation of a cortical somatotopic map. *TINS*. 1995; 18: 402-407

Kim WT, Rioult MG and Cornell-Bell AH. Glutamate induced calcium signalling in astrocytes. *Glia.* 1994; 11: 173-184

Kimelberg HK, Goderie SK, Higman S, Pang,laa S and Waniewski RA. Swelling-Induced Release of Glutamate, Aspartate, and Taurine from Astrocyte Cultures. *J Neurosci.* 1990; I: 1583-1 591

Kinney GA and Spain WJ. Synaptically Evoked GABA Transporter Currents in Neocortical Glia. *J Neurophysiol.* 2002; 88: 2899-2908

Kozlov AS, Angulo MC, Audinat E and Charpak S. Target cell-specific modulation of neuronal activity by astrocytes. *PNAS.* 2006; 103: 10058-10063

Kullman DM and Asztely F. Extrasynaptic glutamate spillover in the hippocampus: evidence and implications. *TINS.* 1998; 21: 8-14

Kvamme E, Torgner IA and Roberg B. Kinetics and localization of brain phosphate activated glutaminase. *J Neurosci Res.* 2001; 66: 5951 - 958

Lee SH, Kim WT, Cornell-Bell AH and Sontheimer H. Astrocytes exhibit regional specificity in gap-junction coupling. *Glia.* 1994; 11:315-25

Lee CJ, Mannaioni G, Yuan H, Woo DH, Gingrich MB and Traynelis SF. Astrocytic control of synaptic NMDA receptors. *J Physiol.* 2007; 581: 1057-1081

Lehre KP, Levy LM, Ottersen OP, Storm-Mathisen J and Danbolt NC. Differential expression of two glial glutamate transporters in the rat brain: quantitative and immunocytochemical observations. *J Neurosci.* 1995; 15: 1835–1853

Lehre KP and Rusakov DA. Asymmetry of Glia near Central Synapses Favors Presynaptically Directed Glutamate Escape. *Biophys J.* 2002; 83:125-134

Levi G and Patrizio M. Astrocyte heterogeneity: endogenous amino acid levels and release evoked by non-*N*-methyl-D-aspartate receptor agonists and by potassiuminduced swelling in type-1 and type-2 astrocytes. *J Neurochem.* 1992; *58:* 1943–1952

Li J, Bickford ME and Guido W. Distinct Firing Properties of Higher Order Thalamic Relay Neurons. *J neurophysiol.* 2003; 90: 291-299

Lin SC and Bergles DE. Synaptic signalling between neurons and glia. *Glia.* 2004; 47: 290-298

Lipton P. Ischemic Cell Death in Brain Neurons. *Physiol Rev.* 1999; 79: 1431-1568

Liu QS, Xu Q, Arcuino G, Kang J and Nedergaard M. Astrocyte-mediated activation of neuronal kainate receptors. *PNAS U S A.* 2004; 101:3172-7

Liu Q-S, Xu Q, Kang J and Nedergaard M. Astrocyte activation of presynaptic metabotropic glutamate receptors modulates hippocampal inhibitory synaptic transmission. *Neuron Glia Biol.* 2004; 1: 307–316

Liu XB, Honda CN and Jones EG. Distribution of four types of synapse on physiologically identified relay neurons in the ventral. *J Comp Neurol.* 1995a; 352: 69-91

Liu XB, Murray KD and Jones EG. Switching of NMDA Receptor 2A and 2B Subunits at Thalamic and Cortical Synapses during Early Postnatal Development. *J Neurosci.* 2004; 24: 8885-8895

Llinas RR and Streriade M. Bursting of thalamic neurons and states of vigilance. *J Neurophysiol.* 2006; 95: 3297-3308

Lu CH, Gonzalez E and Crair MC. Barrel cortex critical period plasticity is independent of changes in NMDA receptor subunit composition. *Neuron.* 2001; 32: 619-634

Lörincz ML, Crunelli V and Hughes SW. Cellular Dynamics of Cholinergically Induced α(8–13 Hz) Rhythms in Sensory Thalamic Nuclei *In Vitro. J Neurosci.* 2008; 28: 660-671

Magistretti PJ and Pellerin L. Astrocytes Couple Synaptic Activity to Glucose Utilization in the Brain. *News Physiol Sci.* 1999; 14: 177-182

Marcaggi P and Attwell D. Role of glial amino acid transporters in synaptic transmission and brain energetics. *Glia.* 2004; 47:217-25

Mares P, Maresová D, Trojan S and Fischer J. Ontogenetic development of rhythmic thalamo-cortical phenomena in the rat. *Brain Res Bull.* 1982; 8: 765-9

Marks GA. Slow rhythmic discharges of thalamic neurons are suppressed during slow wave sleep by iontophoretic application of bicuculline. *Sleep Research.* 1996; 25: 17

Martinez-Hernandez A, Bell KP and Norenberg MD. Glutamine synthetase: glial localization in brain. *Science.* 1977; 195: 1356-1358

Massey PV, Johnson BE, Moult PR, Auberson YP, Brown MW, Molnar E, Collingridge GL and Bashir ZI. Differential roles of NR2A and NR2B-containing NMDA receptors in cortical long-term potentiation and long-term depression. *J Neurosci.* 2004; 24:7821-8

Matthews MA, Narayanan CH, Narayanan Y and St.Onge MF. Neuronal maturation and synaptogenesis in the rat ventrobasal complex: Alignment with developmental changes in rate and severity of axon reaction. *J Comp Neur.* 1977; 173: 4745-772

Mazzani M, Sul JY and Haydon PG. Glutamate on demand: astrocytes as a ready source. *Neuroscientist.* 2001; 7: 396-405

McCormick DA. Neurotransmitter actions in the thalamus and cerebral cortex. *J Clin Neurophysiol.* 1992; 9: 212-23

Meeks JP and Mennerick S. Astrocyte membrane responses and potassium accumulation during neuronal activity. *Hippocampus.* 2007; 17: 1100-8

Meeren HKM, Pijn JPM, Van Luijtelaar ELJM, Coenen AML and Lopes da Silva FH. Cortical Focus Drives Widespread Corticothalamic Networks during Spontaneous Absence Seizures in Rats. *J Neurosci.* 2002; 22: 1480-1495

Miller B, Chou L and Finlay BL. The Early Development of Thalamocortical and Corticothalamic Projections. *J Comp Neurol.* 1993; 335: 1641

Miller RH and Raff MC. Fibrous and protoplasmic astrocytes are biochemically and developmentally distinct. *J Neurosci.* 1984; 4: 585-592

Miller S, Bridges RJ and Cotman CW. Stimulation of phosphoinositide hydrolysis by trans-(±)-ACPD is greatly enhanced when astrocytes are cultured in a serum-free defined medium. *Brain research.* 1993; 618: 175-178

Miyata M and Imoto K. Different composition of glutamate receptors in thalamic synapses. *J Physiol.* 2006; 15: 161-74.

Miyata M and Imoto K. Different composition of glutamate receptors in corticothalamic and lemniscal synaptic responses and their roles in the firing responses of ventrobasal thalamic neurons in juvenile mice. *J Physiol.* 2006; 575: 161–174

Miyata M. Distinct properties of corticothalamic and primary sensory synapses to thalamic neurons. *Neurosci Res.* 2007; 59: 377-382

Montana V, Ni Y, Sunjara V, Hua X and Parpura V. Vesicular Glutamate Transporter-Dependent Glutamate Release from Astrocytes. *J Neurosci.* 2004; 24: 2633-2642

Mooney SM and Miller MW. Postnatal Generation of Neurons in the Ventrobasal Nucleus of the Rat Thalamus. *J Neurosci.* 2007; 27: 5023-5032

Moore CI. Frequency-dependent processing in the vibrissae sensory system. *J Neurophysiol.* 2004; 91: 2390-2399

Najm IM, Janigro D and Babb TL. Mechanisms of epileptogenesis and experimental models of seizures. The Treatment of Epilepsy: Principles and Practise. Wyllie E (Ed.). 33-44. Lippincott, Williams and Wilkins, New York, 2001

Narravete M and Araque A. Endocannabinoids mediate neuron-astrocyte communication. *Neuron.* 2008; 57: 883-893

Nedergaard M, Direct signaling from astrocytes to neurons in cultures of mammalian brain cells. *Science*, 1994; 263:1768-1771

Nedergaard M, Ransom B and Goldman SA. New roles for astrocytes: Redefining the functional architecture of the brain. *TINS.* 2003; 26: 523-530

Nett WJ, Oloff SH and McCarthy KD. Hippocampal Astrocytes In Situ Exhibit Calcium Oscillations That Occur Independent of Neuronal Activity. *J Neurophysiol.* 2002; 87: 528-537

Newman EA. Inward-rectifying potassium channels in retinal glial (Müller) cells. *J Neurosci.* 1993; 13:3333–3345

Newman E and Zahs KR. Calcium Waves in Retinal Glial Cells. *Science.* 1997; 275: 844 – 847

Newman E. Glial modulation of synaptic transmission in the retina. *Glia.* 2004; 15:268-74

Newman E. Calcium Increases in Retinal Glial Cells Evoked by Light-Induced Neuronal Activity. *J Neuroscience.* 2005; 25: 5502-5510

Nimmerjahn A, Kirchhoff F, Kerr JND and Helmchen F. Sulforhodamine 101 as a specific marker of astroglia in the neocortex *in vivo. Nat Methods.* 2004; 1: 31 - 37

Nonaka S, Hough CJ and Chuang D-M. Chronic lithium treatment robustly protects neurons in the central nervous system against excitotoxicity by inhibiting *N*-methyl-d-aspartate receptor-mediated calcium influx. *PNAS U S A.* 1998; 95: 2642–2647

Oberheim NA, Wang X, Goldman S and Nedergaard M. Astrocytic complexity distinguishes the human brain. *TINS.* 2006; 29: 547-53

Oliet SH, Piet R and Poulain DA. Control of glutamate clearance and synaptic efficacy by glial coverage of neurons. *Science.* 2001; 292:923-6.

Olney JW. Brain Lesions, Obesity, and Other Disturbances in Mice Treated with Monosodium Glutamate. *Science.* 1969; 164: 719 – 721

Orkand RK, Nicholls JG and Kuffler SW. Effect of nerve impulses on the membrane potential of glial cells in the central nervous system of amghibia. *J Neurophysiol.* 1966; 29: 788-806

Orthmann-Murphy JL, Abrams CK and Scherer SS. Gap Junctions Couple Astrocytes and Oligodendrocytes. *J Mol Neurosci.* 2008: 35; 101-116

Ottersen OP. Quantitative electron microscopic immunocytochemistry of neuroactive amino acids. *Anat Embryol.* 1989; 180: 1–15

Panatier A, Theodosis DT, Mothet JP, Touquet B, Pollegioni L, Poulain DA and Oliet SH. Glia-derived D-serine controls NMDA receptor activity and synaptic memory. *Cell.* 2006; 125: 775-84

Parpura V, Basarsky TA, Liu F, Jeftinija K, Jeftinija S and Haydon PG. Glutamate-mediated astrocyte-neuron signalling. *Nature.* 1994; 369: 744–747

Parpura V and Haydon PG. Physiological astrocytic calcium levels stimulate glutamate release to modulate adjacent neurons. *PNAS.* 2000; 97: 8629-8634

Parri HR and Crunelli V. Astrocytic Ca2+ increases caused by neurotransmitters in the VB thalamus. *Soc Neurosci Abs.* 2001; 505: 11

Parri HR, Gould TM and Crunelli V. Spontaneous astrocytic Ca^{2+} oscillations in situ drive NMDA-mediated neuronal excitation. *Nat neurosci.* 2001; 4: 803-812

Parri HR and Crunelli V. Astrocytes, spontaneity, and the developing thalamus. *J Physiol.* 2002; 96: 221-230

Parri HR and Crunelli V. The role of Ca2+ in the generation of spontaneous astrocytic Ca^{2+} oscillations. *Neuroscience.* 2003; 120: 979-992

Pascual O, Casper KB, Kubera C, Zhang J, Revilla-Sanchez R, Sul J-Y, Takano H, Moss SJ, McCarthy K and Haydon PG. Astrocytic Purinergic Signaling Coordinates Synaptic Networks. *Science.* 2005; 310: 113-116

Pasti L, Volterra A, Pozzan T and Carmignoto G. Intracellular calcium oscillations in astrocytes: a highly plastic, bidirectional form of communication between neurons and astrocytes in situ. *J Neurosci.* 1997; 17: 7817-7830

Piet R, Vargová L, Syková E, Poulain DA and Oliet SH. Physiological contribution of the astrocytic environment of neurons to intersynaptic crosstalk. *PNAS U S A.* 2004; 101: 2151-5

Perea G and Araque A. Astrocytes Potentiate Transmitter Release at Single Hippocampal Synapses. *Science.* 2007; 317: 1083 – 1086

Perea G and Araque A. Communication between astrocytes and neurons: a complex language. *J Physiol.* 2002; 96: 199-207

Perea G and Araque A. Properties of synaptically evoked astrocyte calcium signal reveal synaptic information processing by astrocytes. *J Neurosci.* 2005; 25: 2192-2203

Petravicz J, Fiacco TA and McCarthy KD. Loss of IP_3 Receptor-Dependent Ca^{2+} Increases in Hippocampal Astrocytes Does Not Affect Baseline CA1 Pyramidal Neuron Synaptic Activity. *J Neurosci.* 2008; 28:4967-4973

Philippe M, Vyklicky L and Orkand RK. Potassium currents in cultured glia of the frog optic nerve. *Glia.* 1996; 17: 72-82

Piet R, Vargova L, Sykova E, Poulain DA and Oliet SHR. Physiological contribution of the astrocytic environment of neurons to intersynaptic crosstalk. *PNAS.* 2004; 101: 2151–2155

Pinault D, Leresche N, Charpier S, Deniau J-M, Marescaux C, Vergues M and Crunelli V. Intracellular recordings in thalamic neurones during spontaneous spike and wave discharges in rats with absence epilepsy. *J Physiol.* 1998; 509.2: 449-456

Pinault D, Slezia A and Acsady L. Cotricothalamic 5-9 Hz oscillations are more pro-epileptogenic than sleep spindles in rats. *J Physiol.* 2006; 547.1: 209-227

Porter JT and McCarthy KD. Hippocampal astrocytes in situ respond to glutamate released from synaptic terminals. *J Neurosci.* 1996; 16: 5073-81

Porter JT and McCarthy KD. Astrocytic neurotransmitter receptors in situ and in vivo. *Prog Neurobiol.* 1997; 51 439-455

Pfrieger FW, Veselovsky NS, Gottmann K and Lux HD. Pharmacological characterization of calcium currents and synaptic transmission between thalamic neurons in vitro. *J Neurosci.* 1992; 12: 4347-4357

Raff MC, Abney ER, Cohen J, Lindsay R and Noble M. Two types of astrocytes in cultures of developing rat white matter: differences in morphology, surface gangliosides, and growth characteristics. *J Neurosci.* 1983: 3; 1289-1300

Rosanova M and Ulrich D. Pattern-specific associative long-term potentiation induced by a sleep spindle-related spike train. *J Neurosci.* 2005; 25: 9398-9405

Rose CR and Konnerth A. Exciting glial oscillations. *Nat Neurosci.* 2001; 4: 773-77

Rothstein JD, Martin L, Levey AI, Dykes-Hoberg M, Jin L, Wu D, Nash N and Kuncl RW, Localization of neuronal and glial glutamate transporters. *Neuron.* 1994; 13: 713–725

Rouach N, Glowinski J and Giaume C. Activity-dependent Neuronal Control of Gap-junctional Communication in Astrocytes. *J Cell Biol.* 2000; 149: 1513-1526

Rutledge EM and Kimelberg HK. Release of [^{3}H]-D-Aspartate from Primary Astrocyte Cultures in Response to Raised External Potassium. *J Neurosci.* 1996; 16: 7803-7811

Rutledge EM, Aschner M and Kimelberg HK. Pharmacological characterization of swelling-induced D-[3H]aspartate release from primary astrocyte cultures. *Am J Physiol Cell Physiol.* 1998; 274: 1511-1520

Safronov BV and Vogel W. Electrical activity of individual neurons: Patch-clamp techniques. Modern Techniques in Neuroscience Research. Windhorst U and Johansson H (Eds.). Springer. 1999. US

Schipke CG and Kettenman H. Astrocyte responses to neuronal activity. *Glia.* 2004; 47: 226-232

Schools GP, Zhou M and Kimelberg HK. Development of Gap Junctions in Hippocampal Astrocytes: Evidence That Whole Cell Electrophysiological Phenotype Is an Intrinsic Property of the Individual Cell. *J Neurophysiol.* 2006; 96: 1383-1392

Seifert G, Schilling K and Steinhäuser C. Astrocyte dysfunction in neurological disorders: a molecular perspective. *Nat Rev Neurosci.* 2006; 7:194-206

Serrano A, Haddjeri N, Lacaille J-C and Robitaille R. GABAergic Network Activation of Glial Cells Underlies Hippocampal Heterosynaptic Depression. *J Neurosci.* 2006; 26:5370-5382

Shelton MK and McCarthy KD. Mature hippocampal astrocytes exhibit functional metabotropic and ionotropic glutamate receptors in situ. *Glia.* 1999; 26: 1-11

Shepherd GM. Neurobiology. 1994. 3rd Ed. Oxford University Press, Inc

Shepherd GM. The synaptic organization of the brain. 2004. 5th Ed. Oxford University Press, Inc

Sherman SM and Guillery RW. Functional organization of thalamocortical relays. *J Neurophysiol.* 1996; 76: 1367-1395

Sherman S and Guillery RW. On the actions that one nerve cell can have on another: Distinguishing "drivers" from "modulators". *PNAS U S A.* 1998; 95:7121–7126

Sherman SM. Tonic and burst firing: dual modes of thalamocortical relay. *TINS.* 2001; 24: 122-126

Shiga H, Murakami J, Nagao T, Tanaka M, Kawahara K, Matsuoka I and Ito E. Glutamate release from astrocytes is stimulated via the appearance of exocytosis during cyclic AMP-induced morphologic changes. *J Neurosci Res.* 2006; 84: 338-347

Shigetomi E, Bowser DN, Sofroniew MV and Khakh BS. Two Forms of Astrocyte Calcium Excitability Have Distinct Effects on NMDA Receptor-Mediated Slow Inward Currents in Pyramidal Neurons. *J Neurosci.* 2008; 28: 6659-6663

Simon RP, Swan JH, Griffiths T and Meldrum BS. Blockade of N-methyl-n-aspartate receptors may protect against ischemic damage in the brain. *Science.* 1984; 226: 850-852

Sontheimer H. Astrocytes, as well as neurons, express a diversity of ion channels. *Can J Physiol Pharmacol.* 1992; 70: 223-238

Spacek J. Three-dimensional analysis of dendritic spines. *Anat Embryol.* 1985; 171; 245-252

Steinhauser C, Beger T, Frotscher M and Kettenmann H. Heterogeneity in the Membrane Current Pattern of Identified Glial Cells in the Hippocampal Slice. *Eur J Neurosci.* 1992; 4: 472

Steriade M. Sleep oscillations and their blockage by activating systems. *J Phychiatr Neurosci.* 1994; 19: 354-358

Steriade M, Contreras D, Amzica F and Timofeev I. Synchronization of fast (30-40 Hz) spontaneous oscillations in intrathalamic and thalamocortical networks. *J Neurosci.* 1996; 16: 2788-2808

Steriade M. Grouping of brain rhythms in corticothalamic systems. *Neuroscience.* 2006; 137: 1087-1106

Sun DA, Sombati S and DeLorenzo RJ. Glutamate Injury-Induced Epileptogenesis in Hippocampal Neurons: An *In Vitro* Model of Stroke-Induced "Epilepsy". *Stroke.* 2001; 32: 2344-2350

Sun L and Liu SJ. Activation of extrasynaptic NMDA receptors induces a PKC-dependent switch in AMPA receptor subtypes in mouse cerebellar stellate cells. *J Physiol.* 2007; 583: 537-553

Szerb JC and O'Regan PA. Glutamine enhances glutamate release in preference to gamma-aminobutyrate release in hippocampal slices. *Can J Physiol Pharmacol.* 1984; 62:919-23

Szerb JC and O'Regan PA. Effect of glutamine on glutamate release from hippocampal slices induced by high K+ or by electrical stimulation: interaction with different Ca2+ concentrations. *J Neurochem.* 1985; 44:1724-31

Takano T, Kang J, Jaiswal JK, Simon SM, Lin JH-C, Yu L, Li Y, Yang J, Deinel G, Zielke HR and Nedergaard M. Receptor-mediated glutamate release from volume sensitive channels in astrocytes. *PNAS.* 2005; 102: 16466-16471

Tanabe T, Yarita H, Iino M, Ooshima Y and Takagi SF. An olfactory projection area in orbitofrontal cortex of the monkey. *J Neurophysiol.* 1975; 38: 1269-83

Theodosis DT and Poulain DA. Neuronal-glial and synaptic remodelling in the adult hypothalamus in response to physiological stimuli. *Ciba Found Symp.* 1992; 168: 209-25

Tian G-F, Azmi H, Takano T, Xu Q, Peng W, Lin J, Oberheim NA, Lou N, Wang X, Zielke HR, Kang J and Nedergaard M. An astrocytic basis of epilepsy. *Nat Med.* 2005; 11: 973 - 981

Vanhatalo S, Palva JM, Holmes MD, Miller JW, Voipio J and Kaila K. Infraslow oscillations modulate excitability and interictal epileptic activity in the human cortex during sleep. *PNAS.* 2004; 101: 5053–5057

Vanhoutte P and Bading H. Opposing roles of synaptic and extrasynaptic NMDA receptors in neuronal calcium signalling and BDNF gene regulation. *Curr Opin Neurobiol.* 2003; 13:366-71

Velazquez JLP and Carlen PL. Development of firing patterns and electrical properties in neurons of the rat ventrobasal thalamus. *Dev Brain Res.* 1996; 91: 164-170

Verkhratsky A and Kettenmann H. Calcium signalling in glial cells. *TINS.* 1996; 19:346–352

Verkhratsky A and Toescu EC. Neuronal-glial circuits as a substrate for CNS integration. *J Cell Mol Med.* 2006; 10: 826-836

Verkhratsky A and Kirchhoff F. NMDA Receptors in glia. *Neuroscientist.* 2007; 13: 28-37

Vesce S, Bezzi P and Volterra A. Synaptic transmission with the glia. *News Physiol Sci.* 2001; 16: 178-184

Volterra A and Meldolesi J. Astrocytes, from brain glue to communication elements: The revolution continues. *Nature.* 2005; 626-640

Walz W and Hertz L. Functional interactions between neurones and astrocytes. II. Potassium homeostasis at the cellular level. *Prog Neurobiol.* 1983; 20: 133-183

Walz W. Controversy surrounding the existence of discrete functional classes of astrocytes in adult gray matter. *Glia.* 2000. 31:95-103

Wang X, Lou N, Xu Q, Tian GF, Peng WG, Han X, Kang J, Takano T and Nedergaard M. Astrocytic Ca2+ signaling evoked by sensory stimulation in vivo. *Nat Neurosci.* 2006; 9:816-23

Wenzel A, Villa M, Mohler H and Benke D. Developmental and regional expression of NMDA receptor subtypes containing the NR2D subunit in rat brain. *J Neurochem.* 1996; 66: 1240-1248

Wenzel A, Fritschy JM, Mohler H and Benke D. NMDA receptor heterogeneity during postnatal development of the rat brain: Differential experrion of the NR2A, NR2B, and NR2C subunit proteins. *J Neurochem.* 1997; 68:469-478

Wittmann M, Bengtson CP and Bading H. Extrasynaptic NMDA receptors: mediators of excitotoxic cell death. Pharmacology of cerebral ischemia. Krieglstein J and Klumpp S (Eds). 253-266. Medpharm Scientific Publishers. 2004. Stuttgart

Wolff JR, Stuke K, Missler M, Tytko H, Schwarz P, Rohlmann A and Chao TI. Autocellular coupling by gap junctions in cultured astrocytes: A new view on cellular autoregulation during process formation. *Glia.* 1998; 24:121-140

Woolsey TA, Anderson JR, Wann JR and Stanfield BB. Effects of early vibrissae damage on neurons in the ventrobasal (VB) thalamus of the mouse. *J Comp Neurol.* 1979; 184: 363-80

Woolsey TA and Van der Loos H. The structural organization of layer IV in the somatosensory region (SI) of mouse cerebral cortex. The description of a cortical field composed of discrete cytoarchitectonic units. *Brain Res.* 1970; 20: 205-242

Xu J, Peng H, Kang N, Zhao Z, Lin JHC, Stanton PK and Kang J. Glutamate-induced Exocytosis of Glutamate from Astrocytes. *J Biol Chem.* 2007; 282: 24185-24197

Yang Y, Ge W, Chen Y, Zhang Z, Shen W, Wu M and Duan S. Contribution of astrocytes to hippocampal long-term potentiation through release of D-serine. *PNAS.* 2003; 100: 15194-15199

Ye Z-C, Wyeth MS, Baltan-Tekkok S and Ransom BR. Functional Hemichannels in Astrocytes: A Novel Mechanism of Glutamate Release. *J Neurosci.* 2003; 23: 3588-3596

Yi JH and Hazell AS. Excitotoxic mechanisms and the role of astrocytic glutamate transporters in traumatic brain injury. *Neurochem Int.* 2006; 48:394-403

Yuan F and Wang T. Glutamate-induced swelling of cultured astrocytes is mediated by metabotropic glutamate receptor. *Sci China C Life Sci.* 1996; 39:517-22

Zhang J, Benveniste H, Klitzman B and Piantadosi CA. Nitric oxide synthase inhibition and extracellular glutamate concentration after cerebral ischemia/reperfusion. *Stroke.* 1995; 26: 298-304

Zhou M and Kimelberg HK. Freshly isolated astrocytes from rat hippocampus show two distinct current patterns and different [K(+)](o) uptake capabilities. *J Neurophysiol.* 2000; 84: 2746-2757

Zhou M and Kimelberg HK. Freshly isolated hippocampal CA1 astrocytes comprise two populations differing in glutamate transporter and AMPA receptor expression. *J Neurosci.* 2001; 21: 7901-8

Zhu L, Blethyn KL, Cope DW, Tsomaia V, Crunelli V and Hughes SW. Nucleus- and species-specific properties of the slow (<1 Hz) sleep oscillation in thalamocortical neurons. *Neuroscience.* 2006; 141: 621-636

Zonta M, Angulo MC, Gobbo S, Rosengarten B, Hossmann KA, Pozzan T and Carmignoto G. Neuron-to-astrocyte signaling is central to the dynamic control of brain microcirculation. *Nat Neurosci.* 2003; 6: 43-50

Appendix 1

Experimental drugs	Chemical name	Function	Supplier
ACPD	(1S,3R)-1-Aminocyclopentane-1,3-dicarboxylic acid	Group I/group II mGlu agonist	Tocris (Bristol, UK)
CCh	Carbachol	Cholinergic receptor agonist	Sigma-Aldrich (Poole, UK)
CPCCOEt	7-Hydroxyiminocyclopropan[b]chromen-1α-carboxylic acid ethyl ester	Selective non-competitive $mGluR_1$ antagonist	Ascent (Weston-super-Mare, UK)
CPG	(S)-4-Carboxyphenylglycine	Competitive group I mGlu antagonist/weak group II agonist	Tocris
D-AP5	D-(-)-2-Amino-5-phosphonopentanoic acid	Selective antagonist for NMDA receptors	Sigma-Aldrich
D-Asp	D-Aspartic acid	EAAT substrate and NMDA-r agonist	Tocris
DHPG	(RS)-3,5-Dihydroxyphenylglycine	Selective group I mGlu agonist	Ascent
Gln	L(+)-Glutamine	EAA	Acros Organics (New Jersey, USA)
Glu	L-Glutamic acid monosodium salt monohydrate	EAA	Sigma-Aldrich
Ifenprodil	4-[2-[4-(cyclohexylmethyl)- 1-piperidinyl]-1-hydroxypropyl]phenol	Selective antagonist for NMDA receptors containing NR2B subunit	Tocris
Isop	(-)-Isoproterenol hydrochloride	Selective β-adrenoceptor agonist	Sigma-Aldrich
Kyn	Kynurenic acid	Non-selective antagonist at NMDA and AMPA/kainate receptors	Sigma-Aldrich
SR95531	gabazine	Selective, competitive GABA-A receptor antagonist	Calbiochem (Nottingham,UK)
MTEP	3-((2-Methyl-1,3-thiazol-4-yl)ethynyl)pyridine	Potent, selective non-competitive mGlu5 antagonist	Tocris
TBOA	L-Threo-beta-benzyloxyaspartate	Potent, selective non-transportable inhibitor of EAATs	Tocris
TTX	Tetrodotoxin	Na^+ channel blocker	Ascent